SHAPE MEMORY ALLOY- MAGNETORHEOLOGICAL FLUID CORE BRACING SYSTEM

By

Shahin Zareie

B.A.Sc. (Mechanical Engineering), Hormozgan University, Iran, 2007

M.A.Sc. (Mechatronic Engineering), Sharif University of Technology, Iran, 2010

A THESIS SUBMITTED IN PARTIAL FULFILLMENT OF

THE REQUIREMENTS FOR THE DEGREE OF

DOCTOR OF PHILOSOPHY

In

THE COLLEGE OF GRADUATE STUDIES

(Civil Engineering)

THE UNIVERSITY OF BRITISH COLUMBIA

(Okanagan)

October 2020

The following individuals certify that they have read, and recommend to the Faculty of Graduate and Postdoctoral Studies for acceptance, a thesis/dissertation entitled:

SHAPE MEMORY ALLOY-MAGNETORHEOLOGICAL FLUID CORE BRACING SYSTEM

submitted by Shahin Zareie in partial fulfillment of the requirements for

the degree of DOCTOR OF PHILOSOPHY

in Civil Engineering

Examining Committee:

Dr. M.Shahria Alam, School of Engineering
Supervisor

Dr. Rudulf J. Seethaler, School of Engineering
Co-supervisor

Dr.Abbas Milani, School of Engineering
Supervisory Committee Member

Dr.Homayoun Najjaran, School of Engineering
Supervisory Committee Member

Dr. Anas Chaaban, School of Engineering
University Examiner

Dr. Anjan Bhowmick, Concordia University
External Examiner

Abstract

Magnetorheological fluid (MRF) and shape memory alloy (SMA) are two smart materials used in many protective systems in civil engineering to mitigate unpredicted hazards. Isolation systems, dampers, and bracing systems are examples of smart protective systems integrated with civil infrastructures, such as building, to enhance their dynamic behaviour. Among them, bracing systems are the most common technique to keep buildings safe and healthy under seismic loads. In this study, both materials are used to develop a new bracing system called the SMA-MRF core-based bracing.

A prototype of the system is fabricated and tested by the loading frame machine to prove the functionality of the system regardless of loading directions. Then, a numerical model of the systems is developed in the Open System for Earthquake Engineering Simulation (OpenSees). This model is implemented in a simplified two-story steel frame and exposed to the simulated ground motions. It is noted that the system improves the structural dynamic behaviour, such as the drift ratio, in the time-domain as well as frequency-domain. A control strategy is applied to the SMA-MRF core bracing systems. It is found that the system enhances the dynamic response with the embedded controller.

The experimental results indicate that pre-straining SMA elements lead to a sharp increase in the energy absorption capacity as well as the recovery ability under short and long-term loadings. It is worth mentioning that the pre-strained SMA maintains the specifications, particularly the recovery capability, rather than conventional SMA under simulated short- and long-term loading.

Lay Summary

The structural integrity of the civil infrastructure is a crucial issue during and after earthquake events. During past decades, it has been observed that the poorly designed and/or inherent weakness in civil infrastructure has been the main reason to damage and collapse them. In the present study, a smart bracing system has been designed conceptually to preserve structural health and stability. A prototype of the system has been fabricated, and its behaviour has been confirmed, characterized by experimental tests under the compression and tension loadings.

To examine the performance of the system in a building, the numerical model of the system has been developed and implemented in a simplified frame structure. Then, the responses of the frame with and without the smart systems have been investigated in the time and frequency domains underground motions. The results have shown that the system has improved the structural behaviour remarkably.

Preface

Publications arising from the work presented in this dissertation are listed as follows:

1. Zareie, S., Alam, M.S., Seethaler, R.J., Zabihollah, A., “Effect of shape memory alloy-magnetorheological fluid-based structural control system on the marine structure using nonlinear time-history analysis”, *Applied Ocean Research*, 2019 Oct, 91:101836.
2. Zareie, S., Alam, M.S., Seethaler, R.J., Zabihollah, A., “A novel shape memory alloy-based element for structural stability control in offshore structures under cyclic loading”, *Ships and Offshore Structures*, 2019 Nov 19:1-8.
3. Zareie, S., Alam, M.S., Seethaler, R.J., Zabihollah, A., “Stability control analysis of the frame structure equipped with shape memory alloy-magnetorheological fluid-based in the frequency domain”, *Applied Ocean Research*, 2020 April, 97: 102091.
4. Zareie, S., Zabihollah, A., “A study of pre-straining shape memory alloy (SMA)-based control elements subject to large-amplitude cyclic loads", *Ships and offshore structures*, 2020 Feb, 1:8.
5. Zareie, S., Zabihollah, A., “A semi-active SMA-MRF structural stability element for seismic control in marine structures”, *Applied Ocean Research*, 2020 July, 100: 102161.
6. Zareie, S., Issa, A., Seethaler, R. J., Zabihollah, A., “Recent Advances in the Applications of Shape Memory Alloys in Civil Infrastructures: A Review", In press, *Structures*.
7. Zareie, S., Issa, A., Seethaler, R. J. Zabihollah, A., “Dynamic response of frame Structures with an SMA-MRF-based bracing system by nonlinear time-history", Revision requested, *Structures*.

8. Zareie, S., Zabihollah A., “Recent Advances Magnetorheological Fluid-based Systems in Civil Infrastructures: A Review”, Submitted to *Journal of Earthquake Engineering*, Manuscript ID: UEQE-2020-4318.
9. Zareie, S., Issa, A., Seethaler, R. J., Zabihollah, A., “A novel SMA-magnetorheological hybrid bracing system for seismic control”, Submitted to *Engineering Structures*, Manuscript ID ENGSTRUCT_2020_2769.

   Zareie, S., Zabihollah, A., “Design and validation of a hybrid shape memory alloy-magnetorheological fluid-based core bracing system under tension and compression”, Submitted to *Smart Materials and Structures*, Manuscript ID: SMS-110724.
10. Zareie, S, Mirzai, N., Alam, M. S., Seethaler, R. J., “An introduction and modeling of novel shape memory alloy-based bracing,” *6th International Conference on Engineering Mechanics and Materials, CSCE,* Vancouver, Canada, 2017.
11. Zareie, S, Mirzai, N., Alam, M. S., Seethaler, R. J., 2017. “A dynamic analysis of a novel shape memory alloy-based bracing system”, *6th International Conference on Engineering Mechanics and Materials, CSCE,* Vancouver, Canada, 2017.
12. Zareie, S., Alam, M.S., Seethaler, R.J., Zabihollah, A., “A shape memory alloy-magnetorheological fluid core bracing system for civil engineering applications: a feasibility study”, *7th International Specialty Conference on Engineering Mechanics and Materials,* Laval, Canada, 2019.

For all papers, I wrote the drafts and co-authors edited them.

The permission has been taken for those my papers which are re-used in this thesis.

Table of Contents

List of Tables

List of Figures

List of Symbols

m_d	TMD mass
m_s	Structural mass
$k_s,$	Stiffness of the structure
k_d	TMD stiffness
ξ_d	TMD damping ratio
ξ_s	Damping ratio of the structure
u	Displacement
$\dot{u}$	Velocity,
$\ddot{u}$	Acceleration of TMD
$\ddot{x}$	Acceleration of the structure
P	External excitation applied to the primary structure
L	length of the cable
g	Ground acceleration
ρ	Fluid density
A_h	Horizontal cross-sectional area
A_v	Vertical the cross-sectional area
ξ_l	Head loss coefficient
L_h	Horizontal length,
L_v	Vertical length
m_t	Mass of TLCD

C_T	damping of TLCD
p	Friction dampers force
μ	Coefficient of dynamic friction
N	Normal force at the sliding interface
α	exponent whose value
$C(\xi)$	Damping coefficient
T	Temperature
A_f	Austenite finish temperature
M_f	Martensite finish temperature
ε_{max}	Maximum applied strain
ε_s	Maximum superelastic strain
A_s	Austenite start temperature
M_d	Martensite phase temperature
F_{sma}	The resistive force of the SMA-elements
σ	Stress
A	Cross-section
E	Young's modulus
ε	strain
ε^T	phase transformation strain
ζ	phase transformation volume fraction
E_M	Young's modulus and in the Martensite phase
E_A	Young's modulus and in the Austenite phases

ε_{ms}	Martensite start strain
ε_{mf}	Martensite finish strain
ε_{as}	Austenite start strain
ε_{af}	Austenite finish strain
σ_{ms}	Martensite start strain
σ_{mf}	Martensite finish strain
σ_{as}	Austenite start strain
σ_{af}	Austenite finish strain
τ_{yeild}	yield stress
τ	shear stress
μ	viscosity
$\dot{y}$	strain rate
F_{MRF}	generated force by MRF-based damper(core)
f_c	frictional force
$\dot{x}$	velocity of external excitation,
c_0	damping coefficient
ξ	Equivalent viscous damping coefficients
A_h	Amount of energy dissipation
D_m	maximum force in one complete stable cycle
F_m	maximum displacement in one complete stable cycle
$Energy_{total}$	The energy absorption capacity
F_i	force at “i-th” coordinate of the “i-th” element

D_i	Displacement at “i-th” coordinate of the “i-th” element
M	Mass matrix
m	Lumped mass
I_c	Moment of inertia
h	Height of floor
f_1	Second natural frequency
f_2	first natural frequency
C	Damping matrix
K	Stiffness matrix
u	displacement of floor
$\ddot{u}_g$	Ground acceleration
C_{eq}	Modified damping matrix
K_{eq}	Modified stiffness matrix
$F_{SMA-MRF}$	Resistive force of the SMA-MRF core bracing system
ε_{UL}^{T}	Maximum phase transformation strain from Martensite to Austenite
ε_{L}^{T}	Maximum phase transformation strain from Austenite to Martensite
F_η	Viscous shear force
F_τ	Magnetic-dependent shear force
f_1	First natural frequency
f_2	Second natural frequency

Acknowledgments

First, I would like to thank my advisors, Prof. M. Shahria Alam and Dr. Rudolf J. Seethaler, for their help and guidance, both professionally and personally. Their guidance helped me in all the time of research and writing of this thesis. I could not have imagined having better advisors and mentors for my Ph.D. study.

I would also like to thank the school of engineering, the University of British Columbia, Okanagan Campus, for support.

My gratitude also goes to many people who have given their time to help me with this effort, especially Dr. A. Zabihollah, as my close friend and my former supervisor.

I would like to dedicate this doctoral dissertation to my lovely parents: Alireza and Fariba, for their unwavering support over the years.

I appreciate the love and support form Maedeh Daghighi.

Chapter 1: Introduction

1.1 Background and motivation

Every year, about 4000 earthquakes happen in Canada. For example, southwestern British Columbia is one of the most active seismic zones in Canada. In the next 50 years, there will be a strong earthquake(s) with a 30% probability of Occurrence [1]. One of the worst scenarios, the earthquake of a magnitude of 9.0, happening in the Cascadia subduction zone, where is about 75 km off the west coast of Vancouver Island [1]. The overall economic loss is about $75 Billion [1]. Civil infrastructures are usually exposed to excessive loading conditions, particularly earthquakes, which may result in catastrophic failure. During the past few decades, a variety of stability and vibration control systems and mechanisms have been developed to enhance the performance and to increase the structural stability of structures. This includes passive, semi-active, and active control systems.

Passive systems, including conventional bracing systems [2], are mainly based on increasing the structural stiffness, the damping, and/or the energy dissipation capacity of the structural elements. The structural design considering all kinds of possible loading scenarios based on passive systems may dramatically increase the size, weight, and construction cost. Furthermore, outputs of these control systems, such as the energy dissipation capacity and the damping, are not controllable and are only functions of the inputs.

On the other hand, active systems, such as active tendon systems [2], need a remarkable source of external energy to be fully activated in civil infrastructure. These systems may enhance the structural characteristics including damping, energy absorption, and/or stiffness. Their effectiveness in civil infrastructure may highly rely on a control mechanism; having a solid

knowledge of users and access to a continuous source of energy are requested to keep them in an optimally functional state. Otherwise, the systems do not meet the desired outputs.

Semi-active control systems, like a semi-active tuned mass damper, can be considered as an optimum alternative solution for civil infrastructures [3]. Such systems use a small amount of external energy compared to active systems while providing a sufficient level of controllability and remove the weakness of passive systems.

The conventional semi-active control systems may not meet the full stability requirements of the structural responses for all loading conditions. During the past few years, different combinations of controllable elements with stiffness elements have been proposed to enhance the functionality of the semi-active system, such as MRF elastomer bearings (MRE bearings) [2]. Recent advances in smart materials and structures provide us with rooms for improving the existing semi-active control systems. This includes modeling, simulation, manufacturing, a different combination of elements, control algorithm, and long-term loading's effect on semi-active performance.

1.2 Problem statement

Although conventional methods such as bracing systems with friction dampers are efficient, they are heavy, huge in size, and occupy costly space in the building [4]. These techniques are passive and impossible to be set for a wide range of earthquakes wave frequencies [4]. In order to surpass these limitations, a semi-active brace damper system is introduced [4]. In the present study, the semi-active bracing system based on shape memory alloy (SMA) and Magnetorheological Fluid (MRF)'s behaviour, called the SMA-MRF core bracing system, is introduced (see Figure 1-1). The main disadvantages of each component are:

- The SMA in the superelasticity is not controllable, and performance is only a function of external excitations coming from external loadings. Additionally, the SMA-based systems' effect on the damping is not much.
- The MRF-based damper is not good for re-recentring purposes in civil infrastructures.

The major advantages of the SMA and the MRF-based damper are as follows:

- SMA-based systems are a good option to provide recovery capability in the civil infrastructures.
- The MRF-based damper can increase the damping of civil infrastructures and energy dissipation capacity. The outputs of the systems are controllable.

The main role of the SMA-based system is to provide the recovery ability in the frame and shifting of the natural frequency of the frame to the higher value. In addition, The SMA-MRF-based core bracing system controls the interstory drift by providing the tunable energy dissipation capacity, the recovery ability, and extra damping. These parameters can not be supplied by the MRF-based damper. So, this smart bracing system minimizes the casualties and decreases dynamic structural responses by dissipating the energy through inherent hysteresis behaviours under dynamic loads.

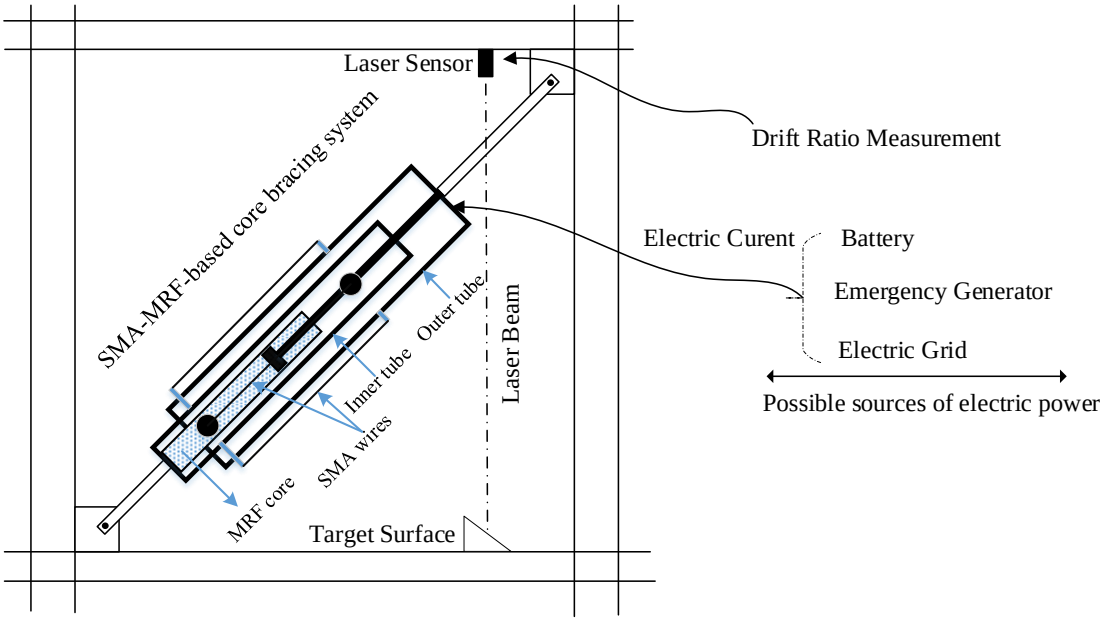

Figure 1-1. The proposed SMA-MRF core bracing system equipped a laser sensor

1.3 Research objectives

To employ the advantages of shape memory alloy (SMA) and MR-fluids and overcome their shortcomings, the novel SMA-MR fluid core bracing system is proposed to be implemented in buildings, as shown in Figure 1-1. In order to design, model, analyze, and validate the system, the general objectives, as shown in Figure 1-2, are defined as:

Objective 1: Developing an analytical model of the SMA-MRF-based bracing system

Objective 2: Proposing and refining the conceptual design, fabrication of a prototype of the proposed bracing systems, and performing experimental tests.

Objective 3: Evaluate the seismic performance of a frame equipped with bracing systems in time and frequency domains

Objective 4: Determine the effect of cyclic loading on SMA

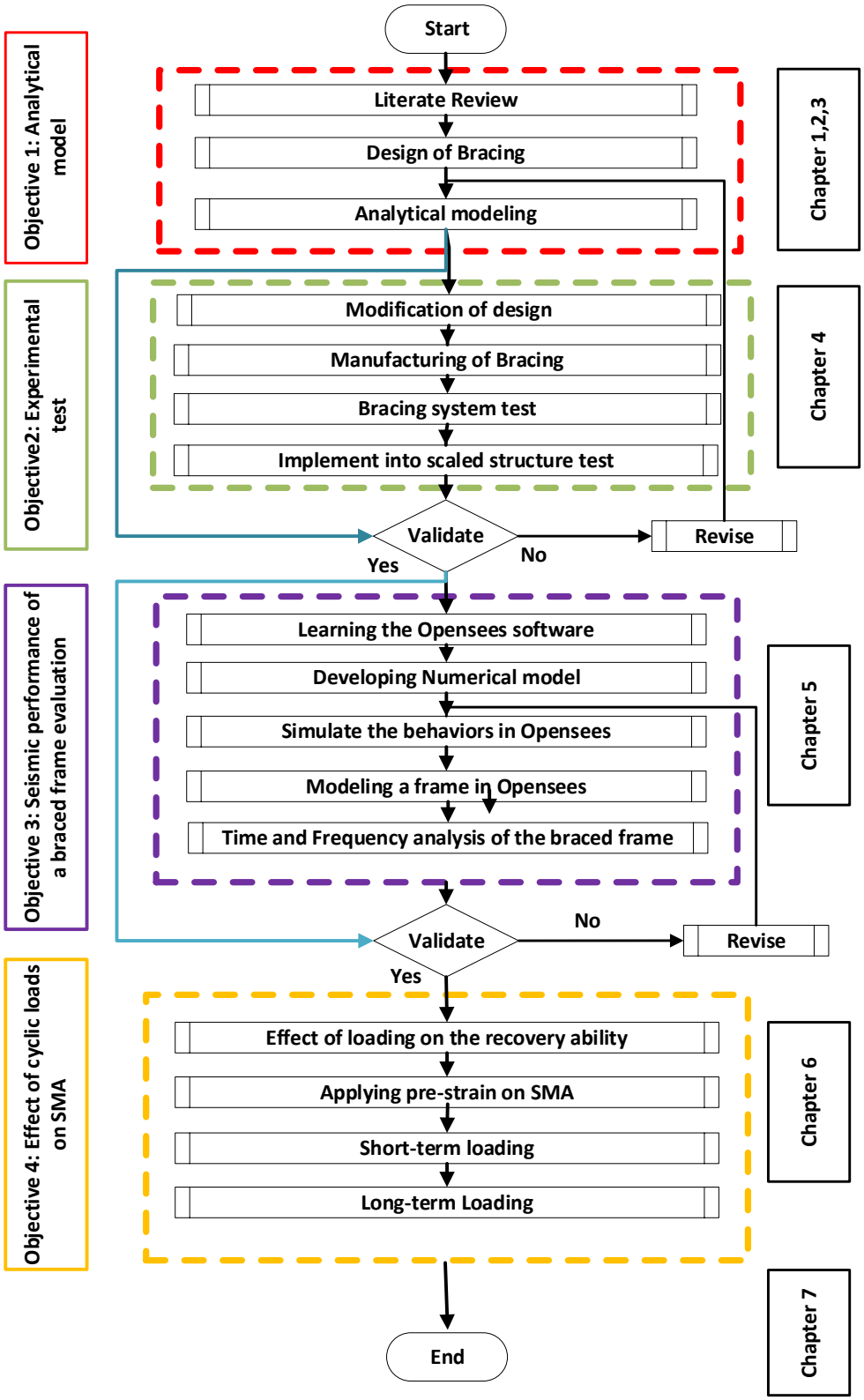

Figure 1-2. Flowchart of goals and topics in this thesis

1.1 Organization of the thesis

- This chapter is focused on the introduction, the motivation, objectives, and the conceptual design of the hybrid semi-active bracing system.
- In Chapter 2, the application of structural control systems in civil infrastructures with respect to the amount of activation energy as well as the equivalent viscous damping coefficient are investigated. A thorough review of the recent publications relevant to the stability control elements in civil structures is performed. The literature review is particularly focused on the development and design of SMA-based and MRF-based bracing systems for civil infrastructures.
- Analytical and numerical models for SMA-based and MRF-based bracing elements are introduced in Chapter 3. Numerical examples are discussed to illustrate the dynamic response of structures integrated with SMA-based and MRF-based elements under various loading conditions.
- Based on the outcomes of chapter 4, the design, the analysis, and the numerical modeling of a hybrid SMA-MRF core bracing system in the OpenSees is introduced in Chapter 4. Numerical simulations have been discussed to illustrate the enhancement in stability control of scaled structures integrated with the hybrid systems under several seismic loadings. The results, including time-history and frequency responses, are compared with the most common control elements.
- The design procedure, prototype fabrication, and experimental set-up for the SMA-MRF core bracing element are presented in chapter 5. Using the MTS machine, a wide range of experimental tests are conducted to study the influences of the implementation of the

hybrid element in structural responses of scaled structures under different loading conditions, including cyclic loading, both steady and progressive loads, and non-deterministic seismic loading.

- Frequency analysis of the frame with the SMA-based, the MRF-based, and the SMA-MRF-based bracing systems under simulated ground motions is conducted in Chapter 6. To enhance the performance of the SMA-MRF based system embedded in the frame, a control algorithm is designed and applied.
- The effect of long-term loading on the SMA component is studied experimentally in Chapter 6. To reduce the degradation' effect on the SMA properties, pre-strain is applied to the SMA. A comparison between 0% prestrained and 1.7% prestrained SMAs is performed.
- Chapter 7 summarizes the present work, highlights the most important outcomes, contributions, and novelty of this thesis. Practical recommendations are provided for work in future researches.

Chapter 2: Literature review

2.1 Introduction

Civil infrastructures are usually exposed to severe and unpredictable loadings, particularly earthquakes, tornados, and storms. To enhance the performance and assure the functionality, civil infrastructures require reliable and efficient mechanisms to provide enough capacity to the structures to maintain their structural integrity under such loadings.

Therefore, seismic control systems are needed to enhance the structural behaviour, such as an increase in the energy dissipation capacity of civil infrastructure. Due to the amount of activation energy, seismic control systems might be classified into passive systems, semi-active systems, and active systems [5] as displayed in Figure 2-1. In this chapter, the comprehensive review of all systems is discussed to portray their advantage and disadvantages.

2.2 Passive systems

Passive systems suppress the seismic loads applied to civil infrastructure and control the structural behaviour without the need for external power [6], which is the main advantage of these systems, to enhance their dynamic response.

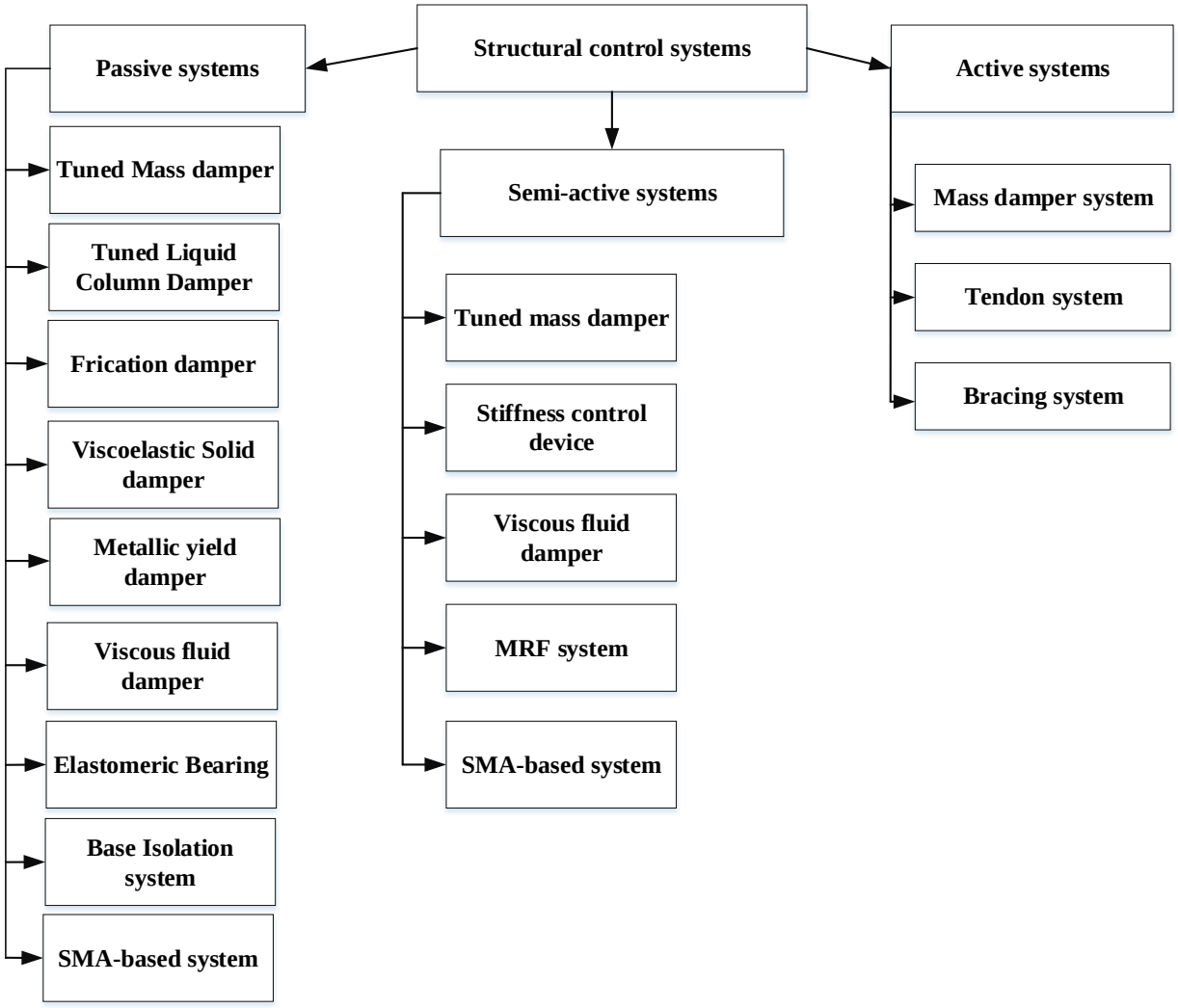

Figure 2-1. The different types of structural control systems adapted from [7]

2.2.1 Tuned mass damper systems

One of the most common passive systems in structural control systems is a Tuned-Mass-Damper (TMD) system. It consists of an extra mass with a damper and a spring added to the main structures to reduce the structural response in the occurrence of the resonance [7]. A schematic diagram of a TMD for a single degree of freedom (SDOF) structure is shown in Figure 2-2.

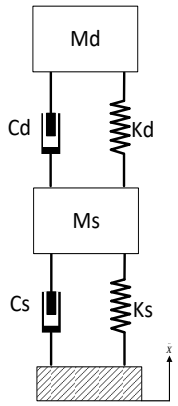

Figure 2-2. SDOF with a Tuned Mass Damper system adapted from [8]

The dynamic response of the SDOF system with the fundamental resonance frequency of the structure (ω_s) and the TMD with the frequency ω_d the system can be modeled with [8]:

$$(1+\mu)\ddot{x} + 2\xi_s\omega_s\dot{x} + {\omega_s}^2 x = \frac{P}{m_d} - \mu\ddot{u} \text{ for the structure} \quad (2.1)$$

$$\ddot{u} + 2\xi_d\omega_d\dot{u} + {\omega_d}^2 x = -\ddot{x} \text{ for the TMD} \quad (2.2)$$

where m_d, m_s, k_s, k_d, ξ_d ,ξ_s, u, $\dot{u}$, $\ddot{u}$, $\ddot{x}$, and P are the TMD mass, the structural mass, the stiffness of the structure, the TMD stiffness, the TMD damping ratio, the damping ratio of the structure, the displacement, the velocity, the acceleration of TMD, the acceleration of the structure, and external excitation applied to the primary structure, respectively [8]. μ corresponds to the ratio of the $m_d$to m_s.

The frequency of TMD is set to the first natural frequency of the primary structure. Thus, the amplitude of vibration of the primary structure decreases in the case of resonance by increasing the equivalent damping ratio, which results in dissipating more energy [7]. The main disadvantages of TMDs are:

- Occupation of large space

- Large mass
- TMDs are only effective at a single a frequency that might not coincide with the seismic loading
- TMD's are very sensitive to de-tuning [8].

2.2.2 Pendulum Tuned Mass Damper

Conventional TMD requires a large space and a very large mass. Hence, a suitable candidate is the Pendulum TMD (PTMD) system [8]. The system consists of a mass that hangs from the top of the main structure by a cable [8], as illustrated in Figure 2-3 schematically. When external excitation is applied to the structure, the PTMD generates opposing forces.

Assumed that θ is small, The equation of motion of an SDOF PTMD can be written as [9]:

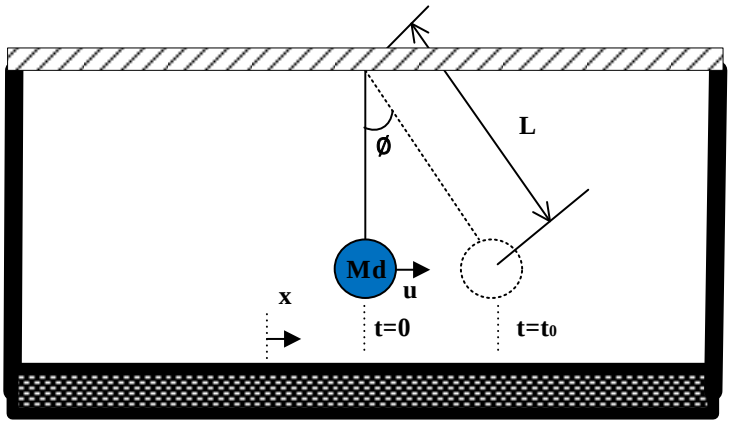

Figure 2-3. Schematic diagram of Pendulum Tuned Mass Dampers [8]

$$m_d\ddot{u} + \frac{m_d g}{L}(u) = -m_d\ddot{x} \tag{2.3}$$

where m_d, L, $\ddot{u}$, and $\ddot{x}$ are PTMD mass, length of the cable, PTMD acceleration, and acceleration of excitation, respectively. The spring stiffness of PTMD is written by [9]:

$$k_d = \frac{m_d g}{L} \tag{2.4}$$

The natural frequency of PTMD is calculated as:

$$\omega_d = \sqrt{\frac{g}{L}} \tag{2.5}$$

The main advantage of the system is the capability of re-tuning the natural frequency of the PTMD by a change in the length of the PTMD cable.

2.2.3 Bidirectional Tuned Mass Damper

A Bidirectional Tuned Mass Damper (BTMD) is a new class of TMD which was introduced by Almaz et al. [10]. The system consists of Y-shape cables connecting the top of the structure to the damper mass and a friction damper between the mass damper and bottom of the structure, as displayed in Figure 2-4. The advantages of this system are:

- Simplicity
- The ability to tune the damper to two independent frequencies of building.

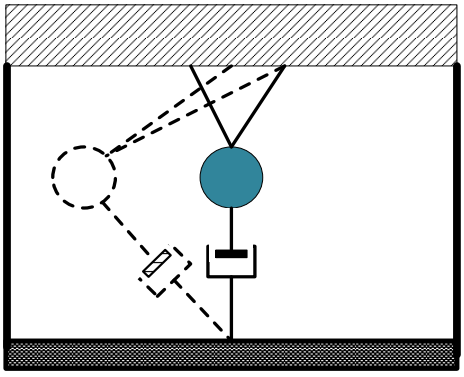

Figure 2-4. Schematic diagram of Bidirectional Tuned Mass Damper Dampers [8]

2.2.4 Tuned Liquid Column Damper (TLCD)

A Tuned Liquid Column Damper (TLCD) is a type of TMD in which the mass, damping, and stiffness are replaced with water [8]. The concept of a TLCD has been used for a long time to stabilize ships; in the 1980s, Sakai et al. [11] proposed to use TLCDs to stabilize buildings. Figure 2-5 displays a schematic diagram of a TLCD.

In this system, the energy applied to the structure by external excitation transfers to the water and eventually converts to heat due to friction. Therefore, the energy from the external excitation is dissipated [7]. The low-cost, easy installation and low required maintenance of this system have attracted much interest from users and designers [12–20].

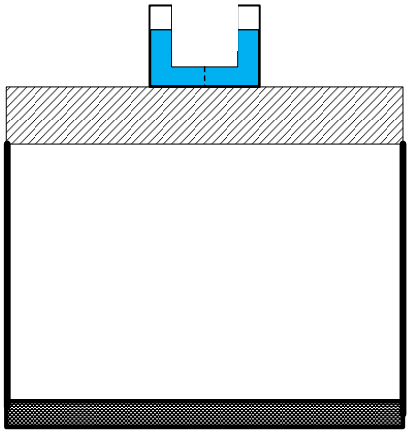

Figure 2-5. Schematic diagram of Tuned liquid damper taken from [8]

The equation of motion of an SDOF TLCD with the cross-sectional area (A) is expressed by [8]:

Primary Structure

$$\left(m_s + \rho A(L_h + L_v)\right)\ddot{x} + c_s\dot{x} + k_s x = \rho - \rho A\ddot{u}(L_h + L_v)\frac{L_h}{L_v} \tag{2.6}$$

TLCD system

$$A(L_h + L_v))\ddot{u} + \frac{\rho A \xi_l}{2}|\dot{u}|u + 2g\rho Au + \mu\rho - \frac{L_h}{L_v}A\ddot{x}(L_h + L_v) \quad (2.7)$$

where ρ, A_h, A_v, L_h, and L_v are the fluid density, the horizontal cross-sectional area, the vertical the cross-sectional area, the horizontal length, and the vertical length, respectively. All parameters are shown in Figure 2-6. u corresponds to the horizontal movement of the primary structure and TLCD system.

m_t which is the mass TLCD, is given by [8]:

$$m_t = \rho A(L_v + L_v) \quad (2.8)$$

$$C_T = \frac{\rho A \xi_l}{2}|\dot{u}| \quad (2.9)$$

where ξ_l stands for the head loss coefficient.

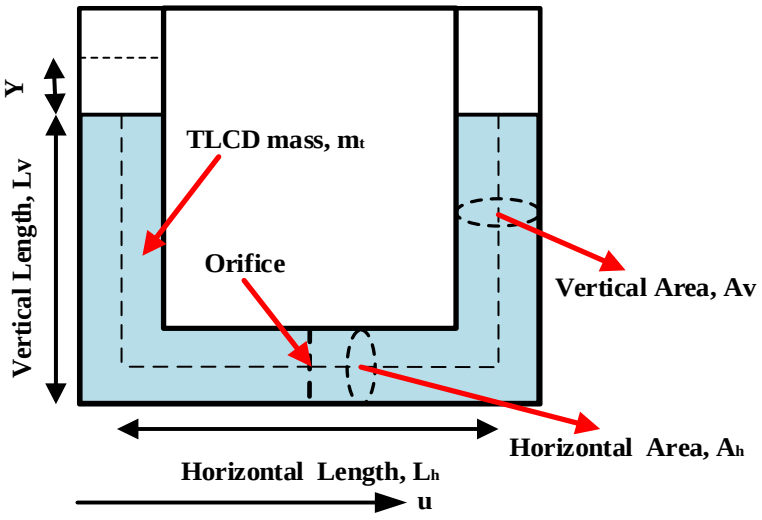

Figure 2-6. Properties of TLCD adapted from [8]

2.2.5 Friction damper

Friction dampers, e.g. Slotted Bolted Connections (SBC) [21], provide relative motion between two bodies. The sliding friction between the bodies dissipates energy [22]. The main purpose of this damper is shifting from the high amplitude to lower amplitude of vibrations, particularly in the resonance [7]. In addition, the energy dissipation capacity is sizable and is not a function of the ambient temperature [2].

Different types of dampers are available, including Pall cross-bracing friction dampers, as displayed in Figure 2-7 [23], and cylindrical friction dampers [24].

The dynamic behaviour of friction dampers is based on experimental tests that can be fitted to the following expression [22]:

$$p = \mu N sgn(\dot{u}) \tag{2.10}$$

where μ, N, and $\dot{u}$ denote coefficient of dynamic friction, normal force at the sliding interface, and velocity, respectively.

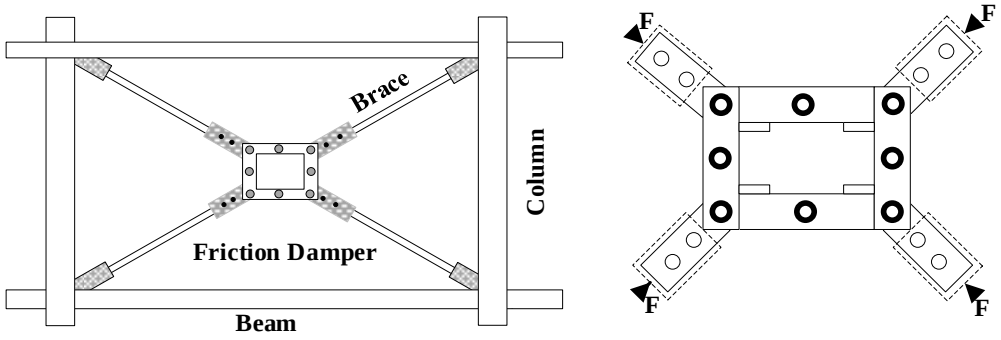

Figure 2-7. Schematic diagram of friction damper and installation in civil infrastructures adapted from [7]

The main disadvantages of the system are no restoring force and permanent deformation. Furthermore, its response is nonlinear and needs nonlinear analysis.

2.2.6 Viscoelastic Solid damper

Viscoelastic solid dampers are composed of solid elastomeric pads of viscoelastic material attached to steel plates, as shown in Figure 2-8 [22]. The characteristics of this damper include both viscous and elastic behaviours [7]. It has the ability to absorb energy during loading and release stored energy while unloading with delay [7].

The dampers are installed in bracing systems and the two ends of the damper move with the movement of the two sides of braces. The relative movement between steel plates and pads dissipates the energy in the viscoelastic material [22].

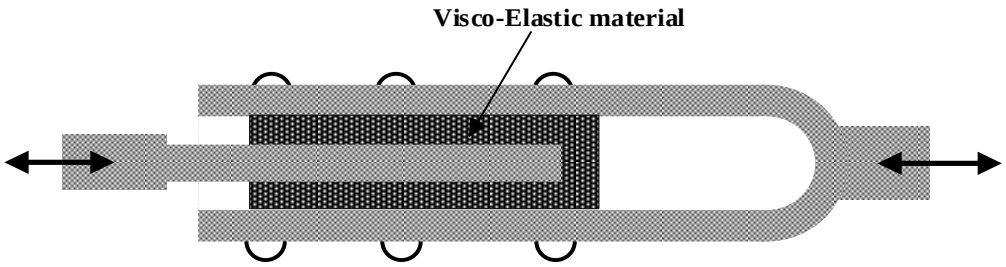

Figure 2-8. Schematic diagram of the viscoelastic solid damper adapted from [22]

It should be noted that the behaviour of this damper depends on the frequency of motion, the strain amplitude, and temperature [22].

In a simplified form, the system can be modeled by "**linear spring in parallel with a linear viscous dashpot**" [22]. The damping force can be computed by:

$$P(t) = Ku(t) + C\dot{u}(t) \tag{2.11}$$

where $K, C,$ and $u(t)$ denote storage stiffness of the damper, damping coefficient, and displacement, respectively.

The system can be activated in a low displacement, and modeling of its behaviour is relatively easy. However, the functionality of the damper strongly depends on the ambient temperature and the loading frequencies. In addition, the deformation capacity is limited [2].

2.2.7 Metallic yield damper

Traditionally, the plastic deformation and ductility of civil infrastructures were designed to dissipate the energy of seismic loads. Metallic yield dampers function in the same way [7,25].

Metallic yield damper (MYD) is a type of damper that uses hysteretic materials, like mild steel, to absorb the dissipated energy as a result of external loadings, such as seismic loads [25]. In many cases, metallic dampers are installed in buildings as a chevron bracing system, as shown in Figure 2-9 [7].

The damping force(P_y) is given by:

$$P_y = (Bt^2/3L)f_y \ , \tag{2.12}$$

$$\Delta_y = (H^2/2Et)f_y \ , \tag{2.13}$$

where B, t, and H represent the width, the thickness, and the height of the damper. Δ_y, f_y , and E denotes the yield displacement, the yield stress, and Young's modulus of the material, correspondingly.

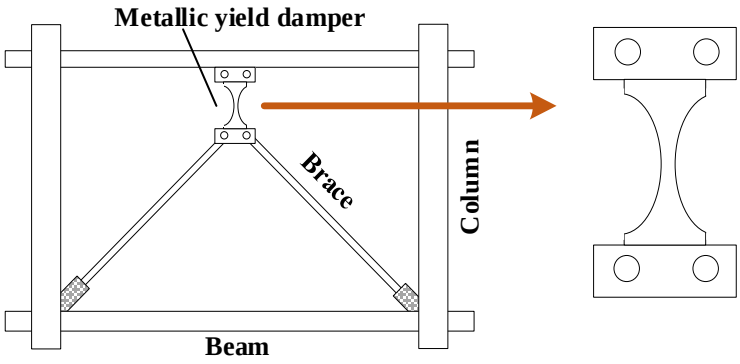

Figure 2-9. Schematic diagram and installation of metallic yield damper adapted from [7]

The metallic yield damper is a good option to improve the structural behaviour due to the stability in its hysteresis response in long-term use. Nevertheless, the system is damaged under strong earthquakes and should be changed [2].

2.2.8 Base Isolation system

Base isolation systems are an efficient method to protect primary structures during earthquakes; the system decreases the vibration amplitude of the main structure by providing more flexibility to the base of the structure [7]. The major effect of isolation is to alter the natural frequency of the structure from a higher magnitude to a lower one [7]. It is suggested to use the system for the low and middle-rise buildings [7].

Base isolation systems are installed between the foundation and the main structure [7]. Figure 2-10 and Figure 2-11 display the applications of base isolation systems in civil infrastructure. Base isolation systems are categorized into; (1) Elastomeric Bearings (2) Friction Bearings, and (3) Lead-Plug Bearings [7], [5].

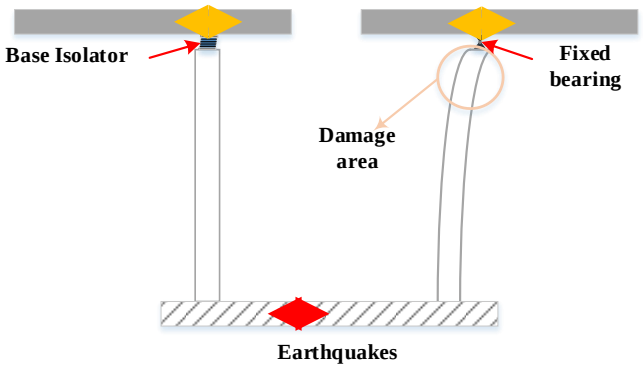

Figure 2-10. Application of base isolation system in bridges [5]

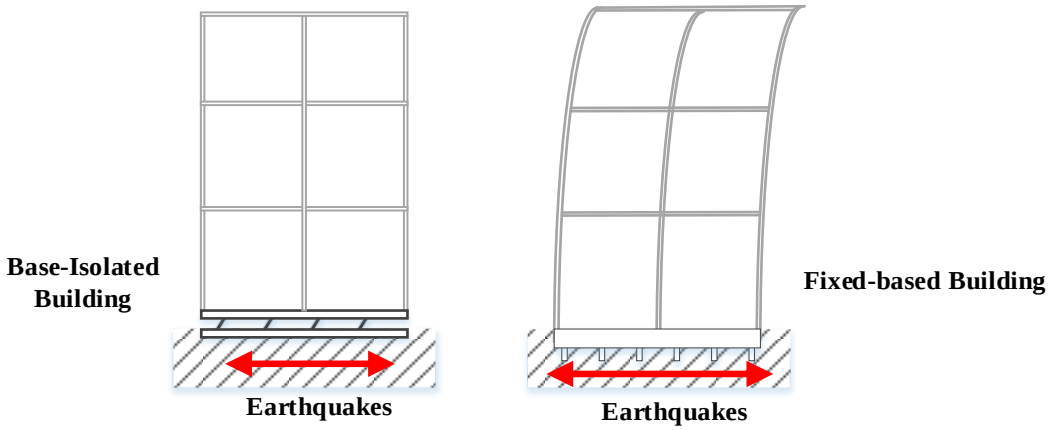

Figure 2-11.Application of base isolation system in buildings [5]

2.2.9 Elastomeric Bearing

Elastomeric bearings are composed of natural rubber that is sandwiched between two steel plates, as illustrated in Figure 2-12 [7]. The key role of the bearing is changing the natural frequency of the primary structure. However, the resistance of the elastomer against the lateral movement is typically very low, requiring larger dampers to achieve sufficient stiffness and damping and to avoid the structural instability [7].

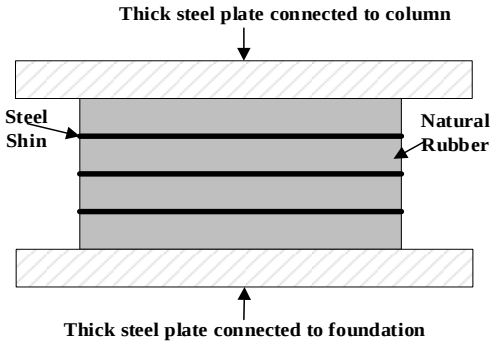

Figure 2-12. Schematic diagram of Elastomeric Bearing adapted from [7]

Lead-Plug Bearing

The low stiffness of the elastomeric bearing is improved by plugging a lead core, as shown in Figure 2-13. The performance of the system is a function of the lateral force. For small forces, the natural rubber provides the desired flexibility. For large forces, the lead core dissipates energy when it yields [7].

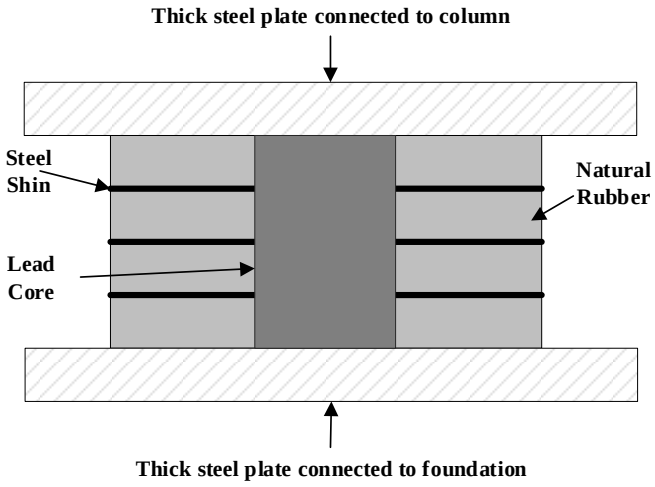

Figure 2-13. Schematic diagram of Lead-Plug Bearing adapted from [7]

Friction Pendulum Bearing

The working principle of Friction Pendulum Bearings (FPB) is based on the friction between sliding surfaces when the forces are applied on surfaces and bearing. The main drawback of this damping system is its inability to return to its initial position after an earthquake, thus resulting in a permanent dislocation of the structure [7]. In order to overcome this problem, a modified FPB was developed in which the core of the bearing is replaced with spherical or concave sliding surfaces. This modification causes the system to move the structure back to its initial position after an earthquake. Figure 2-14 shows this system schematically. To prevent corrosion, the surfaces are coated with a layer of Teflon.

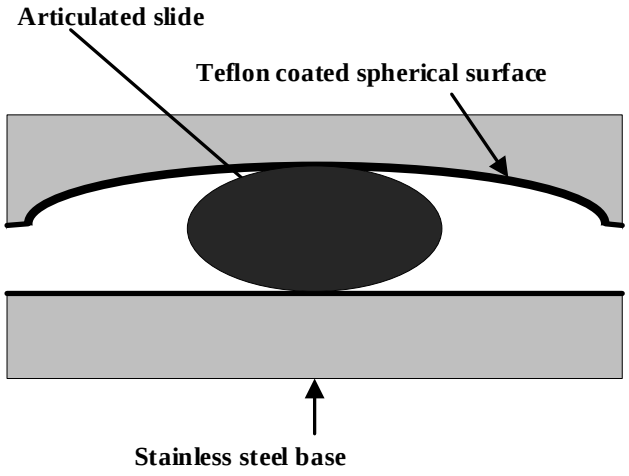

Figure 2-14. Schematic diagram of Friction Pendulum Bearing adapted from [7]

2.2.10 Viscous-based damper

A viscous damper is a cylinder-piston filled with a polymer liquid, as shown schematically in Figure 2-15. The amount of force generated in a viscous damper is proportional to the rate of change in piston displacement, i.e. the velocity of the piston rod.

The relation between force and velocity of a typical viscous damper can be expressed by [26]:

$$F_{Viscous}(t) = C_D|\dot{x}_d|^{\alpha} sgn(\dot{x}) \quad (2.14)$$

where C_D, α, and $x_d(t)$ represent the damping coefficient, the velocity exponent, and the piston rod displacement, respectively.

The performance of the system is proven, but there is a possible leakage [2].

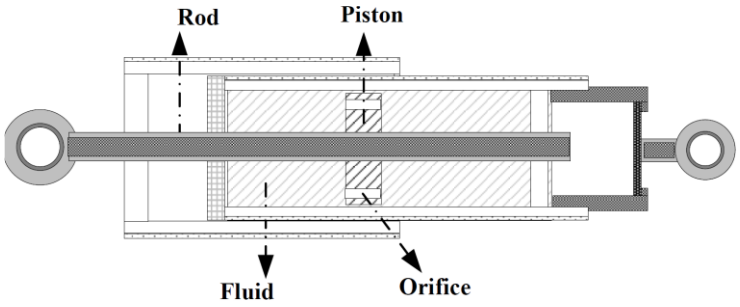

Figure 2-15. The schematic diagram of a viscous-based structural control system [26]

2.3 Semi-active system

Among protective systems, the semi-active systems are commonly used in civil structures as they don't exhibit typical problems of active systems, including capital cost, maintenance, power failure, system reliability, and the lack of knowledge/information [27]. They also don't suffer from passive system problems, such as being unable to adjust to new loading conditions [28]. Semi-active systems combine the best characteristics of both active and passive systems [29]. Different kinds of semi-active systems have been developed for civil structures, such as the friction controllable isolators [30], semi-active tuned mass dampers, semi-active stiffness control devices, and semi-active viscous fluid dampers [7].

2.3.1 Viscous fluid damper

The working mechanism of the semi-active viscous fluid damper is similar to the passive fluid viscous damper, but a closed solenoid valve, which controls the volume of passing flow through the valve, can adjust damping at different levels [31], [7]. This damper is represented schematically in Figure 2-16. This system was introduced by Shinozuka et al. [39] with a two-stage damper [31]. The damping force of this system is written by [31]:

$$F = C(\xi)\dot{u} \tag{2.15}$$

where $C(\xi)$, and $\dot{u}$ denote the damping coefficient and the relative velocity of the piston head, respectively.

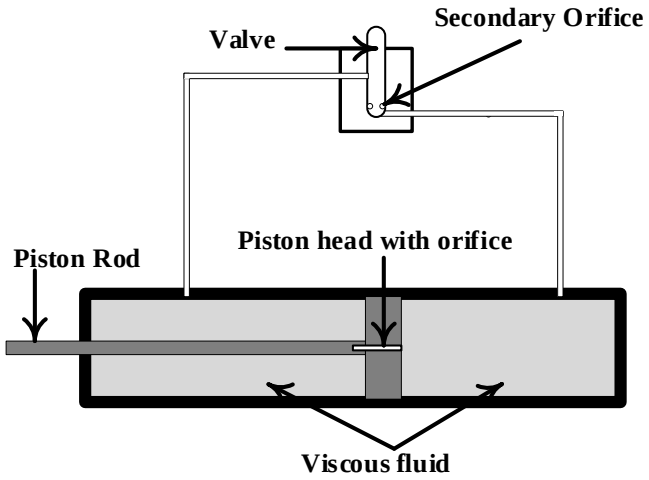

Figure 2-16. Semi-active viscous fluid damper took from [7]**.**

Active systems require the external power to be energized. Basically, these systems need the sensor(s), the controller, and the actuator(s) to apply the proper resistance force. The main advantage of this system is the ability to tune with a wide range of loadings.

2.3.2 SMA-based systems

A smart system is a system with the ability to adapt itself with respect to different loading conditions [32,33]. Smart systems are widely used in many engineering applications, including civil, aerospace, and automotive [34–45]. Smart materials are often the core elements in smart systems/structures. The most common smart materials, which are used in smart systems, include magnetorheological fluid, piezoelectric material, and most recently, Shape Memory Alloy (SMA) [46]. The SMA material refers to a new class of material with the ability to recover its predefined shape after experiencing a large deformation, even up to 14% of its initial length [47]. Although the discovery of SMA goes back to the 1930s [47], the applications of this material have been found interesting in the last few decades [48]. The reasons for the late introduction of SMAs is mainly due to the lack of knowledge in its thermo-mechanical behaviour, the high manufacturing cost, and the low reliability of available SMAs [48]. The recent developments of SMA have led to obtaining an in-depth knowledge of the Austenite-Martensite phase and the Martensite-Austenite phase, decreasing the manufacturing cost, a large number of research works, and thus increasing the reliability of such materials [48]. This can be realized from the huge number of publications in many countries in recent years. Figure 2-17(a) illustrates the number of global publications in the period from 2000 to 2019, which shows a marked increase in the last two decades. While keywords are limited to bridges or buildings and SMAs, the remarkable rise is observed in that period, as presented in Figure 2-17(b). The distribution of publications in bridges and buildings in 10 countries between 2000-2019 is illustrated in Figure 2-18. It is noted that China, the United States, and Canada have the highest number of publications in both kinds of civil infrastructure. The data proves that the SMA and SMA-based applications are very interesting topics for a large research community, particularly in civil infrastructure.

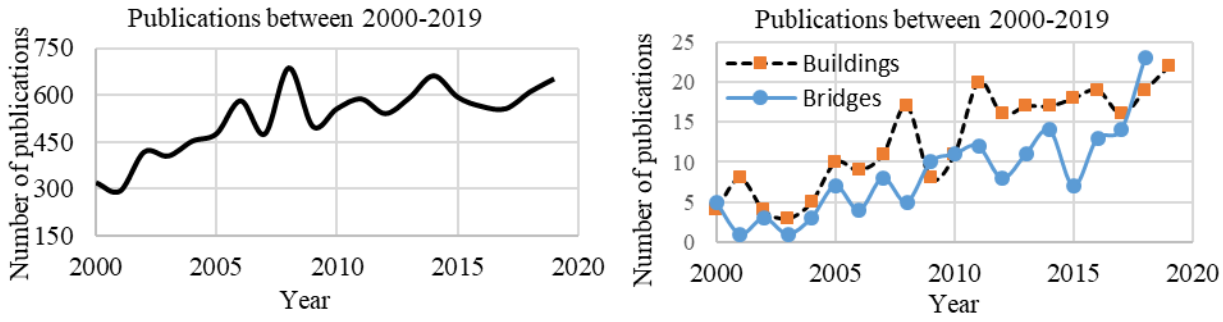

Figure 2-17. Number of publications between 2000-2018 (a) General applications of SMAs (b) SMA applications in bridge and building Source: the engineering village®

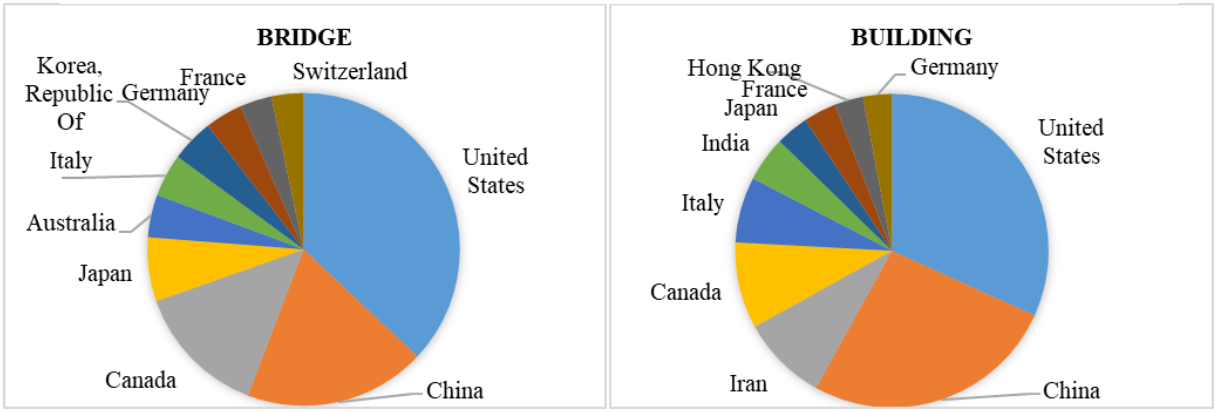

Figure 2-18. Distributions of published papers in SMAs among ten countries between 1990-2018 (a) in buildings (b) in bridges Source: the engineering village®

2.3.2.1 Characteristics of SMA

SMA has distinct thermomechanical properties. When subjected to large plastic strain, it can recover its original shape by applying heat, which is termed as the shape memory effect (SME). Applying heat internally or externally increases the temperature above its phase transformation and causes SMA to recover its initial shape [1]. Another important characteristic of SMA is its superelasticity (SE), which is the capability to recover its original shape from nonlinear strain instantaneously upon load/stress removal [49].

The change in crystal microstructures of SMA is mainly responsible for the SME and the SE. In order to change the crystal structure, the Gibbs free energy should be changed by applying mechanical loading and/or temperature gradient. On the other hand, the temperature and loading have the same effect of changing the crystal phase [50],[51]. It is worth knowing that SMA has three crystal structures, including; twinned Martensite (TM), detwinned Martensite (DM), and Austenite (A) [52]. As presented in Figure 2-19, there are six possible microstructure transformations with respect to the stress and temperature history. Switching procedures from one phase to another phase are given as follows [53]:

The SMA behaviour in the macro-structure level, under the thermal and/or mechanical loading or unloading, is classified into two phases: Martensite phase, which is stable at low temperature and is the weaker phase, and the Austenite phase, which is a stronger phase and stable in high temperature. Nitinol(NiTi), as one of the most common SMA types, has a transformation temperature range between -50 to 110 degrees Celsius [54]. In order to find the phase of SMA subjected to a given applied strain, the characteristics of SMA should be defined. Two important parameters are the applied strain and the working temperature, which are used to determine the stress of the SMA and its phase. The relation between temperature-strain-stress is presented in Figure 2-19. In this figure, M_d and M_f are the maximum temperature, which shapes the Martensite phase and the temperature when the Martensite phase transformation is completed, respectively. The Austenite finish temperature (A_f) is the minimum temperature in which SE occurs. A_s denotes the temperature that the Austenite phase begins. The maximum superelastic strain (ε_s) and maximum applied strain (ε_{max}). The term ε_{max}indicates the maximum reversible strain of SMA, and SMA can recover its strain status after unloading fully. In Figure 2-19, the Young modulus in the Austenite phase and the Martensite phase are denoted as E_A andE_M, respectively.

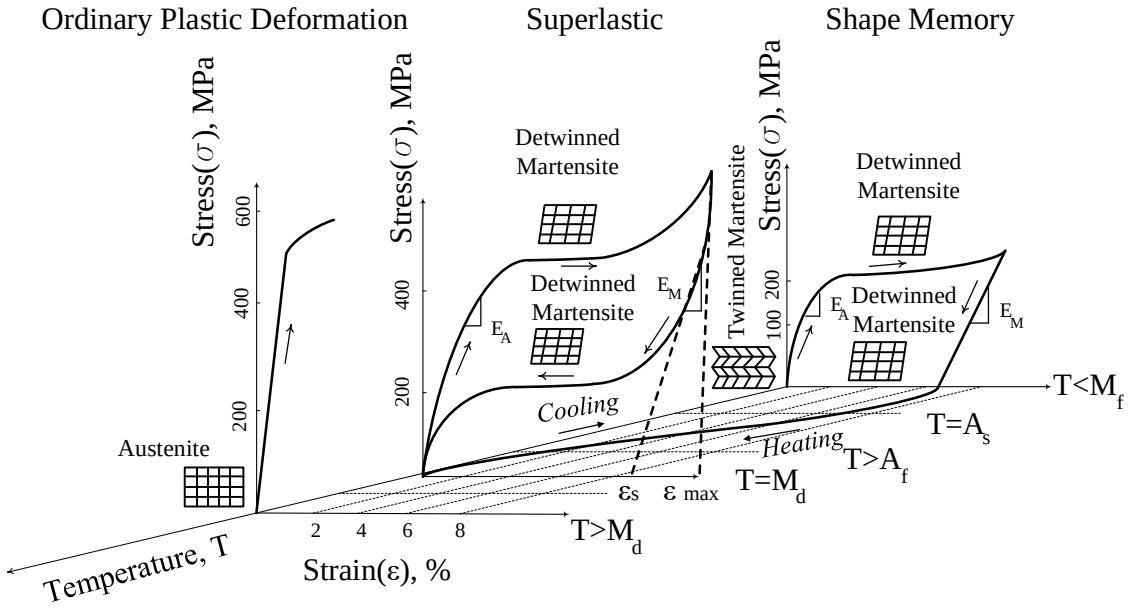

Figure 2-19. The schematic stress-strain-temperature diagram of SMA adapted from [49],[55]

Table 2-1 provides the list of various SMA materials available in the market, exhibiting a wide range of mechanical properties that could lead to different applications. For instance, the maximum and minimum of ε_{max} are 3.1% in $NiTi_{50}$ and 15.0% in FeNiCoAlTaB. E_A also varies from 14.3 GPa in $NiTi_{25}Cu_{25}$ to 117.8 GPa in $NiTi_{50}$. A_f also varies between -62.0^{o}C in FeNiCoAlTaB to 77.8^{o}C in $NiTi_{50}$. These wide ranges of mechanical and thermal properties highlight the usability of such material in many civil related applications.

Table 2-1. Mechanical properties of SMAs

Alloy	$\varepsilon_{max}(\%)$	$\varepsilon_s(\%)$	$E_A(MPa)$	$(A_f°C)$	Reference
$NiTi_{49.1}$	5	3.6	40.4	44.6	[56]
$NiTi_{49.5}$	5.7	4.6	45.3	53.0	[56]
$NiTi_{50}$	3.1	2.2	117.8	77.8	[56]
NiTi	8.2	6.8	30.0	42.9	[57]
$NiTi_{45}$	6.8	6.0	62.5	-10.0	[58]
$NiTi_{44.1}$	6.5	5.5	39.7	0	[58]
$NiTi_{40}Cu_{10}$	4.1	3.4	72.0	66.6	[56]
$NiTi_{41}Cu_{10}$	4.1	3.1	91.5	50.0	[56]
$NiTi_{41.5}Cu_{10}$	3.4	2.8	87.0	60.0	[56]
$NiTi_{25}Cu_{25}$	10.0	2.5	14.3	73	[59]
CuAlBe	3.0	2.4	32.0	-65	[60]
FeMnAlNi	6.1	5.5	98.4	<-50	[61]
FeNiCoAlTaB	15.0	13.5	46.9	-62.0	[62]

2.3.2.2 Damping properties and energy dissipation capacity

Due to the SE and SME phenomena, SMA materials can absorb the induced energy of the external load during the loading-unloading procedure. Figure 2-20(a) shows one complete cycle of loading-unloading for an SMA considering the superelasticity when ($T > A_f$) [50]. Similarly, Figure 2-20(b) shows the same cycle when considering SME. It is noted that SME is given when ($T < M_f$). The shaded areas in Figure 2-20 (inside the loop) indicate the amount of energy dissipation capacity and equivalent viscous damping coefficient [50].

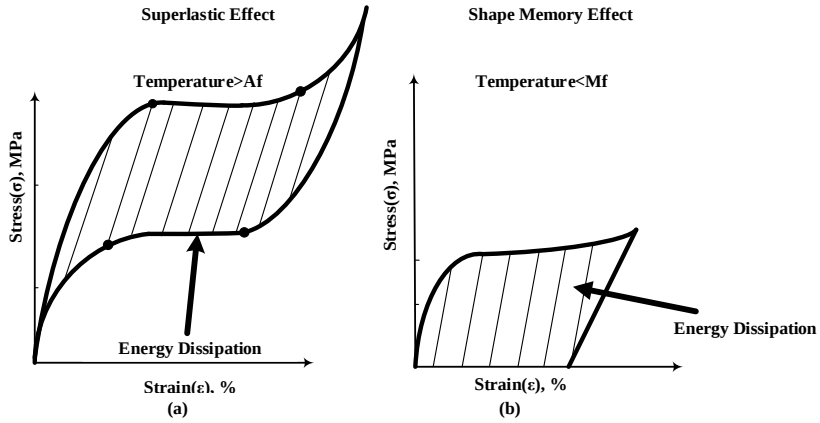

Figure 2-20. The energy dissipation capacity in a complete cycle (a) in the superelasticity (b) in the shape memory effect [50]

The equivalent viscous damping coefficient can be computed by [63]:

$$\xi = \frac{A_h}{2\pi D_m F_m} \tag{2.16}$$

where A_h, D_m, and F_m represent the energy dissipation capacity, the maximum displacement, and the maximum force in one complete cycle, respectively.

2.3.2.3 Protective systems in civil engineering

The energy dissipation and damping capacity, i.e. the SE and the SME of SMA materials, are the keys to develop various devices and components for many engineering applications, such as aerospace, biomedical, automotive, etc. [32],[64]. However, this study is focused on the applications of SMA in civil infrastructures, including steel, concrete, and timber structures, as shown in Figure 2-21 [37,65–68]. In fact, these applications cover a wide range of topics, mainly in the structural control systems, regardless of the system type [50]. It should be noted that different types of SMA-based control systems have not been well explored in research communities [69].

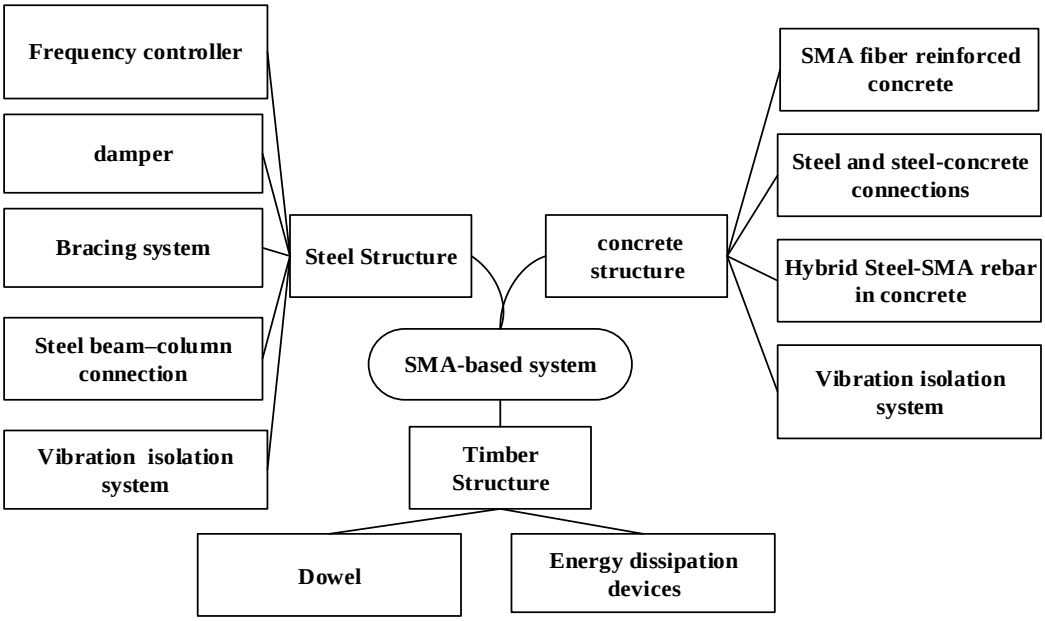

Figure 2-21. SMA-based systems in civil engineering applications

Steel Structures

Steel is a common material to construct the modern civil infrastructure where its flexibility and ductility have made it an ideal contender in the construction industry [70–73]. In order to protect these structures from failure, different techniques such as passive, active, and semi-active systems with conventional materials have been proposed. The following subsections outline the available systems highlight the general features of each one.

Frequency controller

The tuning of the fundamental frequency of civil infrastructure is one of the practical techniques to improve the vibration response of the structure. One of the SMA-based application is to change that frequency [74].

Figure 2-22(a) shows the schematic design of this system installed in buildings. The system is a semi-active control, and it is used to control the structure by applying an electric current. As shown in Table 2-2, the SMA-based system with frequency controllers provides a sharp increase in the natural frequency of the system.

Damper

The SMA-based dampers are widely used in bridges and buildings to upgrade the structural behaviour [50,75–78]. Figure 2-22(a), Figure 2-22(b), and Figure 2-23(a) show the application of SMA-based dampers in buildings and bridges schematically. The detail of an SMA-damper is presented in Figure 2-23(b). The outputs of the system are summarized and presented in Table 2-2. It is observed that SMA-based dampers suppress the vibration response and reduce the relative hinge displacements in the structure. It is evident that damping systems are the most common SMA-based systems in the civil engineering applications to protect the structure against the external excitations.

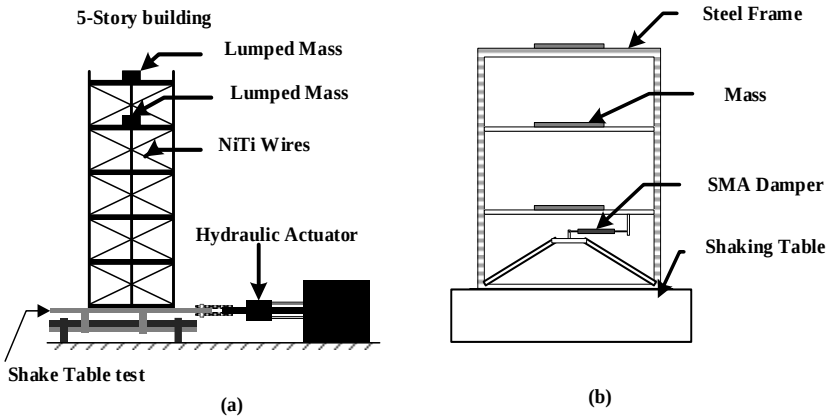

Figure 2-22. (a) The schematic diagram of the frequency controller by SMA wires [74]**, (b) The steel frame with SMA damper** [53]

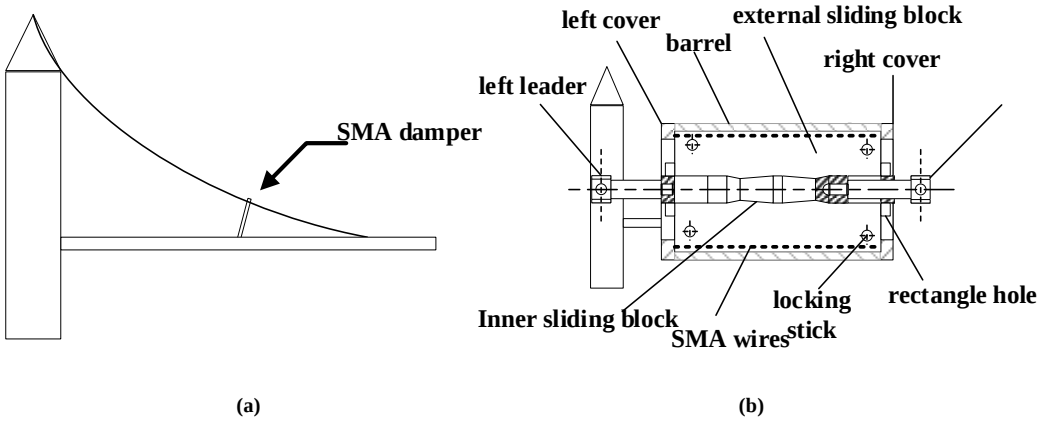

Figure 2-23. (a) The schematic diagram of the stay cable with bridge adopted from [50]**, (b) The schematic diagram of SMA-based damper** [50]

Bracing system

The main role of a bracing system in building structures is to resist lateral loads, such as wind or earthquake loads, and thus help dissipate energy during horizontal movement of the building [73]. The bracing systems can be implemented in a building in different configurations, such as X-type, diagonal-type, V-type, and inverted V-type. The SMA-based bracing system will not only serve the purpose of regular bracing but also it can help self-center the structure. Several researchers have proposed SMA-based self-centering buckling free bracing [67,79–87]. Figure 2-24 presents the SMA-based bracings, which are used to replace the conventional bracings and to study the self-centering behaviour of such systems. Many efforts have been made to design and develop different types of SMA-based bracing systems. Figure 2-25 shows the novel bracing systems used in different civil infrastructure. The structural enhancement by implementing SMA-based systems is presented briefly in Table 2-2 as well. As noted, the SMA-based bracing systems increase the energy absorption and the re-centering capability, reduce the inter-story drift, the roof displacement, and the accelerations of structures and bridges.

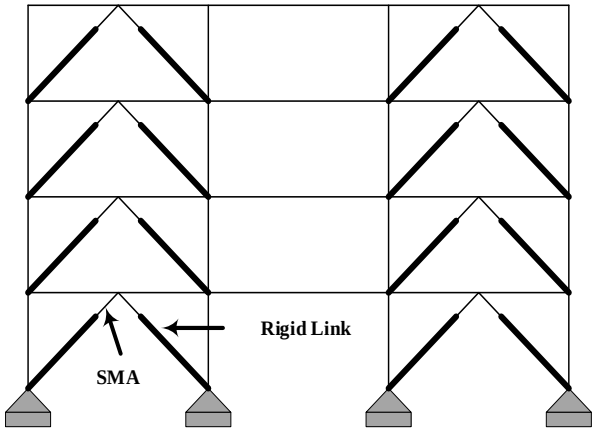

Figure 2-24. Inverted-V SMA based implemented into the 4-story steel frame [81]

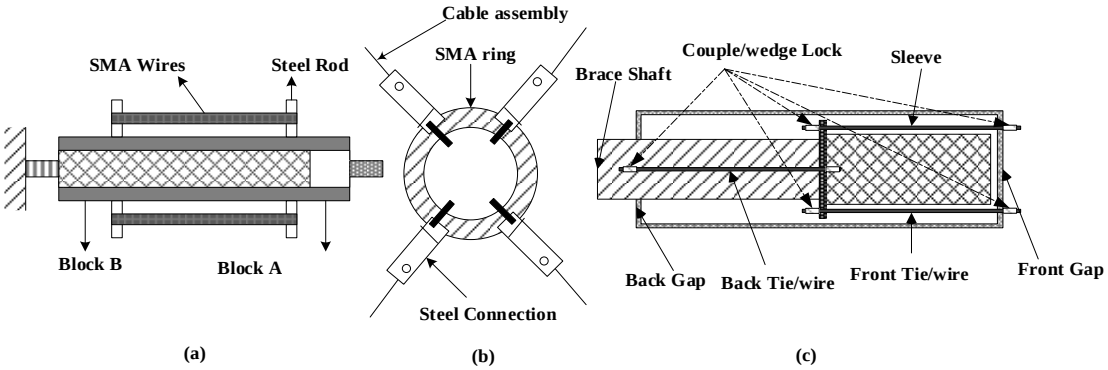

Figure 2-25. (a) Typical diagram of steel braced frames with SMA [88]**, (b) The SMA-based ring bracing system adapted from** [82]**, (c) The schematic diagram of the piston-based self-centering bracing system adapted from** [89]

Steel beam-column connections

The 1995 Kobe and 1994 Northridge earthquakes revealed the importance of the unexpected damage zones in steel moment-resisting frames (MRFs) [90]. One of the common weaknesses in the beam-to-column connections was the brittle failure, which occurred due to the poor welding material, the connection design, and details at that time [90,91]. In addition, studies show that deformation and damages become permanent in MRFs under severe earthquake loads [90]. Consequently, MRFs cannot recover the initial shape after and during strong seismic events [90].

Thus, many researchers proposed the utilization of SMA-based elements into the plastic hinge region of steel beam-column connections [90,92–96]. Figure 2-26 portrays a schematic diagram of these connections [90,97,98]. Figure 2-26(a) presents the configurations of the SMA plates to fasten the steel beam to the column. Figure 2-26(b) and Figure 2-26(c) show SMA-tendons to secure the steel beam to the column or vice versa. As can be seen in Table 2-2, using SMA-tendons improves the energy dissipation capacity and the ductility of the structure. Moreover, the system can remove permanent deformation and prevent local buckling.

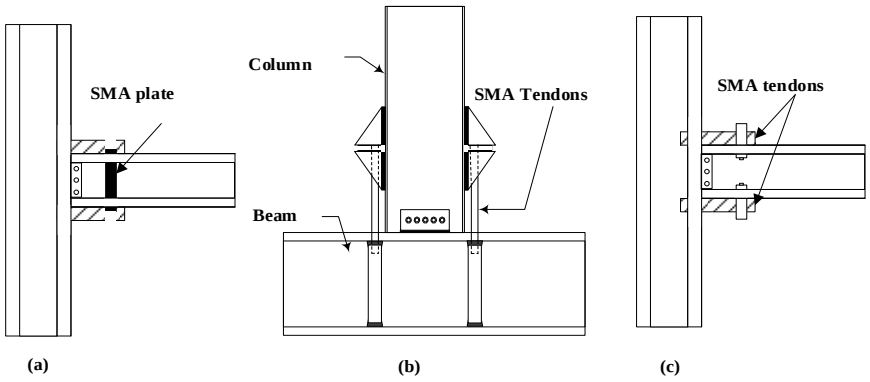

Figure 2-26. (a) A proposed configuration of added SMA plates to steel-beam connections adapted from [90]**, (b) The steel beam-column connection with SMA tendon adapted from** [98]**, (c) SMA tendons adapted from** [97]

Vibration isolation systems

The vibration isolation system is one of the most efficient protective systems in civil structures [70]. As presented in Figure 2-27, these systems are categorized into Sliding Bearings, Fiber-Reinforced Elastomeric Isolators (FREI), and Steel-Reinforced Elastomeric Isolators (SREI). The vibration isolation system in civil infrastructure is composed of three sub-systems, namely, isolators, substructure, and superstructure or main structure [65,99–106], as displayed in Figure

2-28(a). The uncoupled isolators are located between the superstructure and substructure (foundation). In this case, the main structure moves relative to the foundation to prevent seismic hazards by providing variable stiffness. The system makes the structure very stiff for weak earthquakes and very flexible for powerful ones; thus, it minimizes the transferred energy from the earthquake loads to the superstructure [65]. This system acts as a filter between the superstructure and seismic loads to preserve the main structure from seismic hazards [107]. In order to improve the energy dissipation capacity of the isolation system, the SMA, which has the variable stiffness, is the ideal candidate [65]. For example, Lead Rubber Bearings (LRBs), as SREI, are integrated with SMA-bars to enhance the structural dynamic behaviour of conventional LRBs. Figure 2-28 (b) and Figure 2-28 (c) show the two samples of LRBs with SMA [108–110].

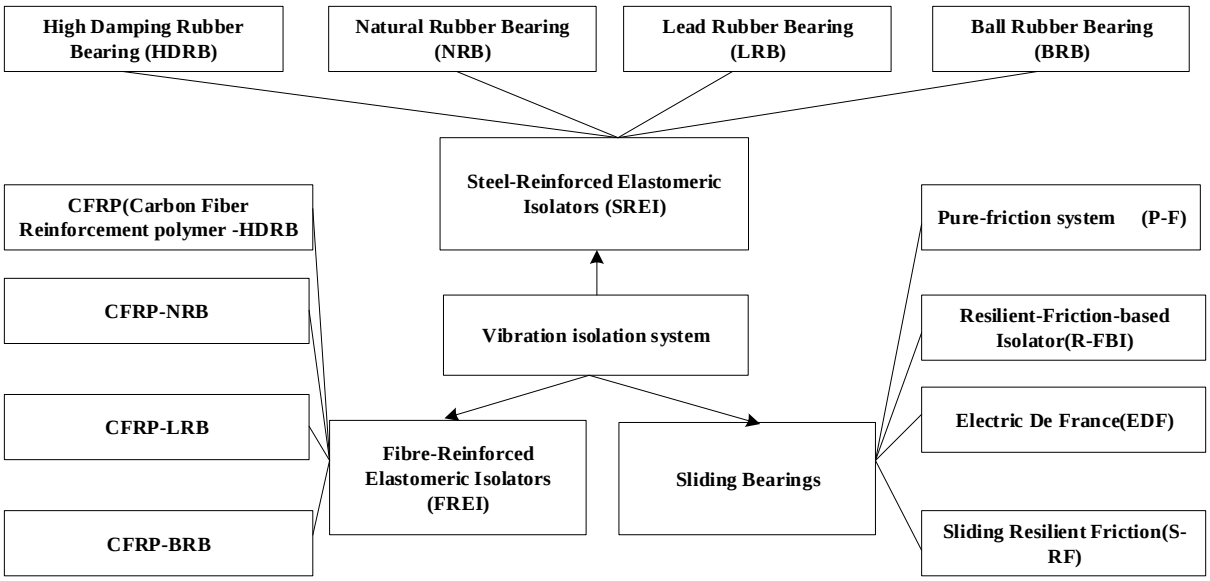

Figure 2-27. The different types of vibration isolation systems taken from [5]

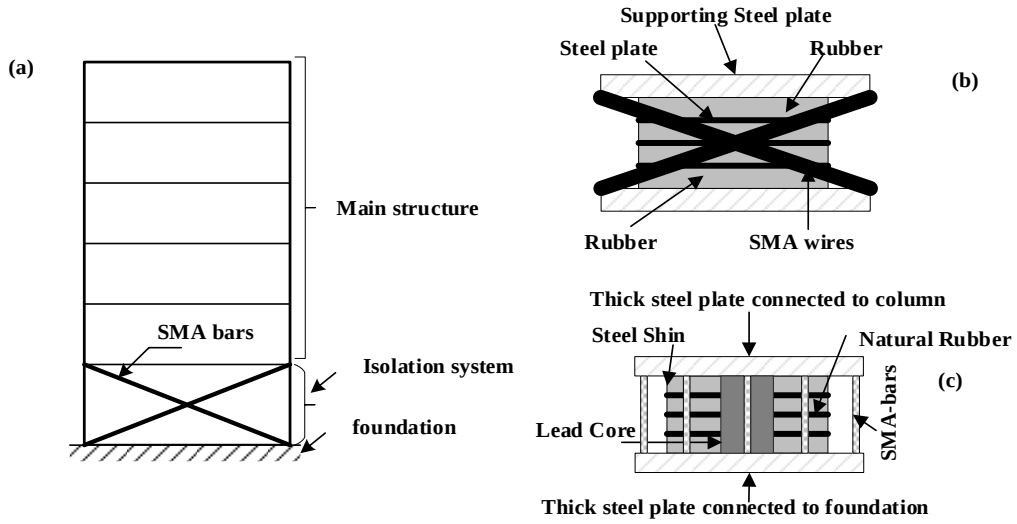

Figure 2-28. (a) The schematic diagram of the vibration isolation system with SMA bars adopted from [1], **(b) The LRB with SMA restrainers adopted from** [19]**, (c) LRB models with SMA bending bars** [70]

The summary of SMAs applications in isolation systems is presented in Table 2-2. As observed in Table 2-2, such systems enhance the different structural parameters. The most desired outputs are improving in the energy dissipation and the re-centering ability, and reduction in the residual displacement.

The different concepts of SMA-based applications in the steel structures have been provided briefly in Table 2-2. It is observed that the SMA-based bracing and the isolation systems are the most common systems in steel structures buildings with more than one story.

Figure 2-29 and Figure 2-30 provide a summary of SMA-based applications in steel structures. The summary is classified as methods and outputs based on the discussed systems. Among the existing methods, the numerical method is the most common approach. The simplicity and relatively low-cost, contrast to other methods, are the main possible reasons to develop SMA-based applications in steel structures. The summary also displays that SMA-based systems using the SE are more applicable than the SME. It may be linked to the simplicity of use since no need

for an external heat source to activate the SE. The effect of SMA-based systems on steel structures' behaviour is also summarized, considering many parameters. Based on the information provided in Table 2-2, it is clearly noted that many forms of displacement, like the inter-story drift and the maximum inter-story drift ration, are the most outputs of different SMA-based applications in steel structures.

Table 2-2. The summary of SMA applications in steel structures

System	Action	Outputs	Referenc
Frequency	Semi-active system with SMA wires in a 5-story	Increases the natural frequency by about 32%	[74]
Damper	SMA-based damper in a stay cable bridge	Suppresses the vibration response, performance	[111]
	SMA restrainer in simply supported bridges	Reduces the relative hinge displacements	[112]
	SMA damper in a stay-cable bridge	Comparable vibration response with SMA	[113]
Bracing	Shape memory alloy based bracing in 6-story steel	Decreases the drift ratio, the peak floor	[88]
system	SMA –based bracing in a 6-story modular steel	Reduces the maximum residual inter storey drift	[80]
	braced frame	up to 98%	
	NiTi bracing system in 4 combinations in a 4-story	Lessens the maximum inter-storey drift and	[81]
	Diagonal SMA-based bracing system in a 4-story	Reduces roof displacement demand	[87,114]
	Pre-strained x-shaped SMA bracing system in 1-	Reduces displacement demand	[67]
	Shape memory alloy friction damper in a 3-story	Improve the interstory drifts, the story	[115]
Steel	SMA tendons (in the Maternsite phase) in the	Provides good energy dissipation capacity and	[97], [98]
beam–	Confined SMA plates in the plastic-hinge region	Mitigate the permanent deformations and	[90]
column	Seismic isolation device with SMA	Increases energy dissipation capacity and the re-	[116]
Vibration	Two seismic isolation devices with SMA in a small	Provides flexibility and supplies good control of	[117]
	SMA supplemented the rubber bearing in a 3-story	Decreases the residual displacement and more	[108]
	Natural Rubber Bearing (NRB) and high damping	The NRB enhances the seismic behaviour greater	[118]
	SMA bending bars into the lead-plug rubber	Reduces residual displacement	[107]

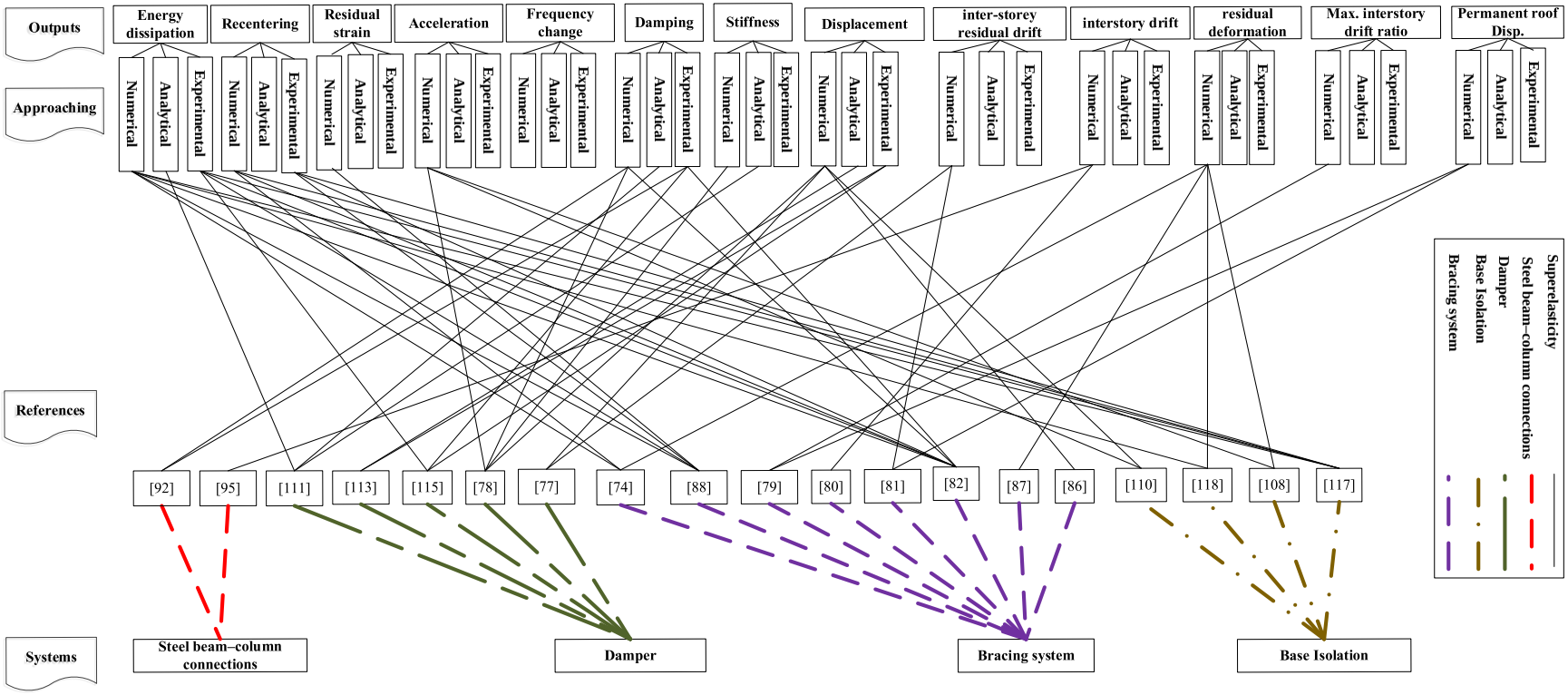

Figure 2-29. The summary of the superelastic SMA-based in applications in steel structures

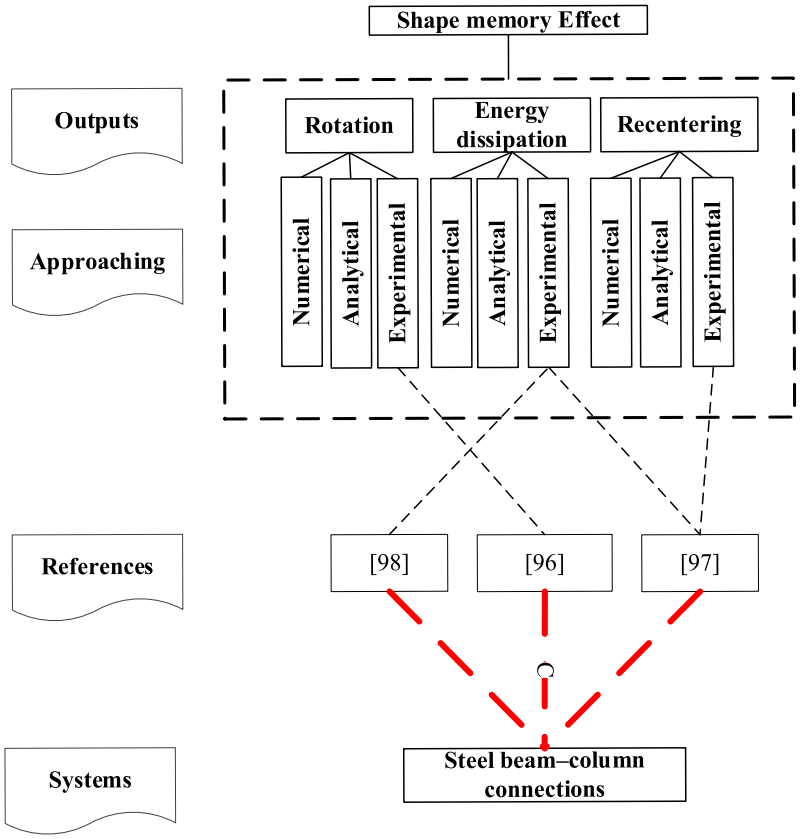

Figure 2-30. The summary of the shape memory effect of SMA-based applications in steel structures

Concrete Structures

Concrete is widely used to construct modern civil infrastructures, such as buildings and bridges. In order to mitigate the seismic hazards, prevent and control the occurrence of damage in concrete, SMA bars and wires have been embedded into the concrete [41,44,119–129], as shown in Figure 2-31. To enhance the stability and performance of concrete structures, many studies have been conducted to investigate the effects of implementing SMA in concrete structures. The applications of SMA-based systems in concrete include SMA fiber reinforced concrete, hybrid steel-SMA rebar in concrete, steel-concrete connections, and isolation systems.

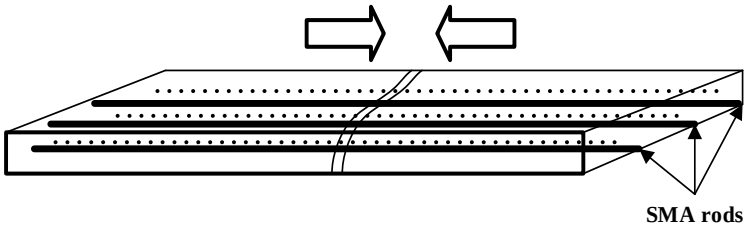

Figure 2-31. The conceptual diagram of concrete with SMA rods adapted from [50]

SMA fiber reinforced concrete

Embedding of SMA strips (bars) into the fiber reinforced concrete is one of the applications of SMA in concrete structures [41,130]. Figure 2-32 depicts the typical diagram of this application. The SMA-reinforced concrete can absorb more energy, reduce the residual drift, and recover the applied stress over the conventional reinforced concrete (RC). In pre-stressed concrete, near-surface mounted (NSM) fiber-reinforced polymers may be replaced with SMA bars in which the need for pre-stressing tools such as mechanical jacks and anchor heads is avoided. This method reduces the crack propagation, stress in the rebar steel and improves the fatigue resistance of the concrete [131,132]. Furthermore, the prestressed SMA increases the crack load and reduces displacement compared to the SMA behaviour in the unstressed condition [131].

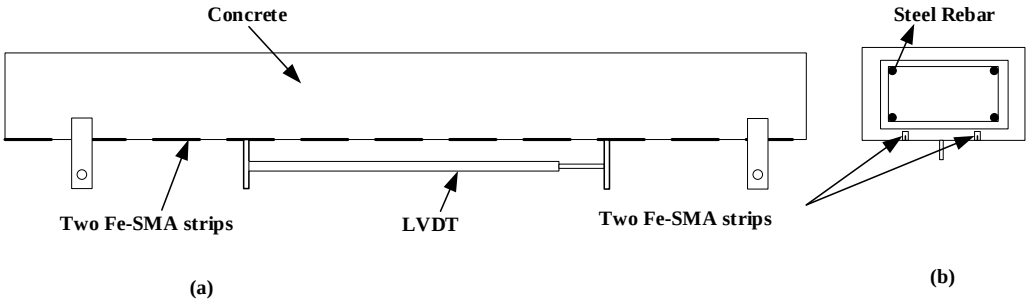

Figure 2-32. The conceptual diagram of concrete with SMA rods adapted from [50]

Steel and steel-concrete connections

In order to give the self-centering ability to the steel connections and steel-concrete (composite) connections, SMA bolts are used to secure the steel beam to the steel column and steel beam/column to concrete slabs connections, as shown in Figure 2-33. In comparison with the conventional steel connections and composite connections, SMA bolts provide higher capacity in terms of energy absorption and equivalent viscous damping [39,133–135].

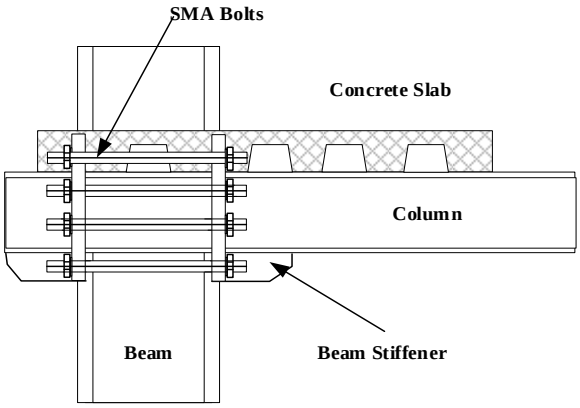

Figure 2-33. The schematic diagram of SMA bolts between the steel to steel elements and steel elements to the concrete slab adapted from [133]

Hybrid Steel-SMA or Fiber-Reinforced Polymer (FRP) -SMA rebar in concrete

A combination of SMA bars and conventional steel bars is a suitable method to increase the capacity of the structure in absorbing energy and, in turn, increasing the lifetime of RC structures [136,137]. The typical diagrams of the hybrid Steel-SMA rebar in concrete are presented in Figure 2-34. In addition, SMA rebar enhances the resistance of structures to corrosion and fatigue [138]. Studies also prove that the structure with hybrid rebar provides significant fire resistance in RC structures [138],[139].

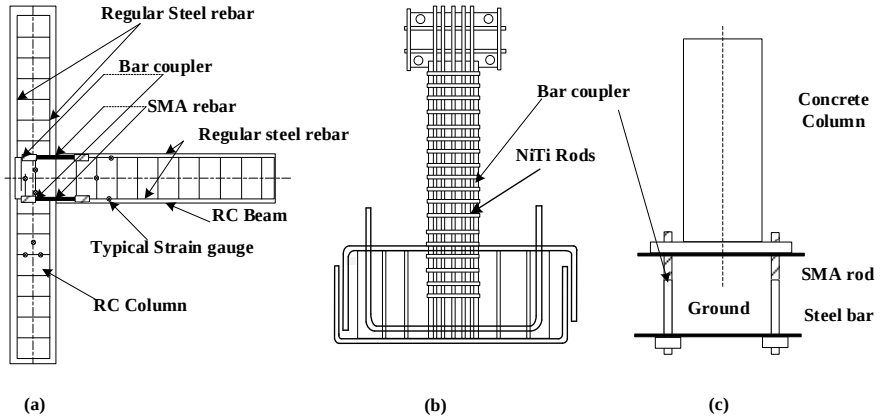

Figure 2-34. The schematic diagrams of the steel-SMA rebar in concrete structures [50,138,140]

Isolation devices

Figure 2-35 shows an SMA isolator system that is integrated into highway bridges [107,109,110,141] to increase the damping and the energy dissipation of the base structure. Such a system provides varying benefits for the main structure, such as controlling the displacement and dissipating the energy of the lateral loads more efficiently [109].

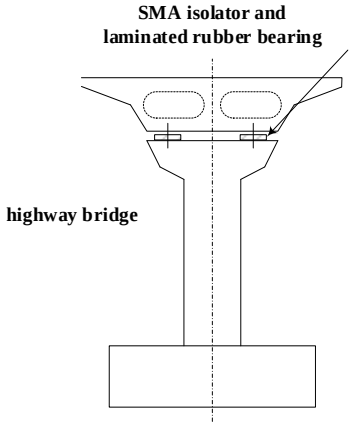

Figure 2-35. Isolator in the highway bridge adapted from [109]

Table 2-3 illustrates the summary of the SMA-based applications in different kinds of concrete structures. It is observed that SMA-based systems provide several functions, including controlling the crack propagation and damage in structures, enhancement in the structural response, preventing damage in the structure, and controlling the vibration. To illustrate the significance of SMA materials in civil structures, several structural parameters, including the energy dissipation capacity, the self-centering, the interstory drift, the flexural capacity, and the damping capacity, must be determined.

Figure 2-36 and Figure 2-37 portrays a brief of SMA-based application in concrete structures. It is categorized based on the methods and outputs for each investigated system. It is clear that the SE is remarkably more common than the SME due to the simplicity in use and no need for any external heat source.

Table 2-3.The summary of SMA-based applications in concrete structure

Goal	Action	Result	Reference
Control Crack propagation	Continuous SMA wires (martensite form) in RC beams	Recovered cracks upon heating	[122]
Enhance structural response	SMA rebar in the plastic hinge region of RC bridge piers	Reduced permanent drift and seismic damages	[109, 112]
	SMA bars in the plastic hinge regions of beams in an 8 story RC	Reduced the inter-story and the top-story residual drifts	[143]
	SMA tension brace in retrofitting RC shear walls	Increased lateral strength, energy dissipation capacity, and re-centering ability	[144]
Damage control	Near-surface mounted SMA-bars anchored underneath RC beams	Increased the yielding and ultimate load capacities and the ductility	[128]
	Prestrained SMA spirals to repair the damaged RC columns	Increased the lateral stiffness about 150%	[145]
Prevent damage	SMA fibers implemented in cement mortar	Improved the tensile and bending strength	[146]
	The SMA wires to install in the concrete beam	Improved the flexural capacity sand supply the large recovery force	[147]
Vibration controls	Laminated rubber bearing isolation system with SMA	Remarkable decrease in the displacement and peak acceleration	[110]
	PTFE isolation system with SMA	Decreased the base displacement and the base shear coefficient	[148]

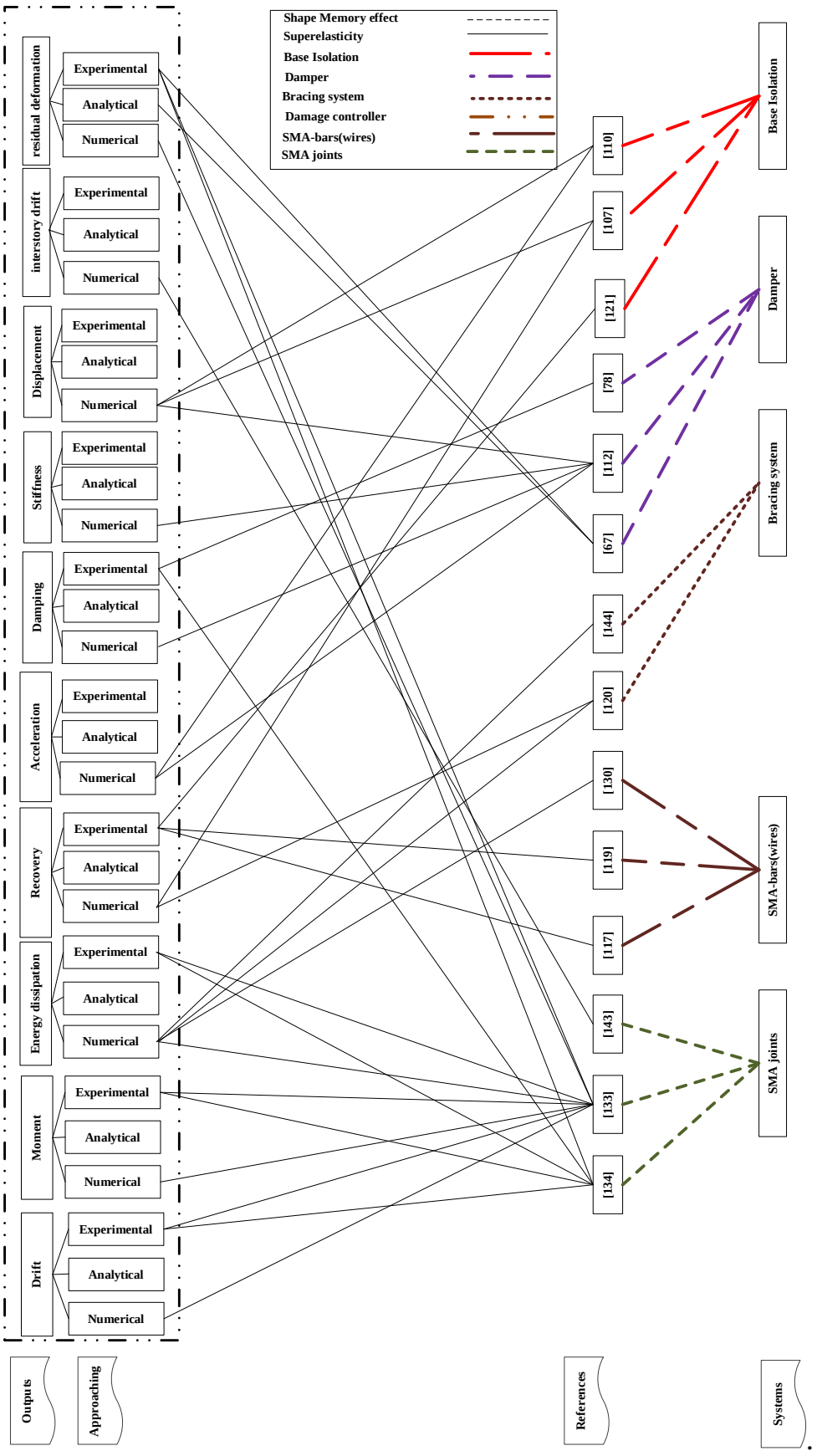

Figure 2-36.The summary of superelastic SMA-based applications in concrete

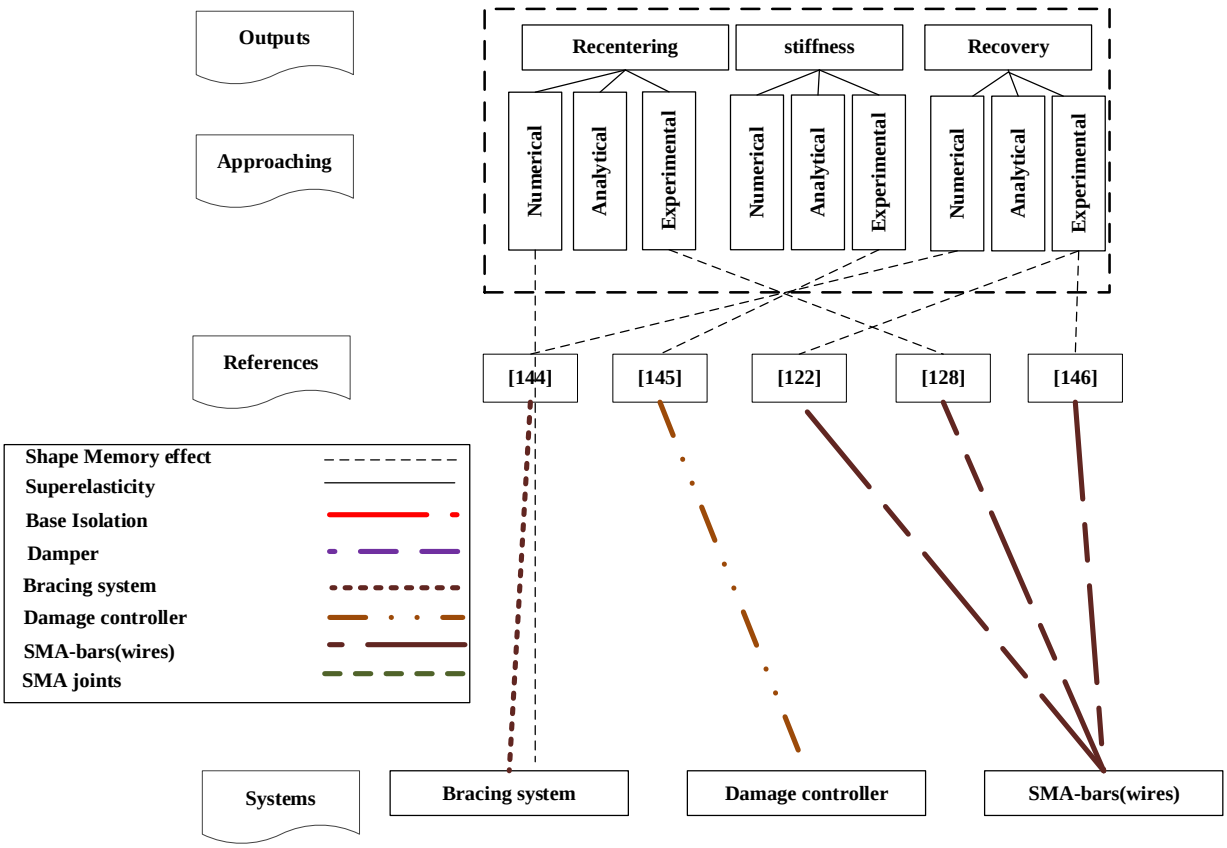

Figure 2-37. The summary of shape memory effect SMA-based applications in concrete structures

Timber Structures

The timber civil infrastructure is very common in North America due to its simplicity in the construction, the low cost, the availability of the raw material, and rapid construction [149–153]. In order to enhance the dynamic behaviour of timber structures, SMA-based systems are utilized and integrated into timber structures [125,154–156]. However, it can be noted that the applications of SMA-based systems in timber and wood structure are not very common.

Recently, few studies have been performed to implement the SMA-bars/wires in timber structures, as shown in Figure 2-38(a), to connect timber walls. Another application, as presented in Figure

2-38(b), is an SMA-based energy dissipater which is embedded in the wood shear wall [157]. The SMA is also used for tuned mass damper (TMD), as displayed in Figure 2-38(c), to reduce the amplitude of vibration response in a timber structure. According to the studies that are conducted on SMA-based systems in timber structures, self-centering, and energy dissipation are the most important aspects of these types of structures. Due to the sensitivity of timber structures to external heat, existing research of the SMA-based system in timber structures is limited to the SE type.

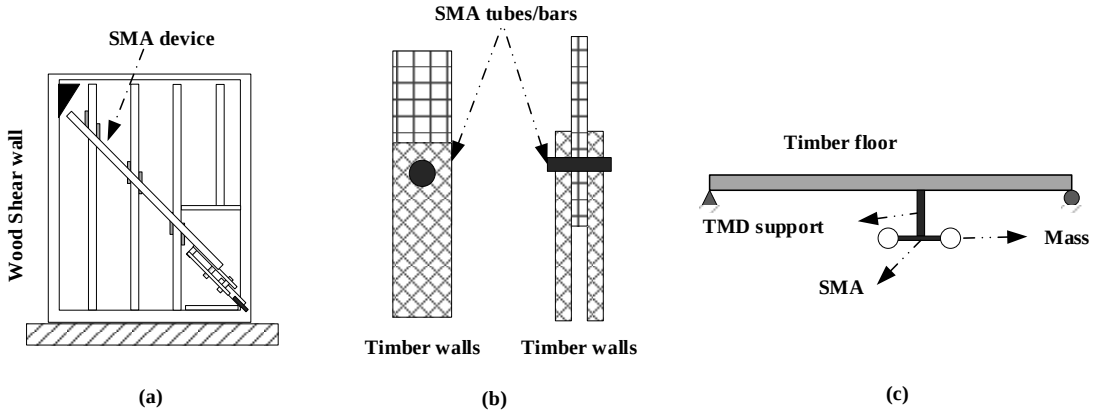

Figure 2-38. (a) SMA device installed in wood shear wall taken from [157]**, (b) SMA tubes/bars in timber walls taken from** [158]**, (c) The tuned mass damper with SMA** [155]

2.3.3 MRF-based semi-active systems

In order to enhance the performance of semi-active systems, magnetorheological fluid (MRF) systems have been used to replace conventional passive systems since they provide fast response, good controllability, and low activation energy.

2.3.3.1 MRF Types

MRF-based systems can be classified into two types, as follows:

Traditional MRF

MRF is a smart fluid with controllable viscosity. It is composed of tiny suspended ferromagnetic particles in a carrier fluid and stabilizers, as displayed in Figure 2-39 [159]. Each component plays

an important role in the MRF's behaviour. Suspended ferromagnetic particles, such as iron, supply variable viscosity. The carrier fluid, typically a synthetic oil, provides the basic viscosity and the media for all components. Stabilizers aim to uphold the smart properties of the MRF by preventing the ferromagnetic particles from settling [160–163].

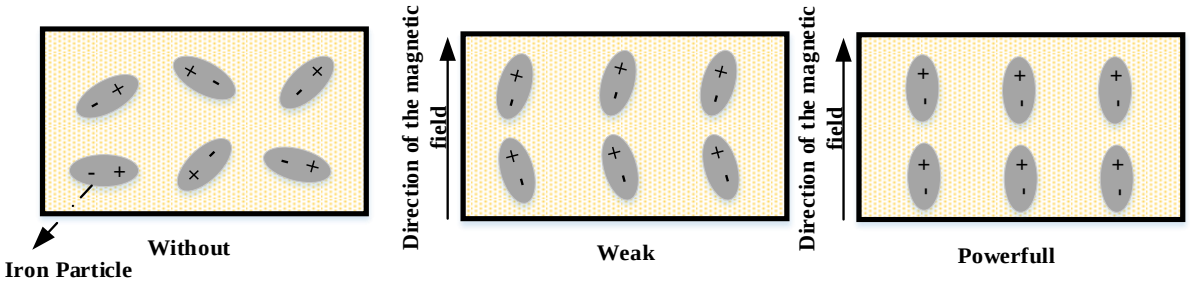

Figure 2-39. The magnetic field on the polarization of MRFs and the effect of magnetic field on MRF [164]

When no magnetic field is applied, an MRF behaves like a Newtonian fluid with the viscosity of its carrier fluid. Once a magnetic field energizes the MRF, the suspended ferromagnetic particles form a chain along the direction of the magnetic field. These chains provide additional shear resistance. Thus, they increase the viscosity of the MRF and turn it into a semi-solid phase that is then a non-Newtonian fluid. When the magnetic field is removed again, the state of the MRF transforms from semi-solid back to liquid, and the viscosity drops to its initial value [165].

When the external shear stress is applied to the semi solid-state, the chain of ferromagnetic particles resists any movement up to shear stress, termed the yield point [8]. After the yield point, the MRF flows like a Newtonian fluid; so, the yield point is a function of the intensity of the applied magnetic field. The maximum achievable yield point is called the saturated yield point.

Shifting between states of MRF occurs very fast (in milliseconds). A graphic figure showing the relationships between applied stress, yield stress, and strain rate is presented in Figure 2-40 [165].

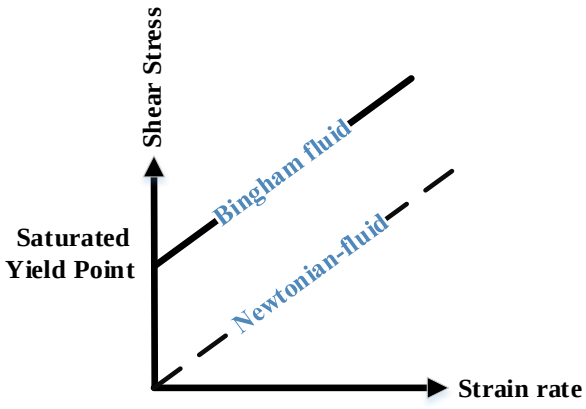

Figure 2-40. The relation between the strain rate and shear stress in the MRF [166]

Due to the unique characteristics of the MRFs and recent developments for the manufacturing of MRFs, MRFs, and MRF-based applications have been attracting the attention of many researchers. It can be noted by the number of published research papers over the last 20 years in many countries. Figure 2-41(a) portrays the number of global publications between 2000-2019, which illustrates - the significant rise of MRF and its applications. As seen in Figure 2-41(b), between 2000-2019, an increase in the number of publications for MRF-based applications in buildings is observed. However, the number of publications almost remains steady for MRF-based systems in bridges in this period. The distribution of publications in ten countries between 2000 -2019 is shown in Figure 2-42(a) for MRFs and their applications and Figure 2-42(b) for MRF-based applications in civil infrastructure. It is noted that the U.S. and China are the pioneer countries in developing and using MRFs in civil infrastructure

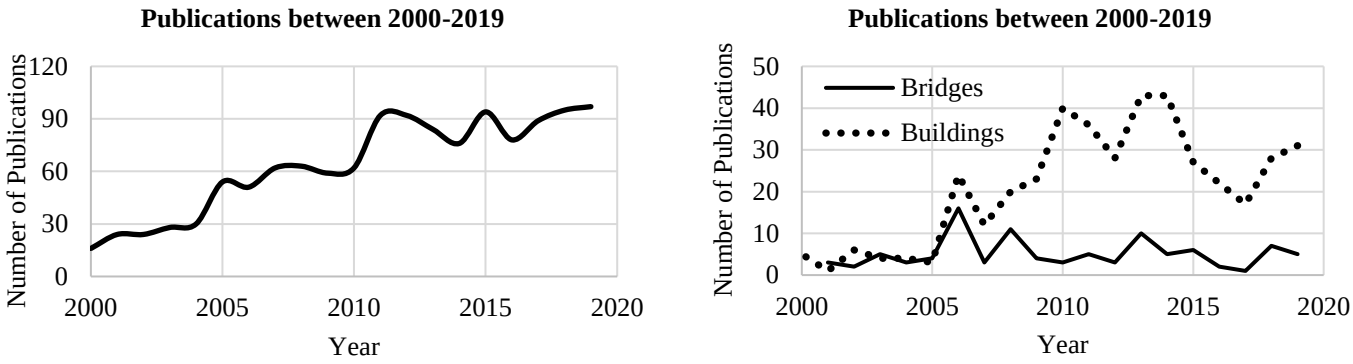

(a) (b)

Figure 2-41. (a) Number of publications between 2000-2019, (a) General applications of MRFs, (b) MRF applications in civil infrastructures Source: the engineering village®

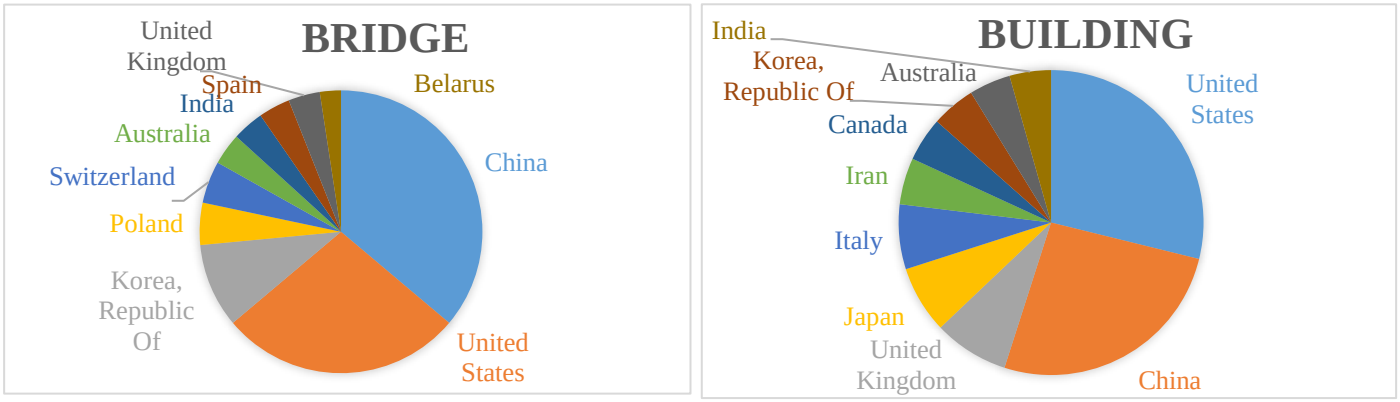

(a) (b)

Figure 2-42. Distributions of published papers in MRFs among ten countries between 2000-2019, (a) in MRFs and their applications, (b) MRF-based applications in civil infrastructures Source: the engineering village®

The effectiveness of MRFs reduces considerably in long-term use. This is mainly due to different densities of the carrier fluid and the suspended ferromagnetic particles, which causes the particles to settle. To reduce this problem, MRF grease (MRG) consisting of "**a base oil, an additive, and a thickener**" [167], was developed as a new matrix for MRF [168,169]. The main advantage of MRG is its long service life while having comparable strength as conventional MRF.

MR elastomers (MRE)

The ferromagnetic particles are combined into a rubber matrix, as a nonmagnetic medium, to make a composites material, which is called an MR elastomer (MRE) [170]. In other words, the fluid in MRFs is altered with rubbers, i.e. natural rubbers, in MREs [171]. Hence, settling down of ferromagnetic particles in MREs is not an issue at all. MREs' mechanical characteristics, like the stiffness in the shear mode, can be changed rapidly under applied magnetic fields [172]. The variable and controllable stiffness of MRE can offer an excellent solution to use in tunable vibration isolation systems [171].

In order to develop tunable vibration isolation systems based on MREs, The MREs are designed and fabricated like laminated rubber bearings vibration isolation systems [172]. However, the steel plate in the conventional laminated vibration isolation systems is replaced with aluminum plates in MRE vibration isolation systems to allow passing the magnetic fields among layers [172].

2.3.3.2 MRF-damping systems in civil infrastructures

Among all types of MRF-based damping systems, MRF dampers and MRF elastomer bearings are most common for structural engineering applications because they are easy to control, and they require little activation energy. Moreover, they are easy to integrate into buildings and bridges since they are compact [173–179]. The enhancement of MRF-based seismic control systems in the dynamic response of civil infrastructures has been examined in many studies [173–175]. For instance, the Keio University building and Tokyo's National Museum of Emerging Science and Innovation (Miraikan) are examples of practical and successful applications of MRF-based damping systems in civil infrastructure [173].

MRF (MRG) dampers

The most common application of MRF in civil engineering is MRF-dampers [174,175,180–186]. Many types of MRF dampers have been developed for improving the dynamic behaviour of civil infrastructure.

MRF dampers are derived from hydraulic dampers, in which MRF or MRG replace conventional working fluids. Magnetic coils are embedded into the piston or installed externally to energize the MRF or MRG when passing through a control valve. The damping force is controlled by adjusting the current through the energizing coils of the MRF damper. Figure 2-44 depicts the force-displacement response of MRF dampers [25]. The de-energized fluid MRF phase behaves like a conventional viscous damper. Energizing and transforming the MRF to the semi-solid phase adds a controllable coulomb damper in order to provide stability in civil infrastructure [187].

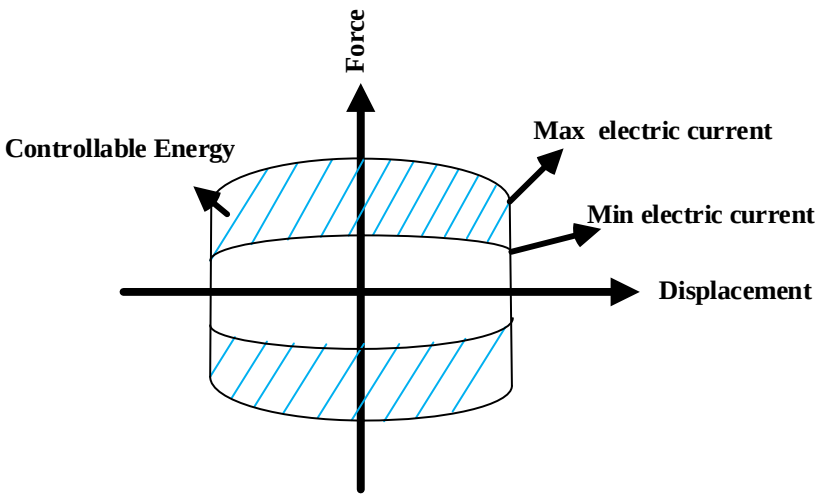

Figure 2-44. The schematic hysteresis diagram of the MRF damper [188]

Figure 2-45-Figure 2-47 show simplified diagrams of the three main types of MRF dampers: the mono-tube MRF damper, the twin-tube MRF damper, and the double-ended MRF damper. Mono-tube dampers are lighter and easiest to fabricate than the other two types, but they are less reliable. Inside of the monotube damper, like a hydraulic cylinder damper, an accumulator as a gas chamber is located to store pressurized gas [189].

In the twin-tube damper, there are two separate cylinders, in which space the outer and inner cylinders are filled by pressurized gas. Hence, the outer cylinder works as an accumulator. In addition, the foot valve is installed in the inner cylinder to control the passing MRF fluid passing through. Recently, the MRG damper shown in Figure 2-48 was introduced to extend the damper's service life [167].

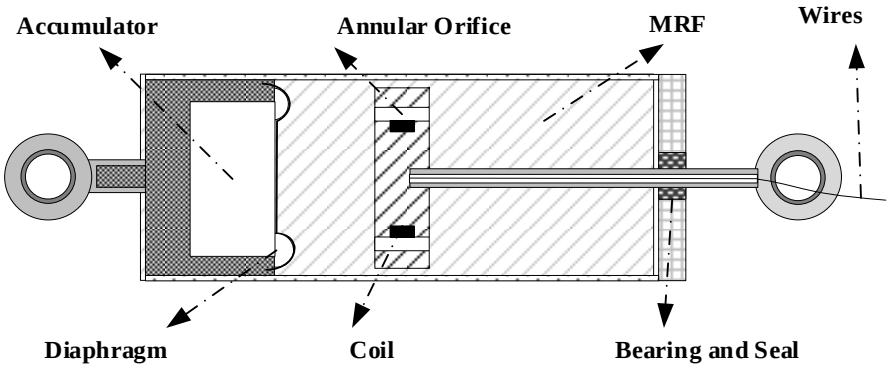

Figure 2-45. Schematic diagram of a mono-tube MRF damper adapted from [189]

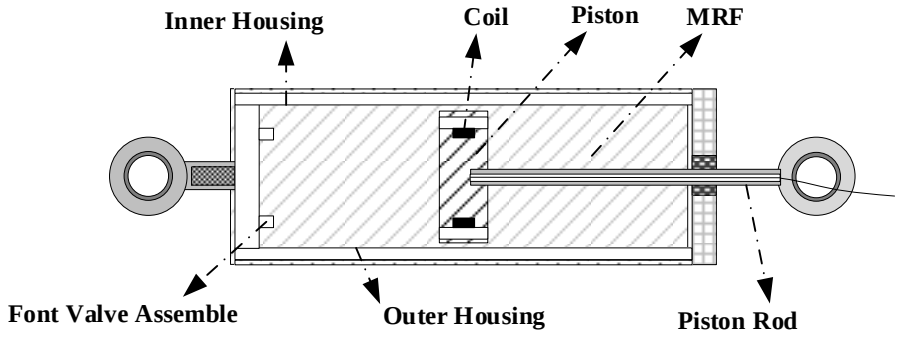

Figure 2-46. Schematic diagram of a twin-tube MRF damper adapted from [189]

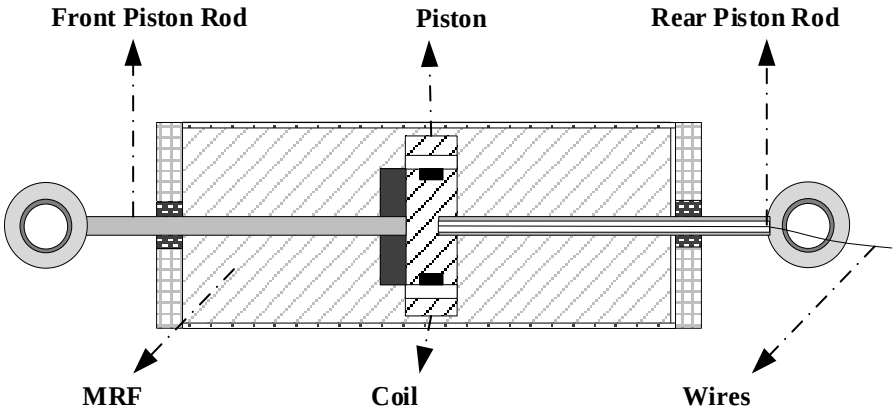

Figure 2-47. Schematic diagram of a double-ended MRF damper adapted from [189]

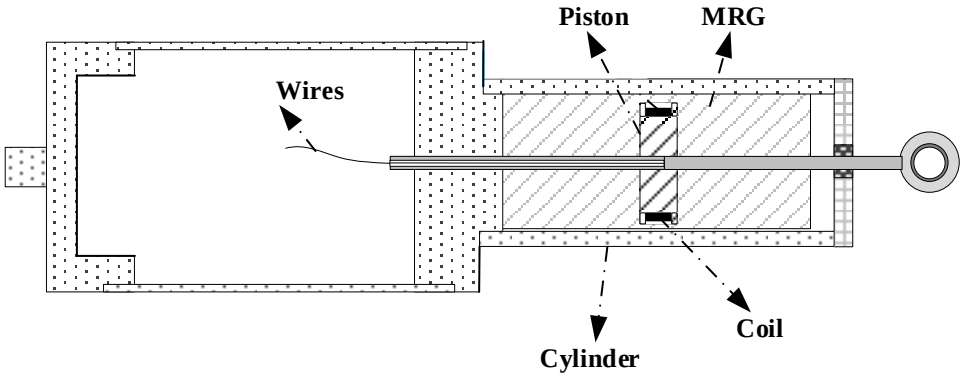

Figure 2-48. Schematic diagram of an MRG damper adapted from [167]

MR elastomer bearings isolation system (MREI))

Conventional vibration isolation systems are designed to minimize the excitation of structural resonant modes of the superstructure during earthquake events. At near-fault locations, this can require large displacements of the bearings supporting the superstructure [173]. Furthermore, the vibration isolation system needs to be carefully designed for the earthquake's magnitude and frequency content. If the earthquake is very different from the design specifications, passive

vibration isolation systems will perform poorly [173]. One solution that allows adapting vibration isolation systems to the type of earthquake encountered is MR elastomer bearings, whose damping characteristics can be adapted to different earthquake characteristics [190–192].

Schematic diagrams of MREI are depicted in Figure 2-49 and Figure 2-50 [193]. They are composed of laminated MREI's layers within steel plates, an electromagnetic coil, and a steel sleeve. These components are secured to the foundation of a structure by a mounting plate. A sliding surface is located at the bottom of the superstructure. There is either a small gap between the laminated structure and the sliding surface, as shown in Figure 2-49, or there are steel balls that fill the gap, as shown in Figure 2-50 [193]. The laminated setup can support large vertical loads. The laminated MRE provides lateral stiffness that can be adjusted with the applied magnetic field to control horizontal displacement. In the absence of a magnetic field, MRE behaves as soft rubber. The variation of stiffness is from 300% softer to 50% stiffer than the rubber carrier [194]. Although MRE dampers have been widely studied for vibration isolation applications in mechanical engineering, their application to civil engineering is relatively new [194]. In order to find the potential applications of MREI in civil infrastructure, many attempts have been made in near-field earthquakes and far-field earthquakes locations [194]. A feasibility study of the MRE isolation system has been performed [194]. It is observed that energizing the system increases the lateral stiffness and the damping force of the MREI up to 37% and 45% than initial values, respectively [194]. Implementing the MREI into the SDOF system shows that the enhancement in stiffness (about 312.67%) and the damping (almost 157.49%) in the SDOF system.

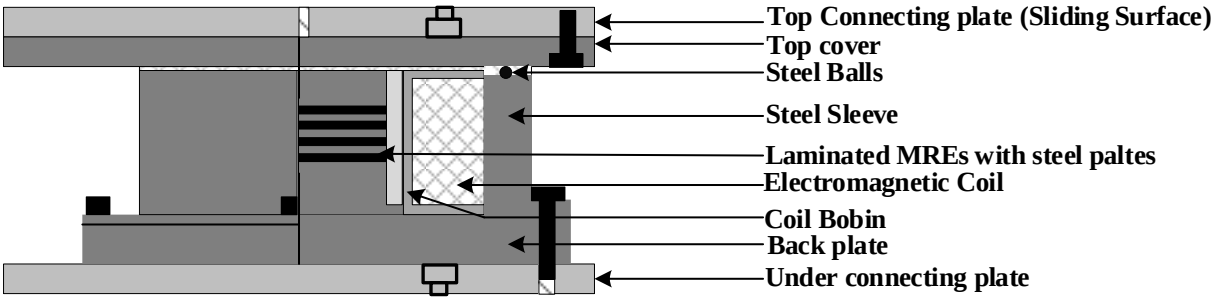

Figure 2-49. Cross-section view of an MRF seismic isolator (MRE) adapted from [195]

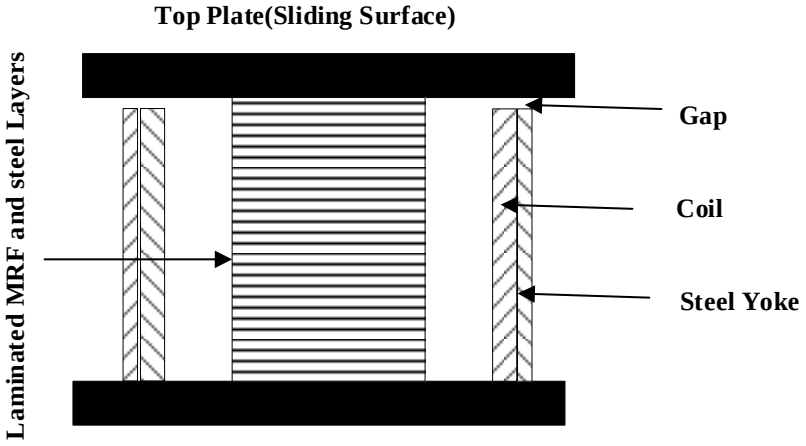

Figure 2-50. The schematic diagram of an MRF seismic isolator (MRE) adapted from [194]

MRF-Tuned Liquid Column Damper (MR-TLCD)

A tuned liquid column damper (TLCD) is a type of TMD in which the mass, the damper, and the spring are replaced with water [8,196], as illustrated in Figure 2-51. TLCDs were originally designed to stabilize ships; however, in the 80s, Sakai et al. [11] proposed implementation for buildings. In TLCD systems, the friction between the fluid and the damper housing, and the turbulent fluid motion are converted to heat, resulting in the dissipation of the main portion of the external excitation energy. Low capital cost, ease of installation, and low maintenance requirements make this an attractive structural vibration control system [12–20,197]. Similar to TMDs, TLCDs can only be tuned to specific excitation frequencies that need not necessarily

overlap with wind and earthquakes loads [198], [199]. The energy dissipation in TLCDs is a function of the liquid through an orifice, and the damping of these systems depends on the velocity of excitations and the "head-loss coefficient" [198]. Thus, the functionality of the system is limited to the specific frequencies and is not controllable. However, natural loadings, such as winds and seismic, have random frequency content [198]. Hence, it is in high demand to develop TLCDs with controllable damping and energy dissipation capacity [198]. One possible solution is replacing the working fluid of a TLCD with MRF (MR-TLCD) [198,200,201], to adjust the damping and the energy dissipation absorption in TLCDs. To tune the damping coefficient, the magnetic field and volume fraction of iron particles in the MR-TLCD can be varied [202]. A schematic diagram of an MR-TLCD is illustrated in Figure 2-51.

It is worth mentioning that the natural frequency and equivalent damping differs from conventional TLCDs [203]. Furthermore, MR-TLCD increases the viscosity of the fluid [199,202]. Moreover, the damping effect of MRF in this system is higher than the resonance of the structure [198,200].

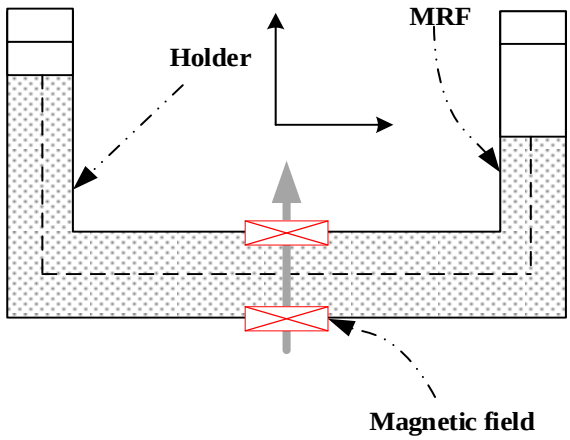

Figure 2-51. Schematic diagram of an MRF tuned liquid column damper [198]

2.3.3.3 The application of MRF damping systems in Buildings

The controllability and stability of MRF-based damping systems open new horizons in structural control systems to improve the dynamic behaviour of buildings [204–206]. The main challenge for introducing MRF-based damping systems is determining the most effective locations for the MRF damping systems in buildings, particularly in high rise buildings [207]. Due to the working principle of MRF based systems, they are best suited in locations of high relative displacements. In general, they can be incorporated into the foundation or the superstructure.

The application of MRF dampers to foundations

Building foundations transfer the ground motions to the building's superstructure. Since there is considerable relative displacement in the bearings between the main structure and the foundation, it is an excellent location for MRF damping systems. They are either added to existing vibration isolation systems, or they can also be added as new structural control systems. Both MRF and MRE dampers are employed in foundations.

MRE isolation systems

MRE isolation systems help to decouple buildings from the source of vibration [173,208,209] [200], [178,178]. Gu et al. studied the MRE isolation system in a five-story benchmark model, with and without, and the real-time control, as frequency control, was designed and implemented in the isolation system. The building was exposed to the simulated earthquakes to study the Root mean square (RMS) of acceleration and the inter-story drift in the building [210]. It showed that the MRE isolation system could decrease the interstory drift, down to 90% with controller and

40% without the controller in contrast to building without this system. It was observed that the controlled MRE isolation could reduce the RMS acceleration by almost 85 %, and the passive MRE isolation could drop about 50% than the original value [210]. Yang et al. [208] examined the performance of the MRE isolation system with a fuzzy logic controller in a scaled three-story building. They investigated structural parameters, including inter-story drift and acceleration. They found that the fuzzy-based controller in the MRE isolation system could decrease acceleration by almost 60% and inter-story drift rather by 20% compared to a fixed building. It can be seen that the MRE isolation systems are an effective system and improve the structural behaviour in building, particularly acceleration and the inter-story drift. They are very effective in reducing inter-story drift when combined with advanced control strategies such as fuzzy logic controllers [208].

MRF dampers in foundations

MRE dampers are semi-active vibration isolation systems that help decouple buildings from the source of vibration [173,208,209]. MRF dampers are easily added to existing vibration isolation systems to enhance their controllability and adaptability [211–215]. When combining MRF dampers to base isolation systems, the MRF damper is connected between the ground and the top of the base isolation system, as shown in Figure 2-52 and Figure 2-53. Experimental and numerical studies show that such systems are very effective in decreasing the base acceleration, the structural acceleration, the base drift, and the peak displacement [211–213].

For instance, Iwata et al. [213] conducted a feasibility study of the MRF damper to base-isolated building structures with a semi-active control algorithm. The simple experimental setup was

composed of a mass, four linear guides, two laminated natural rubber bearings, and the MRF-damper. This set-up was subjected to three ground motions on a shake table. The study showed a 21% reduction in displacement when switching the controller from the off-state to the on-state. Lakhani et al. employed an MRF-damper with a fuzzy logic controller (FLC) and a Lead-bearing system into a five-story single bay frame. The dynamic response of the frame under four ground motions was investigated. A 31% drop in the peak isolator displacement was reported in the frame with the FLC over the fixed frame. It was found that the maximum acceleration of the top floor was reduced by about 83% for the frame equipped with the isolation system compared to the frame without the isolation system.

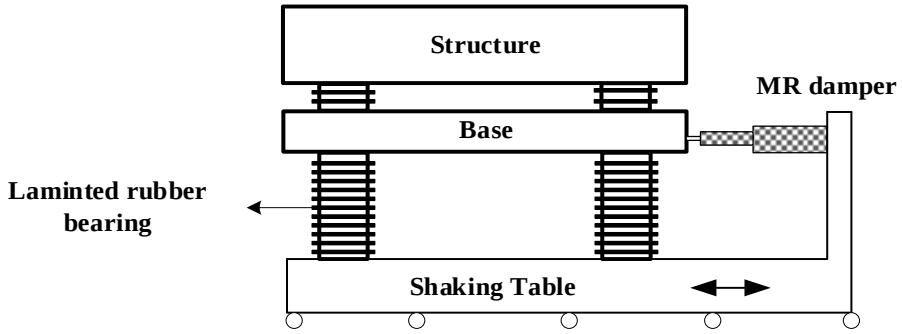

Figure 2-52. Schematic diagram of a combination of an MRF damper and a base isolation system adapted from [212]

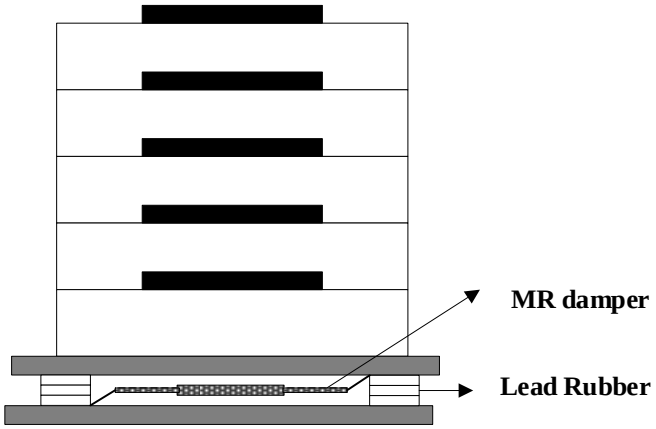

Figure 2-53. Schematic diagram of a combination of an MRF damper and a base isolation system adapted from [212]

MRF-based seismic control systems in structural components

Due to controllability, energy dissipation ability, and fast-responding of the MRF-based seismic control systems, they are installed independently like MRF-based damper in the bracing systems, or dependently, like the MRF-based damper with isolation based systems as structural components in buildings; they preserve buildings during and after seismic activities. MRF-based systems can be used as follows:

MRF bracing system

MRF dampers are well suited for bracing systems, in both regular or irregular buildings [7,216]. The bracing system is installed between two floors to control the interstory drift between them [7], as presented in Figure 2-54 [7].

Estaki incorporated an MRF-based bracing system with a linear–quadratic regulator (LQR) control system in the numerical model of a 20-story steel frame that is designed based on the national building code of Canada (NBCC 2005). MRF-based bracing systems were utilized in every story.

The dynamic response of the structure was examined under six ground motions. The contrast between the frame with active control MRF-based system and the passive system showed a marked decline of about 68.5% in top floor displacement compared to the MRF-based system without controller [2].

Lee et al. developed a numeral and experimental small scale three-story building structure [217]. In the first story of the structure, (a) chevron, (b) upper toggle, and (c) scissor-jack toggle MRF-based bracing system were incorporated in the structure, as shown in Figure 2-55. The distributions of the peak and the RMS acceleration along all stories were calculated. It was seen that all bracing systems decreased the peak acceleration and RMS acceleration. The scissor-jack toggle bracing system was able to reduce the peak and the RMS accelerations by up to 75%. The existing studies show that the MRF-based bracing system is capable of preserving the building subjected to strong ground motions.

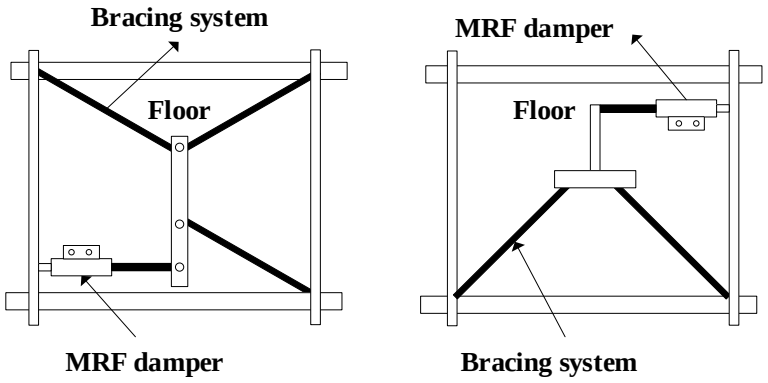

Figure 2-54. Applications of MRF dampers in bracing systems adapted from [7]

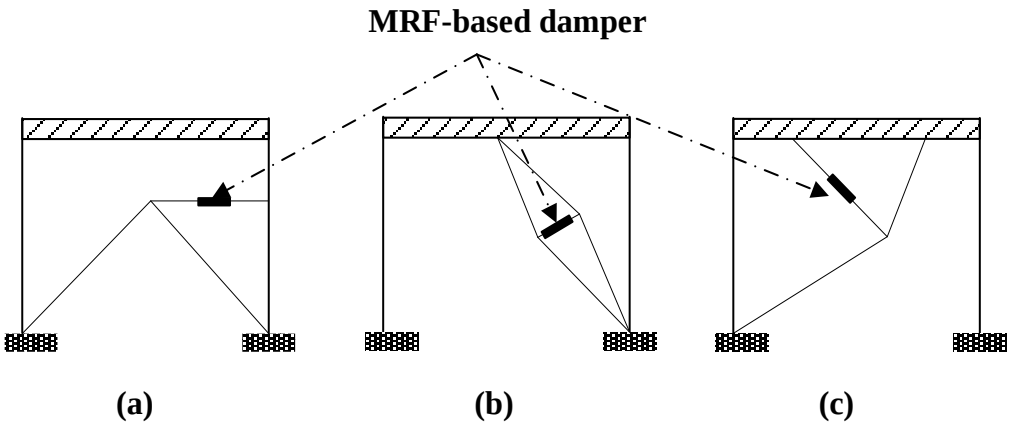

Figure 2-55 The schematic diagram of bracing systems based MRF-based damper, (a) chevron, (b) upper toggle, and (c) scissor-jack toggle taken from [217,218]

Tuned Mass-MRF dampers (TMMRD)

In a tuned mass damper (TMD) system, a mass is attached to the main structure of the building with a spring and a damper [5]. This additional vibration-mass is used to reduce the main resonance peak of the structure by increasing the equivalent damping ratio. Subsequently, this results in dissipating more energy [219]. Unfortunately, TMDs are massive structures that are typically only effective for damping a single building resonance; however, earthquakes are expected to excite several structural resonances. Multiple tuned mass dampers (MTMD) systems are further development that can protect several building resonances. However, MTMDs are also very sensitive to de-tuning, and they cannot be tuned in real-time [8,220].

A Semi-active tuned mass damper (SATMD) is a TMD system with an external small tunable damper that adds real-time adaptability [178,220,221]. This system was originally developed to suppress wind-induced vibrations in tall buildings [222]. It is similar in performance to fully active TMD systems, but it is simpler, more robust, and it requires substantially less power [222].

Figure 2-56 illustrates a TMMRD, where an MR damper is integrated into a SATMD [207,223]. The MR damper then allows for actively controlling the damping force applied to the TMD [178]. Zemp et al. suggested installing two tuned pendular inertial masses (TMs), which are 160-ton masses and magnetorheological fluid (MRF) damper in an RC structure with 21 stories tall building. Both TMs were added on the 21st story, and the LQR control strategy was applied to the proof-of-concept MR damper. The structural behaviour under seven different ground motions illustrated that the performance of the building improved by about 50% for peak and RMS displacements compared to the conventional one.

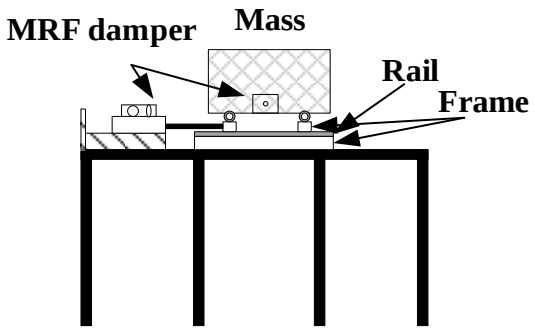

Figure 2-56.Schematic diagram of the SATMD with MRF damper [223]

MRE isolation systems-Tuned mass dampers (MREI-TMD)

The application of MRE isolation systems is not limited to the foundation of buildings [224]. They can also be combined with the conventional structural control systems, such as the TMDs [224], to increase their effectiveness and controllability [224]. Sun et al. developed a magnetorheological elastomers-based tuned mass damper installed on the top of a scaled three-story frame for seismic protection, as displayed in Figure 2-70. A frequency analysis of the structural behaviour subject to a scaled 1940 El Centro earthquake record was performed. It was noted that the first natural frequency of the structure could be shifted from 3.1Hz to 7.1Hz by switching electric current from 0A to 2.5A. Hence, dynamic behaviour significantly improved.

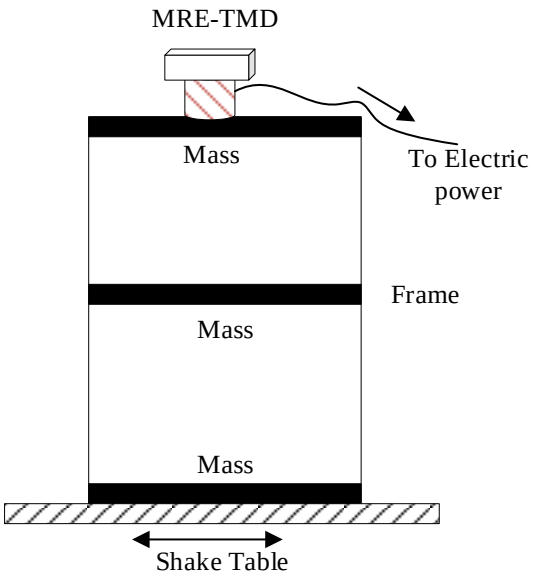

Figure 2-57. Typical diagram of the MRE-TMD in a frame adapted from [224]

2.3.3.4 Summary of MRF-based systems in buildings

Figure 2-58 and Figure 2-59 summarize MRF-based systems for building applications. It is worth noting that the MRF-dampers are the most established MRF-based structural control system in buildings; they are integrated into foundations as well as the main structures. However, other MRF-based damping systems, such as MREs and MR-TLCDs are currently being developed and still need to prove their effectiveness in future studies.

It is observed that the MRF-based systems could significantly reduce different response parameters, such as peak drift, inter-story drift, and accelerations, i.e. peak and absolute acceleration. It is worth mentioning that the MRF-based systems have also been capable of increasing the structural energy dissipation and damping coefficient.

Among all the discussed systems, it is noted that MRF-based TLCDs, as the structural protection systems, are the most common system to decrease the acceleration and displacement in buildings.

In the foundation of buildings, MRF-based dampers are commonly used to decrease dynamic accelerations and displacements.

The main advantage of semi-active vibration control systems over passive systems is their controllability. A wide range of control systems, such as LQR, LQG, On-Off, skyhook, and Fuzzy Logic strategies have been utilized to improve the dynamic behaviour of buildings. Among these strategies, fuzzy logic controllers the most common for seismic MRF-based systems due to their high robustness.

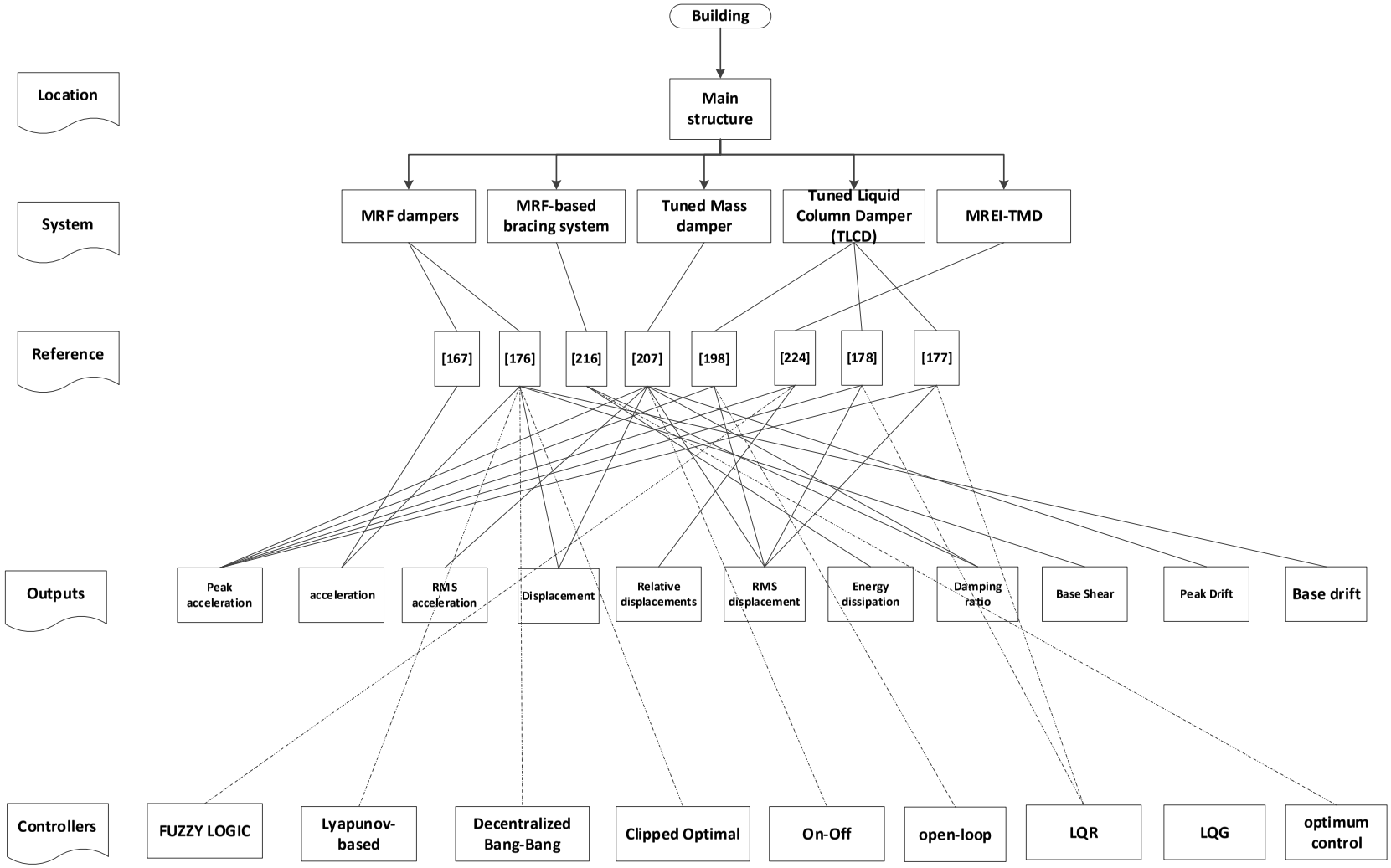

Figure 2-58. The summary of MRF-based applications in the main structure of buildings

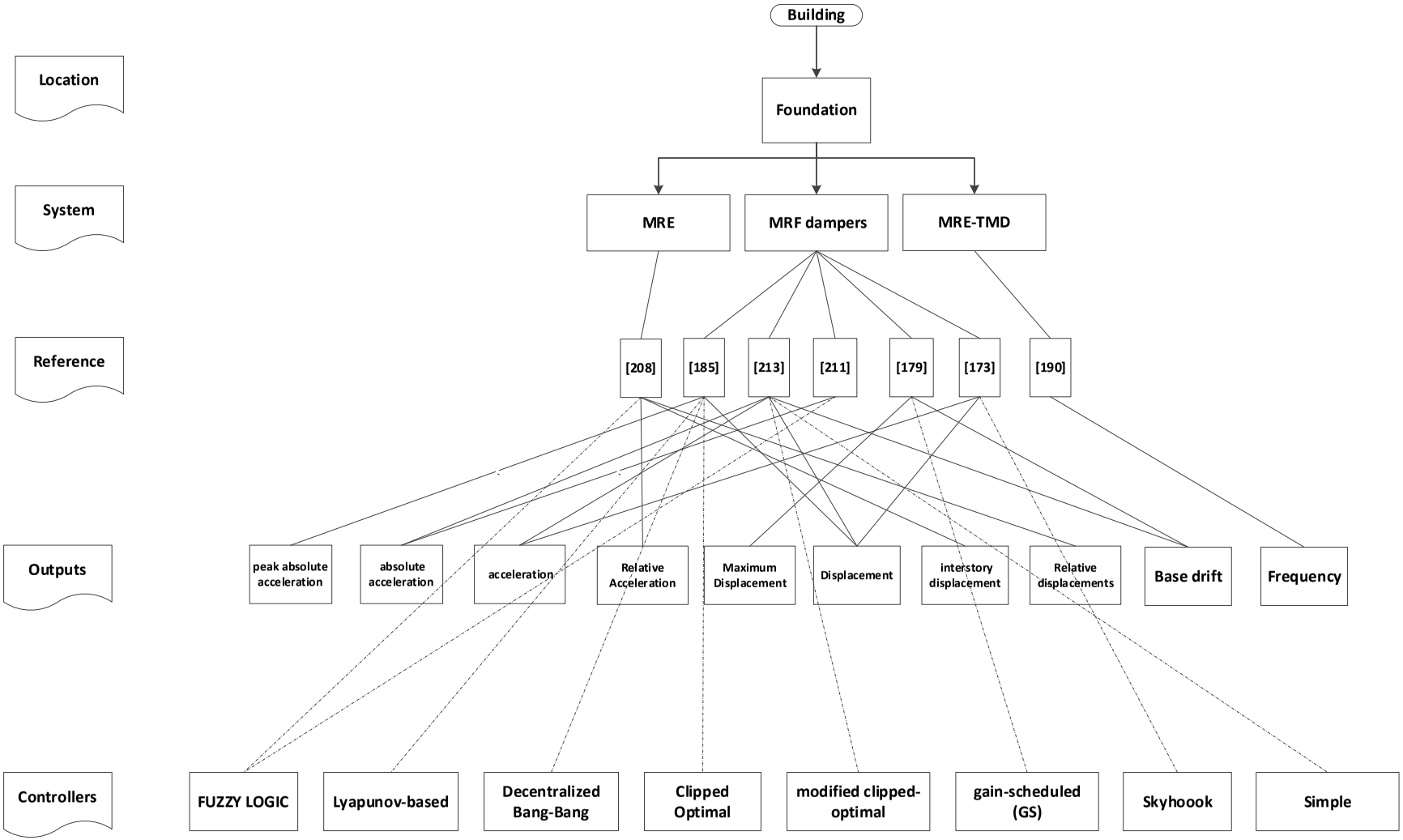

Figure 2-59. The summary of MRF-based applications in the foundation of buildings

2.3.3.5 The Application of MRF damping systems to Bridges

In the 1989 Loma Prieta, the1995 Hyogo-ken Nanbu, and the 2001 Bhuj earthquakes, severe bridge damages were observed. Many studies focus on mitigation techniques involving structural control systems [225]. The conventional method to ensure bridge stability is to insert secured gaps between the bridge components. This is impractical for bridges with close adjoining components. MRF based structural control systems are one solution to this problem. They can be installed between the pier and deck, or they can also be embedded directly into the main structure [226–234]. This section discusses the integration of MRF damping systems into different bridge components.

Damping between the pier and main structure

There is a significant relative displacement between the pier and the main structure of bridges. Thus, this is an ideal location for placing MRE and MRF dampers.

MRF-damper

To prevent pounding in bridges, MRF dampers can be installed between its spans [235–239], as illustrated in Figure 2-60. Alternatively, MRF dampers can also be utilized to decrease the relative displacement between the abutment and the deck, as presented in Figure 2-61 [239].

Heo et al. examined the functionality of the MRF-based damper with a lumped mass, as portrayed in Figure 2-60, for a two-span bridge to prevent the spans from pounding [225]. They used a numerical single-degree-of-freedom (SDOF) system to model a bridge made of an RC slab and an I-type beam. The numerical model was verified against an experimental setup of the bridge equipped with the controlled and uncontrolled MRF-based damper under simulated ground motions. The experimental results showed that the relative peak displacement between the two

spans sharply decreased from 85.04 mm without an MRF-based damping system to 20.29 mm with a passive MRF-based damping system, 13.61 mm with a Lyapunov controlled MRF-based damping system, and 12.74 mm with a Clipped-optimal controlled MRF-based damping system. The root-mean-square (RMS) relative displacement from 7.58 mm in the un-controlled bridge surprisingly drops to 1.40 mm and 1.23 mm for the Lyapunov and Clipped-optimal controlled MRF-based systems. Similarly, Sheikh et al. [238] proposed an MRF Damper in an RC Highway Bridge to mitigate the pounding effect of its base-isolation system, as illustrated in Figure 2-61. A simplified analytical model was developed and exposed to the El-Centro earthquake. The model's response without an MRF-based damper was compared to a Bang-bang controlled MRF-based damper; it illustrated a remarkable reduction in displacement and acceleration of 39% and 40%, respectively.

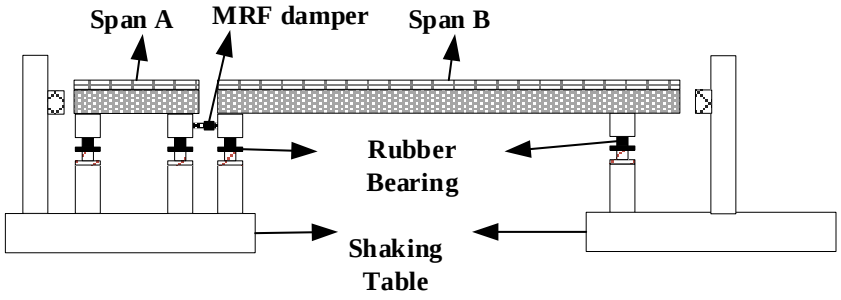

Figure 2-60. Application of MRF dampers in preventing bridge poundings, adapted from [225]

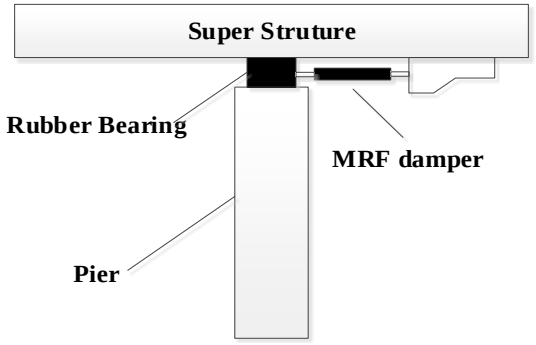

Figure 2-61. Application of MRF dampers between the pier and superstructure in bridges, adapted from [238]

MREI

MREI can be used to decouple the relative motion between the bridge piers and the main structure [193,240]. The stiffness and damping of MREIs of the main structure are growing up. Li et al. [241] studied an MREI located between the pier and deck for a scaled bridge system, as presented in Figure 2-62. The structure consisted of a steel deck and an Acrylonitrile-butadiene-styrene(ABS) polymer pier. To assess the functionality of this damping system, a sinusoidal shaking table with two loading frequencies, including 1Hz and 2Hz, was utilized to test the dynamic response of the bridge. Active and inactive MREI system reduced the displacement of the deck by about 30% and acceleration by up to 75%. It may be noted that MREI are relatively new systems to mitigate the seismic hazards in bridge and the research work in this area is very rare.

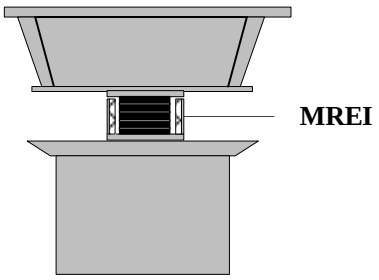

Figure 2-62. The typical MREI in bridge [195]

Main Structure

MRF-damping systems have also been embedded into the main structure of bridges to improve their structural behaviour. The following subsections discuss how they affect the dynamic response of bridges.

MRF damper

MRF dampers are effective structural control systems for bridges, particularly cable-stayed bridges [242,243], which are very common for large spans [244]. The Shandong Binzhou Yellow River

Highway Bridge, China, is a typical example of a cable-stayed bridge, whose flexibility and low damping coefficient are not enough to suppress vibrations adequately. MRF dampers with and without controllers significantly suppress these vibrations. Figure 2-63 and Figure 2-64 illustrate applications of MRF-based damping systems in bridges [244].

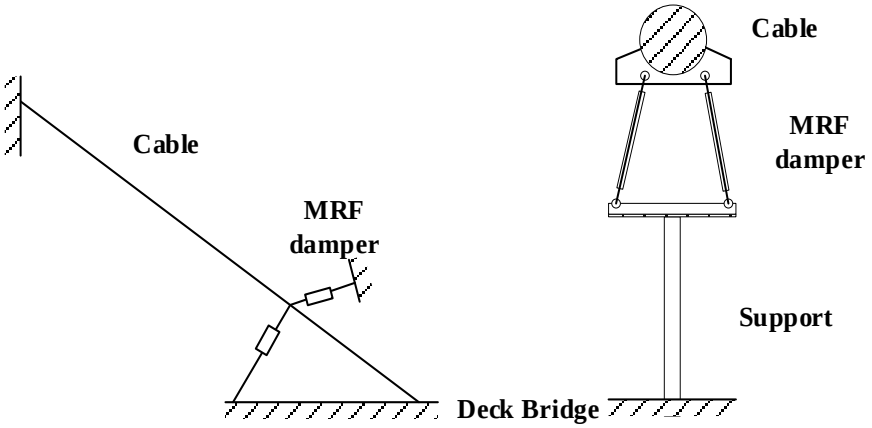

Figure 2-63. The schematic diagram of an MRF damper in a cable-stayed bridge adapted from [244]

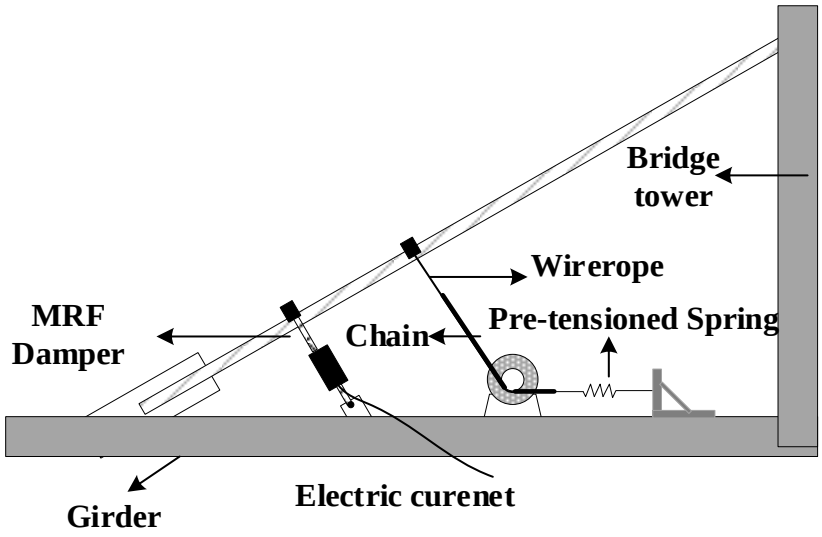

Figure 2-64. An application of the MRF damper in the cable-stayed bridge [242]

TMMRD

The combination of an MRF damper with a tuned mass damper (TMMRD) is an attractive semi-active vibration mitigation system that provides an adjustable, real-time, fail-safe, and low power

solution [66]. Numerical and experimental studies indicate that TMMRDs provide sufficient stability during transient and steady-state loadings to the main structure of bridges [245–247]. Figure 2-65 displays a typical application of a TMMRD in the Wolgograd Bridge [245–247]. The result showed an increase in resonance frequency and a decrease in the damping ratio of the primary structure [66]–[68].

To supply a controlled damping force for setting the amount of energy dissipation and the stiffness force for controlling the natural frequencies of the superstructure, many control approaches have been utilized. For instance, the system becomes more effective by tracking errors of forcing in the MRF damper in the TMMRD [246]. TMMRD systems are a relatively new technology for controlling the dynamic response of bridges, and there are only a few studies available.

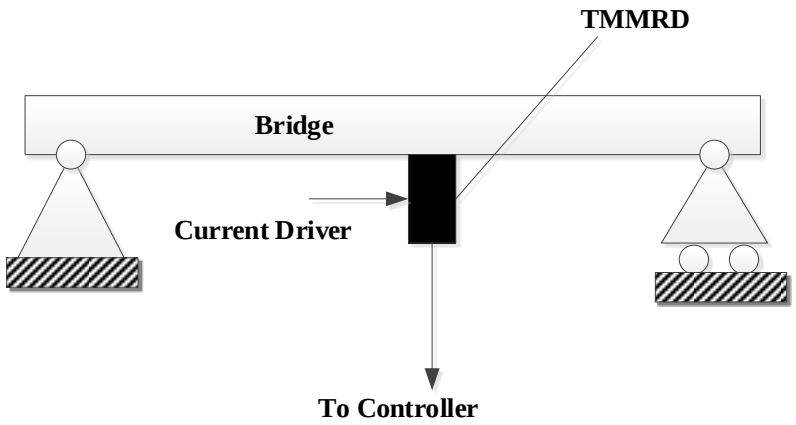

Figure 2-65.The application of TMMRD in a bridge [245]

2.3.3.6 Summary of MRF dampers in Bridges

Figure 2-66 and Figure 2-67 summarize publications of MRF-based damping systems in bridges. It is noted that the diversity of MRF-based damping systems in bridges is much lower than in

buildings. They are limited to the TMMRD, MRF dampers, and MREI. In bridges, MRF damping systems are mainly located between the pier and the main structure, and in some cases, they are installed into superstructures.

To achieve optimum dynamic behaviour, a variety of closed-loop control algorithms, including LQG, LQR, and fuzzy logic, have been studied. To find the effect of MRF-based systems on the bridge's response, the structural dynamic behaviour, such as accelerations, displacements, and the damping coefficient, have been investigated. It is observed that accelerations and displacements of bridges are the most desired structural control parameters to ensure the stability and integrity of bridges.

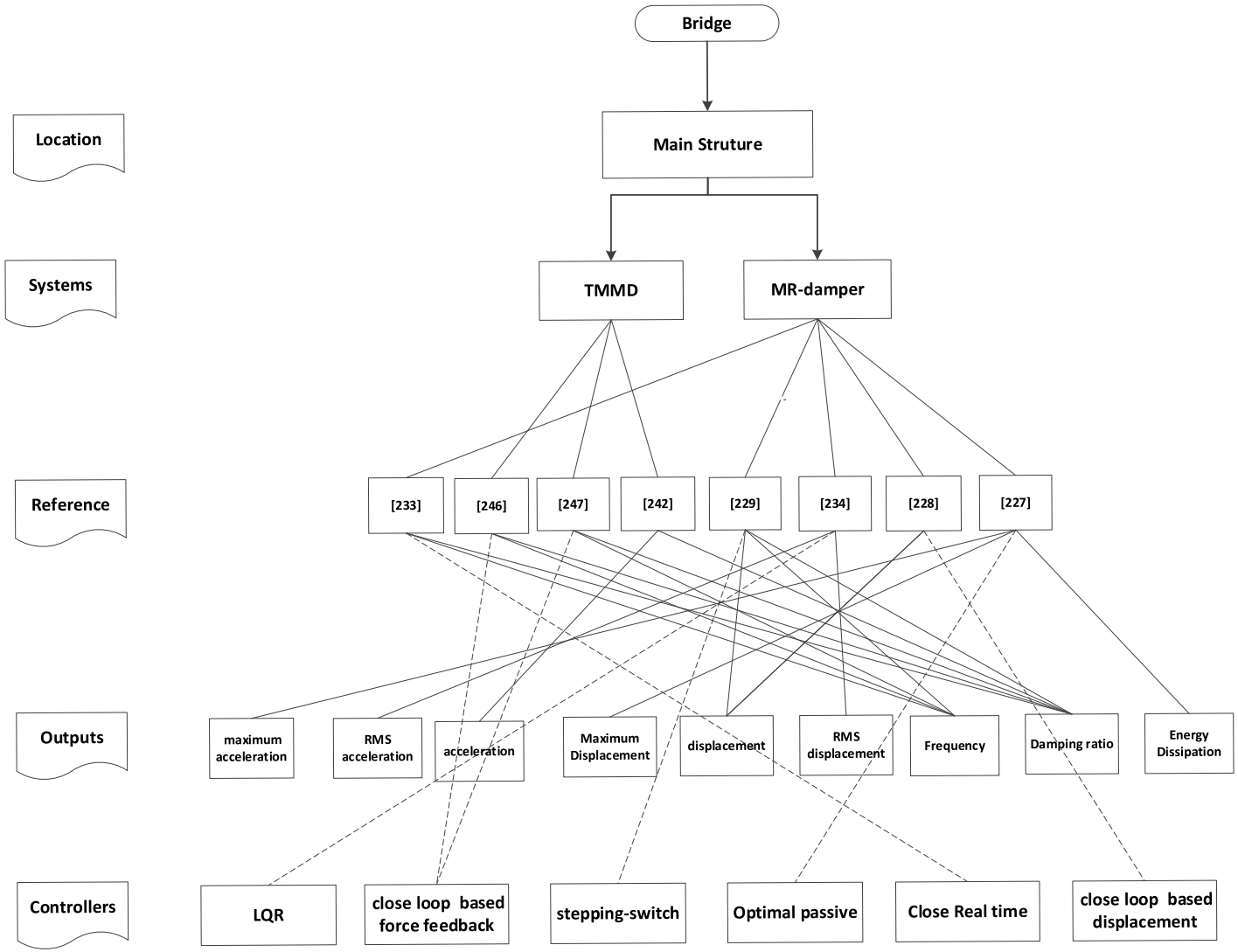

Figure 2-66. The summary of MRF-based applications in the main structure of bridges

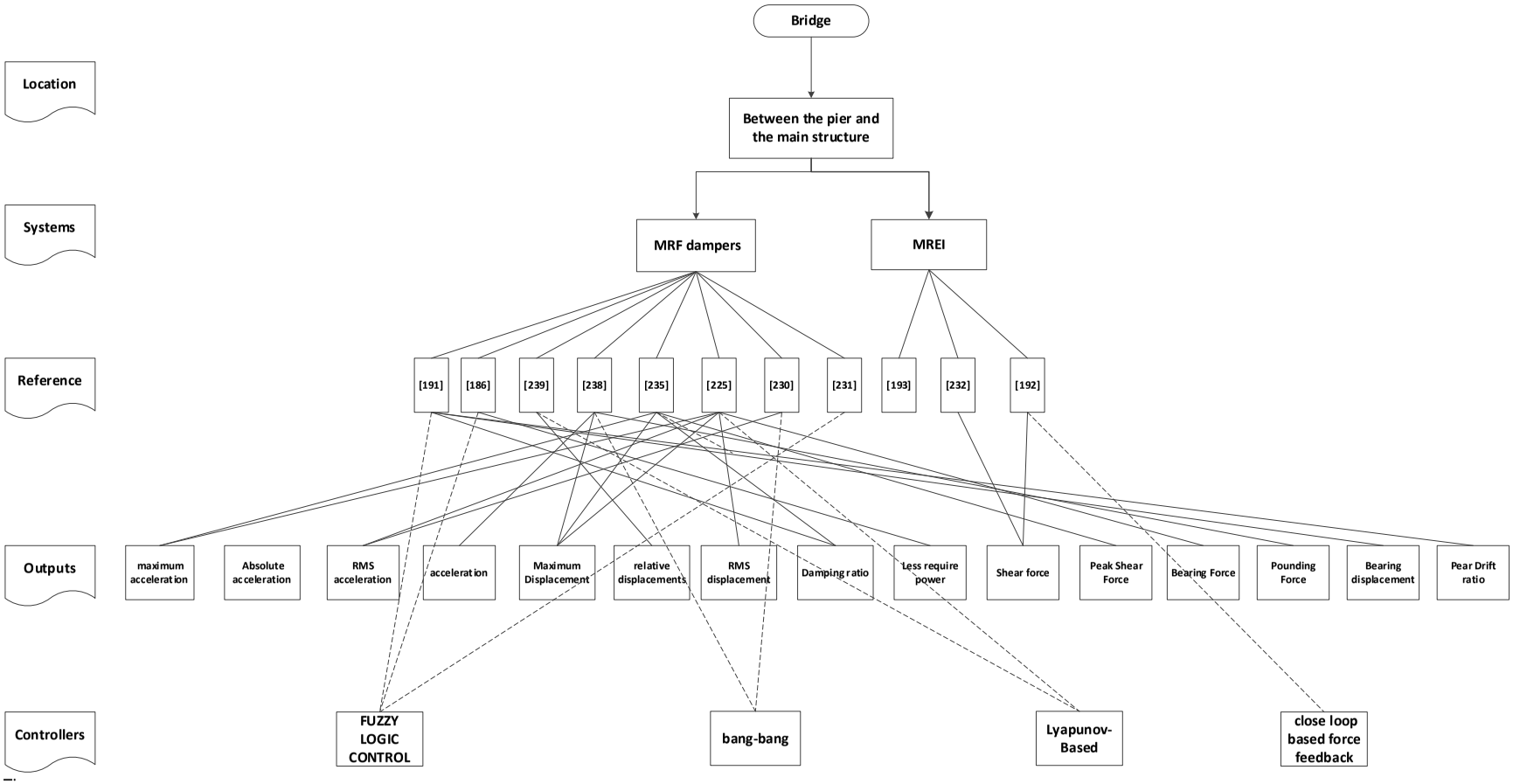

Figure 2-67. The summary of MRF-based applications between the pier and the main structure of bridges

2.3.4 Stiffness control device

Semi-active stiffness control devices change the natural period of the structure by modifying the stiffness [248]. Thus, the vibration response of the structure changes. The system, as displayed in Figure 2-68, is made up of a hydraulic cylinder, a piston rod, a solenoid control valve, and a tube. The valve can either be open (On) or close (Off) mode. When the mode is open, the fluid can move freely through two-cylinder chambers. So, the stiffness of the structure reduces [248]. In Off mode, the fluid cannot move, and the brace and beam lock; hence, structural stiffness increases. Besides the simple On-Off system, several other control algorithms have been developed to enhance the dynamic performance of the structure by controlling the flow rate of the stiffness control device [7].

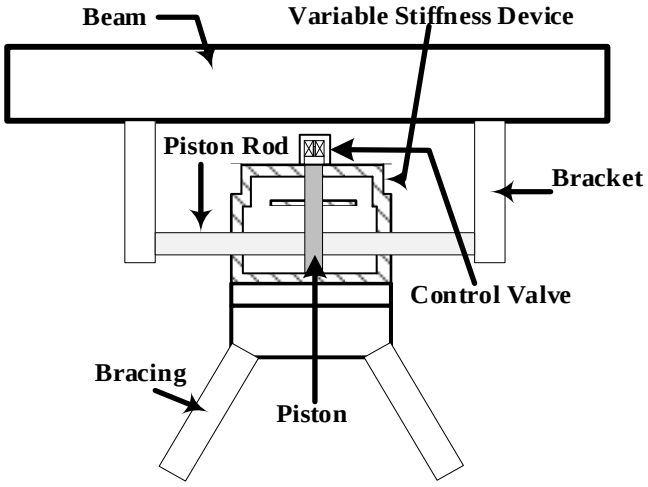

Figure 2-68. Semi-active variable-stiffness device adapted from [248]

2.4 Active systems

The active systems require an external power to be energized. Basically, these systems need sensor(s), controller(s), and actuator(s) to apply the proper resistance force. The main advantage

of these systems is the ability to tune with a wide range of loadings. However, this advantage is offset by the potentially large power required to actuate the control system.

2.4.1 Mass damper system

The main role of the conventional TMD system is changing the natural period (frequency) of the primary structure [7]. Many efforts have been made to enhance the performance of the TMD system, such as SATMD [249]. However, the external loadings with a wide range of frequencies, such as wind, are applied to civil infrastructure and affect the structural response deeply [249]. Hence, these loadings make TMDs inefficient. An alternative solution is the implementation of an actuator into TMD, which is called: an active mass damper system [7], which can set itself to the load frequencies. The actuator is located between the main structure and TMD. The typical diagram of the system is shown in Figure 2-69. The actuator can control the movement of TMD to "**increase structural control effectiveness**" [7], which depends on the control strategy.

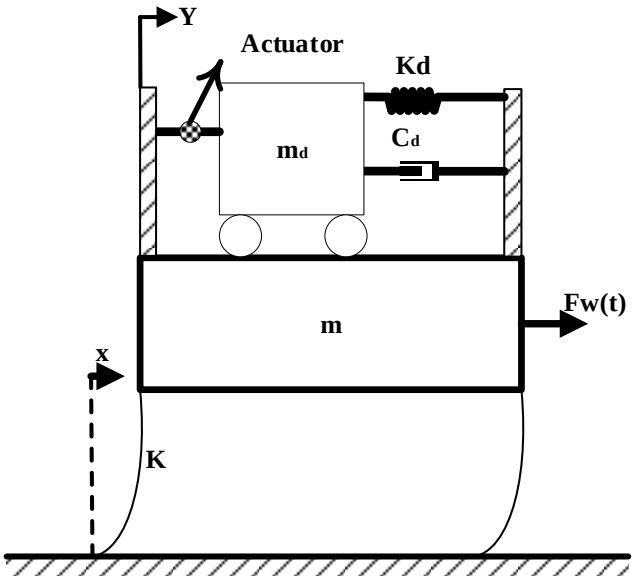

Figure 2-69. Active tuned mass damper adapted from[249]

2.4.2 Tendon system

An active tendon system is composed of prestressed tendons, which are controlled by electrohydraulic servomechanisms [250], as displayed in Figure 2-70. The system is installed between two stories. While the structure shakes, the interstory drift pulls or pushes the tendons, and the amount of tension is adjusted by the actuators. This system can actuate continuously or discretely [7].

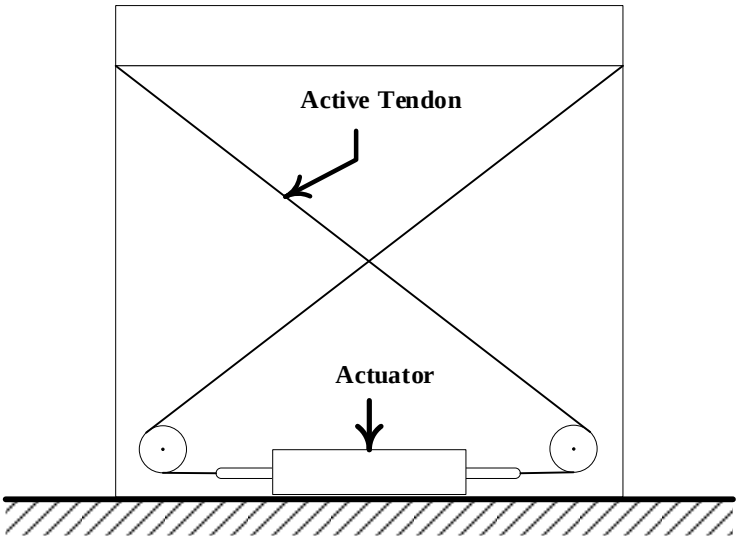

Figure 2-70. Typical diagram active tendon system adapted from [7]

2.4.3 Bracing system

An active bracing system has an actuator embedded into the bracing system, as displayed in Figure 2-71 [7]. The bracing system is installed between two floors to control the interstory drift between two stories [7]. The different control strategies have been applied experimentally and numerically to tune the actuator and minimize the displacement [249].

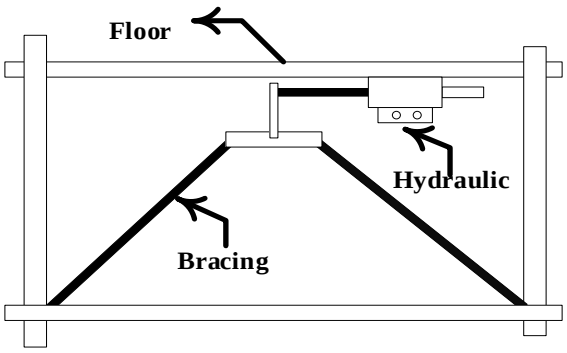

Figure 2-71. Semi-active bracing system

2.5 Summary

To maintain the stability of civil infrastructure, many seismic control systems have been developed. Such systems have been thoroughly discussed in the literature and summarized in Table 2-4. Among controlled systems damping systems, SMA and MRF-based systems have attracted significant attention due to their effectiveness.

MRF-based systems are promising candidates to replace conventional seismic control systems, entirely or partially in different kinds of civil infrastructure such as buildings and bridges. It has been found that most MRF-based systems have been developed based on the MRF-based dampers, which enhance the structural behaviour of civil infrastructure. However, the self-centering is missing capability in MRF-based applications.

An SMA is an excellent alternative as a replacement, partially or entirely, for conventional protective systems in steel, timber, and concrete civil infrastructure. The review shows that SMA-based systems are the most common systems in steel structures as well as concrete structures. In most protective system applications, SE-SMA-based systems have many practical characteristics rather than SME in all discussed civil infrastructure. For instance, it is not required to apply the source by external source. However, this study shows that the SMA-based applications have good potential to enhance the structural response in civil infrastructure, particularly the displacements

and the interstory drift. Nevertheless, it is observed that controllability is the missing feature in most SMA-based systems, and cannot adopt under different loading conditions. Being passive in the SE makes a good alternative for those applications when the frequency of applied loading is less than the natural frequency of primary structures. The following chapters will introduce an SMA-MRF core-based bracing system for civil infrastructures. It combines the recovery ability of SMA-bases damper systems with the controllability of MRF-based damper systems.

Table 2-4. The summary of structural control systems and their advantages and disadvantages

Passive system	Disadvantages	Advantages	Semi-active system	Disadvantages	Advantages	Active system	Disadvantages	Advantages
Tuned mass Damper	Occupation of large space, Occupation of large space, sensitive to de-tuning	Increasing the equivalent damping ratio, Shifting natural frequency	Viscous fluid damper	Under development	A few information about structural properties and measured structural parameters,	Mass damper system	Costly, Complexity, require energy, high maintenance , Design of controller	Robust to multiple-frequency lording
Pendulum Tuned Mass Damper	sensitive to frequency deviation	capability of re-tuning the natural frequency	SMA-based systems	Need source of heat	Re-centering	Tendon system	require energy, Design of controller	pulsed- and the continuous state
Bidirectional Tuned Mass Damper	Not-common	Simplicity, tuneable the damper to two independent frequencies	MRF-based systems	No Re-centering	Controllability, High equivalent Damping	Bracing system	require energy, Design of controller	large control force
Tuned Liquid Column Damper	low inherent damping	The low-cost, easy installation and low required maintenance	Stiffness control device	Need controller	a large forces			
Friction damper	no restoring force and permanent deformation, needs nonlinear analysis	Large energy dissipation						
Viscoelastic Solid damper	Function of frequency of motion, the strain amplitude, and temperature	Linear Behaviour, restoring force, active in low displacement						
Metallic yield damper	damaged under strong earthquakes and should be changed	long-term use.						
iscous-based damper	Possible fluid leakage	Easy modeling High reliability , active in low displacement						
SMA-based systems	No-controllable	Re-centering						
Friction Pendulum Bearing	Limited availability	very low maintenance						
Elastomeric Bearing	resistance against the lateral movement is typically very low,	Proved performance						
Lead-Plug Bearing	Complicated fabrication	Good for small and large force						

Chapter 3: Analytical Model of the SMA-MRF core bracing Elements

3.1 Introduction

Maintaining the stability of civil structures under excessive dynamic loads, including earthquakes and windstorms, has always been a big challenge for researchers and designers in structural engineering communities. Recent advances in the development of multi-functional smart materials, design, and construction of structural control systems, particularly bracing systems, with the capability to retain the stability of civil infrastructures, have opened a new horizon in civil engineering to keep the structural integrity. In the present study, a hybrid smart, bracing system based on Magnetorheological Fluid (MRF) and Shape Memory Alloy (SMA) has been developed, as presented in Figure 3-1(a). Analytical models are conducted to elaborate on the performance and functionality of the developed model under the quasi-static load. The proposed SMA-MRF core bracing element is composed of an MRF damper, as a core, and surrounded SMA wires secured by two hollow cylinders, as shown in Figure 3-1(b). The conceptual 3D design and the fabricated SMA-MRF based system is presented in Figure 3-2.

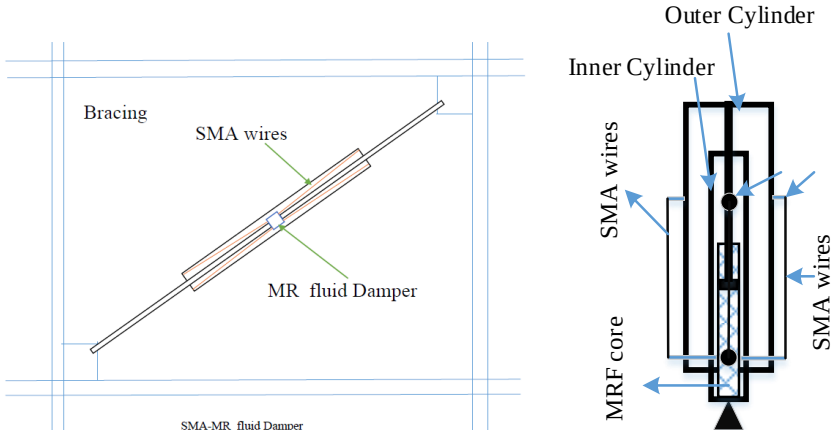

Figure 3-1. (a) The proposed SMA-MRF core bracing system (b) The conceptual design of SMA-MRF core

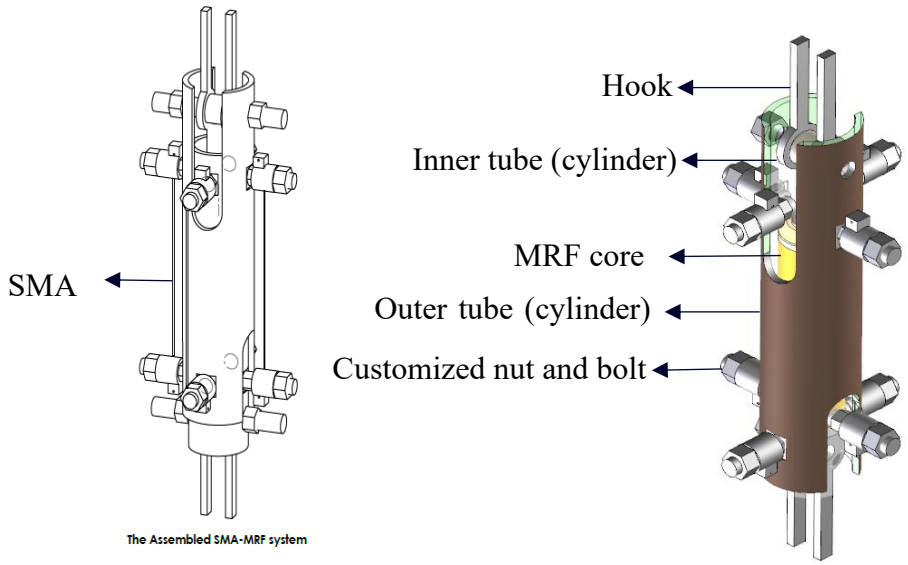

Figure 3-2. The 3D conceptual design of the scaled prototype of the SMA-MRF-based system

Considering some simplification, such as rotation, the proposed bracing system is a one-degree-of-freedom system, while it is installed in a building. As the mechanism is set to move only in the axial direction, the rotation and movement in the other direction are negligible. Therefore, the mechanism is free to move in one direction only, as shown in Figure 3-3(a).

The MRF-based damper is a two-way damper. So, this damper is functional under tension and compression. The main issue is how to keep the SMA-wires under tension regardless of loading direction. In order to resolve this issue, a novel design is considered to attach two SMA wires to the inner cylinder(tube) and outer cylinder(tube). Similarly, the other two wires are kept to the inner as well as the outer cylinders(tubes). This mechanism puts the SMA-wires under tension loading, always.

When the external excitation tensions the system, the MRF damper and SMA wires held between the bottom of the inner cylinder and the top of the outer cylinder supply the damping force, as shown in Figure 3-3(b). In the same way, when the external loading compresses the system, as

presented in Figure 3-3(c), again, the MRF core and SMA wires are secured by the top of the inner cylinder, and the bottom of the outer cylinder provide the resistance force.

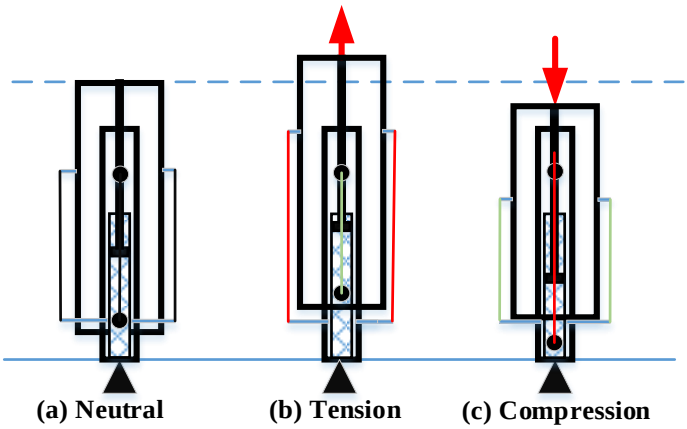

Figure 3-3. Possible states of the SMA-MRF core bracing system (a). the neutral position (b). Under tension (c). under compression

In order to evaluate the functionality of the hybrid system (seen in Figure 3-4(a)), it is compared with the SMA and the MRF bracing systems, as presented in Figure 3-4(b) and Figure 3-4(c), respectively The components of the SMA system are derived from SMA elements in the SMA-MRF bracing system. Similarly, the MRF-based bracing system's element comes from the MRF core of the suggested system.

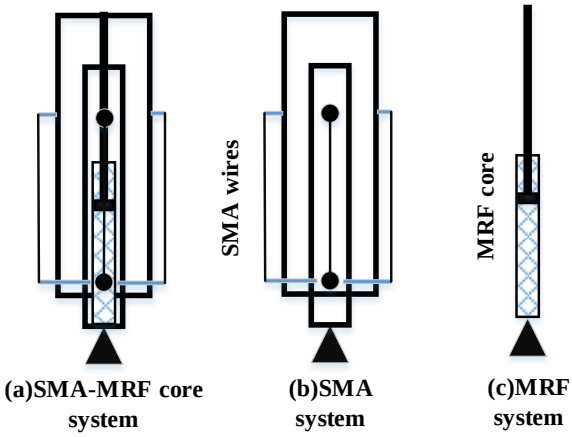

Figure 3-4. Schematic diagram of (a) SMA-MRF core bracing system, (b) SMA bracing system, (c) MRF bracing system

3.2 Analytical approach

The analytical procedure of the SMA-MRF bracing element is illustrated in Figure 3-5. As shown in the working mechanism in the figure, the displacement of the SMA and the MRF core are equal. This is a key point to calculate the damping force generated by each of them in the hybrid system. In addition, the displacements and the forces are needed to find the hysteresis responses, not only in the hybrid system but also in the sub-systems, including the SMA-based and the SMA-MRF-based systems. For simplicity, in the following subsections, the procedure is separately explained for SMA and MRF.

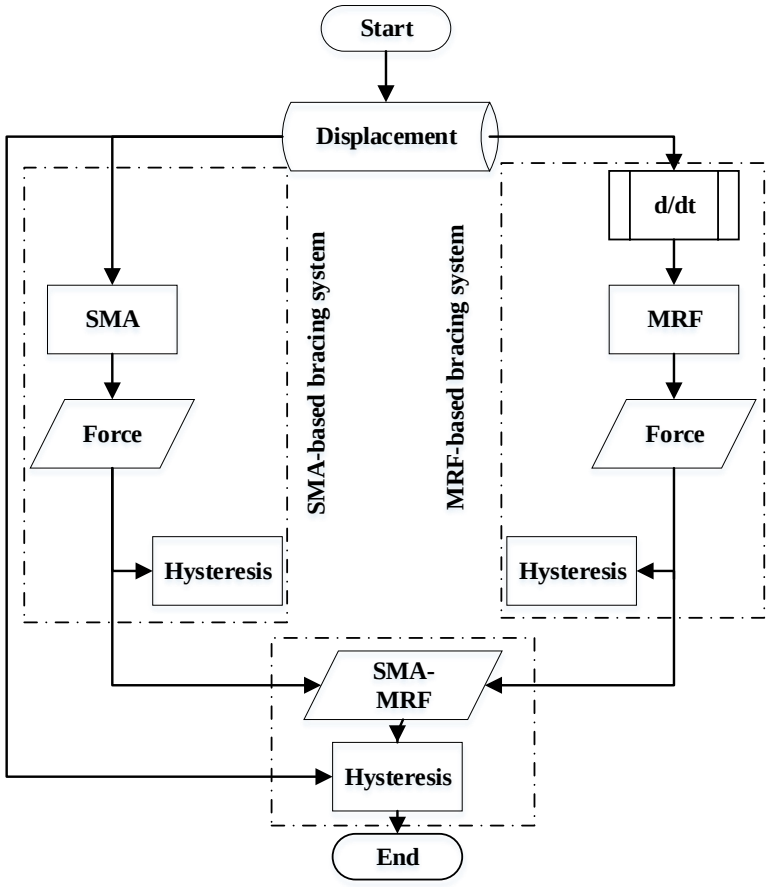

Figure 3-5. The flowchart of dynamic response calculation of the SMA-based, the SMA-MRF-based, the SMA-MRF core bracing systems

3.2.1 SMA element

The resistive force of the SMA-elements can be computed by:

$$F_{sma} = \sigma A \tag{3.1}$$

where σ and A denote the stress and the cross-section, respectively

The constitutive law for analytical modeling of σ in SMA wires is given as: [251]:

$$\sigma(\varepsilon) = E(\varepsilon - \varepsilon^T) \tag{3.2}$$

where σ, E, ε, and $\varepsilon^T$are the stress, Young's modulus of the SMA, the strain, and the phase transformation strain, respectively.

The Young's modulus of the SMA is defined by [251]:

$$E = E_A + \zeta(E_M - E_A) \tag{3.3}$$

where E_A and E_M are Young's modulus in the Austenite and Martensite phases, respectively. ζ denotes the phase transformation volume fraction.

The relation between strain-stress in the Martensite phase and the Austenite phase is shown in Figure 3-6(a). The loading state starts from zero and reaches the Martensite start strain (ε_{ms}) that is the end of the elastic response of the SMA. As the load increases, the state of SMA changes into an inelastic mode to the Martensite finish strain (ε_{mf}). Increasing the applied load beyond this point, the strain goes to the inelastic phase. In this study, the system is designed in a way that loading does not exceed ε_{mf}. In the unloading phase, it starts from ε_{mf}, and moves to the Austenite start strain (ε_{as}). Continuing the load release changes the strain from ε_{as} to ε_{af} (Austenite finish strain) in the inelastic state. By removing more load, it goes back to the initial shape.

In Eq.(3.2), ε^T is defined for the loading and the unloading phases given by [113]:

$$\varepsilon^T = \zeta \varepsilon_L^T \tag{3.4}$$

$$\varepsilon^T = \zeta \varepsilon_{UL}^T \tag{3.5}$$

where ε_L^T and ε_{UL}^T are the maximum phase transformation strain from Austenite to Martensite and Martensite to Austenite, correspondingly.

The relation between ε_L^T and ε_{UL}^T is given by [113]:

$$\varepsilon_{UL}^T = \varepsilon_L^T + \frac{\sigma_{ms} - \sigma_{af}}{E_A} - \frac{\sigma_{mf} - \sigma_{as}}{E_M} \tag{3.6}$$

where σ_{ms} and σ_{mf} are the Martensite start and the finish stresses, respectively. Similarly, σ_{as} and σ_{af} denote the Austenite start and finish stresses. These stresses and the relevant strains are shown schematically in Figure 3-6(a).

3.2.2 MRF core

The MRF damper is the core element of the proposed hybrid SMA-MRF bracing system. The behaviour of MRF damper is based on the phenomena that the polarized iron particles stop moving along the direction of the magnetic pole until the yield stress. After this point, the relation between shear stress and strain rate becomes linear [29]. The mathematical model of the MRF based on the Bingham model is expressed by [7]:

$$\tau < \tau_{yeild} \rightarrow \dot{y} = 0 \tag{3.7}$$

$$\tau \geq \tau_{yeild} \rightarrow \tau = \tau_{yeild}\, sgn(\dot{y}) + \mu \dot{y}$$

where τ_{yeild}, τ, μ, and $\dot{y}$ indicate the yield stress, shear stress, viscosity, and strain rate, respectively. This behaviour is plotted in Figure 3-6 (b).

In the MRF-based damper, μ is a variable viscosity and is a function of the applied magnetic field upon the MRF.

In the regular damper, it can be assumed that the fluid cannot resist the shear stress. However, the MRF can do. It is linked to the semi-solid state of the MRF exposed to the magnetic field. This is a key point and the main difference between the conventional damper, like Viscous-based and the MRF-based dampers.

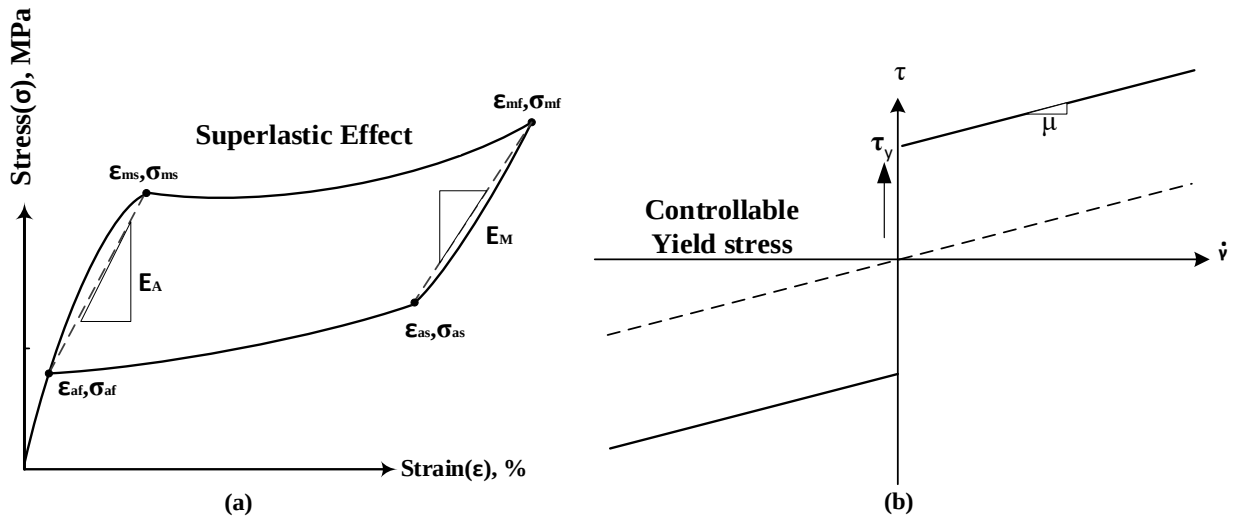

Figure 3-6. The schematic diagram of (a) stress-strain relations in SMA (b) Shear stress-strain rate in the MRF

The MRF-based dampers are developed in a way that MRF is the working fluid with variable viscosity. The magnetic field in the control valve is provided by the electromagnetic coil and supplies damping force by energizing the MRF and changing the yield stress of the fluid. The magnetic flux path in this field governs the orientation of MRF polarization [252], and without applying a magnetic field to the MRF, the resistance force is generated only as a result of the viscosity of the MRF [253].

Many models have been proposed to describe the behaviour of MRF dampers. One of the most widely used models is the Bingham [164], which describes the visco-plastic MRF damper

behaviour. The schematic diagram of the Bingham model is presented in Figure 3-7. In this model, the generated force is computed by [254]:

$$F_{MRF} = f_c.sgn(\dot{x}) + c_0\dot{x} \tag{3.8}$$

where c_0, $\dot{x}$, and f_c are the damping coefficient, a function of the variable viscosity, the velocity of external excitation, and the frictional force, respectively. The variable viscosity depends on the intensity of the magnetic field [255].

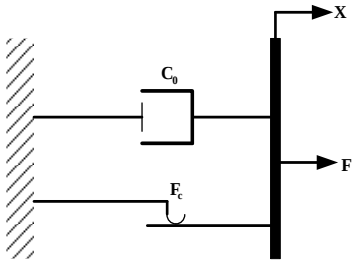

Figure 3-7. The typical diagram of the Bingham model [254]

3.2.3 Equivalent viscous damping

Insertion of an energy dissipation device into the main structure adds an extra damping effect into structures, reduces the displacement demand, and protect the structure against seismic loads. The damping can be expressed in the equivalent viscous damping form, which is calculated by the area of the hysteresis response of the system in the stress-strain curve. Considering the hysteresis response, damping coefficients is given by [63]:

$$\xi = \frac{A_h}{2\pi D_m F_m} \tag{3.9}$$

where $A_h, F_m,$ and D_m are the amount of energy dissipation, maximum force and maximum displacement in one complete stable cycle, respectively.

Figure 3-8(a) illustrates a typical force-displacement relation of the MRF damper under one loading protocol. Due to the variable viscosity of the MRF damper, the force produced by the MRF damper is variable and increases from the passive state of MRF damper (without applied electric current) up to the saturated state (applied maximum electric current). Thus, the energy dissipation capacity is varied from the minimum to the maximum electric current. Figure 3-8 (b) shows the schematic diagram of the force-displacement of the SMA-based bracing system. The energy absorption capacity is only a function of the applied displacement where the energy dissipation is not controllable. Figure 3-8 (c) shows the schematic energy dissipation capacity of the SMA-MRF system in the inactive state (the minimum electric current) to the active state (the maximum electric current).

3.3 Materials

As mentioned earlier, the present bracing system combines the SMA and the MRF properties to develop a novel hybrid bracing system. In this section, the main characteristics of the material used in each system are discussed.

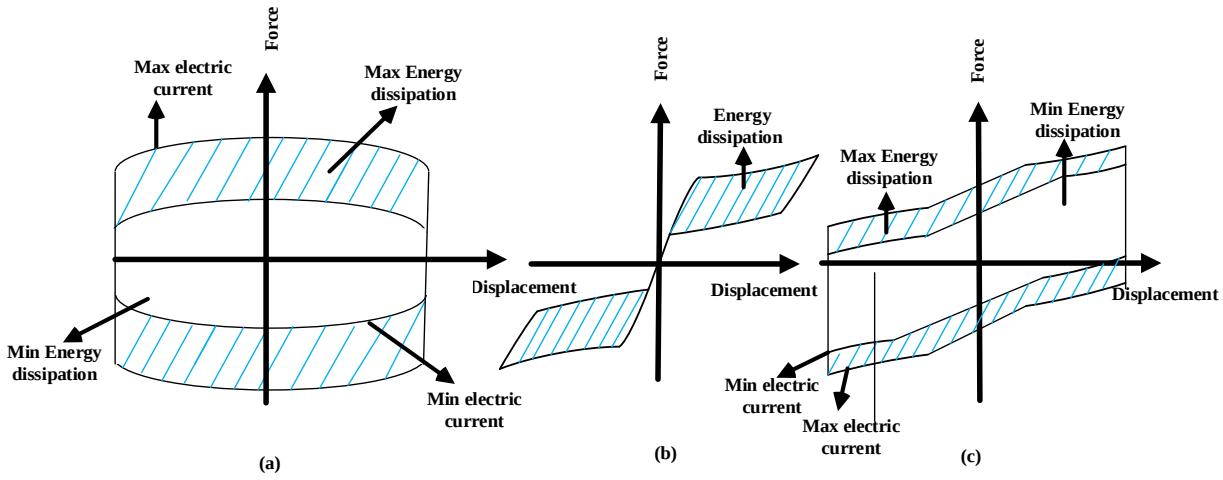

Figure 3-8. The schematic diagram of energy dissipation of (a) the MRF-based bracing system (b) the MRF-based bracing system (c) the SMA-MRF core bracing system

3.3.1 Shape memory alloys (SMA)

Shape memory alloys (SMAs) with different compositions, such as Cu-Zn, Fe-Pd, Mn-Cu, and NiTi, are available in the market. SMAs exhibit two unique properties, which differentiate them from conventional alloys, namely, shape memory effect (SME) and superelasticity (SE). The shape memory effect explains the ability of SMA to return to its initial state by heating. The superelasticity effect results in recovering the original shape by removing the load upon it. In this study, as the working temperature for most civil applications is above the Austenite finish temperatures of SMA alloys; therefore, only SE is considered.

Table 3-1 provides the different parameters for two SMAs (e.g., NiTi and FeNiCuAlTaB) considered in this study. One may note that the A_f is the minimum temperature in which the superelasticity occurs and ε_{max} represents the superelastic strain range, which is the maximum reversible strain without having the permanent deformation. The A_f and ε_{max} in NiTi and FeNiCuAlTaB are 53^{o}C and 5.7%, and -62^{o}C and 15%, respectively.

To develop the SMA-based and the SMA-MRF-based systems, each system had either four NiTi or four FeNiCuAlTaB wires where the length of each wire was 1000 mm with a cross-sectional area of 218.05 mm^2 and 116.80 mm^2, respectively, as presented in Table 3-2.

Table 3-1. The SMA material properties

Alloy	$\varepsilon_s(\%)$	$E_A Gpa)$	$\varepsilon_{max}(\%)$	$A_f(\,^o c)$	Reference
NiTi	4.6	45.3	5.7	53	[256]
FeNiCuAlTaB	13.5	46.9	15	-62	[256]

Table 3-2. The dimensions of the SMA bracing system

Material	Length(mm)	Area of each SMAs(mm^2)	Number of SMA wires
NiTi	1000	218.05	4
FeNiCuAlTaB	1000	116.80	4

3.3.2 MRF core

As the present work focuses on seismic applications for civil structures, a large-scale double MR fluid damper with the nominal maximum force 200 kN is selected [21]. The MRF damper can provide a wide range of force capacity, based on the value of the applied magnetic field. In this research, the system is studied for two electric current values, namely, 0 A and 1 A, which present the minimum and maximum possible electric currents to provide the minimum and maximum intensity of the magnetic field for this damper, respectively.

3.4 Results

In order to find the effect of SMAs, particularly superelasticity, in the SMA-based and SMA-MRF-based bracing systems, a lateral displacement, as shown in Figure 3-9, has been applied to the systems. This loading protocol increases steadily to investigate all of the possible phases in the SMAs and different velocities in the MRF-based damper in those bracing systems. As seen, the maximum and minimum applied displacements are 30.6 mm and -27.9 mm, respectively.

Another important parameter is the velocity of the applied load, which is required to calculate the loading in the MRF system with respect to the applied axial displacement. The loading protocol displayed in Figure 3-9 has a 0.5 Hz frequency. Hence, a wide range of velocities is applied to the MRF-based and SMA-MRF-based systems. The calculated velocity for the applied lateral displacement is illustrated in Figure 3-10 with the maximum and minimum velocity of 62mm/s and -64 mm/s, respectively.

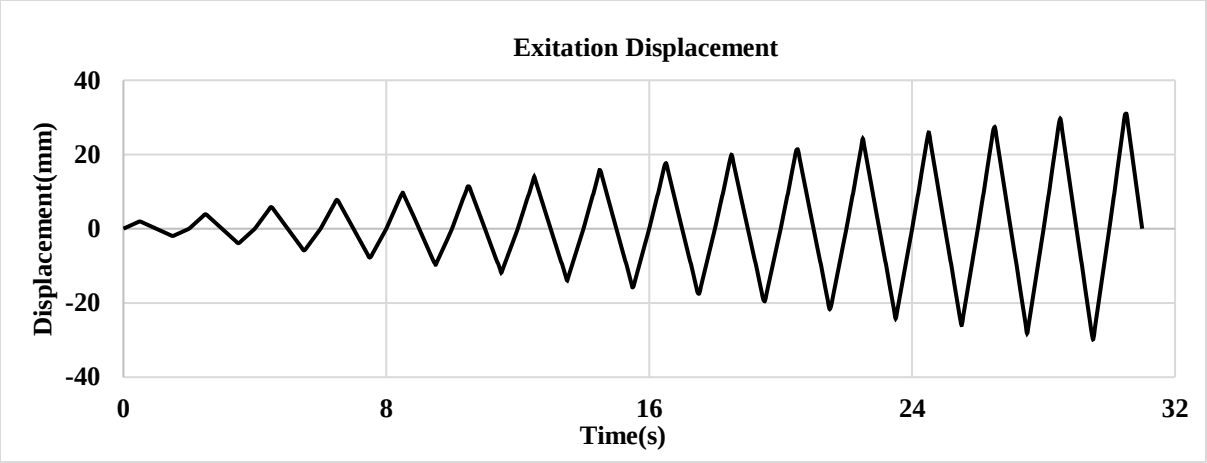

Figure 3-9. The axial excitation of SMA bracing systems and SMA-MRF core bracing system

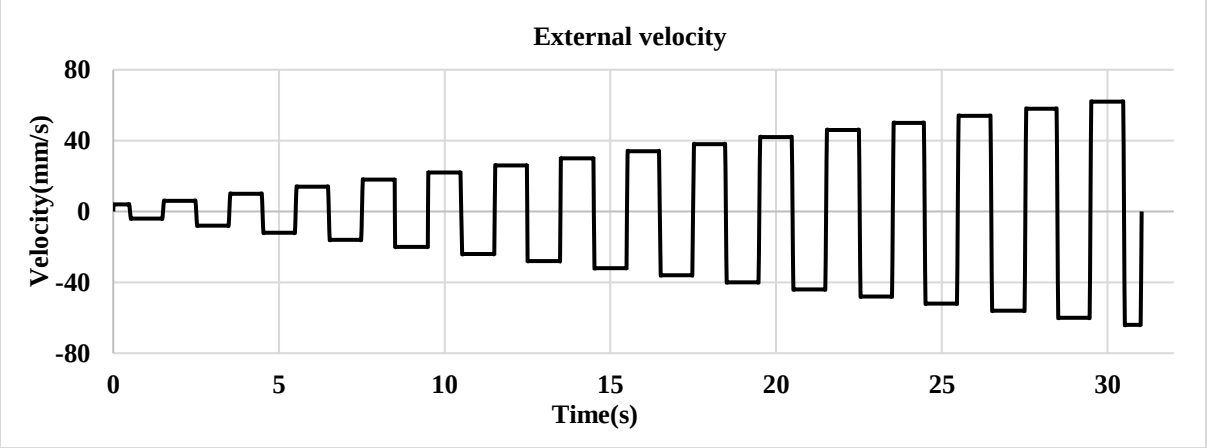

Figure 3-10. The equivalent velocity excitation of MRF-bracing systems and SMA-MRF bracing system

3.4.1 Hysteresis responses

The hysteresis responses of the SMA and MRF-based bracing systems with the suggested materials under the applied loading protocol are illustrated in Figure 3-11 to Figure 3-14, whereas the SMA-based, the MRF-based, and the SMA-MRF-based bracing systems with different SMA materials in inactive and active modes are presented. As depicted in Figure 3-11, the SMA-based systems are capable of working in both tension and compression states. The Martensite start forces for all SMA systems are about 175 kN. However, the corresponding Martensite finish forces of

FeNiCuAlTaB and NiTi are 181 kN and 190 kN, respectively. It is also noticed that by removing the external excitations, all the SMA-based bracing systems move back to the initial state. Therefore, the system can recover the original shape after unpredictable excitation, such as earthquakes. In the MRF bracing system, the peak force in inactive mode is about 52 kN, as presented in Figure 3-12(a), and it reached 175 kN in active mode, as illustrated in Figure 3-12(b). In the case of an emergency such as a severe earthquake, the electric power may not be available to energize the MRF core. Hence, Figure 3-12(a) represents the worst-case scenario.

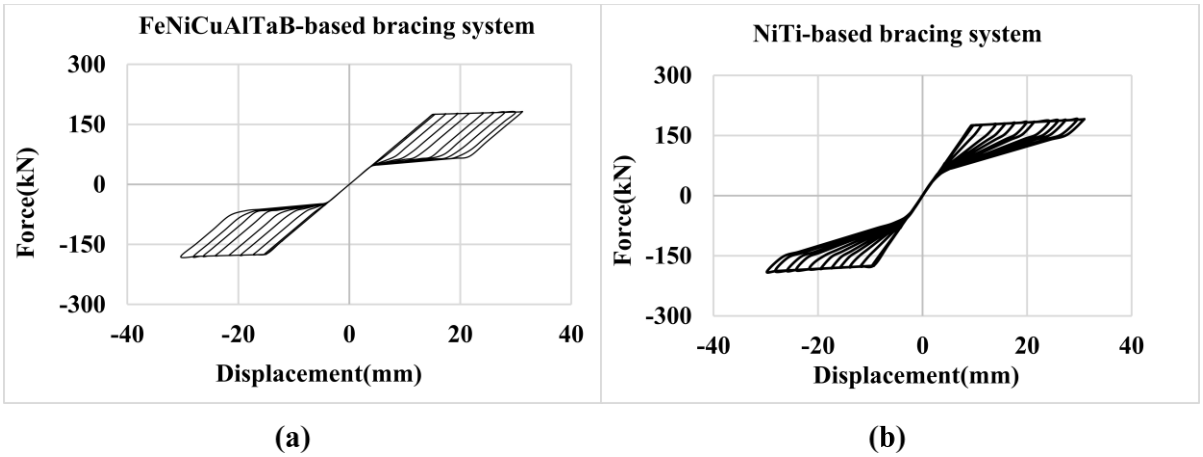

Figure 3-11. (a) Hysteresis of FeNiCuAlTaB SMA-bracing system, (b) Hysteresis of NiTi SMA-bracing system

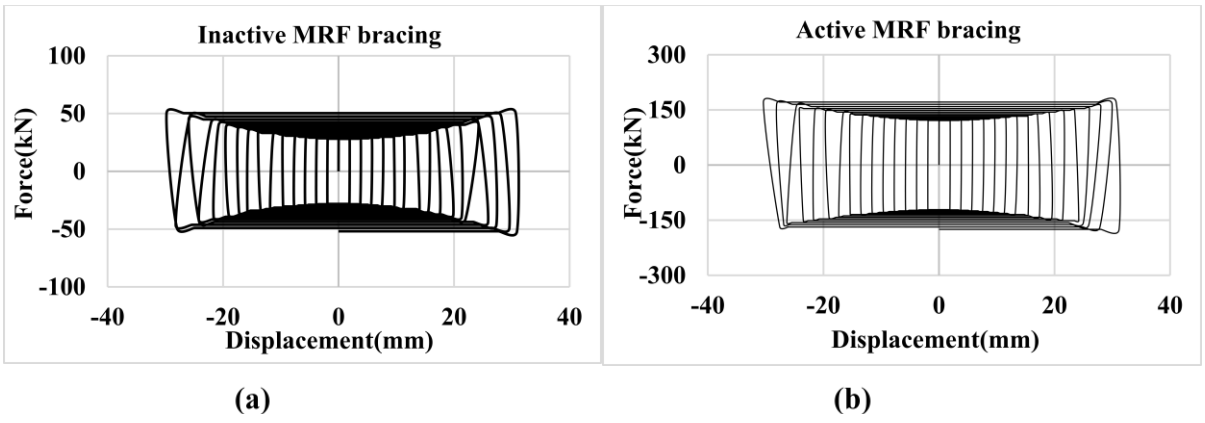

Figure 3-12. (a)Hysteresis of inactive MRF bracing system (Off state) (b) Hysteresis of activated MRF bracing system (On mode)

In the absence of the magnetic field in the SMA-MRF core bracing system, the hysteresis responses have been revealed in Figure 3-13. The peak force is almost 240 kN in FeNiCuAlTaB-based and increases to 250 kN in NiTi-based systems. It is noted that without energizing the MRF core, the SMA-MRF core bracing systems in all the SMA materials provide remarkably greater resisting force compared to the systems in which there are only SMA or MRF bracing systems.

The dynamic behaviours of all the SMA-MRF core bracing systems in the presence of a magnetic field are shown in Figure 3-14. It is found that the active systems provide greater resistance than those of the MRF-based and SMA-based bracing systems. It is also observed that the ratio of damping forces of active mode to inactive mode increases about 50.1% and 50.5% in the FeNiCuAlTaB-based and NiTi-based system, respectively. The hysteresis responses of the bracing systems (see Figure 3-14) indicate a significant drop in the recovery capability of the bracing systems while implementing MRF core to the bracing system. Moreover, energizing the MRF core up to the saturated value results in decreasing the re-centering ability of the systems. In order to activate the recovery ability of the SMA-MRF based system, the MRF core-based bracing can be switched from active mode to inactive mode. In other words, by implementing suitable controllers in the SMA-MRF-based system, the re-centering ability of this system is tuned. This feature can be used during and after seismic events, by switching the system from On to Off mode.

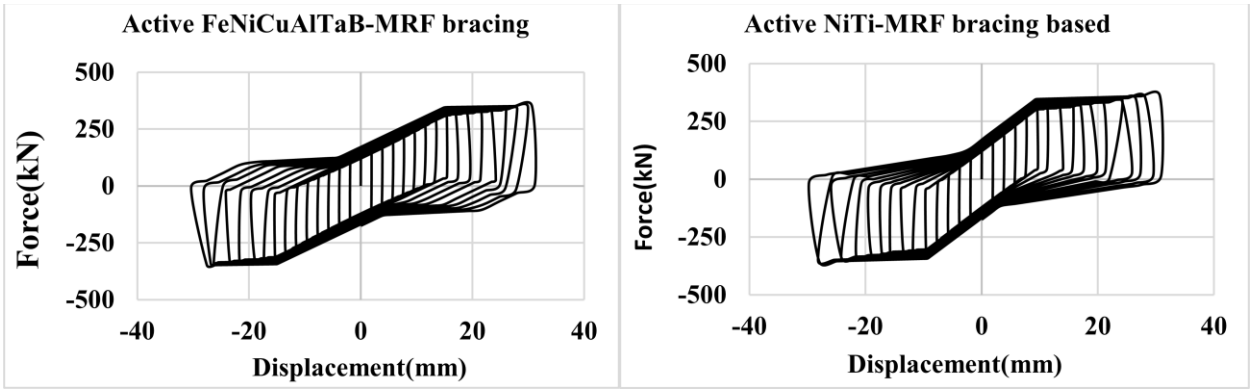

(a) **(b)**

Figure 3-13. (a) Hysteresis of an active SMA-MRF core FeNiCuAlTaB NiTi-based bracing system based, (b) Hysteresis of an activate SMA-MRF core NiTi based bracing system based

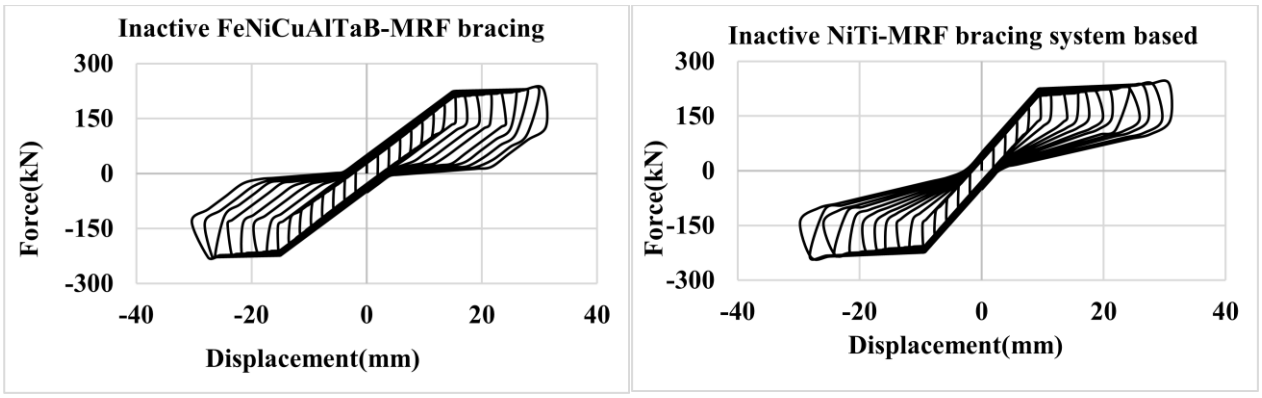

(a) **(b)**

Figure 3-14. (a) Hysteresis of an inactive SMA-MRF core FeNiCuAlTaB NiTi-based bracing system based, (b) Hysteresis of an inactivate SMA-MRF core NiTi based bracing system based

3.4.2 Energy dissipation capacity

One important finding is the amount of energy dissipation in bracing systems subjected to the loading, as displayed in Figure 3-15. This amount in the "Off" mode of MRF bracing is about 39.4 kJ, and in "On" mode, it increases to 145.92 kJ. As observed that the SMA bracing systems dissipate energy about 16.27 kJ and 17.3 kJ in FeNiCuAlTaB-based, and NiTi-based system,

respectively. Enforcing the MRF core into the SMA bracing system provokes to boost the magnitude in an inactive mode from 55.88 kJ to 162.22 kJ in NiTi-based MRF and shifts from 56.71 kJ to 163.2 kJ in FeNiCuAlTaB-based in active mode. It is observed that the systems with MRF core, even in inactive mode, dissipates a higher amount of energy compared to the systems with only SMA wires.

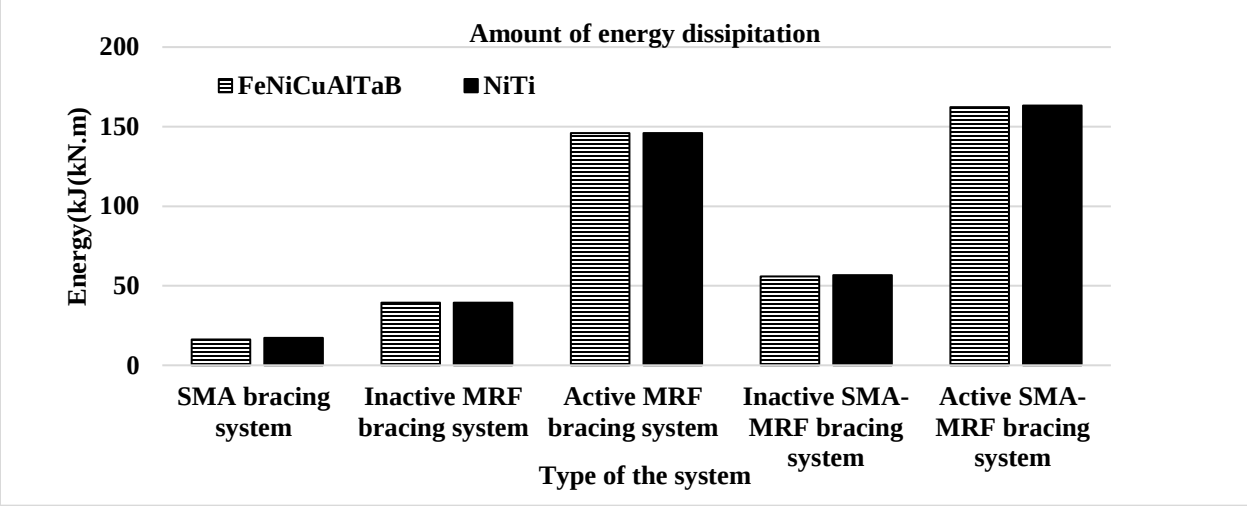

Figure 3-15. Amount of energy dissipations for all the systems

3.4.3 Equivalent viscous damping

In order to compare the equivalent viscous damping of all systems, the hysteresis responses for all the systems are computed for the last positive and negative applied loading, which has the maximum and the minimum displacement, respectively, as displayed in Figure 3-16 and Figure 3-17. Hence, there are two complete force-displacement cycles. In order to find the maximum equivalent viscous damping between the two complete cycles, which is a function of the maximum force, maximum displacement, and the energy dissipation capacity (see Eq.6), the absolute maximum damping force and displacement have to be calculated which occur under a positive

load, as displayed in Figure 3-16 and Figure 3-17. Thus, this load is used to calculate one parameter, namely equivalent viscous damping.

The equivalent viscous damping coefficients of all the systems are also computed based on the hysteresis responses of the bracing systems, as presented in Figure 3-18. The coefficient is about 0.32 in the MRF bracing systems with and without applying a magnetic field. However, the use of SMAs reduces this amount in SMA-MRF core bracing systems to 0.18 in FeNiCuAlTaB-based, and 0.17in NiTi-based systems. In the "Off" mode, it drops to 0.11 for FeNiCuAlTaB-based and 0.10 for the NiTi-based system. The comparison among all the systems proves that the minimum coefficient is about 0.04, which occurred in the NiTi-based SMA-bracing system whereas, the FeNiCuAlTaB provides 0.05 equivalent damping.

As observed, the equivalent viscous damping coefficients are calculated based on the amount of energy dissipation, the maximum displacement, and the damping force. Hence, these values are close in On and Off states of the MRF-based core are close.

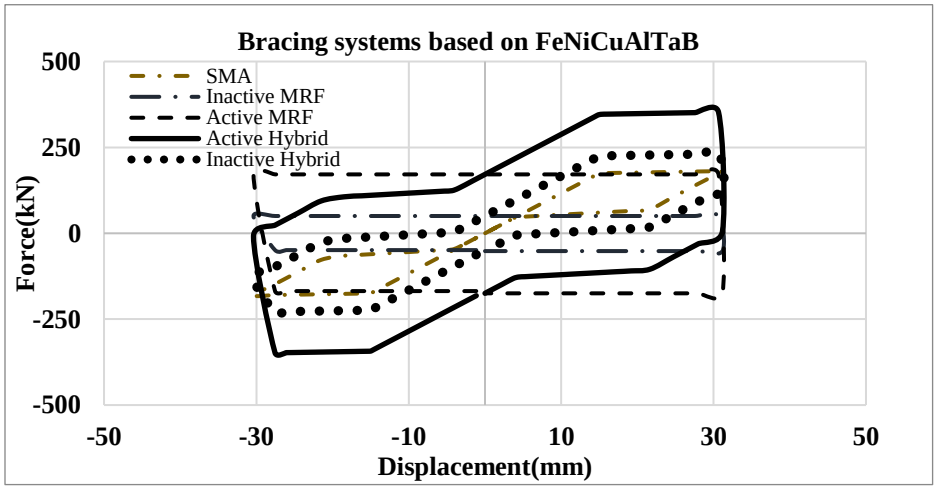

Figure 3-16. Hysteresis of FeNiCuAlTaB-based bracing systems and MRF-based systems

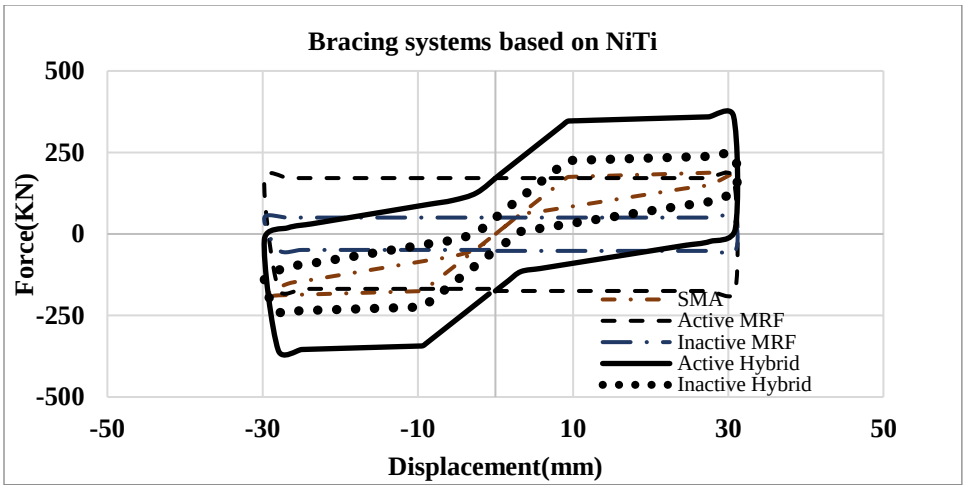

Figure 3-17. Hysteresis of NiTi-based based bracing systems and MRF-based system

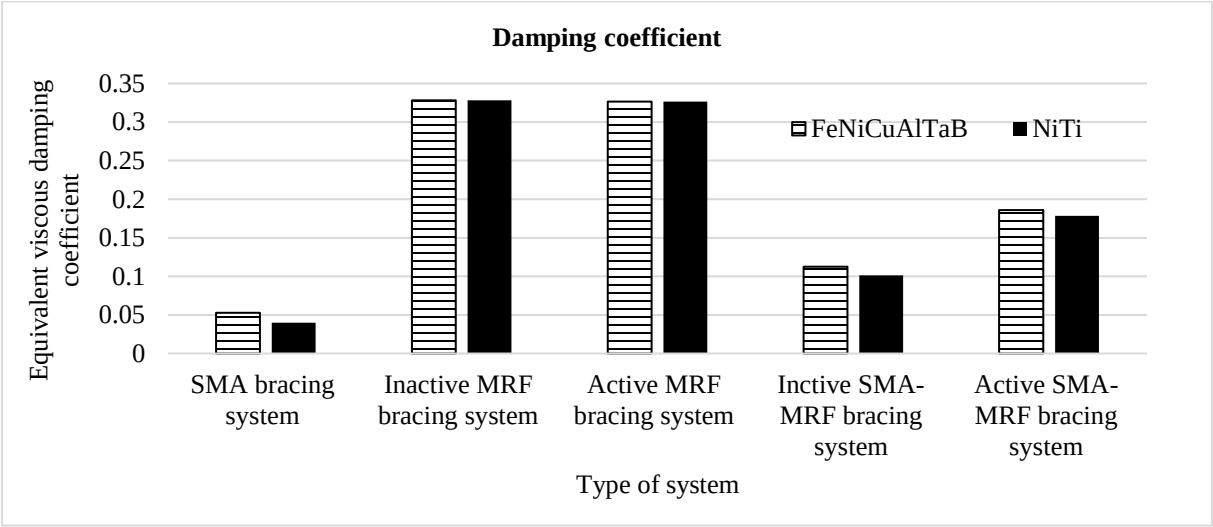

Figure 3-18. Equivalent viscous damping coefficients of all bracing systems

3.5 Conclusion

A novel efficient -semi-active SMA-MRF core bracing system has been introduced to be installed in building frames. This smart, bracing element significantly improves the stability of the structure by dissipating more energy of the applied dynamic loads and minimizing the permanent deformations. Several analytical models have been provided to illustrate the performance and functionality of the proposed model. The obtained hysteresis responses can be different from

Figure 3-8 because of loading conditions and assumptions for the analytical approach, SMA properties, and applied electric currents. The main conclusions of this study are as follows:

1. The implementation of the MRF core into the SMA bracing system increases the amount of energy dissipation even without applying a magnetic field in comparison with the SMA-based system. The increment of about 250% is observed in the active state of the SMA-MRF-based systems. It is noted that the difference between active and inactive SMA-MRF based system is about 190% for both used SMAs.
2. In the unloading phase, switching from active to inactive (On to Off mode) - in SMA-MRF bracing systems enhance the ability of the structure to re-center.
3. It is noted that ε_{max} of FeNiCuAlTaB is 15%, and that of NiTi is 5.7%. This value helps the system to recover the pre-defined state in larger strain. However, the applied strain on the bracing system does not go beyond 3% in real civil infrastructure.
4. The main advantage of FeNiCuAlTaB systems is the value of A_f which provides the ability of SMA to recover to the initial shape in the ambient temperature that is not possible for NiTi.
5. The study shows that recentering ability, energy dissipation capacity, and equivalent viscous damping coefficient are controllable. Hence. Each and/or all of them could be set with respect to a structural target(s).

Chapter 4: Design and Analysis of an SMA-MRF core-based bracing system

4.1 Introduction

In order to take the benefits of the SMA-MRF-based core bracing system in the civil infrastructure, the numerical model is required to be developed. A state-of-art hybrid SMA-MRF-based core bracing system is fabricated in-house to enhance the structural behaviour of the bracing system, including energy dissipation capacity and the equivalent damping coefficient. Experimental tests are conducted to illustrate the functionality of the system and the benefits of the SMA and the MRF systems. Furthermore, the numerical model of the SMA-based, the MRF-based, and the SMA-MRF-based systems are developed and validated.

4.2 Sizing the SMA-based bracing system

The SMA-based bracing, as displayed in Figure 4-1, used in this study, is similar to the one introduced by [87]. To develop the SMA-based, as well as the SMA-MRF-based systems, SMAs in the form of wires are used to insert into those systems. To select SMA wires' dimensions properly among all commercial available NiTi, two main constraints are considered. Firstly, the total maximum resistive force by SMA wires under tension and compression should be close to the damping force supplied by the activated MRF-damper. Another factor is the maximum allowable strain in SMA wires keeping wire between the Martensite start strain and the Martensite finish strain; it takes advantage of the recovery capability in the inelastic phase and the energy dissipation capacity in SMAs.

According to the fundamental properties of SMA and experimental tests, two wires having a 1.5 mm diameter and length of 170 mm are chosen for the tension loading. Similarly, two wires having the same dimensions are used for the compression loading.

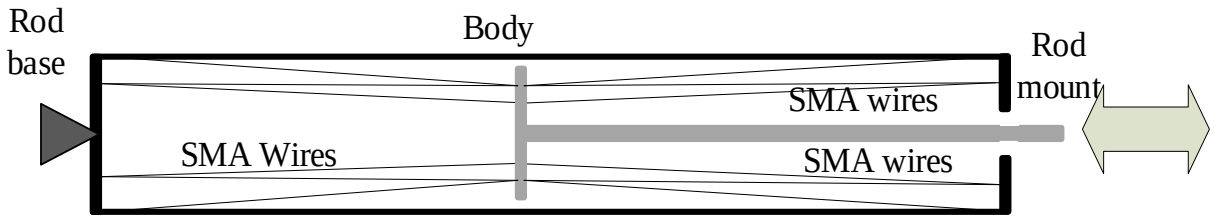

Figure 4-1. The schematic diagram of the SMA-based system developed by [114]

4.3 Sizing the MRF-based bracing system

The MRF-based bracing system, as shown in Figure 4-2, is originally a typical MRF damper which is installed diagonally in the frame. The damper, as the most common MRF-based system, is developed based on the direct shear mode of the MRF based [189].

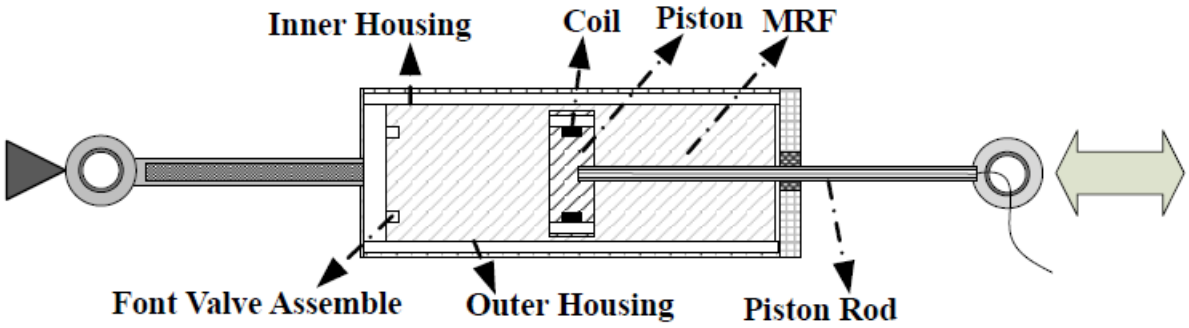

Figure 4-2. The Schematic diagram of the MRF-based system

Due to the natural characteristics of the MRF, as the working fluid, the damping force of the damper is a function of the magnetic field. The total amount of force, as presented in Figure 4-3, in MRF shear mode, can be computed by [258]:

$$F_{MRF} = F_{\eta} + F_{\tau} \tag{4.1}$$

where F_{η} and F_{τ} denote the viscous shear force and the magnetic-dependent shear force, respectively. The detail of the different transformation phases between F_{η} andF_{τ} can be found in [258].

In this study, it is assumed that the MRF damper and SMA-based system are massless and only have the damping and stiffness effect due to negligible masses of the MRF damper and SMA-based system compared to the structure.

In order to match the resistive force by the SMA-elements to the MRF-damper, the maximum force of the active MRF-damper is considered. Assuming the peak force of the scaled active MRF-based damper (max (F_{MRF})), the cross-sectional area of n SMA wires can be computed as:

$$A_{wire} = (3/n)\left(\frac{\max(F_{MRF})}{\sigma_{ms}}\right) \tag{4.2}$$

where σ_{ms} is the martensite stress of the SMA specimen. In the present study, two SMA-wires for the tension and two wires for the compression are used in the SMA-based systems as well as the SMA-MRF core bracing system.

Concerning the maximum allowable displacement in the MRF-damper, the length of each SMA-wire is determined to move to the beyond the Martensite start strain(ε_{ms}).

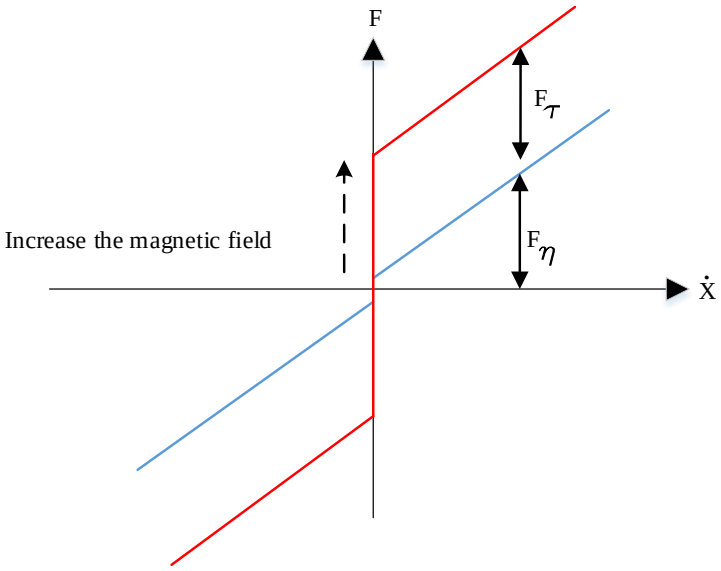

Figure 4-3. The schematic damping force vs. velocity by an MRF damper

4.4 Experimental Characterization of SMA and MRF dampers

4.4.1 Experimental Setup

In order to perform the experimental tests, a universal servo-hydraulic testing machine-MTS model 370.5 has been used. This loading frame machine has a 500 kN loading capacity with a 150 mm dynamic stroke with an in-built actuator and displacement sensor to run tests and collect data. The system also has a control scheme and software to execute the desired measurement, such as displacement. For most loads, the frequency range between 0.1-1 Hz, which is in the acceptable range. The schematic diagram of the system is shown in Figure 4-4.

The data monitoring and gathering have been conducted by software developed by the MTS machine's manufacturer. The experimental setup of the machine and the accessories in the Applied Laboratory for Advanced Materials and Structures (ALAMS) at the University of British Columbia, Okanagan campus, is illustrated in Figure 4-5.

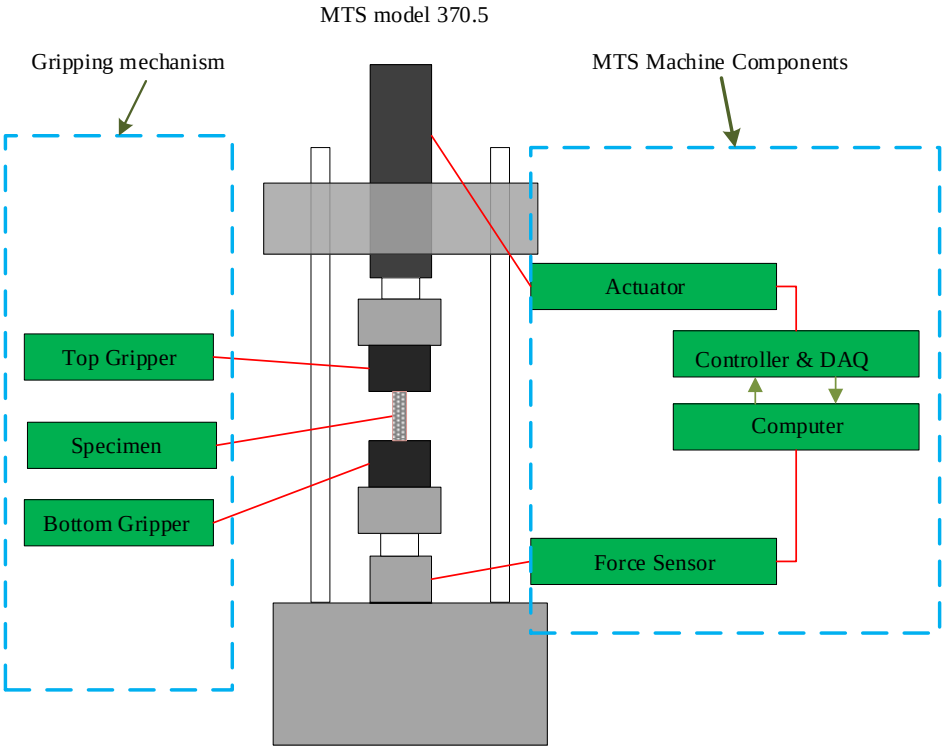

Figure 4-4. The schematic diagram of the setup configuration the experimental test

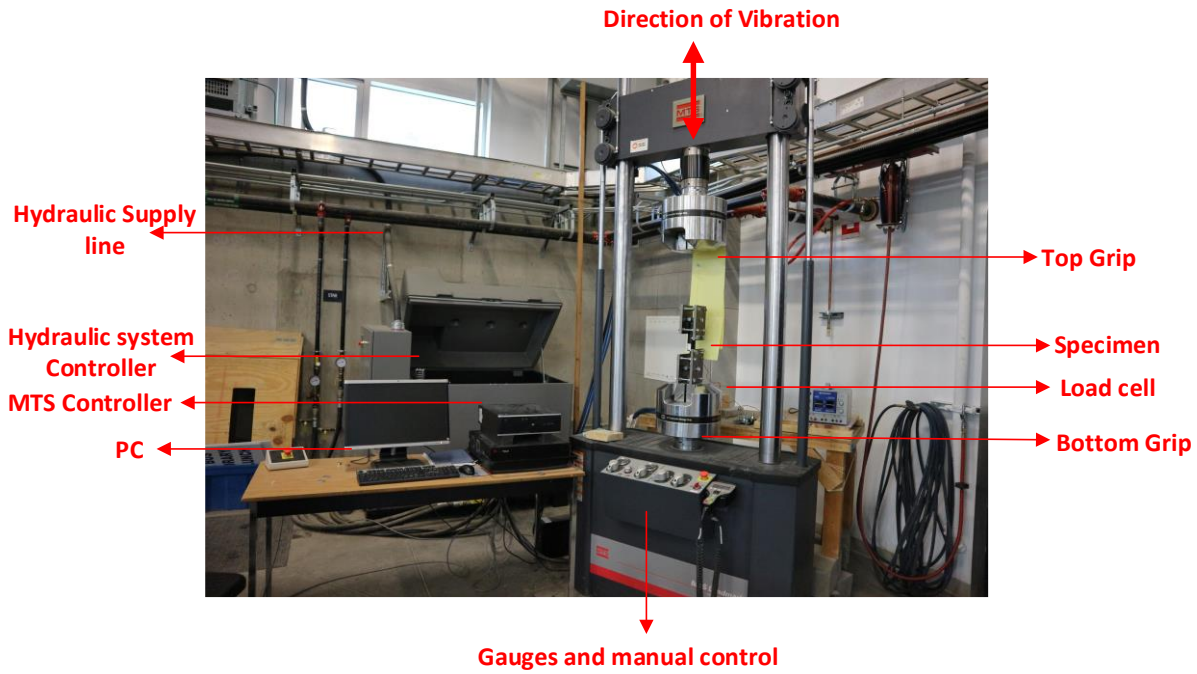

Figure 4-5. The MTS loading frame and the accessories

4.4.2 Shape Memory Alloy (SMA)

NiTi is the most common SMA among all SMAs [5]. In this study, the NiTi wire specimen manufactured by Confluent Medical Technologies Co. is used. Its characteristics are given in Table 4-1.

In order to determine the strain-stress response of the SMA, the specimen having a 1.5 mm diameter and 560 mm length is chosen. Due to the difficulty of keeping SMA in place by the machine grippers, two steel plates at the top and bottom grippers are used. Two ends of SMA wire are secured by steel bolts having 10 mm diameter and 145 mm in length and nut having 20 mm width across flat and 10 mm thickness of each plate. In addition, this action reduces the possibility of disconnection of the SMA specimen as a result of the fatigue due to the stresses at the ends of the specimen, as presented in Figure 4-6.

Table 4-1. The properties of NiTi shape memory alloy

PHYSICAL PROPERTIES	Value
Melting point (^oC)	1310
Density (g/cm^3)	6.5
Electrical resistivity (μohm-cm)	82
Modulus of Elasticity (GPa)	41
Coefficient of Thermal Expansion(\^oC)	11×10^{-6}
Ultimate Tensile Strength (MPa)	~1070
Total Elongation	~10%
Straight length(mm)	560
Diameter(mm)	1.5

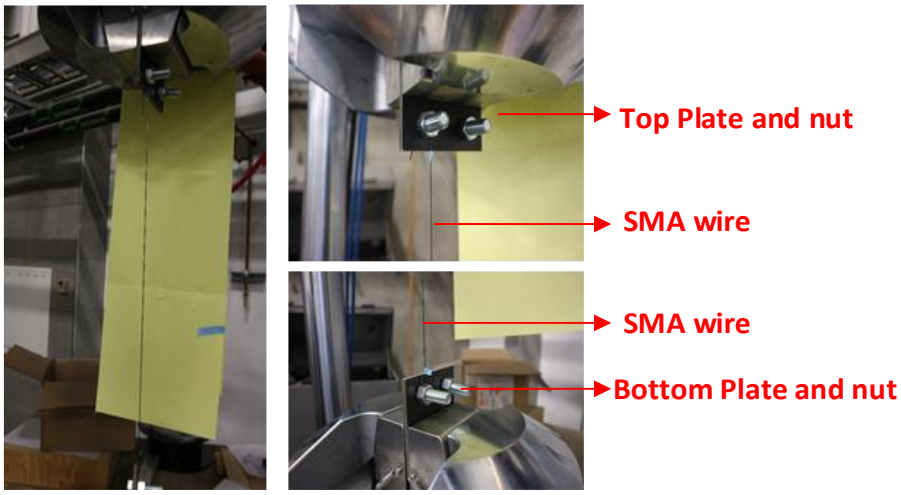

Figure 4-6. The experimental setup for the SMA specimen

In order to find the hysteresis response of the SMA, the loading protocol, as illustrated in Figure 4-7, is performed by the loading frame machine. To find the hysteresis responses of the SMA specimen, the static loading is applied by the MTS machine. The time period of this loading is remarkably greater than the loading introduced in Chapter 3 (Figure 3-9). The main reason for that is giving enough time to the specimen to change its state gradually and recover the original state

eventually. The maximum amplitude is about 4.7%the strain in the SMA, which is applied along ten cycles with a constant frequency [259].

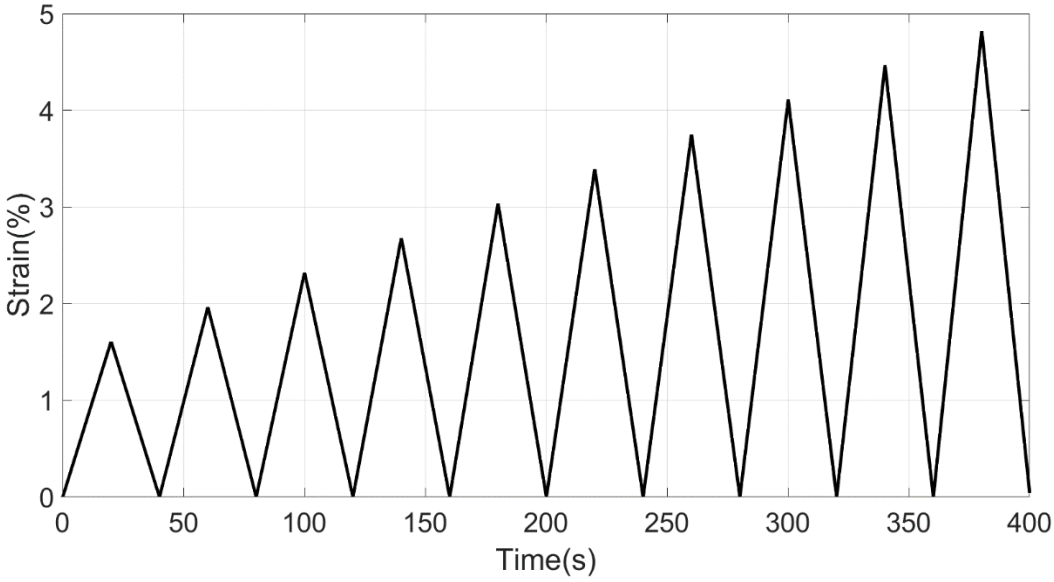

Figure 4-7. The applied load to the SMA specimen

The “uniaxial self-centering material” is selected to model the SMA part of the bracing system in OpenSees. The hysteresis behaviour of this material is displayed in Figure 4-8. It is observed that there are many parameters, such as “Initial Stiffness”, “Post-Activation Stiffness”, “Forward Activation Force”, “Ratio of Forward to Reverse Activation Force”, “Slip Deformation”, “Bearing Deformation, Ratio of Bearing Stiffness to Initial Stiffness”, that should be set to model the system in Opensees.

All parameters are set, as given in Table 4-2. After tuning, the strain-stress response of the uniaxial self-centering material is compared to the experimental data, as displayed in Figure 4-9.

The numerical hysteresis responses show that strains and stresses, particularly the Martensite strains and stresses and Austenite strains and stresses, are close to experimental results. In other

words, hysteresis responses in the OpenSees follow the experimental hysteresis responses in the loading and the unloading phase of every complete cycle. So, a good agreement between numerical and experimental results is found. After tuning the SMA model, the SMA dimensions are also scaled up with respect to the maximum force in the MRF-based damper; more details can be found in [259].

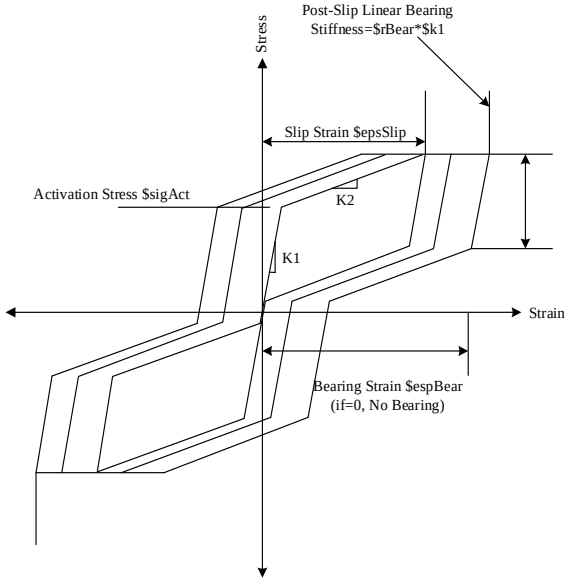

Figure 4-8. The strain-stress behaviour of "uniaxial self-centering Material" in the OpenSees [260]

Table 4-2. Parameters of self-centering materials

Properties	Value
Initial Stiffness	37,500 kN/mm^2
Post-Activation Stiffness	4500 kN/mm^2
Forward Activation Stress (Force)	450 MPa
Ratio of Forward to Reverse Activation Stress (Force)	0.86

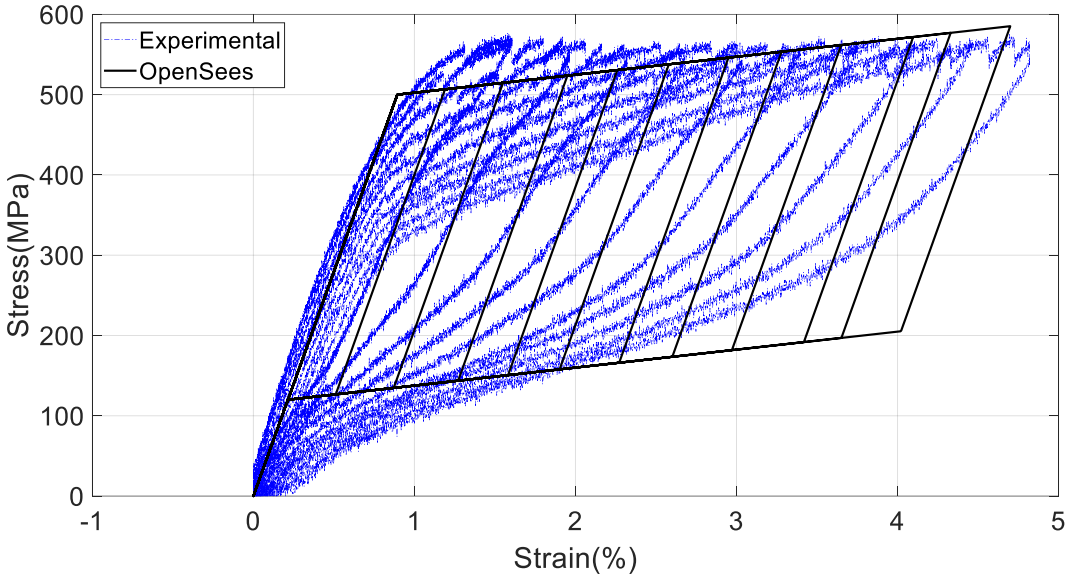

Figure 4-9. The comparison between hysteresis responses of the numerical and experimental responses

4.4.3 Magnetorheological fluid (MRF) damper

In order to find the dynamic response, namely force-displacement and velocity-force, an MRF damper model RD-8041-1 fabricated by LORD Co. is chosen, portrayed in Figure 4-10. The characteristics of the MRF damper is given in Table 4-3. The damper can provide a force greater than 2447N (peak to peak) with 1A electric current and also supplies the damping force in off-state (0 A), which is less than 667N (peak to peak). To activate the damper, it requires a 12 V DC to be activated. The continuous-time to keep the system fully energized for 1A is about 30s. It is also possible to apply a maximum intermittent of 2A to activate the damper.

In order to find the dynamic behaviour of the MRF-based damper, the loading protocol, as shown in Figure 4-11, is applied by the MTS machine [86,259]. The maximum amplitude is about 8 mm. the frequencies are between 1 Hz in the first cycle to 2 HZ in the last cycle.

Figure 4-10. The experimental setup for MRF damper

Table 4-3. The properties of the MRF damper (LORD®)

PHYSICAL PROPERTIES	Value
Stroke (mm)	74
Extended Length (mm)	248
Body Diameter(mm)	42.1
Shaft Diameter(mm)	10
Tensile Strength(N)	8896 max
Damper Forces (N), Peak to Peak, 5 cm/sec @ 1 A	>2447
Damper Forces N), Peak to Peak, 20 cm/sec @ 0 A	<667
Maximum Operating Temperature(°C)	60
Input Current, Continuous for 30 seconds(A)	1 max
Input Current, Intermittent(A)	2 max
Input Voltage(V)	12 V

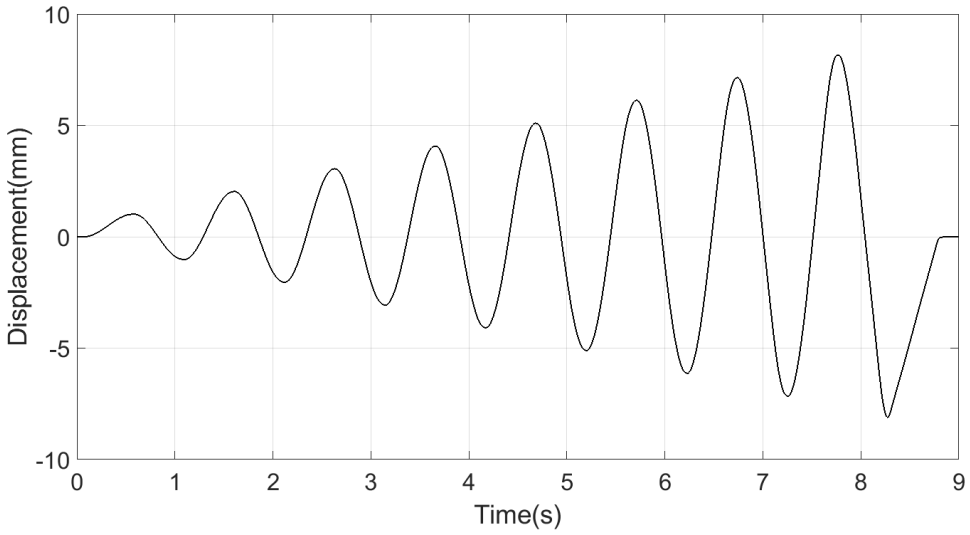

Figure 4-11.The applied load to the MRF damper

In order to characterize the MRF-based damper, the response of the different states of MRF –based damper, from the zero applied electric current (inactive, off-state) to the maximum applied current (the saturated state, active) have been investigated. To this end, the following activation currents were applied: 0 A, 0.2 A. 0.4 A, 0.6 A, 0.8 A, and 1A, to the studied MRF damper.

It is worth mentioning that there is no direct way to model the MRF damper in OpenSees. Hence, modeling the MRF damper is performed based on the working principles of this device. Two suitable alternatives are the "Viscous Damper Material" and "Viscous Material" which are available in OpenSees's library

In the present work, "Viscous Damper Material" is chosen to model the MRF damper [261], due to the similar actuation mechanism with the viscous damper. "Elastic stiffness of linear spring", "Damping coefficient", and "Velocity exponent", as the relevant parameters, are tuned by the trial and error method to achieve a good comparison with the experimental results. After setting those parameters, the force-displacement and the force-velocity of the numerical and the experimental models are compared, as presented in Figure 4-12 and Figure 4-13, respectively. In the minimum state (0A), the remarkable noise in the experimental data is observed due to the limitations of the testing machine. Overall, it is found that there is a good match between the numerical and experimental results.

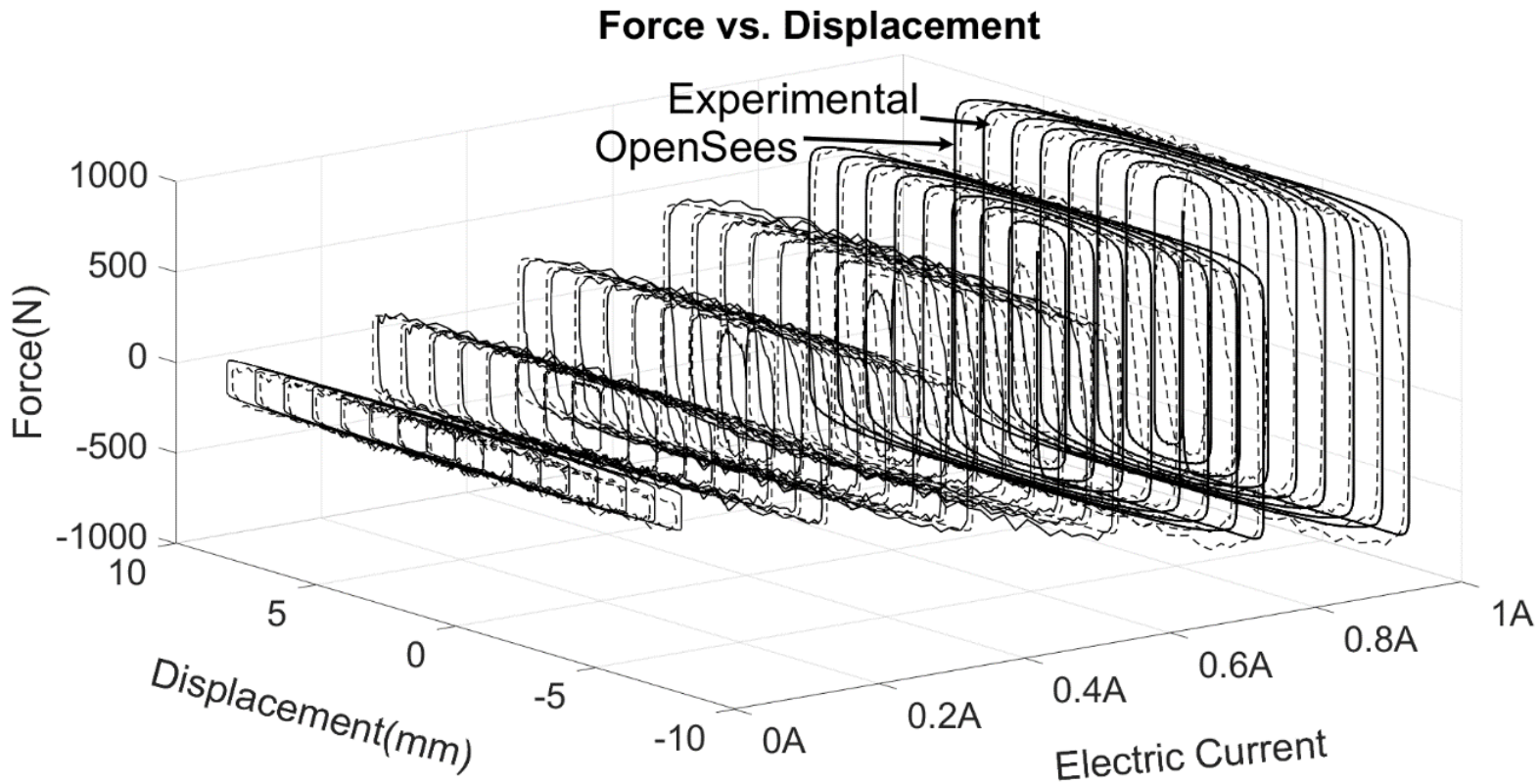

Figure 4-12. The comparison between hysteresis responses of the numerical and the experimental results of the MRF damper

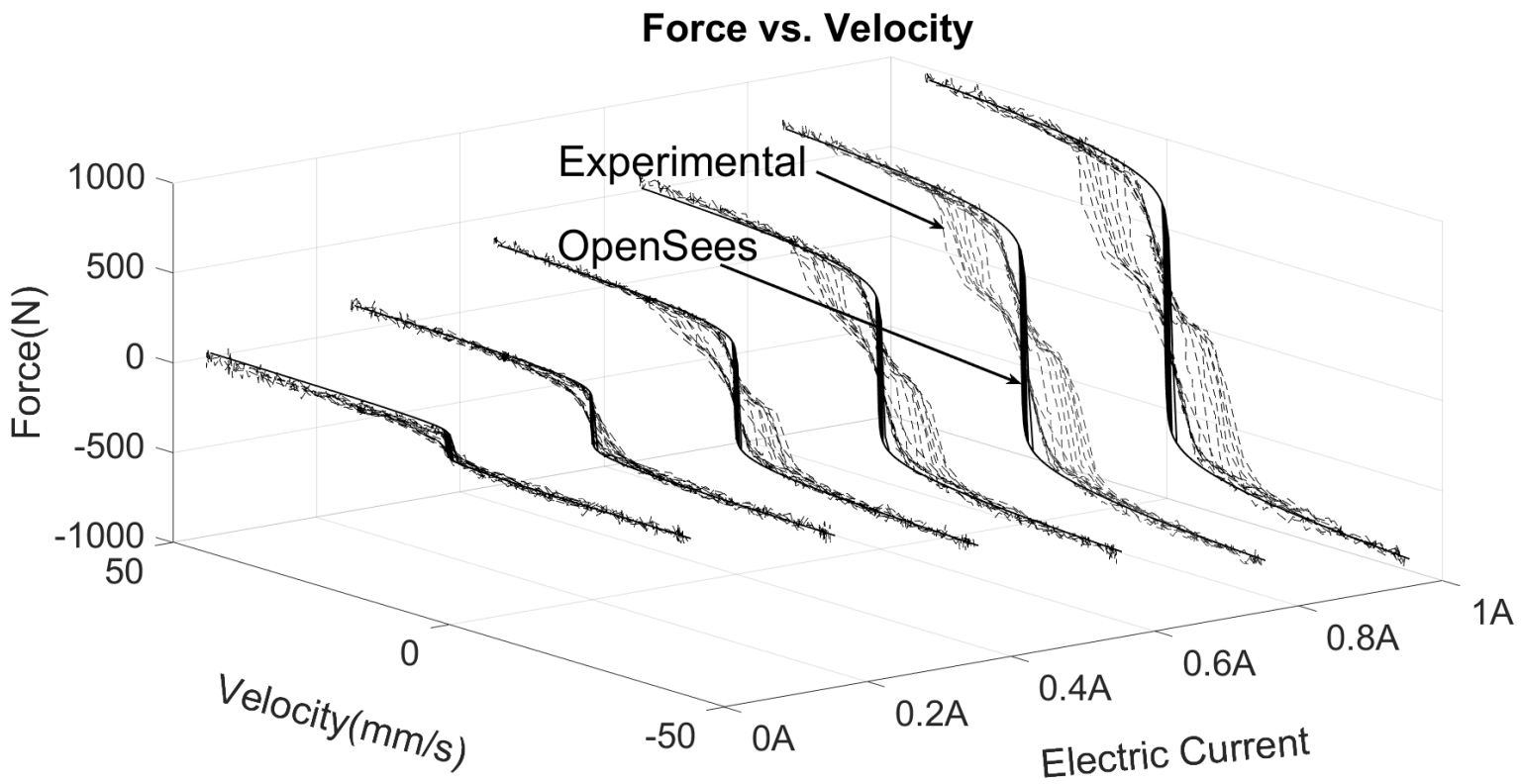

Figure 4-13. The comparison between force vs. velocity of the numerical and the experimental results of the MRF damper

4.5 The conceptual design of the SMA-MRF core bracing system:

The proposed system is composed of two steel tubes, MRF-based damper, SMA-wires, customized nuts, and bolts. The outer tube has a greater height than the inner one. Four customized nuts and bolts are connected to the outer cylinder, and four customized nuts and bolts are attached to the inner cylinder. The two ends of each SMA wire are held by customized nuts and secured to the body of the cylinder by customized bolts, as introduced in Figure 3-2. Each end of the MRF-based damper in the proposed system is fixed by two customized hooks.

4.6 Fabrication of the bracing system

In order to develop the prototype of the SMA-MRF core bracing system, the conceptual 3D design of the system is developed, as presented in Figure 4-14. As observed, two steel cylinders surround the MRF damper. The inner with the outside diameter (OD) 25.29 mm and outer steel cylinder with OD 26.22 mm are considered. The height of the inner and outer cylinders are about 252.00 mm and 278.40 mm, correspondingly.

The cylinders hold the two SMA wires by four customized nut and bolts for the tension state and keep another two SMA wires for the compression state by the other four nut and bolts. Two ends of each SMA wire having 1.50 mm diameter and 170.00 mm length are secured to the body of the cylinder by the customized bolts and nuts.

The bottom of the MRF damper and the inner cylinder are kept in place by a bolt with a 10.77 mm diameter passing throughout them; the two sides of this bolt are kept by two customized steel hooks. Similarly, the top of the MRF damper and the outer cylinder are secured by two hooks. These hooks have been designed so that the device can properly be grabbed in the MTS machine. Figure 4-14 shows the two-way SMA-MRF core bracing system. The details of the system are presented in Annex F.

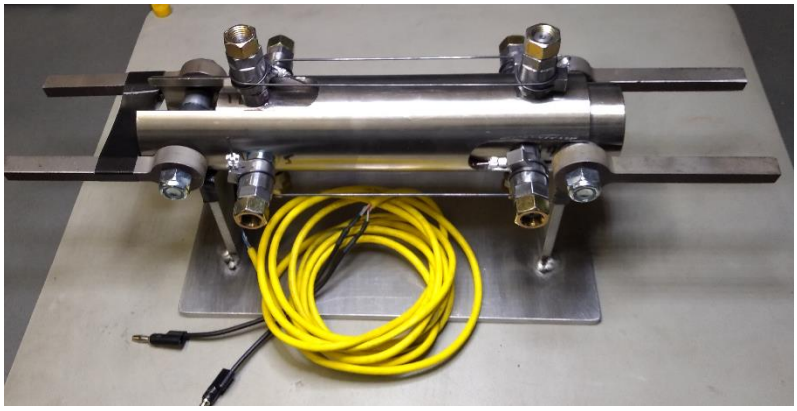

Figure 4-14. The prototype of two-ways SMA-MRF core bracing system

4.7 Experimental setup

In order to evaluate the performance of the proposed system, it has been experimentally tested by the loading frame machine. Figure 4-15 illustrates the experimental setup at ALAMS at the University of British Colombia, Okanagan campus. The loading frame machine and its main components are presented in Figure 4-16.

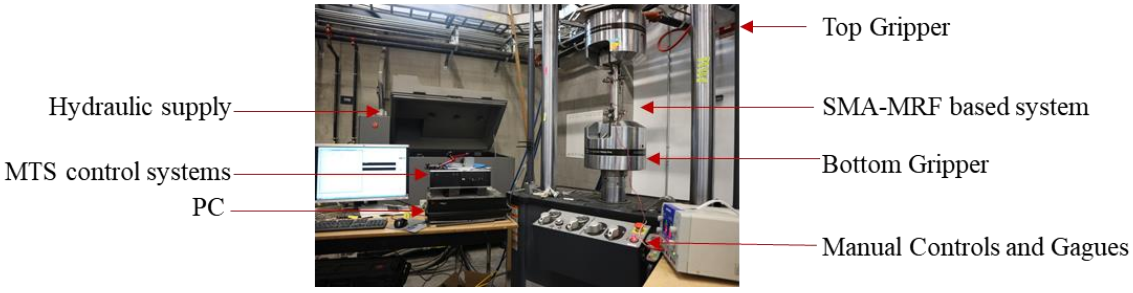

Figure 4-15. The MTS loading frame machine with its accessories

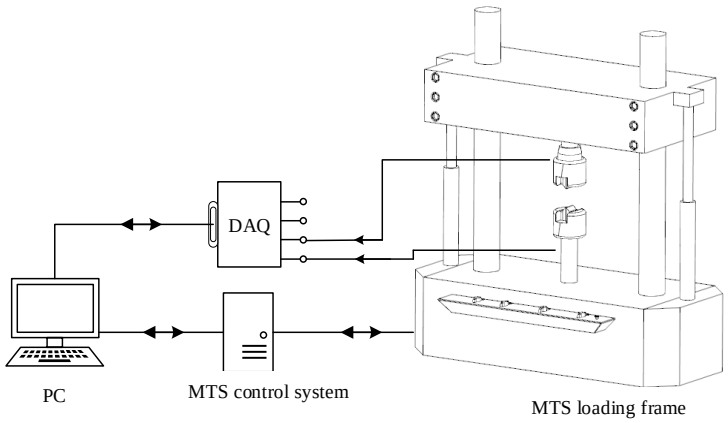

Figure 4-16. The typical diagram of the setup configuration the experimental test

4.8 Characterization of the SMA-MRF damper

In order to find the hysteresis behaviour of the SMA-MRF core bracing system, it is secured between the top and the bottom gripper of the MTS machine directly, as presented in Figure 4-17. In the next step, a loading protocol, as displayed in Figure 4-18, is applied to the specimen. As observed, the loading protocol includes one complete cycle, with a frequency of 1 Hz, which is the maximum allowable frequency in the MTS machine, and the maximum amplitude of 7 mm.

Figure 4-17. The two ways SMA-MRF core bracing system

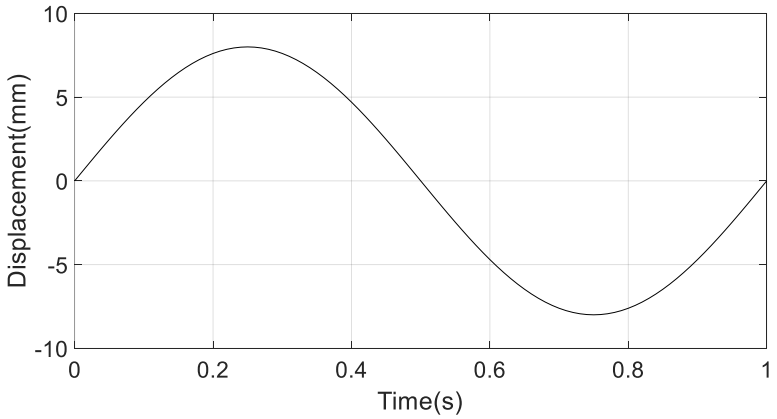

Figure 4-18. The loading protocol applied by the MTS machine

The SMA-MRF-based system is tested under applied 0A and 1A under the same loading protocol. The experimental results are presented in Figure 4-19. It is observed that the system is capable of providing the damping force under the tension as well as the compression with and without applied electric current. Furthermore, activated and inactivated hysteresis responses are symmetrical. It means the system behaves the same in tension and compression, regardless of loading's direction. It is seen that the maximum forces of the system are controllable and varied between 3076 N and 2355 N under 0A and 1A, respectively.

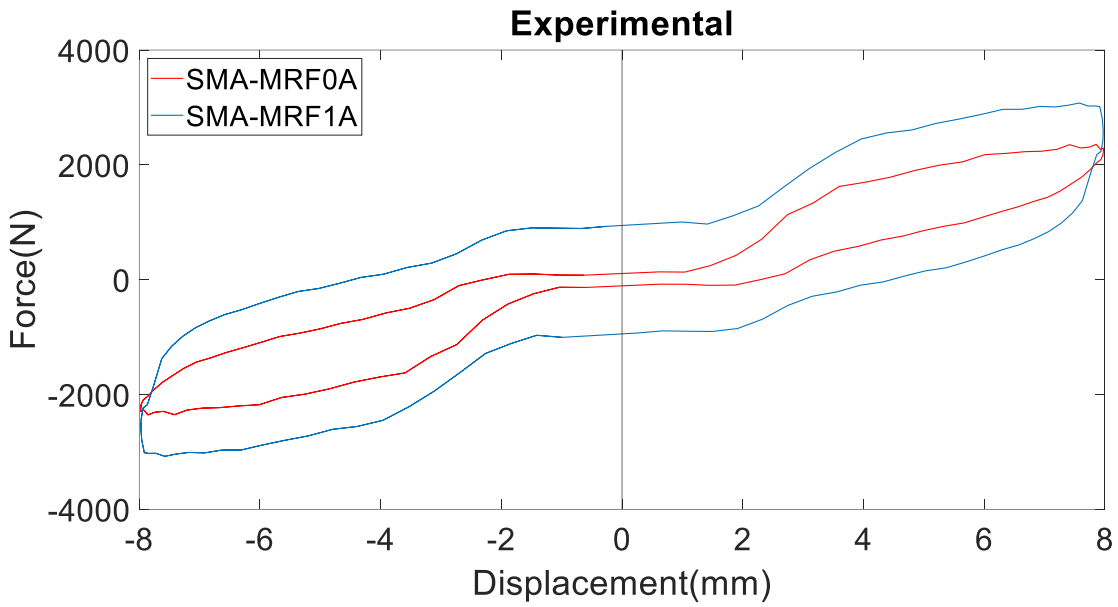

Figure 4-19. The experimental results of the SMA-MRF based core bracing system

4.8.1 Energy dissipation capacity

The energy dissipation capacity of the SMA-MRF-based system is calculated and shown in Figure 4-20. In the inactive state of the system, the system can absorb about 18 kJ of energy and changes up to 51 kJ in the active state of the system. It is noted that the SMA components of the system in an inactive system make a major contribution to the absorption energy capacity. Since the system is energized, the MRF-core-based system enhances the capacity of the systems, a remarkable

increase of about 183%. Thus, the energy dissipation capacity of the system is controllable and can be changed upon the applied electric current. It is a vital outcome of the system to enhance the dynamic behaviour of the civil infrastructure equipped with this novel bracing system by impending a good control strategy.

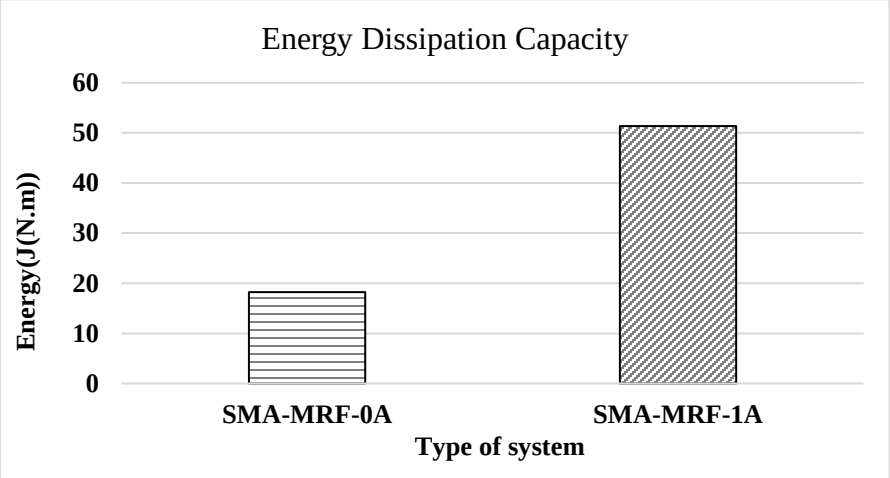

Figure 4-20. The comparison between the energy dissipation capacity of the active and the inactive SMA-MRF-based system

4.8.2 The equivalent viscous damping coefficient

The equivalent viscous damping coefficient is another studied parameter for this novel system. To compute the damping, fully activate (1A) and inactive (0A) systems are considered, as shown in Figure 4-21. It is seen that the damping coefficients are about 0.08 and 0.24 in the inactive and active modes of the system, respectively. It means that the activation of the MRF-core based system increases the damping of the system. Hence, the controllability of the damping coefficient is a significant feature of the SMA-MRF-based system and can be tuned between the minimum and the maximum value with respect to the amount of the applied electric field. It is also observed that the system can provide the damping coefficient in the inactive state of the system. Rephrasing,

the system, as a passive system, is capable of damping the dynamic response of the civil infrastructure experiencing external loading.

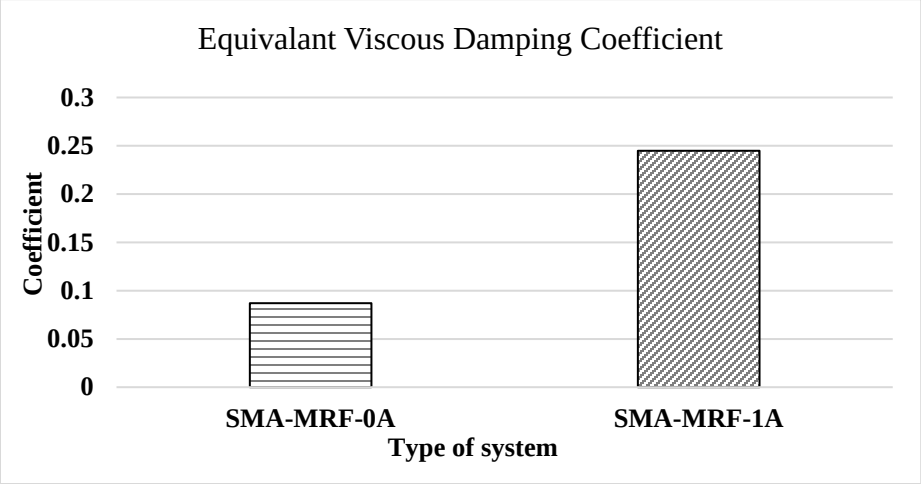

Figure 4-21. The comparison between the equivalent viscous damping coefficient of active and inactive SMA-MRF-based system

4.8.3 Validation results:

To validate the numerical results of the SMA-MRF based system, the OpenSees is used to develop the numerical model of the SMA-MRF based system. From the library materials of OpenSees, the "SelfCentering" materials and "ViscousDamper" are chosen to model the SMA wires and the MRF-based damper, respectively.

The two material models are modeled parallel to simulate the behaviour of the SMA-MRF based system, which can be considered as a new model. Then, the model is exposed to the same loading protocol introduced in Figure 4-23.

The comparison between the numerical and experimental results is conducted and displayed in Figure 4-22 and Figure 4-23. As observed, there is a good match between numerical results and experimental results in the 0A state as well as the 1A state. In other words, the numerical model actuates in the pressure as well as compression loading and absorbs the energy in both ways.

However, a slight difference between experimental and numerical results close to the center is observed. It is mainly due to slipping SMA wires around the customized nuts and bolts, which affect the recentring capacity.

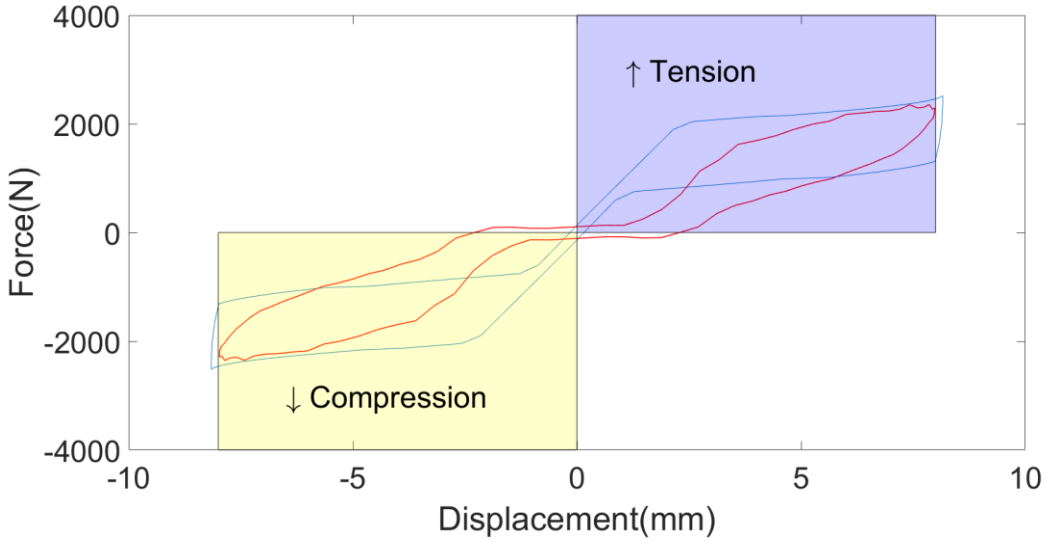

Figure 4-22. OpenSees and experimental results in the inactive state (0A) of the SMA-MRF based system

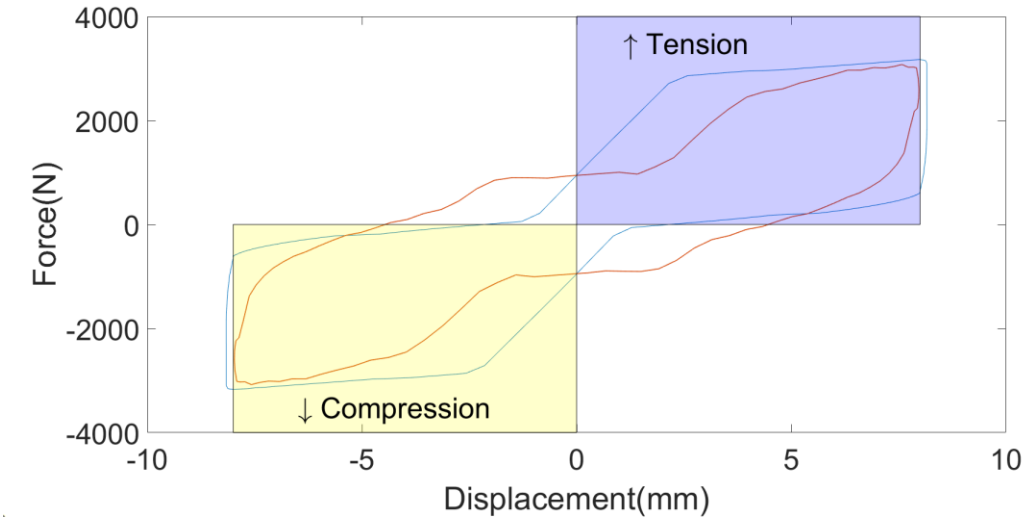

Figure 4-23. OpenSees and experimental results in the active state (1A) of the SMA-MRF based system

4.9 Conclusion

In this study, the proof of concept of the semi-active bracing systems based on the SMA-MRF has been proposed to implement into civil infrastructure. According to novelty in design, the system is a two-way system. In other words, the system can work while the systems move forward and backward (the tension and compression mode) under external excitation. The main outcome of the research are as follows:

1. The system supplied the tunable resistive force subjected to the tension as well as compression loads equally. Thus, the performance of the system is verified experimentally.
2. The hysteresis responses and the maximum resistive forces of the system can be changed regarding the amount of activation of the MRF-based core.
3. It is found that the energy dissipation capacity of the system is a function of SMA and applied electric currents upon the MRF-based core. Hence, the energy dissipation ability is controllable and can be tuned concerning desired outputs.
4. It is observed that the equivalent viscous damping coefficient of the proposed system can be set due to the amount of applied electric currents.
5. The dynamic response of an SMA-based, MRF-based, and SMA-MRF based bracing systems have been generated and obtained in OpenSees. The numerical models of the main components of the bracing system have been validated numerically and experimentally.

Chapter 5: Numerical study of SMA-MRF Bracing Systems

5.1 Introduction

Civil infrastructures are vulnerable to catastrophic failure when exceeding the limit loading, requiring a reliable structural control mechanism to enhance the integrity and stability of the structure. Bracing systems improve the performance of the structures through increasing the stiffness of structures, the damping coefficient, and/or the energy absorption capacity. However, the functionality of those bracing systems is not controllable and may be altered after strong seismic events.

In this study, a smart bracing system based on multifunctional materials, particularly the shape memory alloy (SMA) and the magnetorheological fluid (MRF) has been developed. The superelasticity properties of SMA gives the capability of recovering the original state after remarkable deformation. Furthermore, the SMA dissipates the energy of the applied load in the loading-unloading mechanism. The viscosity of MRF is variable and depends on the intensity of the applied magnetic fields.

In the present chapter, to study its effect on the performance of the buildings, a numerical model of a two-story frame is developed by the Open System for Earthquake Engineering Simulation (OpenSees) software. Then, nonlinear time-history analysis is performed to compare the results of the modeled frame with and without the Viscous-based, the SMA-Viscous-based, and the SMA-MRF-based bracing systems under three simulated ground motion profiles. The comparison between drifts of all frames proves that the SMA-MRF-based bracing systems significantly preserve the structural integrity and result in a better seismic performance

5.2 Analytical Model of the SMA-MRF Structural Bracing System

In order to study the effect of a bracing system on the dynamic response of a structure, an idealized two-story frame similar to the one used in [262] is considered, as shown in Figure 5-1. The mass and stiffness matrix of the frame are given by [262]:

$$M = m\begin{bmatrix}2 & 0\\ 0 & 1\end{bmatrix} \tag{5.1}$$

$$K = \frac{24EI_c}{h^3}\begin{bmatrix}3 & -1\\ -1 & 1\end{bmatrix} \tag{5.2}$$

where M, and K are the mass and the stiffness matrixes of the frame. h, E and I represent the height, Young's modulus, and the moment of inertia, respectively. m represents in lumped mass.

The first two natural frequencies of the frame are given by [262]:

$$f_1 = \frac{3.464}{2\pi}\sqrt{\frac{EI_c}{mh^3}}, f_2 = \frac{6.928}{2\pi}\sqrt{\frac{EI_c}{mh^3}} \tag{5.3}$$

To find the dynamic equation of motion for the frame model, the equation of motion is expressed by [262]:

$$M\ddot{u} + C\dot{u} + Ku = -M\ddot{u}_g(t) \tag{5.4}$$

where $\ddot{u}_g$ and u is the ground acceleration and the displacement of the floor, respectively.

Inserting the structural control systems given into the frame, the damping and/or the stiffness of the frame are changed. Assuming massless control elements and ignoring their horizontal effect, Eq.(5.4) is modified to:

$$M\ddot{u} + C_{eq}\dot{u} + K_{eq}u = -M\ddot{u}_g(t) \tag{5.5}$$

where C_{eq} and K_{eq} are the damping matrix and modified stiffness matrix.

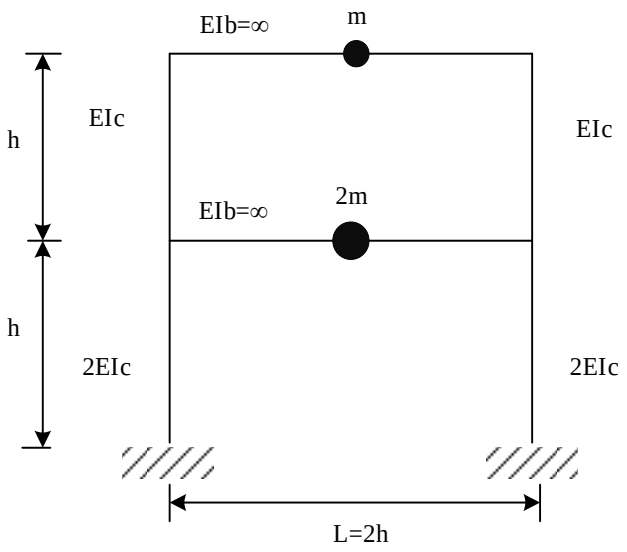

Figure 5-1. The two-story frame adapted from [262]

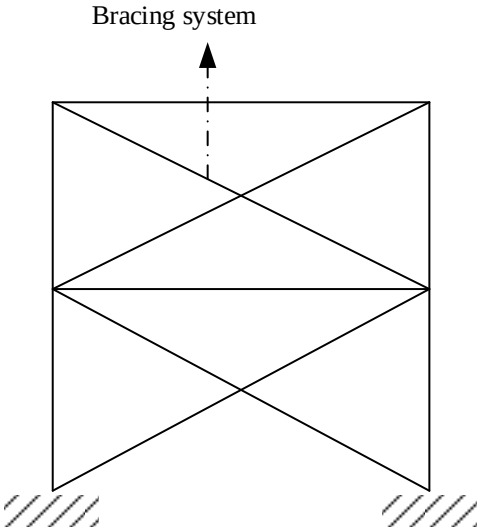

Figure 5-2. The schematic diagram of a 2DOF frame with structural control elements

Structural control system:

In order to improve the dynamic behaviour of the frame, the SMA-MRF (hybrid) based bracing system is installed in the frame, as shown in Figure 5-2. While the hybrid bracing system is under loading, it provides the resistive force ($F_{SMA-MRF}$).

In terms of the effect, the hybrid system on the equation of motion, Eq. (5.4) is rewritten as:

$$M\ddot{u} + C\dot{u} + Ku = -M\ddot{u}_g(t) - F_{SMA-MRF} \quad (5.6)$$

The SMA-MRF core bracing system is originally composed of a parallel arrangement of the SMA-based and the MRF-based systems. The force is composed of F_{SMA} and F_{MRF} by:

$$F_{SMA-MRF} = F_{SMA} + F_{MRF} \quad (5.7)$$

where F_{SMA} and F_{MRF} denote the force supplied by the SMA-damper and the MRF-damper, respectively. These dampers add stiffness and damping forces to the structure that are used to control the natural frequency and equivalent damping ratio of the structure.

5.3 Modeling the SMA-MRF damper into a two-story frame

In order to model and analyze the introduced frame, as presented in Figure 5-1, OpenSees software is used, and the proper material models are chosen for the model from the materials library in OpenSees to develop an accurately representative model of the frame [259]. It is an idealized two-story frame, fixed to the ground, four massless column, and two rigid floors.

In the first step, for modeling purposes, the two-story frame with a height of 3657.6 mm and a bay length of 7315.2 mm is considered. The weight of the first and second floor are about 2000 kN and 1000 kN, respectively. Each column has the moment of inertia 133.194×10^6 mm^4 and the area of 40909.5 mm^2. The material of columns has the Young modulus of 206.84 kN/mm^2.

In order to validate the numerical model of the frame in OpenSees, the first two-natural frequencies are obtained in OpenSees and compared to the analytical results using Eq.(5.3). The first and second natural frequencies, using the two approaches, are about 1.28 Hz (f_1) and 2.63 Hz (f_1), respectively. Hence, the numerical model is a good match with the analytical

5.4 Seismic control of frame structure integrated with the SMA-MRF core bracing system

The effectiveness of Viscous-based, the SMA-Viscous-based, and particularly the SMA-MRF-based systems in providing the structural stability in the time-domain subjected to dynamic loading is studied. Then, to control the structural behaviour of civil infrastructures in the time-domain, many structural elements need to be considered. However, an alternative and more efficient approach to investigate the control issues in civil infrastructure is transforming the time-domain responses to frequency-domain responses. Hence, the control approach is based on structural amplitude responses for a specific bandwidth of the frequencies. Commonly, the bandwidth is the first few natural frequencies of the civil infrastructure.

In this chapter, a frequency analysis of the simplified frame with and without the structural control element has been performed to study the influence of the conventional and novel structural control system in the frequency domain.

In order to enhance the functionality of the SMA-MRF based system, a simple On-Off control algorithm has been designed and embedded in the modeled frame to suppress the structural amplitude in the desired frequency bandwidth. The dynamic response of a simplified 2DOF structure equipped with the Viscous-based, the Viscous-SMA-based, and the developed hybrid SMA-MR-based systems have been conducted using the OpenSees. A comparison between the present SMA-MRF-based and the Viscous-based systems has been performed. It is observed that, upon activation, the developed SMA-MRF-based structural control system reduces the amplitude of the maximum drift ratio of both degrees of freedom in a wide range of the frequency spectrum of the structure.

5.5 Design and modeling of structural stability control elements for earthquake

While presenting a novel hybrid control element, the present work compares the performance of a simplified two-degrees of freedom (2 DOFs) structure equipped with the present hybrid SMA-MRF-based element, the Viscose-based, and the SMA-Viscous-based under three earthquake profiles. In chapter 3, the SMA-MRF-based system has been introduced in detail. However, one of the most conventional systems is the viscous-based system. Here, the brief of the viscous-based system is discussed.

5.5.1 Viscous-based control element

Due to the similarity of the working mechanism between the MRF-based system and the Viscous-based damper, the Viscous-based system is as a common passive system is considered to compare their performance on the frame. A viscous damper is a cylinder-piston filled with a polymer liquid, as shown schematically in Figure 5-3. The amount of force generated in a viscous damper is proportional to the rate of change in piston displacement, i.e. the velocity of the piston rod. The relation between force and velocity of a typical viscous damper can be expressed by [26,263,264]:

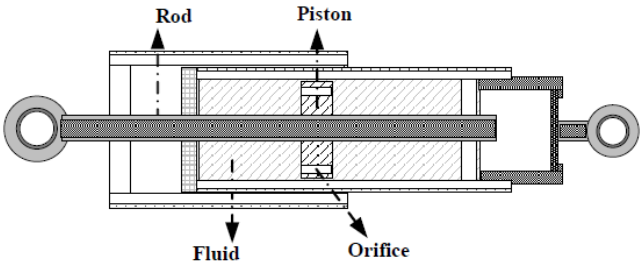

Figure 5-3. The schematic diagram of a viscous-based structural control system adapted from [263]

$$F_{Viscous}(t) = C_d|\dot{x}|^{\alpha} sgn(\dot{x}(t)) \quad (5.8)$$

where C_d, α, and $\dot{x}(t)$ represent the damping coefficient, the velocity exponent, and the piston rod displacement, respectively.

To model a viscous-damper in the OpenSees, the behaviour of the damper has been considered as the superposition of a spring and a dashpot, as shown in Figure 5-4 [264].

$$F_{Viscous}{}'(t) = [(x_m(t) - sgn(F_{Viscous}(t))(|F_{Viscous}(t)|^{\frac{1}{\alpha}}/C_d)]K_d \tag{5.9}$$

where k_d and x_m represent the total spring displacement and the internal stiffness of the system.

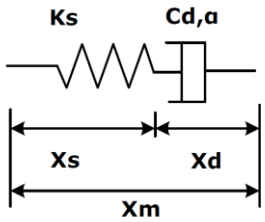

Figure 5-4. A linear spring element and a linear viscous dashpot element for modeling of a nonlinear viscous damper [26,263]

5.5.2 Modeling a 2 DOFs Frame

To study the influence of the structural control systems on the dynamic response, a 2D two-story frame with embedded bracing systems (X-shape) is considered, as shown in Figure 5-2. The dynamic response for the first and second stories have been determined; the results have been compared with that of the idealized 2D frame.

5.5.3 Frequency analysis

The drift ratio, an important structural parameter used in the structural stability assessment criterion, is defined as:

$$\mathrm{Dr} = \frac{\mathrm{u^r}}{\mathrm{h}} \tag{5.10}$$

where u^{r} and h stand for the relative displacement between two consecutive floors and the height of the floor, correspondingly.

To analyze the structural response of the frame in the frequency domain, the Discrete Fourier Transform (DFT) is applied to transform the drift ratio in the time-domain to the DRIFT RATIO (DR) in the frequency domain. The DFT for the given Dr with the length of n is computed by:

$$\mathrm{DRIFT\ RATIO(DR)[j\omega]} = \sum_{0}^{n-1} \mathrm{Dr[k]exp(-j\omega kT)} \tag{5.11}$$

For better presentation, Eq. (5.11) is simplified to:

$$(\mathrm{DR})_{\mathrm{n}} = \frac{1000}{\mathrm{n}} |\mathrm{DR[j\omega]}| \tag{5.12}$$

where $|DR[j\omega]|$ stands for the absolute value of the $DR[j\omega]$. $(\mathrm{DR})_{\mathrm{n}}$ is the normalized drift ratio.

5.6 Simulation of the stability control elements for earthquake

The effects of the stability control elements have been simulated for three ground motions (GM), namely, Christchurch (New Zealand. 2011), Darfield (New Zealand, 2010), and Parkfield (the USA, 1979). In the following subsections, the earthquake profiles have been presented. The response of the frame has been provided, and the influences of the frame under three ground motions have been studied.

5.6.1 Modeling Earthquakes

The properties of GMs are given in Table 5-1. It is seen that the strength of the earthquake is varied from 6.2 MW in Christchurch, 7MW in Darfield, and 6.0 MW in Parkfield. The acceleration profile of Christchurch, Darfield, and Parkfield are presented in Figure 5-5. As it is seen, the maximum absolute acceleration in Christchurch, Darfield, and Parkfield is 0.715 g, 0.238g, and 0.57g, respectively [265]. One may note that the GMs have been scaled down 1:2 original values.

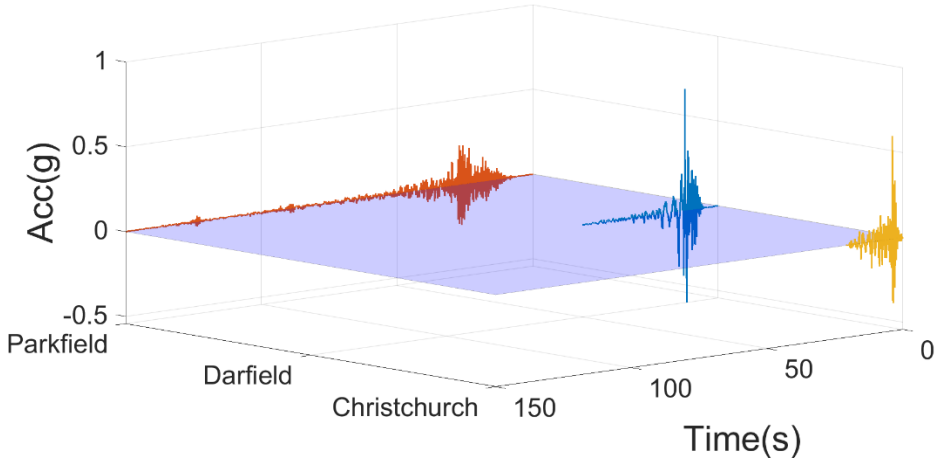

Figure 5-5. Acceleration time history of selected earthquake

Table 5-1. Selective ground motions and characteristics in three tectonic environments [265]

Earthquake	Year	Site	Mw	R(km)	Vs30(m/s)
Christchurch, NZ	2011	Resthaven	6.2	5	141
Darfield, NZ	2010	Resthaven	7.0	19	141
Parkfield	1979	P.F.Z.-1	6.0	3	178

5.6.2 Matching The MRF-damper to Viscus damper

In order to use the MRF-based damper in the SMA-MRF-based system bracing system, the numerical model is scaled up about 30.5 times greater than the original values [259]. The main reason is to match the maximum force in the MRF-based bracing system to the viscous-based bracing system, developed in OpenSess, as presented in Figure 5-6.

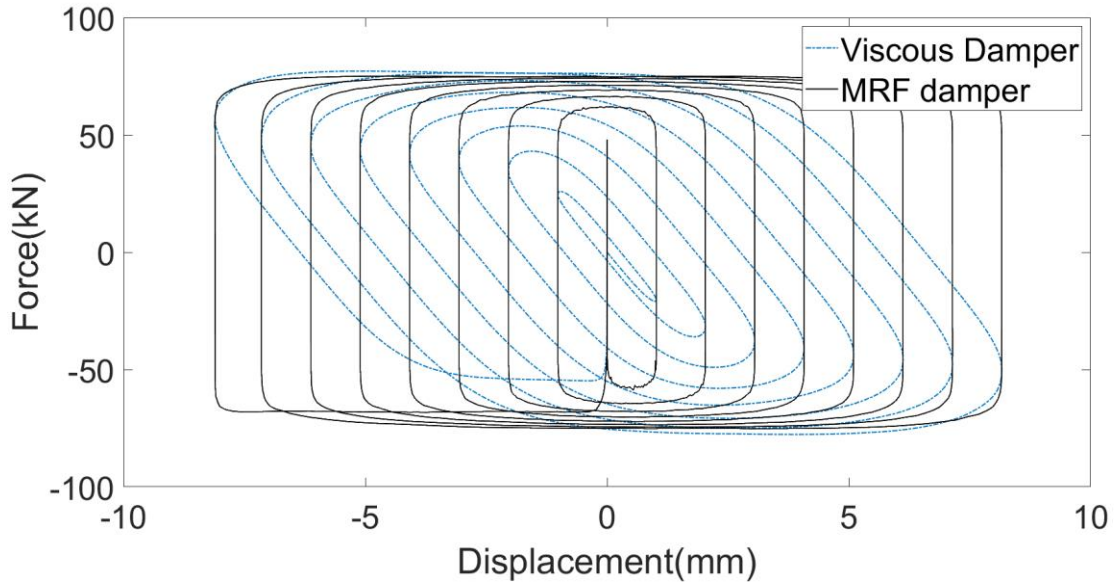

Figure 5-6. The matching the MRF-based bracing system's hysteresis respond to the viscous-based bracing system's hysteresis response

5.6.3 Effect of control element on GMs: time-domain response

To compare the functionality of the structural control systems, the displacement of the first story of the frame with and without the control systems has been determined under Parkfield GM, shown in Figure 5-7 and Figure 5-8. It has been observed that displacements of the frame surprisingly reduced by the SMA-MRF-based system in Off-state and particularly On-state. A comparison between maximum displacements under all GMs is presented in Figure 5-9 and Figure 5-10. It is seen that adding the SMA-MRF element reduces the maximum displacement of the first story for all GMs. On the other hand, activating the SMA-MRF system reduces the maximum displacement to 36, 24, and 13 for Christchurch, Parkfield, and Darfield, respectively. This approximately results in 45.4%, 54.7%, and 71.7% reduction for the three GMs, respectively.

Similarly, the maximum displacement of the second story has been determined for the three GMs when adding structural control elements and shown in Figure 5-10. Once again, one may realize

that activating the hybrid SMA-MRF system results in a sharp reduction, approximately 43%-83%, compared to the conventional system.

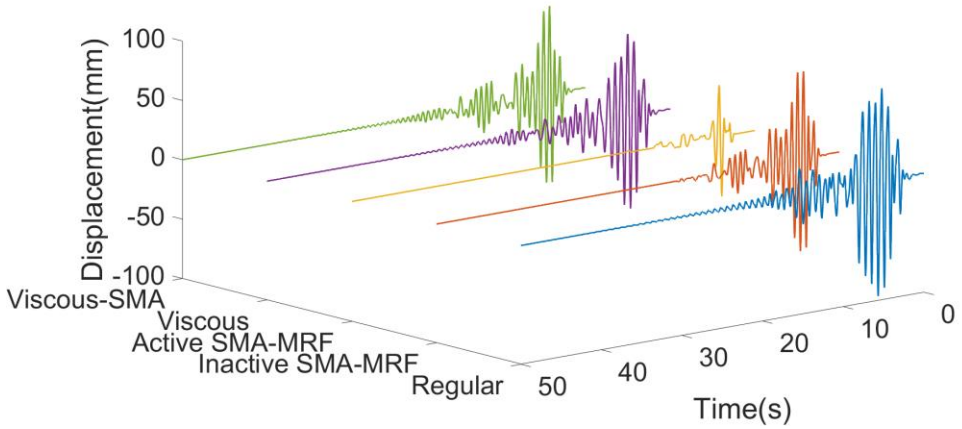

Figure 5-7. The displacement of the first floor under the Parkfield ground motion

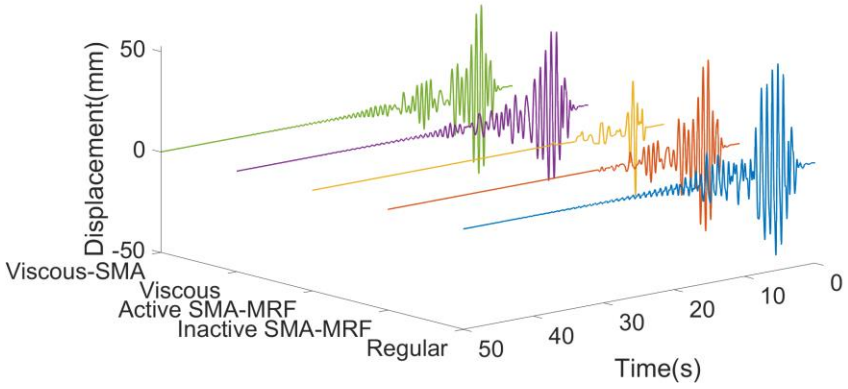

Figure 5-8. The displacement of the second floor under the Parkfield ground motion

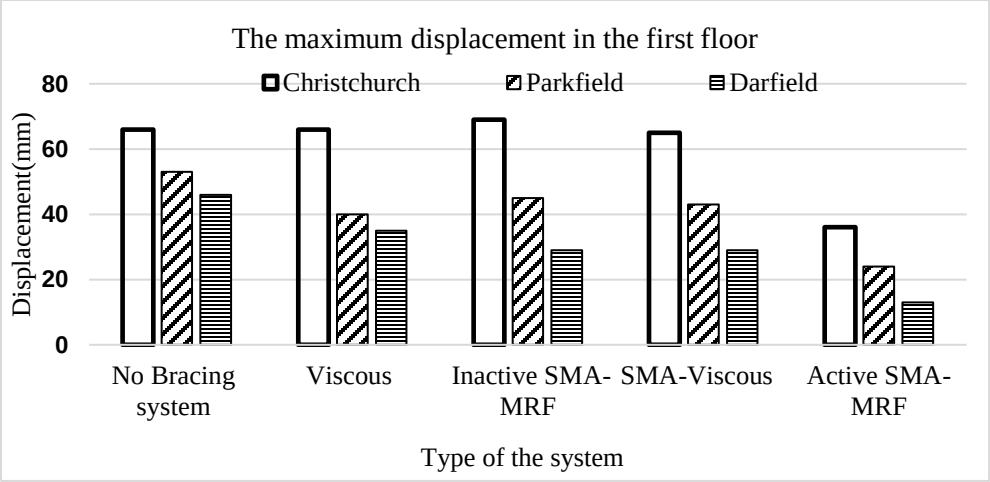

Figure 5-9. The maximum displacement of the first story on GMs

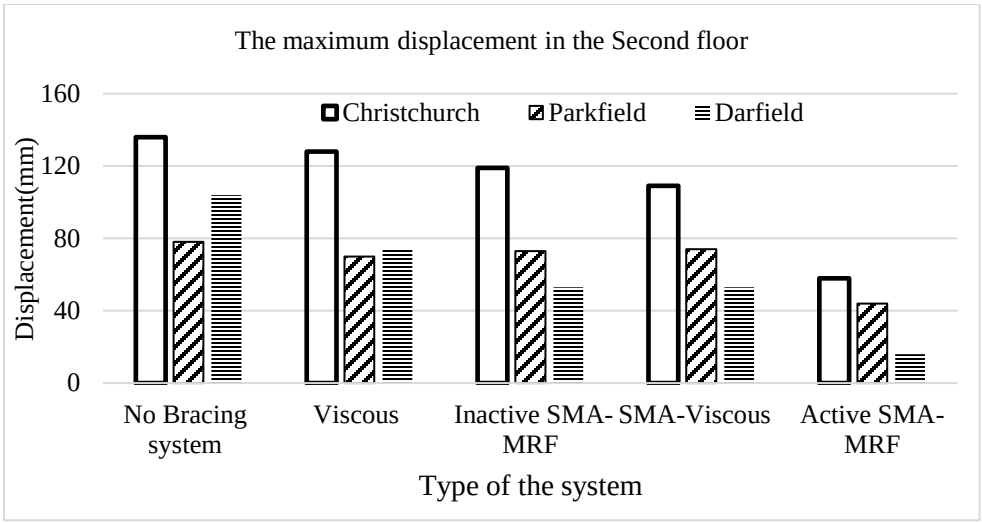

Figure 5-10. The maximum displacement of the second story on GMs

5.6.4 Effects of control elements on the structural stability: frequency domain

In the previous section, the functionality of the structural control systems under different GMs has been shown in the time domain analysis. However, understanding the functionality of the system for different applied frequencies is essential in the design and development of the stability control element for dynamic loadings. In this section, the effects of adding control elements in structural stability have been investigated in the frequency domain. For the sake of brevity, only one GM, the Christchurch earthquake, has been considered for the simulation.

In order to illustrate the performance of the structures under external dynamic loading, three regions, namely safe zone (SZ), warning zone (WZ), and danger zone (DZ), have been introduced. The safe zone is considered as the zone in which the maximum normalized drift ratio is less than 0.01; the warning zone is where the drift ratio is between 0.01 to 0.1. The drift ratio above 0.1 is considered as the danger zone where the structure will be at a high risk of failure. One may note that for loading frequency close to the natural frequency, the structure begins to resonance leading to high instability.

In order to compare the effect of structural control systems on both floors of the frame, the frequency responses of each floor are studied separately. Figure 5-11 and Figure 5-12 compare the effects of adding control elements in the drift ratio for the first and second stories under the Christchurch earthquake. The peak Drift Ratio of the SMA-viscous system significantly changes down drift ratio to 0.08 while it leads to a 1.5 Hz shift in the natural frequency of the structure embedded with the control system. The inactive SMA-MRF-based system decreases the drift ratio by 68.5%. One may realize that activating the hybrid SMA-MRF system may keep the stability for the structure in the safe zone for a wide range of loading frequencies. Similar results are observed for the first and the second floors for all GMs.

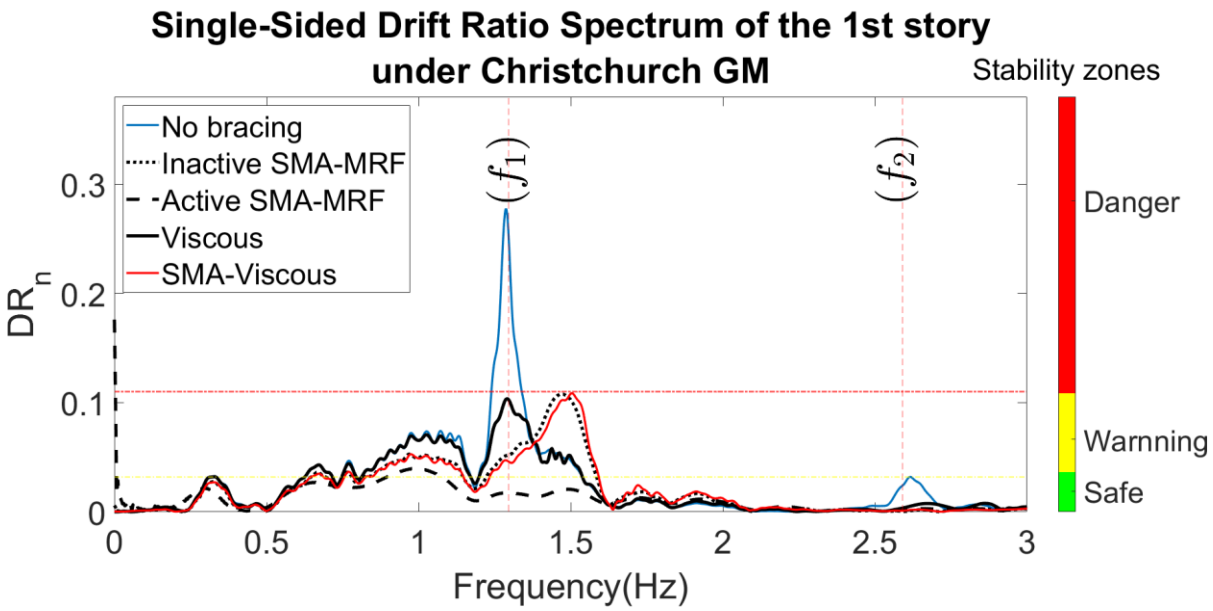

Figure 5-11. The frequency response of the first floor with structural control systems under the scaled Christchurch GM

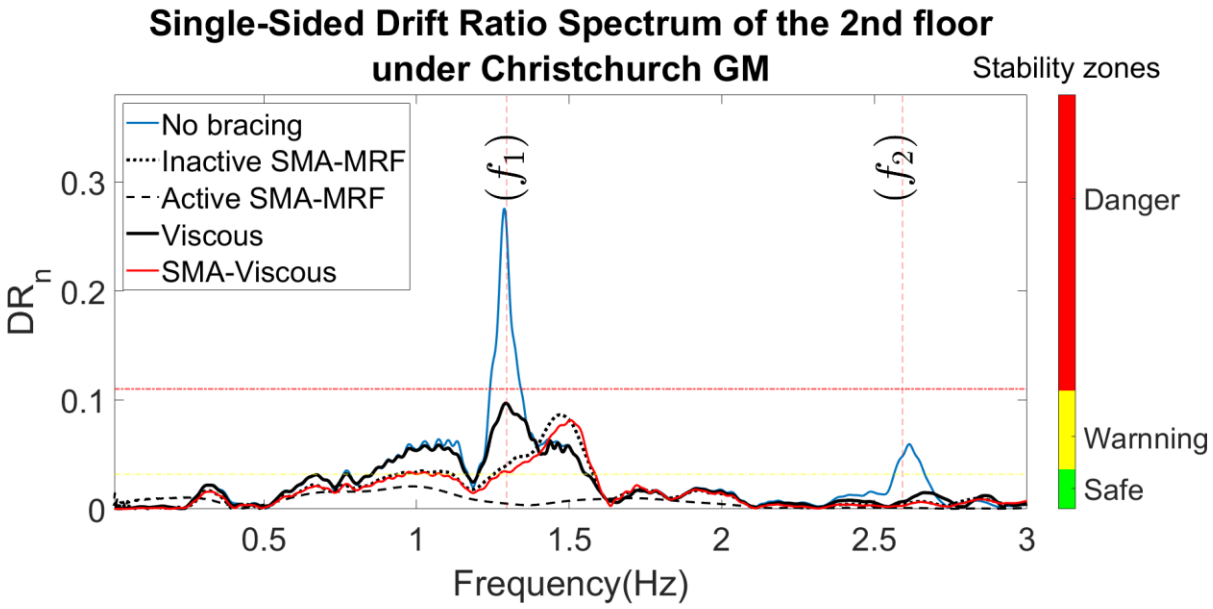

Figure 5-12. The frequency response of the second floor with structural control systems under the scaled Christchurch GM

5.6.5 The semi-active control algorithm for the frequency response of drift ratios

According to the stability limitation, such as drift displacement, given by structural design, a safe zone (SZ) is defined for safe structural stability. The drift displacements at selected locations are measured constantly; accordingly, for drift displacement lower than the safe zone, no electric field is induced to MR damper (system activated). Once the drift displacement goes beyond the safe zone, a constant electric current will be induced to the MRF damper (system deactivated). Although the present system is capable of adjusting for the different magnitudes of drift displacements, for the sake of simplicity, the present system is just an "On-Off" system, as presented in Figure 5-13. One may be noted that when the value of the drift displacement increases from the safe zone, a fixed electric current will be applied to the MRF damper supplying a constant control force to bring back the drift to the safe zone. Once the magnitude of the drift falls in the safe zone, the electric source will be disconnected. Therefore, this algorithm minimizes the risk of structural destabilization.

Figure 5-14 and Figure 5-15 illustrate the frequency response of the drift ratio of the first and second floors of the structure. It is observed that in the frequency band 0.8-1.7 Hz, the response of the system exceeds the safe zone. Therefore, the control system needs to be activated in this frequency range. To save energy, the control system is activated before 0.8 Hz and deactivated after 1.7 Hz. This ensures the frequency response of the system to fall in the safe zone when subjecting to a wide range of loading frequencies.

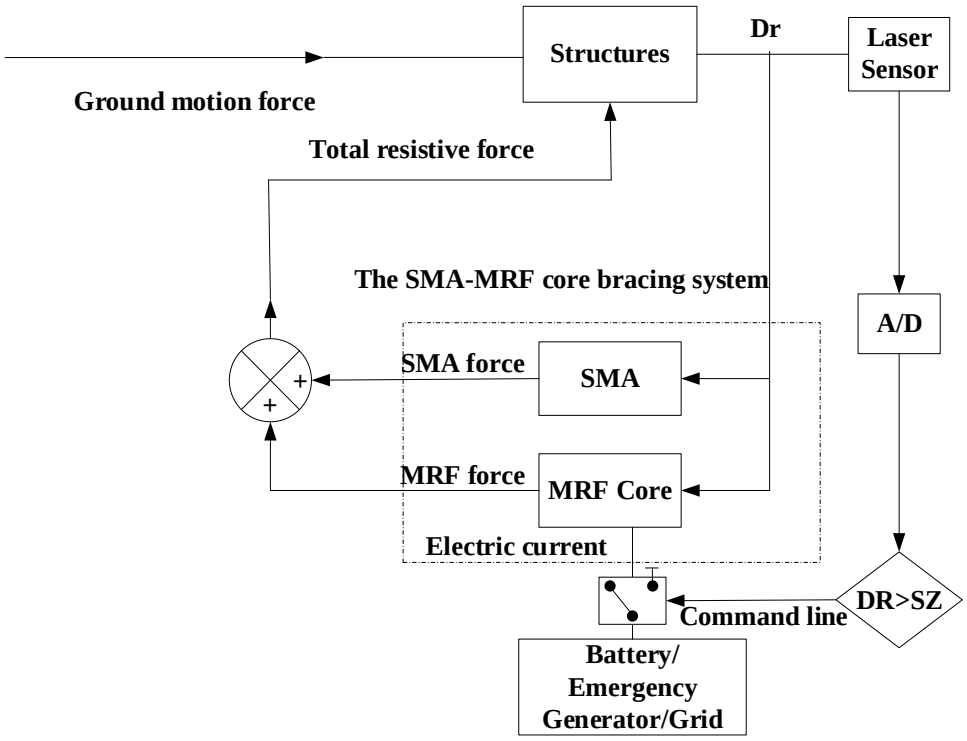

Figure 5-13. The schematic diagram of the closed-loop controller

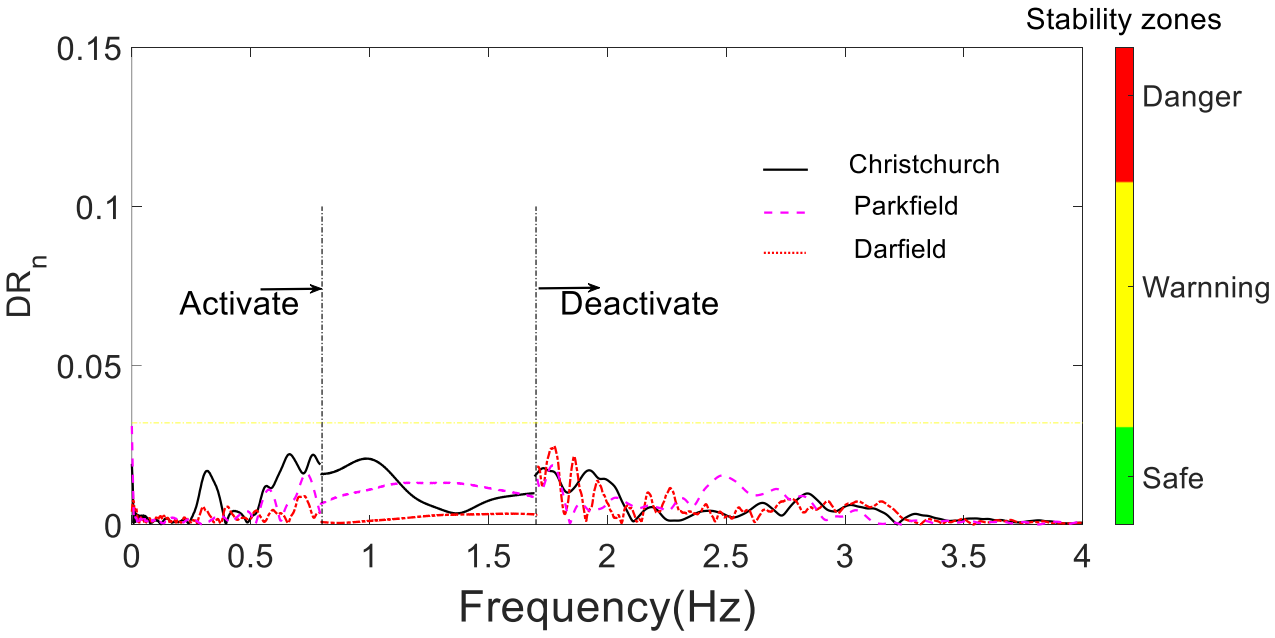

Figure 5-14. The frequency response of the first story with structural control systems under the scaled Christchurch GM

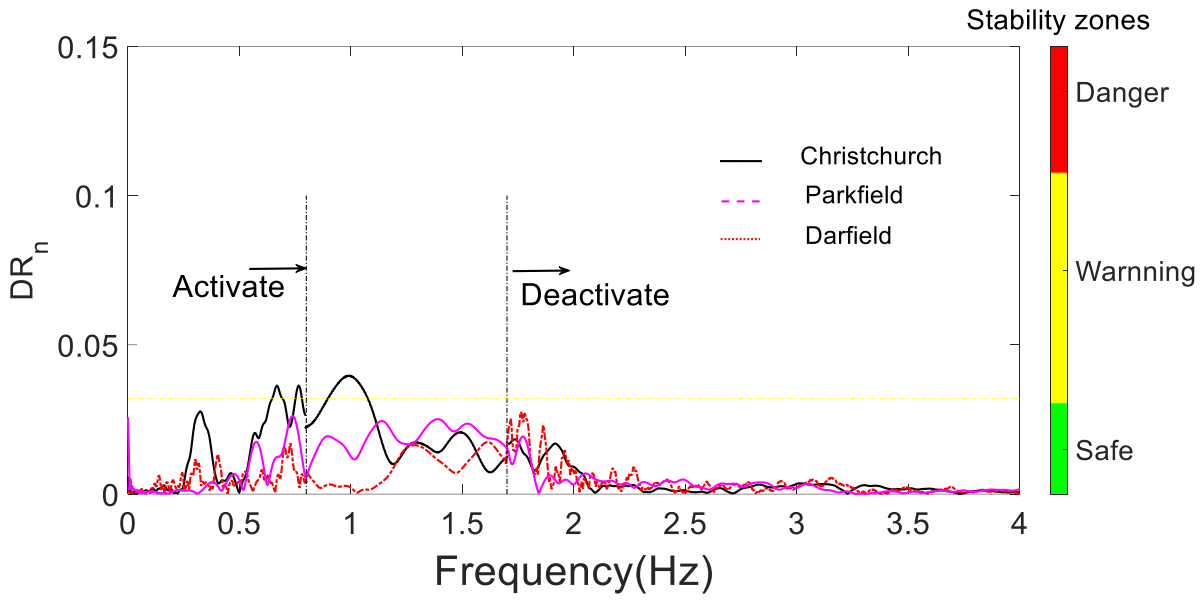

Figure 5-15. The frequency response of the second-story with structural control systems under the scaled Christchurch GM

5.7 Conclusion

The dynamic response of the Viscous-based, the SMA-Viscous-based, and the SMA-MRF based bracing systems have been generated and obtained in the OpenSees. In the first step, a two-story frame is modeled in the OpenSess and validated by analytical results. This frame is used to study the effect of the different proposed bracing systems. Then, the effects of adding structural control elements in stability control of the structures have been investigated. Several structural control elements, namely the SMA-MRF-based system, the Viscous-base, and the SMA-Viscous-base, have been examined for drift ratios for a simplified two-degrees of freedom structures both in the time domain and in the frequency domain. It was observed that adding control elements reduces the drift ratio for both stories subjected to three earthquakes under the study. The SMA-MRF control system provided more reduction in the drift ratio for both stories subjected to the three earthquakes. To illustrate the performance and functionality of the systems, three zones, namely safe zone, warning zone, and danger zone, have been introduced. It was observed that activating

the SMA-MRF system makes the frequency response of the structure fall in the safe zone for a wide range of loading frequencies.

In the aspect of the electric energy consumption, the MRF-based and the SMA-MRF-based systems, systems are studied for two states with(On) and without(Off) maximum electric current. In the Off state, there is no electric power; but in the On state, the maximum allowable current is applied to the SMA-MRF-based system, as well as the MRF-based system.

Chapter 6: Effect of cyclic loading on the SMA behaviour

6.1 Introduction

In the previous chapters, the prototype of the SMA-MRF core bracing system has been proposed, designed, and fabricated. It aims to protect the civil infrastructures subjected to seismic activities. Furthermore, it is assumed that the system should be fully functional in the lifespan of real buildings. Hence, any change from the ideal behaviour of each element of the proposed system affects the outcomes of the entire system significantly.

The MRF-based damper has been fabricated and tested after 2 million cycles by manufacturer, and results have shown a negligible difference from its initial behaviour [266]. Another material is the SMA, which is used in the form of wire in this smart system. Few studies have been conducted on the effect of long-term use. Hence, the investigation of that condition is in demand to find any possible change over the initial response.

In this chapter, experimental responses of SMA wires by focusing on dissipation capacity and residual deformation are studied to compare responses of SMAs with and without applied prestraining. Among all applying prestrained, ranging from 1.5% to 2 %, 1.7% is chosen due to reasonable experimental results. Comparisons between 0% and 1.7% prestrained SMA's specimen under short and long-term cyclic loads are conducted.

6.2 Energy absorption calculation

SMA-based systems absorb the energy of external excitation through their hysteresis. In order to calculate the energy dissipation capacity, the obtained hysteresis response should be divided into n elements, as presented in Figure 6-1. Each element can be assumed as a trapezoid with an area equal to the energy dissipation between two small displacements. Due to the SE SMA's flag shape hysteresis, the energy dissipation strip shown in Figure 6-1 seems to consider portion beyond the

hysteresis. However, this additional portion will cancel out when the full cycle of hysteresis is considered. The sum of all elements is the total energy dissipation capacity under the specific loads.

The total energy dissipation is computed by [86]:

$$Energy_{total} = \sum_{i=1}^{n-1} 0.5(F_i + F_{i-1})(D_i - D_{i-1}) \tag{6.1}$$

where F_i and D_i denote the force and displacement of the "i-th" node of the "i-th" element, respectively.

When energy dissipation is normalized by the volume of the SMA material, it can be calculated from force (strain) and force (stress) data, as illustrated in Figure 6-1.

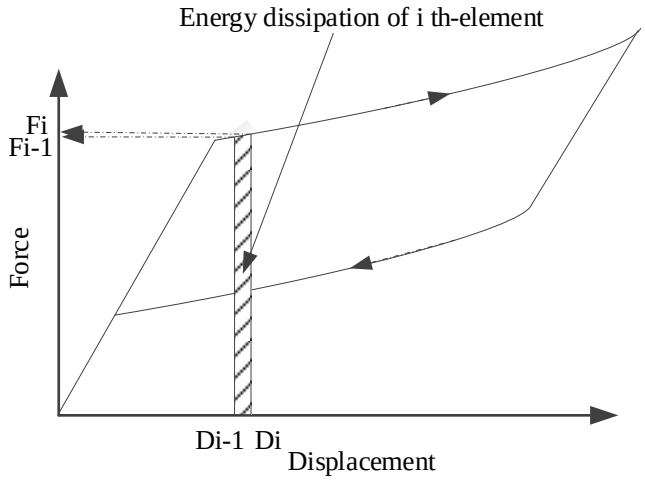

Figure 6-1. The energy absorption of a typical hysteresis response of the SMA

Effect of cyclic loading on the deformation of SMA

The load shown in Figure 6-2 is applied 100 times to the specimen to simulate the cyclic loads, and similarly, 1000 cycles are used to model the long-term cyclic loads. It is assumed that the load is strong enough to pull the element into the inelastic region up to 3.5% longer than the original

length. This limit is set to not go beyond the fully superelastic response in all cases, including the pre-strained cases. One hundred cycles of such loads are anticipated to happen in critical situations. The hysteresis responses for both loading conditions are obtained experimentally using an MTS load frame. The SMA wires have been subjected to a 1.7% initial pre-straining prior to the application of external loading.

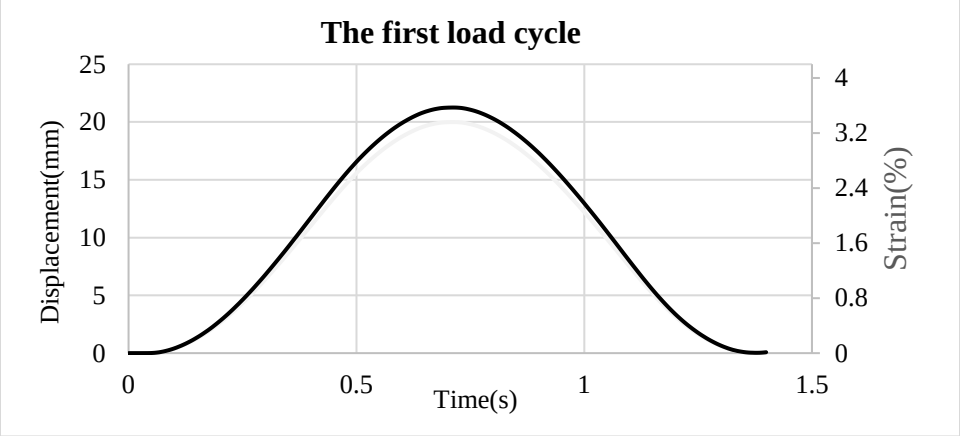

Figure 6-2. One load cycle applied by the MTS machine

The permanent (residual) deformation is an index to estimate how much the SMA loses its ability to recover its original state. The SMA specimen has been subjected to 1000 load cycles with a typical loading shown in Figure 6-2. Figure 6-3 illustrates the effects of cyclic loading on the residual deformation of the SMA specimens. It is seen that the major rise occurs between 1 to 100 cycles, which is approximately about 1.5 mm (0.30 % strain) after the first 100 cycles. Beyond 300 cycles, the residual deformation can be assumed as constant. The range of the residual deformation is between 1.9 mm (0.34% strain) to 2.2 mm (0.40% strain) from cycle 300 to cycle 1000. One may be noted that SMA, such as conventional materials, loses its characteristics under cyclic loads [267].

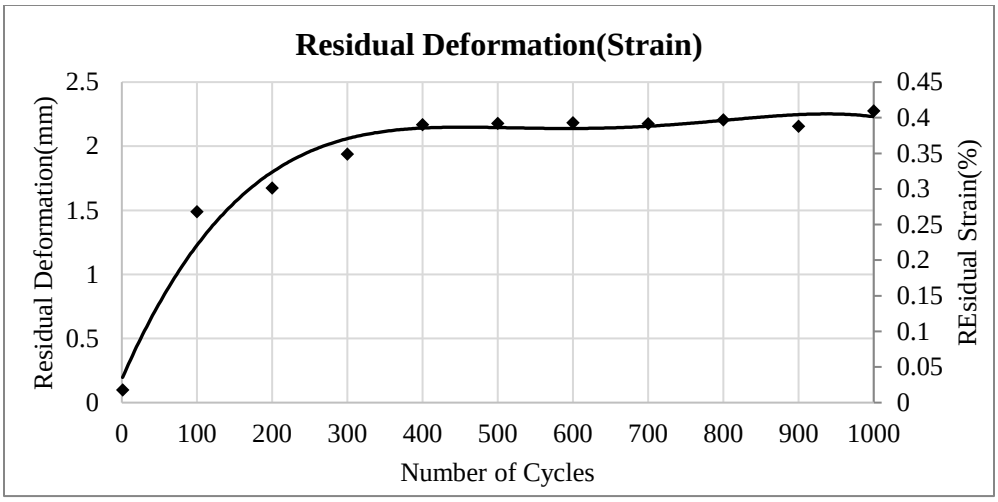

Figure 6-3. Effect of cyclic loading on residual(strain) deformation of SMA

6.3 Pre-straining SMA

In order to select the pre-strain point for the SMA during loading and unloading phases, two possible points are considered in the hysteresis response of the SMA as shown in Figure 6-4. The first option is σ_1, in the loading phase and the second option is σ_2, in the unloading phase. In this study, the pre-straining point, which is about 1.7 % in the loading phase, is selected to apply to the SMA specimen. It is mainly due to avoid applying the maximum allowable strain and reduce the possibility of the degradation under cyclic loadings, while the pre-straining is applied.

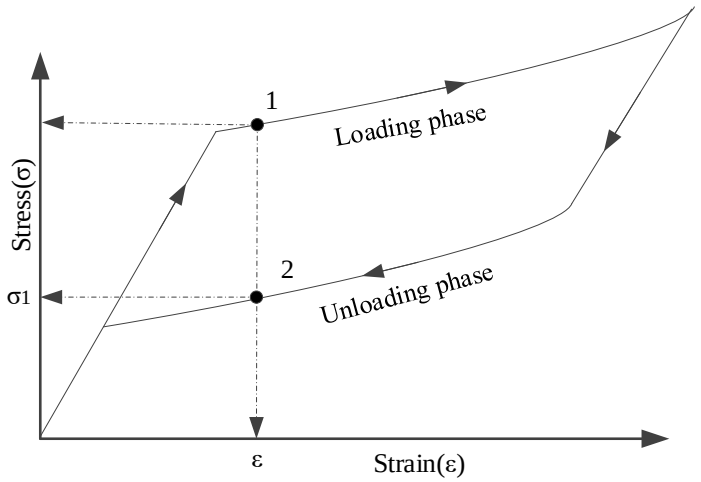

Figure 6-4. The typical hysteresis response of the SMA

6.4 Results and discussions

In order to simulate the external periodical dynamic live loads, such as winds and earthquakes, the SMA's short and long terms behaviour is investigated.

6.4.1 Short-term loading

The hysteresis responses of the 0% and 1.7% pre-strained SMA specimens under short-term cyclic loads are displayed in Figure 6-5. For the 0% pre-strained cycle, a small initial force, about 40 N, is applied by the MTS machine to fix the specimen in place.

Significant differences in the hysteresis responses are observed between initial responses and responses under cyclic loads. One of the main differences is that the considerable residual deformation appears in the 0% pre-strained SMA specimen after ten cycles, whereas the 1.7% pre-strained specimen does not exhibit this deformation under the short-term cyclic loads. The second change is the decrease in the under-the-curve area.

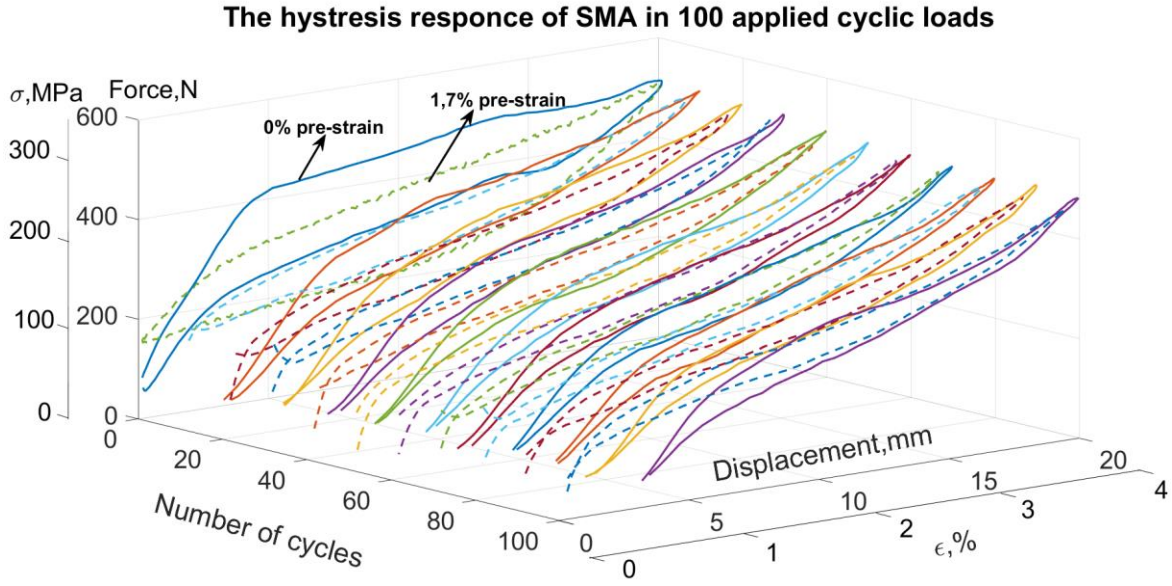

Figure 6-5. The hysteresis responses of the 0% and 1.7% pre-strained specimen along 100 cycles

The amount of energy dissipation capacity for up to 100 cyclic loads is shown in Figure 6-6. The energy dissipation capacity drops remarkably with an increasing number of cycles for both SMAs. The sharpest drop from 2.5 J/cm^3 to 1 J/cm^3 occurs in the first ten cycles. Thereafter, the energy dissipation capacity decreases more gradually and reaches 0.7J/cm^3 after 100 cycles for both the 0% and 1.7% pre-strained specimens. It is worth mentioning that the reduction is linked to the degradation of the SMA. It is s that the degradation has a similar effect on the energy dissipation capacity reduction on all SMA specimens regardless of level applied prestraining.

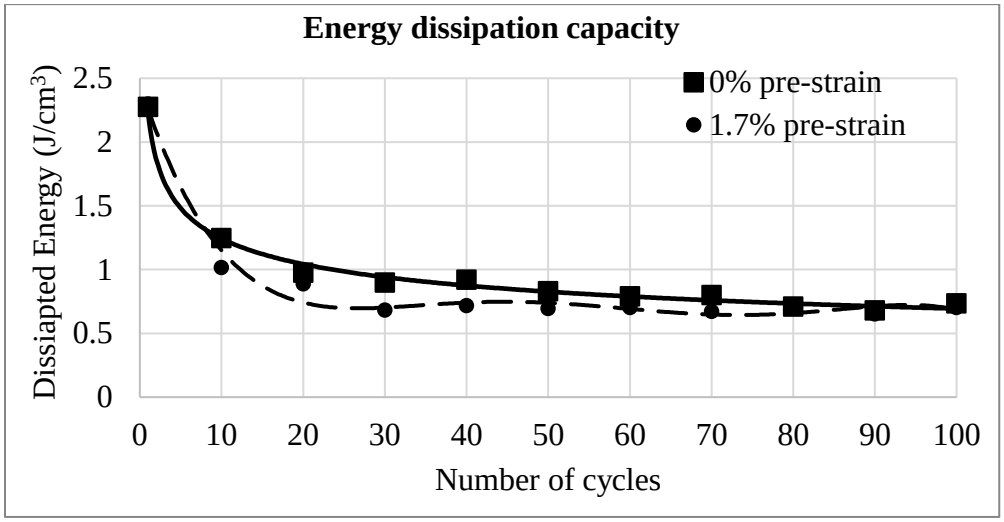

Figure 6-6. The amount of energy dissipation capacity in 0% and 1.7% pre-strained specimen

6.4.2 Long-term loading

The hysteresis responses of the SMA specimen for up to 1000 cyclic loads are shown in Figure 6-7. A significant improvement in the term of full recovery capability of hysteresis response after 100 cycles are observed when the SMA wires are subjected to pre-strain.

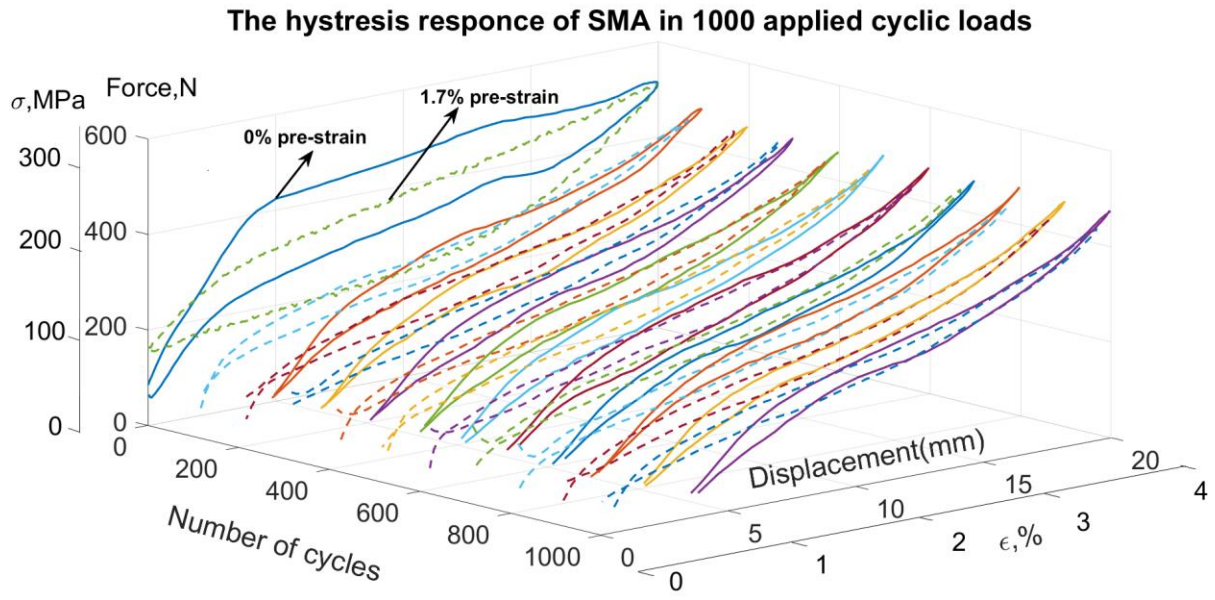

Figure 6-7. The hysteresis responses of the 0% and 1.7% pre-strained specimen along 1000

The effect of long-term loads on the energy absorption capacity is presented in Figure 6-8. It shows a similar trend for both specimens. In the first 100 cycles, energy absorption capacity drops sharply from 2.3 J/cm^3 to 0.7 J/cm^3. This is followed by a much more gradual decrease to 0.5 J/cm^3 at 1000 cycles.

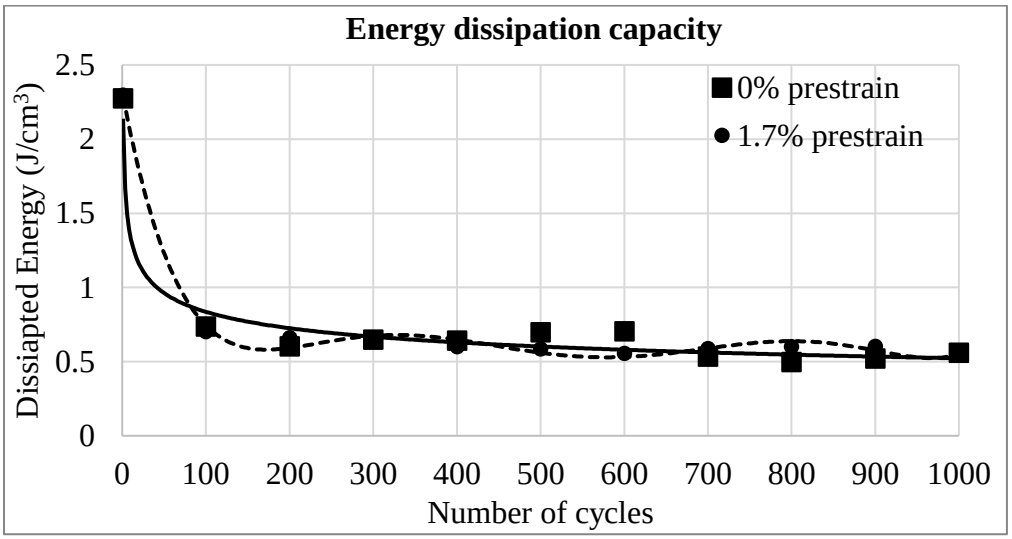

Figure 6-8. The amount of energy dissipation capacity in 0% and 1.7% prestrained specimen

6.5 Conclusion

The effects of high-amplitude cyclic loadings (i.e. loads that pull the structures beyond the elastic region) on the dynamic behaviour of SMA-based structural control elements have been studied experimentally. The study demonstrates that SMA-elements in the SE mode are good passive structural control elements that provide excellent energy absorption and self-centering capacity. To develop these components, two important parameters should be considered: the loss of energy dissipation capacity and residual deformation. The experimental study indicates:

- The energy dissipation capacity of an SMA-element drops by about 75% in the first 100 cycles. Thus, a safety factor of approximately 2.5 is required in the design of SMA based structural control elements.
- During the initial 100 cycles, the residual strain of about 0.26% takes place in the conventional SMA specimen. Hence, SMA-based structural control elements require adequate preload in order to provide optimum self-centering capacity.

Chapter 7: Summary, Conclusion, and Future works

In this study, a novel smart bracing system has been proposed to enhance the stability of civil infrastructure. The proposed system ensures the functionality and serviceability of structures when subjected to unpredicted external loads, such as seismic loads. To illustrate the performance and functionality of the proposed system, several issues, including analytical, numerical, experimental, and simulation of case studies, have been tackled. The following subsections provide brief descriptions and contributions of the present study. Regarding the controllability of output, the proposed system can be considered as a suitable structural control for the low, medium, and high seismic zone.

7.1 Conceptual design

The conceptual design of the novel hybrid system, called SMA-MRF core bracing, has been developed in which the controllability of MR dampers and the superelasticity effect of SMA have been combined. The hybrid bracing system has a core MRF damper surrounded by SMA wires. The design ensures that the SMA wires are under tension when subject to both compression as well as tension loadings.

7.1.1 Analytical study

An analytical model has been developed to simulate the performance of the novel hybrid system in Chapter 3. This model captures the simultaneous effects of magnetic, electrical, and mechanical fields.

The model has been utilized to investigate the controllable energy dissipation capacity, the recentering ability, and the damping coefficient in the tension and the compression modes.

7.1.2 Fabrication

Based on the conceptual design, a prototype of the system has been designed, and accordingly, the system has been fabricated. The system is composed of two sliding cylinders, a core MR damper fixed in the inner cylinder, and four SMA wires attached and fixed at the outer cylinder.

7.1.3 Experimental analysis

The prototype models have been subjected to the dynamic loads (Chapter 4) by an MTS load frame machine to obtain the experimental data.

The comparison between the performance of the SMA-MRF core bracing system to the SMA-based system and the MRF-based system has been conducted. The experimental results in the proposed systems have been compared with that of the numerical approach (Chapter 4).

It is understood that the performance of SMA-based systems in the long-term may alter because of material degradation. To compensate for the degradation effects in the energy absorption capacity as well as increasing in the residual deformation in the SMA-based bracing systems, the SMA wires have been subjected to predefined pre-straining. The remarkable enhancement has been found in the pre-strained mode after applied cyclic loads.

7.1.4 Numerical analysis

The numerical model of the hybrid bracing system has been developed in the OpenSees. Moreover, the numerical model of the SMA-based bracing system, the MRF bracing, and the conventional bracing system have been explored in Chapter 5. The numerical and experimental models have been compared to validate the accuracy of the numerical models. The numerical model of the two-story frame has been developed. To find the structural behaviour, the frame has been equipped with the hybrid bracing and subjected to three scaled simulated ground motions.

The performance of all systems has been compared to study the effect of the bracing systems on the structural behaviour of the frame.

7.2 Conclusion

The SMA-MRF core bracing system has been proposed to enhance structural stability under external seismic loadings. The main outcomes of the present hybrid system are summarized as follows:

7.2.1 Energy dissipation capacity

The hybrid SMA-MRF core bracing system can play a major role in the energy dissipation of the external loadings. In fact, the energy dissipation capacity of the present systems is much greater than that of the SMA-based and inactive MRF-based bracing systems. The force-displacement responses of the smart bracing system have displayed that the amount of energy dissipation varies by the applied electric current.

It is observed that the implementation of the SMA-MRF core bracing system dramatically increases the absorption energy capacity of civil infrastructure.

7.2.2 Re-centering ability

Re-centering is one of the most important issues in structural stability. The results from analytical and experimental works proved that the re-centering ability of civil structures equipped with the proposed hybrid system had been significantly improved. It is worth noting that the re-centering ability of structure may be controlled by changing the strength of the magnetic field. Therefore, the plastic deformation of the structural members under the ground motions may be decreased or fully eliminated.

7.2.3 The equivalent viscous damping coefficient

The equivalent viscous damping coefficient, which shows the damping capability of the system, has been calculated analytically and validated by experimental results. It has been observed that the equivalent viscous damping coefficient is a function of the viscosity of MR fluid in the MRF core and SMA wires. Therefore, energizing the MRF damper increases this coefficient. Similar results have been computed numerically for the energized hybrid SMA-MRF system installed in civil infrastructure and subjected to the simulated earthquake profiles.

7.2.4 Pre-straining effect

The degradation in SMA wires in the SMA-based bracing systems leads to permanent deformation, and in turn, decreases the energy dissipation capacity as well as its equivalent viscous damping. The side-effects of the degradation have been decreased by applying pre-straining on SMA wires in the system. It has been noted that pre-straining SMA wires significantly reduced the residual strain. Besides, the pre-strained wires have kept the functionality of the SMA-based system much better than the standard system.

7.2.5 Other structural parameters

The nonlinear time-history analysis of civil infrastructure has been conducted; the inter-story drift, and the maximum displacement, as the structural behaviour's parameters, have been obtained. The results have proved that the effect becomes much better than civil infrastructure equipped with the SMA system and the MRF-based system. Hence, it is a suitable alternative to be replaced with systems.

7.3 Contribution

The outcomes of this work have been summarized into several major contributions followed by the relevant details and minor ones:

- Numerical modeling
    - Introduced practical finite element (FEA) codes to model the SMA and the MRF core
    - Developing the FEA model for the SMA-MRF based system
- Investigation on the effects of cyclic loadings on the response of the SMA, MRF, and SMA-MRF -based control elements
    - Defined correction factors to involve the effects of cyclic loading on the stress-strain response of SMA and SMA-hybrid based systems
    - Study the effects of pre-straining SMA on the stress-strain response of SMA wires
    - Conducting experimental tests on the stress-strain responses of SMA to study the effect of pre-straining under simulated short- and long-term cyclic loading
    - Conducting research to study the effect of cyclic loading on the hysteresis response of SMA wires.
- Experimental investigation
    - Designing the prototype of the SMA-MRF core bracing system
    - Fabrication of the SMA-MRF system's components
    - Performance testing of critical components
    - Assembly all components and delivering a practical and ready-use SMA-MRF element
    - Conducting experimental tests upon the SMA-MRF core bracing system in the MTS machine
    - Validation of numerical results with corresponding experimental ones

- ❖ Dynamic analysis of a simplified frame structure integrated with the SMA-MRF core bracing system
    - o Developed the numerical model of the frame in OpenSees
    - o Modeling the frame with SMA-based, the MRF-based, the SMA-MRF-based systems in OpenSees
    - o Conducting the time-history analysis for frame equipped the SMA-MRF-based systems
    - o Performing the frequency analysis for the frame with the SMA-MRF-based systems

7.4 Future works:

The study has shown the huge potential of the novel system to enhance the dynamic behaviour of civil infrastructure under simulated ground motions. In order to extend the various civil engineering applications of this system, some suggestions should be considered. For instance, the size, the length of SMA wire and MRF-based damper, the source of electric power, kind of control system, the static and the dynamic tests of the inner and the outer cylinders, and customized nuts, which meet the requirements for actual applications in civil infrastructure.

7.4.1 Actual size fabrication and testing

Civil infrastructure, such as building and bridge, has its own specifications. To find the proper structural responses, the actual size of the SMA-MRF bracing system should be designed and manufactured with respect to the specification of the target structure, which determines the size of each component, particularly SMAs and MRF-based core. Moreover, testing the actual size of the proposed system and obtaining its dynamic behaviour under different loading conditions will help develop a more accurate numerical model of the system.

Today, SMA materials, mostly NiTi-based, are available in the market in many forms and dimensions. In order to have a fully functional SMA-MRF-based system, a better mechanism for SMA-based components should be designed and developed to prevent sliding in SMA-wires around the nuts and bolts. However, most MRF-based dampers are prototype. In order to develop an MRF-based damper for civil engineering applications, particularly in buildings, more studies should be performed considering the prototype's fabrication as well as the mass production’s cost.

7.4.2 Implementation of real civil infrastructure

At least one type of civil infrastructure, such a steel building, should be selected and integrated with the proposed system and explore its structural behaviour in order to prepare the system for industrial applications. Then, this system can also be extended in a wide range of civil engineering applications such as RC structure.

7.4.3 Control system

It has been observed that a 20 ton-MRF-based damper just needs 50 Watt electric power to be fully energized. This amount of required activation energy can be supplied by the battery, emergency generator, or electric grid. So, the controllability of the system, as a primary advantage of the semi-active system, can be set the applied electric current in order to take the desired outputs by a suitable controller. A wide range of control strategies, from the classics like a PID controller to modern control, like a fuzzy controller, can be developed.

References

[1] Worldwide AIR. Study of impact and the insurance and economic cost of a major earthquake in British Columbia and Ontario/Québec. Insur Bur Canada 2013;345.

[2] Kambiz Esteki, Esteki K. Developing new analytical and numerical models for mr fluid dampers and their application to seismic design of buildings. Concordia University, 2014.

[3] Preumont A. Semi-active Control. Vib. Control Act. Struct., 2011, p. 403–16.

[4] Aly Sayed Ahmed AM, Zasso A, Resta F. Proposed configurations for the use of smart dampers with bracings in tall buildings. Smart Mater Res 2012;2012:Article ID 251543.

[5] Hedayati Dezfuli F. Hysteretic behaviour of steel-and fibre-reinforced elastomeric isolators fitted with superelastic shape memory alloy wire. University of British Columbia, 2015.

[6] Kunde MC, Jangid RS. Seismic behavior of isolated bridges: A-state-of-the-art review. Electron J Struct Eng 2003;3:140–69.

[7] Esteki K. Developing new analytical and numerical models for mr fluid dampers and their application to seismic design of buildings. The Department of Building, Civil, and Environmental Engineering,Concordia University, 2014.

[8] Soto MG, Adeli H. Tuned mass dampers. Arch Comput Methods Eng 2013;20:419–31.

[9] Connor JJ. Introduction to structural motion control. Prentice Hall; 2003.

[10] Almazán JL, Juan C, Inaudi JA, López-Garc\'\ia D, Izquierdo LE. A bidirectional and homogeneous tuned mass damper: A new device for passive control of vibrations. Eng Struct 2007;29:1548–60.

[11] Sakai F, Takaeda S, Tamaki T. Tuned liquid column damper-new type device for suppression of building vibrations. Int. Conf. Highrise Build. Nanjing, China, Mar, 1989, p. 25–7.

[12] Xu YL, Samali B, Kwok KCS. Control of along-wind response of structures by mass and liquid dampers. J Eng Mech 1992;118:20–39.

[13] Balendra T, Wang CM, Cheong HF. Effectiveness of tuned liquid column dampers for vibration control of towers. Eng Struct 1995;17:668–75.

[14] Gao H, Kwok KCS, Samali B. Optimization of tuned liquid column dampers. Eng Struct 1997;19:476–86.

[15] Balendra T, Wang CM, Rakesh G. Effectiveness of TLCD on various structural systems. Eng Struct 1999;21:291–305.

[16] Hruska A, Dorfmann A. Elastic shear frames with tuned liquid column dampers a controlled study of small-scale models. Struct. Control Civ. Infrastruct. Eng., World Scientific; 2001, p. 281–92.

[17] Yalla SK, Kareem A. Optimum absorber parameters for tuned liquid column dampers. J Struct Eng 2000;126:906–15.

[18] Liu M-Y, Chiang W-L, Chu C-R, Lin S-S, others. Analytical and experimental research on wind-induced vibration in high-rise buildings with tuned liquid column dampers. Wind Struct 2003;6:71–90.

[19] Samali B, Mayol E, Kwok KCS, Mack A, Hitchcock P. Vibration control of the wind-excited 76-story benchmark building by liquid column vibration absorbers. J Eng Mech 2004;130:478–85.

[20] Al-Saif KA, Aldakkan KA, Foda MA. Modified liquid column damper for vibration control of structures. Int J Mech Sci 2011;53:505–12.

[21] Grigorian CE, Yang T-S, Popov EP. Slotted bolted connection energy dissipators. Earthq Spectra 1993;9:491–504.

[22] Symans MD, Charney FA, Whittaker AS, Constantinou MC, Kircher CA, Johnson MW, et al. Energy dissipation systems for seismic applications: current practice and recent developments. J Struct Eng 2008;134:3–21.

[23] Pall AS, Marsh C. Response of friction damped braced frames. J Struct Eng 1982;108:1313–23.

[24] Soong TT, Dargush GF. Passive energy dissipation systems in structural engineering. Wiley; 1997.

[25] Shen H, Zhang R, Weng D, Gao C, Luo H, Pan C. Simple design method of structure with metallic yielding dampers based on elastic--plastic response reduction curve. Eng Struct 2017;150:98–114.

[26] Akcelyan S, Lignos DG, Hikino T. Adaptive numerical method algorithms for nonlinear viscous and bilinear oil damper models subjected to dynamic loading. Soil Dyn Earthq Eng 2018;113:488–502.

[27] Dyke, SJ and Spencer Jr B, Dyke SJ, Spencer Jr BF, Sain MK, Carlson JD. Modeling and control of magnetorheological dampers for seismic response reduction. Smart Mater Struct 1996;5:565. https://doi.org/10.1088/0964-1726/5/5/006.

[28] Yang G, Spencer Jr BF, Jung H-J, Carlson JD. Dynamic modeling of large-scale magnetorheological damper systems for civil engineering applications. J Eng Mech 2004;130:1107–14.

[29] Iqbal MF. Application of magneto-rheological dampers to control dynamic response of buildings. Concordia University, 2009.

[30] ee, Sang-Hyun, Kyung-Won Min, Lan Chung, Sung-Kyung Lee, Myoung-Kyu Lee, Jae-Seung Hwang, Seung-Bok Choi and H-GL. Experimental verification of an MR damper

controlled highway bridge. J Intell Mater Syst Struct 2007;18:1111-1120.

[31] Symans MD, Constantinou MC, Taylor DP, Garnjost KD. Semi-active fluid viscous dampers for seismic response control. First World Conf. Struct. Control, 1994, p. 3–12.

[32] Jani JM, Leary M, Subic A, Gibson MA. A review of shape memory alloy research, applications and opportunities. Mater Des 2014;56:1078–113.

[33] Zareie S, Zabihollah A, Azizi A. Buckling control of morphing composite airfoil structure using multi-stable laminate by piezoelectric sensors/actuators. Proc. SPIE - Int. Soc. Opt. Eng., vol. 7978, 2011. https://doi.org/10.1117/12.880409.

[34] Morais J, de Morais PG, Santos C, Costa AC, Candeias P. Shape Memory Alloy Based Dampers for Earthquake Response Mitigation. Procedia Struct Integr 2017;5:705–12.

[35] Shrestha B, Li C, Hao H, Li H. Performance-Based Seismic Assessment of Superelastic Shape Memory Alloy-Reinforced Bridge Piers Considering Residual Deformations. J Earthq Eng 2017;21:1050–69.

[36] Aryan H, Ghassemieh M. Mitigation of vertical and horizontal seismic excitations on bridges utilizing shape memory alloy system. Adv. Mater. Res., vol. 831, 2014, p. 90–4.

[37] Zareie. S, Alam. MS, Seethaler. RJ, Zabihollah. A. An experimental study of SMA wire for tendons of a Tension Leg Platform. 5th Annu. Eng. Grad. Symp., Kelowna: 2019.

[38] Rojob H, El-Hacha R. Fatigue performance of RC beams strengthened with self-prestressed iron-based shape memory alloys. Eng Struct 2018;168:35–43.

[39] Yan S, Xiao ZF, Lin MY, Niu J. Numerical analysis of dynamic behavior of pre-stressed shape memory alloy concrete beam-column joints. IOP Conf. Ser. Mater. Sci. Eng., vol. 348, 2018, p. 12013.

[40] Bajoria KM, Kaduskar SS. Modeling of a reinforced concrete beam using shape memory

alloy as reinforcement bars. Act. Passiv. Smart Struct. Integr. Syst. 2017, vol. 10164, 2017, p. 101640S.

[41] Michels J, Shahverdi M, Czaderski C. Flexural strengthening of structural concrete with iron-based shape memory alloy strips. Struct Concr 2018;19:876–91.

[42] Zhou P, Liu M, Li H, Song G. Experimental investigations on seismic control of cable-stayed bridges using shape memory alloy self-centering dampers. Struct Control Heal Monit 2018:e2180.

[43] Mahmoudi M, Montazeri S, Abad MJS. Seismic performance of steel X-knee-braced frames equipped with shape memory alloy bars. J Constr Steel Res 2018;147:171–86.

[44] Ghassemieh M, Rezapour M, Sadeghi V. Effectiveness of the shape memory alloy reinforcement in concrete coupled shear walls. J Intell Mater Syst Struct 2017;28:640–52.

[45] Wang B, Zhu S. Cyclic tension--compression behavior of superelastic shape memory alloy bars with buckling-restrained devices. Constr Build Mater 2018;186:103–13.

[46] Hietanen S. ER fluids and MR materials-Basic properties and some application developments. VTT Symp., vol. 225, 2003, p. 33–50.

[47] Andrawes B, DesRoches R. Unseating prevention for multiple frame bridges using superelastic devices. Smart Mater Struct 2005;14:S60.

[48] Graesser EJ, Cozzarelli FA. Shape-memory alloys as new materials for aseismic isolation. J Eng Mech 1991;117:2590–608.

[49] DesRoches R, McCormick J, Delemont M. Cyclic properties of superelastic shape memory alloy wires and bars. J Struct Eng 2004;130:38–46.

[50] Song G, Ma N, Li H-N. Applications of shape memory alloys in civil structures. Eng Struct 2006;28:1266–74.

[51] Saadat S, Salichs J, Noori M, Hou Z, Davoodi H, Bar-On I, et al. An overview of vibration and seismic applications of NiTi shape memory alloy. Smart Mater Struct 2002;11:218.

[52] Lagoudas D. 2008, Shape Memory Alloys: Modeling and Engineering Applications n.d.

[53] Sun L, Huang WM. Nature of the multistage transformation in shape memory alloys upon heating. Met Sci Heat Treat 2009;51:573–8.

[54] Seo J, Kim YC, Hu JW. Pilot study for investigating the cyclic behavior of slit damper systems with recentering Shape Memory Alloy (SMA) bending bars used for seismic restrainers. Appl Sci 2015;5:187–208.

[55] Seo J, Hu JW, Davaajamts B. Seismic performance evaluation of multistory reinforced concrete moment resisting frame structure with shear walls. Sustainability 2015;7:14287–308.

[56] Strnadel B, Ohashi S, Ohtsuka H, Ishihara T, Miyazaki S. Cyclic stress-strain characteristics of Ti-Ni and Ti-Ni-Cu shape memory alloys. Mater Sci Eng A 1995;202:148–56. https://doi.org/https://doi.org/10.1016/0921-5093(95)09801-1.

[57] Boyd JG, Lagoudas DC. A thermodynamical constitutive model for shape memory materials. Part I. The monolithic shape memory alloy. Int J Plast 1996;12:805–42. https://doi.org/https://doi.org/10.1016/S0749-6419(96)00030-7.

[58] Alam MS, Youssef MA, Nehdi M. Analytical prediction of the seismic behaviour of superelastic shape memory alloy reinforced concrete elements. Eng Struct 2008;30:3399–411. https://doi.org/https://doi.org/10.1016/j.engstruct.2008.05.025.

[59] Liu Y. Mechanical and thermomechanical properties of a Ti50Ni25Cu25 melt spun ribbon. Mater Sci Eng A 2003;354:286–91. https://doi.org/https://doi.org/10.1016/S0921-5093(03)00018-2.

[60] Zhang Y, Hu X, Zhu S. Seismic performance of benchmark base-isolated bridges with superelastic Cu–Al–Be restraining damping device. Struct Control Heal Monit 2009;16:668–85. https://doi.org/10.1002/stc.327.

[61] Omori T, Ando K, Okano M, Xu X, Tanaka Y, Ohnuma I, et al. Superelastic Effect in Polycrystalline Ferrous Alloys. Science (80-) 2011;333:68–71. https://doi.org/10.1126/science.1202232.

[62] Tanaka Y, Himuro Y, Kainuma R, Sutou Y, Omori T, Ishida K. Ferrous Polycrystalline Shape-Memory Alloy Showing Huge Superelasticity. Science (80-) 2010;327:1488–90. https://doi.org/10.1126/science.1183169.

[63] Priestley MJN, Calvi GM, Kowalsky MJ. Displacement-based Seismic Design of Structures. IUSS Press,; 2007.

[64] Hartl DJ, Lagoudas DC. Aerospace applications of shape memory alloys. Proc Inst Mech Eng Part G J Aerosp Eng 2007;221:535–52.

[65] Zhang Y, Zhu S. A shape memory alloy-based reusable hysteretic damper for seismic hazard mitigation. Smart Mater Struct 2007;16:1603.

[66] Savi MA, Pacheco PMCL, Braga AMB. Chaos in a shape memory two-bar truss. Int J Non Linear Mech 2002;37:1387–95.

[67] Sun S, Rajapakse RKND. Dynamic response of a frame with SMA bracing. Proc SPIE 2003;5053:262–70. https://doi.org/10.1117/12.484201.

[68] Zareie S, Alam MS, Seethaler RJ, Zabihollah A. Effect of cyclic loads on sma-based component of cable-stayed bridge. 7th Int. Spec. Conf. Eng. Mech. Mater., Laval: 2019.

[69] Aryan H, Ghassemieh M. A superelastic protective technique for mitigating the effects of vertical and horizontal seismic excitations on highway bridges. J Intell Mater Syst Struct

2017;28:1533–52.

[70] Mansouri I, Safa M, Ibrahim Z, Kisi O, Tahir MM, Baharom S, et al. Strength prediction of rotary brace damper using MLR and MARS. Struct Eng Mech 2016;60:471–88.

[71] Mansouri I, Shariati M, Safa M, Ibrahim Z, Tahir MM, Petković D. Analysis of influential factors for predicting the shear strength of a V-shaped angle shear connector in composite beams using an adaptive neuro-fuzzy technique. J Intell Manuf 2017:1–11.

[72] Mansouri I, Ghodrati Amiri G, Hu JW, Khoshkalam M, Soori S, Shahbazi S. Seismic fragility estimates of LRB base isolated frames using performance-based design. Shock Vib 2017;2017.

[73] Zeynali K, Monir HS, Mirzai NM, Hu JW. Experimental and numerical investigation of lead-rubber dampers in chevron concentrically braced frames. Arch Civ Mech Eng 2018;18:162–78.

[74] McGavin GL, Guerin G. Real-time seismic damping and frequency control of steel structures using Nitinol wire. SPIE's 9th Annu. Int. Symp. Smart Struct. Mater., 2002, p. 176–85.

[75] NourEldin M, Naeem A, Kim J. Life-cycle cost evaluation of steel structures retrofitted with steel slit damper and shape memory alloy--based hybrid damper. Adv Struct Eng 2018:1369433218773487.

[76] Lee J, Kim J. Development of box-shaped steel slit dampers for seismic retrofit of building structures. Eng Struct 2017;150:934–46.

[77] Li H-N, Liu M-M, Fu X. An innovative re-centering {SMA}-lead damper and its application to steel frame structures. Smart Mater Struct 2018;27:75029. https://doi.org/10.1088/1361-665x/aac28f.

[78] Seelecke S, Heintze O, Masuda A. Simulation of earthquake-induced structural vibrations in systems with SMA damping elements. SPIE's 9th Annu. Int. Symp. Smart Struct. Mater., 2002, p. 238–45.

[79] Vafaei D, Eskandari R. Seismic performance of steel mega braced frames equipped with shape-memory alloy braces under near-fault earthquakes. Struct Des Tall Spec Build 2016;25:3–21.

[80] Sultana P, Youssef MA. Str-834: seismic performance of modular steel frames equipped with shape memory alloy braces 2016.

[81] Moradi S, Alam MS, Asgarian B. Incremental dynamic analysis of steel frames equipped with NiTi shape memory alloy braces. Struct Des Tall Spec Build 2014;23:1406–25.

[82] Gao N, Jeon J-S, Hodgson DE, DesRoches R. An innovative seismic bracing system based on a superelastic shape memory alloy ring. Smart Mater Struct 2016;25:55030.

[83] Qiu C, Zhu S. Shake table test and numerical study of self-centering steel frame with SMA braces. Earthq Eng Struct Dyn 2017;46:117–37.

[84] Haque ABMR, Alam MS. Hysteretic Behaviour of a Piston Based Self-centering (PBSC) Bracing System Made of Superelastic SMA Bars--A Feasibility Study. Structures, vol. 12, 2017, p. 102–14.

[85] Issa AS, Alam MS. Seismic Performance of a Novel Single and Double Spring-Based Piston Bracing. J Struct Eng 2018;145:4018261.

[86] Zareie S, Alam MS, Seethaler RJ, Abolghassem Z. A shape memory alloy-magnetorheological fluid core bracing system for civil engineering applications: a feasibility study. 7th Int. Spec. Conf. Eng. Mech. Mater., Montreal: 2019.

[87] Zareie S, Mirzai N, Alam MS, Seethaler RJ. An introduction and modeling of novel shape

memory alloy-based bracing. CSCE 2017, Vancouver, Canada: 2017.

[88] Qiu C-X, Zhu S. Performance-based seismic design of self-centering steel frames with SMA-based braces. Eng Struct 2017;130:67–82.

[89] Haque ABM, Alam MS. Cyclic Performance of a Piston Based Self-Centering Bracing System. Struct. Congr. 2015, 2015, p. 2360–71.

[90] Moradi S, Alam MS. Feasibility study of utilizing superelastic shape memory alloy plates in steel beam--column connections for improved seismic performance. J Intell Mater Syst Struct 2015;26:463–75.

[91] Wang W, Fang C, Yang X, Chen Y, Ricles J, Sause R. Innovative use of a shape memory alloy ring spring system for self-centering connections. Eng Struct 2017;153:503–15.

[92] Fang C, Yam MCH, Chan T-M, Wang W, Yang X, Lin X. A study of hybrid self-centring connections equipped with shape memory alloy washers and bolts. Eng Struct 2018;164:155–68.

[93] Cissé C, Zaki W, Ben Zineb T. Numerical simulation of the behavior of steel T-stubs connected by Fe-based shape memory alloy bolts. J Intell Mater Syst Struct 2018:1045389X18781263.

[94] Farmani MA, Ghassemieh M. Steel beam-to-column connections equipped with SMA components and web energy dissipating devices. J Constr Steel Res 2017;135:30–48.

[95] Nastri E, D'Aniello M, Zimbru M, Streppone S, Landolfo R, Montuori R, et al. Seismic response of steel Moment Resisting Frames equipped with friction beam-to-column joints. Soil Dyn Earthq Eng 2019;119:144–57.

[96] Abolmaali A, Treadway J, Aswath P, Lu FK, McCarthy E. Hysteresis behavior of t-stub connections with superelastic shape memory fasteners. J Constr Steel Res 2006;62:831–8.

[97] Leon RT, DesRoches R, Ocel J, Hess G. Innovative beam column connections using shape memory alloys. SPIE's 8th Annu. Int. Symp. Smart Struct. Mater., 2001, p. 227–37.

[98] Ocel J, DesRoches R, Leon RT, Hess WG, Krumme R, Hayes JR, et al. Steel beam-column connections using shape memory alloys. J Struct Eng 2004;130:732–40.

[99] Hedayati Dezfuli F, Alam MS. Performance of carbon fiber-reinforced elastomeric isolators manufactured in a simplified process: experimental investigations. Struct Control Heal Monit 2014;21:1347–59. https://doi.org/10.1002/stc.1653.

[100] Dezfuli FH, Alam MS. Shape memory alloy wire-based smart natural rubber bearing. Smart Mater Struct 2013;22:13–45.

[101] Dezfuli FH, Alam MS. Performance-based assessment and design of FRP-based high damping rubber bearing incorporated with shape memory alloy wires. Eng Struct 2014;61:166–83.

[102] Dezfuli FH, Alam MS. Sensitivity analysis of carbon fiber-reinforced elastomeric isolators based on experimental tests and finite element simulations. Bull Earthq Eng 2014;12:1025–43.

[103] Li S, Hedayati Dezfuli F, Wang J-Q, Alam MS. Displacement-Based Seismic Design of Steel, FRP, and SMA Cable Restrainers for Isolated Simply Supported Bridges. J Bridg Eng 2018;23:4018032.

[104] Li S, Dezfuli FH, Wang J, Alam MS. Longitudinal seismic response control of long-span cable-stayed bridges using shape memory alloy wire-based lead rubber bearings under near-fault records. J Intell Mater Syst Struct 2018;29:703–28.

[105] Dezfuli FH, Alam MS. Seismic vulnerability assessment of a steel-girder highway bridge equipped with different SMA wire-based smart elastomeric isolators. Smart Mater Struct

2016;25:75039.

[106] Dezfuli FH, Alam MS. Hysteresis model of shape memory alloy wire-based laminated rubber bearing under compression and unidirectional shear loadings. Smart Mater Struct 2015;24:65022.

[107] Hu JW. Seismic analysis and parametric study of SDOF lead-rubber bearing (LRB) isolation systems with recentering shape memory alloy (SMA) bending bars. J Mech Sci Technol 2016;30:2987–99.

[108] Gur S, Mishra SK, Chakraborty S. Performance assessment of buildings isolated by shape-memory-alloy rubber bearing: Comparison with elastomeric bearing under near-fault earthquakes. Struct Control Heal Monit 2014;21:449–65.

[109] Wilde K, Gardoni P, Fujino Y. Base isolation system with shape memory alloy device for elevated highway bridges. Eng Struct 2000;22:222–9.

[110] Mishra SK, Gur S, Roy K, Chakraborty S. Response of Bridges isolated by shape memory--alloy rubber bearing. J Bridg Eng 2015;21:4015071.

[111] Li H, Liu M, Ou J. Vibration mitigation of a stay cable with one shape memory alloy damper. Struct Control Heal Monit 2004;11:21–36.

[112] DesRoches R, Delemont M. Seismic retrofit of simply supported bridges using shape memory alloys. Eng Struct 2002;24:325–32.

[113] Zuo X-B, Li A-Q, Sun W, Sun X-H. Optimal design of shape memory alloy damper for cable vibration control. J Vib Control 2009;15:897–921.

[114] Zareie S, Mirzai N, Alam MS, Seethaler RJ. A dynamic analysis of a novel shape memory alloy-based bracing system. CSCE 2017, Vancouver, Canada: 2017.

[115] Qian H, Li H, Song G. Experimental investigations of building structure with a superelastic

shape memory alloy friction damper subject to seismic loads. Smart Mater Struct 2016;25:125026.

[116] Attanasi G, Auricchio F, Crosti C, Fenves GL. An innovative isolation bearing with shape memory alloys. Proc. 14th World Conf. Earthq. Eng. (Beijing, China, 12--17 Oct. 2008), 2008.

[117] Dolce M, Cardone D, Marnetto R. SMA recentering devices for seismic isolation of civil structures. SPIE's 8th Annu. Int. Symp. Smart Struct. Mater., 2001, p. 238–49.

[118] Alam MS, Dezfuli FH. Performance Comparison between SMA-based Natural Rubber Bearing and SMA-based High Damping Rubber Bearing. 7th Natl. Seism. Conf. Bridg. Highw. Oakland, Calif., 2013.

[119] Ghafoori E, Neuenschwander M, Shahverdi M, Czaderski C, Fontana M. Elevated temperature behavior of an iron-based shape memory alloy used for prestressed strengthening of civil structures. Constr Build Mater 2019;211:437–52.

[120] Roh H, Reinhorn AM. Hysteretic behavior of precast segmental bridge piers with superelastic shape memory alloy bars. Eng Struct 2010;32:3394–403.

[121] Thomson P, Balas GJ, Leo PH. The use of shape memory alloys for passive structural damping. Smart Mater Struct 1995;4:36.

[122] Deng Z, Li Q, Sun H. Behavior of concrete beam with embedded shape memory alloy wires. Eng Struct 2006;28:1691–7.

[123] Davis A, Mirsayar M, Sheahan E, Hartl D. Structural health monitoring for DOT using magnetic shape memory alloy cables in concrete. Nondestruct. Charact. Monit. Adv. Mater. Aerospace, Civ. Infrastructure, Transp. XII, vol. 10599, 2018, p. 10599-10599–8.

[124] Sherif MM, Tanks J, Ozbulut OE. Acoustic emission analysis of cyclically loaded

superelastic shape memory alloy fiber reinforced mortar beams. Cem Concr Res 2017;95:178–87.

[125] Liu X, Li J, Tsang H-H, Wilson J. Enhancing seismic performance of unbonded prestressed concrete bridge column using superelastic shape memory alloy. J Intell Mater Syst Struct 2018;29:3082–96.

[126] Parvin A, Raad J. Internal and External Reinforcement of Concrete Members by Use of Shape Memory Alloy and Fiber Reinforced Polymers under Cyclic Loading—A Review. Polymers (Basel) 2018;10:376.

[127] Jung D, Wilcoski J, Andrawes B. Bidirectional shake table testing of RC columns retrofitted and repaired with shape memory alloy spirals. Eng Struct 2018;160:171–85.

[128] Rojob H, El-Hacha R. Self-Prestressing Using Iron-Based Shape Memory Alloy for Flexural Strengthening of Reinforced Concrete Beams. ACI Struct J 2017;114:523.

[129] Abdulridha A, Palermo D. Behaviour and modelling of hybrid SMA-steel reinforced concrete slender shear wall. Eng Struct 2017;147:77–89.

[130] Azadpour F, Maghsoudi AA. Crack Width Study for Two-Span RC Beams Strengthened with Ni-Ti Strands under Cyclic Loading. Smart Mater Struct 2019.

[131] Shahverdi M, Czaderski C, Motavalli M. Iron-based shape memory alloys for prestressed near-surface mounted strengthening of reinforced concrete beams. Constr Build Mater 2016;112:28–38.

[132] Moni M. Performance of shape memory alloy reinforced concrete frames under extreme loads. University of British Columbia, 2011.

[133] Fang C, Wang W, He C, Chen Y. Self-centring behaviour of steel and steel-concrete composite connections equipped with NiTi SMA bolts. Eng Struct 2017;150:390–408.

[134] Oudah F, El-Hacha R. Innovative Self-Centering Concrete Beam-Column Connection Reinforced Using Shape Memory Alloy. ACI Struct J 2018;15.

[135] Chowdhury MA, Rahmzadeh A, Moradi S, Alam MS. Feasibility of using reduced length superelastic shape memory alloy strands in post-tensioned steel beam--column connections. J Intell Mater Syst Struct 2019;30:283–307.

[136] Billah AHMM, Alam MS. Seismic performance of concrete columns reinforced with hybrid shape memory alloy (SMA) and fiber reinforced polymer (FRP) bars. Constr Build Mater 2012;28:730–42. https://doi.org/https://doi.org/10.1016/j.conbuildmat.2011.10.020.

[137] Nehdi M, Alam MS, Youssef MA. Development of corrosion-free concrete beam–column joint with adequate seismic energy dissipation. Eng Struct 2010;32:2518–28. https://doi.org/https://doi.org/10.1016/j.engstruct.2010.04.020.

[138] Youssef MA, Alam MS, Nehdi M. Experimental investigation on the seismic behavior of beam-column joints reinforced with superelastic shape memory alloys. J Earthq Eng 2008;12:1205–22.

[139] Saiidi MS, Wang H. Exploratory study of seismic response of concrete columns with shape memory alloys reinforcement. ACI Struct J 2006;103:436.

[140] Song G, Ma N, Li H-N. Review of applications of shape memory alloys in civil structures. Eng. Constr. Oper. Challenging Environ. Earth Sp. 2004, 2004, p. 559–66.

[141] Turkington DH, Carr AJ, Cooke N, Moss PJ. Seismic design of bridges on lead-rubber bearings. J Struct Eng 1989;115:3000–16.

[142] Billah AHMM, Alam MS. Plastic hinge length of shape memory alloy (SMA) reinforced concrete bridge pier. Eng Struct 2016;117:321–31.

[143] Alam MS, Nehdi M, Youssef MA. Seismic performance of concrete frame structures

reinforced with superelastic shape memory alloys. Smart Struct Syst 2009;5:565–85.

[144] Cortés-Puentes WL, Palermo D. SMA tension brace for retrofitting concrete shear walls. Eng Struct 2017;140:177–88.

[145] Shin M, Andrawes B. Emergency repair of severely damaged reinforced concrete columns using active confinement with shape memory alloys. Smart Mater Struct 2011;20:65018.

[146] Moser K, Bergamini A, Christen R, Czaderski C. Feasibility of concrete prestressed by shape memory alloy short fibers. Mater Struct 2005;38:593–600.

[147] Song G, Mo YL. Increasing concrete structural survivability using smart materials. A Propos Submitt to Grants to Enhanc Adv Res (GEAR), Univ Houst 2003.

[148] Dolce M, Cardone D, Ponzo FC. Shaking-table tests on reinforced concrete frames with different isolation systems. Earthq Eng Struct Dyn 2007;36:573–96.

[149] Ceccotti A. Timber-concrete composite structures. Timber Eng Step 1995;2.

[150] Chen J, Chen YF, Shi X, Zhao Y, Li T. Hysteresis behavior of traditional timber structures by full-scale tests. Adv Struct Eng 2018;21:287–99.

[151] Köhler J. Reliability of timber structures. vdf Hochschulverlag AG; 2007.

[152] Xue J, Xu D. Shake table tests on the traditional column-and-tie timber structures. Eng Struct 2018;175:847–60.

[153] Izzi M, Casagrande D, Bezzi S, Pasca D, Follesa M, Tomasi R. Seismic behaviour of Cross-Laminated Timber structures: A state-of-the-art review. Eng Struct 2018;170:42–52.

[154] Cardone D, Sofia S. Experimental Evaluation of a Device Prototype Based on Shape Memory Alloys for the Retrofit of Historical Buildings. J Mater Eng Perform 2012;21:2719–28. https://doi.org/10.1007/s11665-012-0414-x.

[155] Huang H, Chang W-S, Mosalam KM. Feasibility of shape memory alloy in a tuneable mass

damper to reduce excessive in-service vibration. Struct Control Heal Monit 2017;24:e1858. https://doi.org/10.1002/stc.1858.

[156] Chang W-S, Murakami S, Komatsu K, Araki Y, Shrestha K, Omori T, et al. Technical note: Potential to use shape memory alloy in timber dowel-type connections. Wood Fiber Sci 2013;45:330–4.

[157] van de Lindt JW, Potts A. Shake table testing of a superelastic shape memory alloy response modification device in a wood shearwall. J Struct Eng 2008;134:1343–52.

[158] Huang H, Chang W-S. Seismic resilience timber connection—adoption of shape memory alloy tubes as dowels. Struct Control Heal Monit 2017;24:e1980.

[159] Ahamed R, Choi S-B, Ferdaus MM. A state of art on magneto-rheological materials and their potential applications. J Intell Mater Syst Struct 2018;29:2051–2095.

[160] Ashour O, Rogers CA, Kordonsky W. Magnetorheological fluids: materials, characterization, and devices. J Intell Mater Syst Struct 1996;7:123–30.

[161] Ashour ON, Kinder D, Giurgiutiu V, Rogers CA. Manufacturing and characterization of magnetorheological fluids. Smart Struct. Mater. 97, 1997, p. 174–84.

[162] Naji J, Zabihollah A, Behzad M. Vibration characteristics of laminated composite beams with magnetorheological layer using layerwise theory. Mech Adv Mater Struct 2017:1–10.

[163] Naji J, Zabihollah A, Behzad M. Layerwise theory in modeling of magnetorheological laminated beams and identification of magnetorheological fluid. Mech Res Commun 2016;77:50–9.

[164] Sapiński B, Filuś J. Analysis of parametric models of MR linear damper. J Theor Appl Mech 2003;41:215–40.

[165] Yang S, Li S, Wang X, Gordaninejad F, Hitchcock G. A hysteresis model for magneto-

rheological damper. Int J Nonlinear Sci Numer Simul 2005;6:139–44.

[166] Grunwald A. Design and optimization of magnetostrictive actuator. Dublin City University, 2007.

[167] Sakurai T, Morishita S. Seismic response reduction of a three-story building by an MR grease damper. Front Mech Eng 2017;12:224–33.

[168] Sahin H, Gordaninejad F, Wang X, Fuchs A. Rheological behavior of magneto-rheological grease (MRG). Act. Passiv. Smart Struct. Integr. Syst. 2007, vol. 6525, 2007, p. 65250D.

[169] Ze-bing DAI, Jin-zhi H, Hong-xia W. Semi-active control of a cable-stayed bridge under multiple-support excitations. J Zhejiang Univ A 2004;5:317–25.

[170] Danas K, Kankanala S V, Triantafyllidis N. Experiments and modeling of iron-particle-filled magnetorheological elastomers. J Mech Phys Solids 2012;60:120–38.

[171] Jung H-J, Lee S-J, Jang D-D, Kim I-H, Koo J-H, Khan F. Dynamic characterization of magneto-rheological elastomers in shear mode. IEEE Trans Magn 2009;45:3930–3.

[172] Eem SH, Jung H-J, Koo JH. Seismic performance evaluation of an MR elastomer-based smart base isolation system using real-time hybrid simulation. Smart Mater Struct 2013;22:55003.

[173] Oliveira F, Botto MA, Morais P, Suleman A. Semi-active structural vibration control of base-isolated buildings using magnetorheological dampers. J Low Freq Noise, Vib Act Control 2017:1461348417725959.

[174] Reichert BA. Application of magnetorheological dampers for vehicle seat suspensions. Virginia Polytechnic Institute and State University, 1997.

[175] Ebrahimi B. Development of hybrid electromagnetic dampers for vehicle suspension systems. University of Waterloo, 2009.

[176] Dumne SM, Shrimali MK, Bharti SD. Earthquake performance of hybrid controls for coupled buildings with MR dampers and sliding base isolation. Asian J Civ Eng 2017;18:63–97.

[177] Zemp R, de la Llera JC, Roschke P. Tall building vibration control using a TM-MR damper assembly: Experimental results and implementation. Earthq Eng Struct Dyn 2011;40:257–71.

[178] Zemp R, De La Llera JC, Almazán JL. Tall building vibration control using a TM-MR damper assembly. Earthq Eng Struct Dyn 2011;40:339–54. https://doi.org/10.1002/eqe.1033.

[179] INOUE N, NISHIMURA H, IWATA N, MIYAHARA Y, NAKASONE J, WATAKABE M, et al. Study on semi-active isolation system with magneto-rheological fluid damper 2004.

[180] Khan SU-R. The effects of unmitigated idle time on the performance of magnetorheological dampers as a structural protective system. 2018.

[181] Lara L, Brito J, Gallego CAG. Structural control strategies based on magnetorheological dampers managed using artificial neural networks and fuzzy logic. Rev UIS Ing 2017;16:227–42.

[182] Al-Fahdawi OAS, Barroso LR, Soares RW. Utilizing the Adaptive Control in Mitigating the Seismic Response of Adjacent Buildings Connected with MR Dampers. 2018 Annu. Am. Control Conf., 2018, p. 912–7.

[183] Winter BD, Swartz RA. Low-force magneto-rheological damper design for small-scale structural control. Struct Control Heal Monit 2017;24:e1990.

[184] Dyke, SJ and Spencer Jr B. Developing New Analytical and Numerical Models for Mr

Fluid. 2nd Int. Work. Struct. Control, 1996, p. 163--173.

[185] Dyke SJ, Spencer BF. A comparison of semi-active control strategies for the MR damper. Intell. Inf. Syst. 1997. IIS'97. Proc., 1997, p. 580–4.

[186] Liu Y, Gordaninejad F, Evrensel CA, Hitchcock GH, Wang X. Variable-structure-system-based logic fuzzy control of bridge vibration using fail-safe magnetorheological fluid dampers. Smart Struct. Mater. 2002 Smart Syst. Bridg. Struct. Highw., vol. 4696, 2002, p. 219–28.

[187] Zareie S, Zabihollah A. The Recent Advances in Magnetorheological Fluids-Based Applications. Emerg. Trends Mechatronics, IntechOpen; 2020.

[188] Jimnez R, Alvarez L. Real time identification of structures with magnetorheological dampers. Decis. Control. 2002, Proc. 41st IEEE Conf., vol. 1, 2002, p. 1017–22.

[189] Zhu, Xiaocong and Jing, Xingjian and Cheng L. Magnetorheological fluid dampers: a review on structure design and analysis. J Intell Mater Syst Struct 2012;23:839–73.

[190] Wang Q, Dong X, Li L, Ou J. Study on an improved variable stiffness tuned mass damper based on conical magnetorheological elastomer isolators. Smart Mater Struct 2017;26:105028.

[191] Symans MD, Kelly SW. Fuzzy logic control of bridge structures using intelligent semi-active seismic isolation systems. Earthq Eng Struct Dyn 1999;28:37–60.

[192] Behrooz M, Yarra S, Mar D, Pinuelas N, Muzinich B, Publicover NG, et al. A self-sensing magnetorheological elastomer-based adaptive bridge bearing with a wireless data monitoring system. Sensors Smart Struct. Technol. Civil, Mech. Aerosp. Syst. 2016, vol. 9803, 2016, p. 98030D.

[193] Xing Z-W, Yu M, Fu J, Wang Y, Zhao L-J. A laminated magnetorheological elastomer

bearing prototype for seismic mitigation of bridge superstructures. J Intell Mater Syst Struct 2015;26:1818–25.

[194] Li Y, Li J, Li W, Samali B. Development and characterization of a magnetorheological elastomer based adaptive seismic isolator. Smart Mater Struct 2013;22:35005.

[195] Zhao L, Yu M, Fu J, Zhu M, Li B. A miniature MRE isolator for lateral vibration suppression of bridge monitoring equipment: design and verification. Smart Mater Struct 2017;26:47001.

[196] Behbahani HP, Bin Adnan A, Vafaei M, Shad H, Pheng OP. Vibration Mitigation of Structures through TLCD with Embedded Baffles. Exp Tech 2017;41:139–51.

[197] Dziedziech K, Ghosh A, Iwaniec J, Basu B, Staszewski WJ, Uhl T. Analysis of tuned liquid column damper nonlinearities. Eng Struct 2018;171:1027–33.

[198] Wang JY, Ni YQ, Ko JM, Spencer BF. Magneto-rheological tuned liquid column dampers (MR-TLCDs) for vibration mitigation of tall buildings: Modelling and analysis of open-loop control. Comput Struct 2005;83:2023–34. https://doi.org/10.1016/j.compstruc.2005.03.011.

[199] Miandoab EM, Yousefi-Koma A. Control of dry friction oscillator using semi-active magneto-rheological tuned liquid column damper. Proc Inst Mech Eng Part C J Mech Eng Sci 2014;228:2495–502.

[200] Ni YQ, Ying ZG, Wang JY, Ko JM, Spencer Jr BF. Stochastic optimal control of wind-excited tall buildings using semi-active MR-TLCDs. Probabilistic Eng Mech 2004;19:269–77.

[201] Yalla SK, Kareem A, Kantor JC. Semi-active tuned liquid column dampers for vibration control of structures. Eng Struct 2001;23:1469–79.

[202] Cheng C-W, Lee HH, Luo Y-T. Experimental study of controllable MR-TLCD applied to the mitigation of structure vibration. Smart Struct Syst 2015;15:1481–501.

[203] Sun HX, Wang XY. An investigation on a semi-active magnetorheological tuned liquid column damper (MR-TLCD). Act. Passiv. Smart Struct. Integr. Syst. 2016, vol. 9799, 2016, p. 979933.

[204] Braz-César MT, Folhento PLP, Barros RC. Numerical Simulation of Torsional Response Control of a Plan-Eccentric Mass Distribution Building by Using Magnetorheological Dampers. 2018 13th APCA Int. Conf. Control Soft Comput., 2018, p. 358–63.

[205] Bhaiya V, Bharti SD, Shrimali MK, Datta TK. Genetic Algorithm Based Optimum Semi-Active Control of Building Frames Using Limited Number of Magneto-Rheological Dampers and Sensors. J Dyn Syst Meas Control 2018;140:101013-101013–13.

[206] Bozorgvar M, Zahrai SM. Semi-active seismic control of buildings using MR damper and adaptive neural-fuzzy intelligent controller optimized with genetic algorithm. J Vib Control 2018;25:273–285.

[207] Aly AM. Control of wind-induced motion in high-rise buildings with hybrid TM/MR dampers. Wind Struct 2015;21:565–95.

[208] Yang J, Sun S, Tian T, Li W, Du H, Alici G, et al. Development of a novel multi-layer MRE isolator for suppression of building vibrations under seismic events. Mech Syst Signal Process 2016;70–71:811–20. https://doi.org/10.1016/j.ymssp.2015.08.022.

[209] Hadzir MNH, Norfaidayu ZA, Sabri MSM, Abu-Bakar M-H. Investigation of Damping Coefficient For Magnetorheological Elastomer. MATEC Web Conf., vol. 217, 2018, p. 2003.

[210] Gu X, Li J, Li Y. Adaptive base isolation system with magnetorheological elastomer base

isolators: numerical investigations. 6th World Conf. Struct. Control Monit., 2014.

[211] Lakhani MT, Soni DP. Comparative Study of Smart Base-Isolation Using Fuzzy Control and Neural Network. Procedia Eng 2017;173:1825–32.

[212] Yoshioka H, Ramallo JC, Spencer Jr BF. "Smart" base isolation strategies employing magnetorheological dampers. J Eng Mech 2002;128:540–51.

[213] Iwata N, Hata K, Sodeyama H, Sunakoda K, Fujitani H, Hiwatashi T, et al. Application of MR damper to base-isolated structures. Smart Struct. Mater. 2002 Smart Syst. Bridg. Struct. Highw., vol. 4696, 2002, p. 352–63.

[214] Zamani A-A, Tavakoli S, Etedali S, Sadeghi J. Adaptive fractional order fuzzy proportional--integral--derivative control of smart base-isolated structures equipped with magnetorheological dampers. J Intell Mater Syst Struct 2018;29:830–44.

[215] Fu W, Zhang C, Sun L, Askari M, Samali B, Chung KL, et al. Experimental investigation of a base isolation system incorporating MR dampers with the high-order single step control algorithm. Appl Sci 2017;7:344.

[216] Vulcu C, Dubin\ua D, Popa N, Vekas L, Ghi\ct\ua G, Sireteanu T, et al. Hybrid seismic protection system: Buckling restrained brace of nano-micro composite magneto rheological damper. Ce/Papers 2017;1:2936–45.

[217] Lee S-H, Min K-W, Chung L, Lee S-K, Lee M-K, Hwang J-S, et al. Bracing systems for installation of MR dampers in a building structure. J Intell Mater Syst Struct 2007;18:1111–20.

[218] Sigaher-Boyle AN, Constantinou MC. Scissor-Jack-Damper Energy Dissipation System 2004.

[219] Weber F, Boston C, Maślanka M. An adaptive tuned mass damper based on the emulation

of positive and negative stiffness with an MR damper. Smart Mater Struct 2010;20:15012.

[220] Spencer Jr BF, Nagarajaiah S. State of the art of structural control. J Struct Eng 2003;129:845–56.

[221] Jung HJ, Jang DD, Lee HJ, Moon SJ. Experimental Investigation of Effectiveness of Smart Passive System for Seismic Protection of Building Structures. Adv. Sci. Technol., vol. 56, 2008, p. 355–62.

[222] Hrovat D, Barak P, Rabins M. Semi-active versus passive or active tuned mass dampers for structural control. J Eng Mech 1983;109:691–705.

[223] Cesmeci S, Gordaninejad F, Ryan KL, Eltahawy W. A liquid spring--magnetorheological damper system under combined axial and shear loading for three-dimensional seismic isolationof structures. J Intell Mater Syst Struct 2018;29:3517–3532.

[224] Sun S, Yang J, Du H, Zhang S, Yan T, Nakano M, et al. Development of magnetorheological elastomers–based tuned mass damper for building protection from seismic events. J Intell Mater Syst Struct 2018;29:1777–89. https://doi.org/10.1177/1045389X17754265.

[225] Heo G, Kim C, Jeon S, Lee C, Seo S. A study on a MR damping system with lumped mass for a two-span bridge to diminish its earthquake-induced longitudinal vibration. Soil Dyn Earthq Eng 2017;92:312–29.

[226] Li H, Liu J, Ou J. Seismic response control of a cable-stayed bridge using negative stiffness dampers. Struct Control Heal Monit 2011;18:265–88.

[227] Choi K-M, Jung H-J, Cho S-W, Lee I-W. Application of smart passive damping system using MR damper to highway bridge structure. J Mech Sci Technol 2007;21:870–4.

[228] Maślanka M, Sapiński B, Snamina J. Experimental study of vibration control of a cable with

an attached MR damper. J Theor Appl Mech 2007;45:893–917.

[229] Lou WJ, Ni Y-Q, Ko JM. Modal damping and stepping-switch control of stay cables with magnetorheological fluid dampers. Smart Struct. Mater. 2001 smart Syst. Bridg. Struct. Highw., vol. 4330, 2001, p. 354–65.

[230] Yang M-G, Chen Z-Q, Hua X-G. An experimental study on using MR damper to mitigate longitudinal seismic response of a suspension bridge. Soil Dyn Earthq Eng 2011;31:1171–81.

[231] Lin P-Y, Lin T-K. Control of seismically isolated bridges by magnetorheological dampers and a rolling pendulum system. Struct Control Heal Monit 2012;19:278–94.

[232] Yarra S, Behrooz M, Pekcan G, Itani A, Gordaninejad F. A large-scale adaptive magnetorheological elastomer-based bridge bearing. Act. Passiv. Smart Struct. Integr. Syst. 2017, vol. 10164, 2017, p. 1016425.

[233] Weber F, Distl H. Amplitude and frequency independent cable damping of Sutong Bridge and Russky Bridge by magnetorheological dampers. Struct Control Heal Monit 2015;22:237–54.

[234] Duan YF, Ni YQ, Ko JM. State-derivative feedback control of cable vibration using semiactive magnetorheological dampers. Comput Civ Infrastruct Eng 2005;20:431–49.

[235] Guo A, Li Z, Li H, Ou J. Experimental and analytical study on pounding reduction of base-isolated highway bridges using MR dampers. Earthq Eng Struct Dyn 2009;38:1307–33.

[236] Sheikh MN, Xiong J, Li WH. Reduction of seismic pounding effects of base-isolated RC highway bridges using MR damper. Struct Eng Mech 2012;41:791–803.

[237] Renzi E, Serino G. Testing and modelling a semi-actively controlled steel frame structure equipped with MR dampers. Struct Control Heal Monit 2004;11:189–221.

[238] Sheikh MN, Xiong J, Li W. MR damper in reducing pounding effect of base-isolated rc highway bridge. AEES Conf. 2010 Aust., Australian Earthquake Engineering Society.; 2011.

[239] Wang X, Gordaninejad F. Lyapunov-based control of a bridge using magneto-rheological fluid dampers. J Intell Mater Syst Struct 2002;13:415–9.

[240] Li R, Zhou M, Wu M, Tang X. Semi-Active Predictive Control of Isolated Bridge Based on Magnetorheological Elastomer Bearing. J Shanghai Jiaotong Univ 2019;24:64–70. https://doi.org/10.1007/s12204-018-2009-7.

[241] Li R, Mu W, Zhang L, Wang X. Design and testing performance of a magneto-rheological elastomer isolator for a scaled bridge system. J Intell Mater Syst Struct 2018;29:171–82. https://doi.org/10.1177/1045389X17721033.

[242] Wang Z, Chen Z, Gao H, Wang H. Development of a Self-Powered Magnetorheological Damper System for Cable Vibration Control. Appl Sci 2018;8:118.

[243] Kim Y, Mahajan AA. Smart Control of Seismically Excited Highway Bridges. Comput. Methods Earthq. Eng., Springer; 2017, p. 387–403.

[244] Li H, Liu M, Li J, Guan X, Ou J. Vibration control of stay cables of the shandong binzhou yellow river highway bridge using magnetorheological fluid dampers. J Bridg Eng 2007;12:401–9.

[245] Weber F, Maślanka M. Precise stiffness and damping emulation with MR dampers and its application to semi-active tuned mass dampers of Wolgograd Bridge. Smart Mater Struct 2013;23:15019.

[246] Weber F, Maślanka M. Frequency and damping adaptation of a TMD with controlled MR damper. Smart Mater Struct 2012;21:55011.

[247] Weber F. Dynamic characteristics of controlled MR-STMDs of Wolgograd Bridge. Smart Mater Struct 2013;22:95008.

[248] Symans MD, Constantinou MC. Semi-active control systems for seismic protection of structures: a state-of-the-art review. Eng Struct 1999;21:469–87.

[249] Loh C-H, Lin P-Y, Chung N-H. Experimental verification of building control using active bracing system. Earthq Eng Struct Dyn 1999;28:1099–119.

[250] Ghaffarzadeh H, Younespour A. Active tendons control of structures using block pulse functions. Struct Control Heal Monit 2014;21:1453–64.

[251] Zuo X-B, Li a.-Q, Sun X-H. Optimal Design of Shape Memory Alloy Damper for Cable Vibration Control. J Vib Control 2009;15:897–921. https://doi.org/10.1177/1077546308094916.

[252] Wang DH, Ai HX, Liao WH. A magnetorheological valve with both annular and radial fluid flow resistance gaps. Smart Mater Struct 2009;18:115001.

[253] Boese H, Ehrlich J. Performance of magnetorheological fluids in a novel damper with excellent fail-safe behavior. J Intell Mater Syst Struct 2009.

[254] Butz T, Von Stryk O. Modelling and simulation of electro-and magnetorheological fluid dampers. ZAMM 2002;82:3–20.

[255] Gillespie T. Development of semi-active damper for heavy off-road military vehicles. Masters Abstr. Int., vol. 45, 2006.

[256] Hedayati Dezfuli F, Alam MS. Shape memory alloy wire-based smart natural rubber bearing. Smart Mater Struct 2013;22:45013. https://doi.org/10.1088/0964-1726/22/4/045013.

[257] Yang G, Spencer Jr BF, Carlson JD, Sain MK. Large-scale MR fluid dampers: modeling

and dynamic performance considerations. Eng Struct 2002;24:309–23.

[258] Poynor JC. Innovative designs for magneto-rheological dampers. Virginia Polytechnic Institute and State University, 2001.

[259] Zareie. S, Shahria Alam M, Seethlaer RJ, Zabihollah. A. Effect of shape memory alloy-magnetorheological fluid-based structural control system on the marine structure using nonlinear time-history analysis. Appl Ocean Res J 2019;91:101836. https://doi.org/https://doi.org/10.1016/j.apor.2019.05.021.

[260] McKenna F, Fenves GL, Scott MH, others. Open system for earthquake engineering simulation. Univ California, Berkeley, CA 2000.

[261] Mazzoni S, McKenna F, Scott MH, Fenves GL, others. OpenSees command language manual. Pacific Earthq Eng Res Cent 2006.

[262] Chopra AK. Dynamics of structures: theory and applications to earthquake engineering. Prentice-Hall; 2001.

[263] Akcelyan S, Lignos DG, Hikino T, Nakashima M. Evaluation of simplified and state-of-the-art analysis procedures for steel frame buildings equipped with supplemental damping devices based on E-Defense full-scale shake table tests. Soil Dyn Earthq Eng 2016;142:488–502.

[264] Akçelyan S. Seismic retrofit of existing steel tall buildings with supplemental damping devices. McGill University Libraries, 2017.

[265] Pieper CG. Seismic analysis and design of hybrid concrete timber structures with 2015 national building code of Canada. University of British Columbia, 2018.

[266] Compnay, Lord. RD-8041-1 MR Damper Technical Drawing. 2009.

[267] Shigley JE. Shigley's mechanical engineering design. Tata McGraw-Hill Education; 2011.

Appendix A SMA modeling

```
# ------------------------------------------------------------------------
-----------------------
# Example 1. cantilever 2D
# EQ ground motion with gravity
# all units are in kip, inch, second
# elasticBeamColumn ELEMENT
#  Silvia Mazzoni & Frank McKenna, 2006
#
# ^Y
# |
# 2   __
# |    |
# |    |
# |    |
# (1)  4.2 m
# |    |
# |    |
# |    |
# =1= ---- -------->X
#

# SET UP ---------------------------------------------------------------------
--------
wipe;         # clear opensees model
model basic -ndm 2 -ndf 3;    # 2 dimensions, 3 dof per node
file mkdir data;      # create data directory

# define GEOMETRY -----------------------------------------------------------
--
# nodal coordinates:
# node 1 0. 0.;      # node#, X Y
# node 2 0. 432.
node 1 0. 0.000
node 2 0. 4200.0



# Single point constraints -- Boundary Conditions
fix 1 1 1 1;       # node DX DY RZ

# nodal masses:
mass 2 5.18 0. 0.;     # node#, Mx My Mz, Mass=Weight/g.

# Define ELEMENTS ------------------------------------------------------------
--
# define geometric transformation: performs a linear geometric transformation
of beam stiffness and resisting force from the basic system to the global-
coordinate system
geomTransf Linear 1;     # associate a tag to transformation
```

```
# sma
# set SMA  3
# set k1  28000
# set k2  [expr 0.128*$k1]
# set sigmaMs 375.0
# set sigmaAf 160.0
# set epsilonl 0.06


set SMA  3
set k1  43000
set k2  [expr 0.08*$k1]
set sigmaMs 500.0
set sigmaAf 160.0
set epsilonl 0.06




set sigAct $sigmaMs
set beta [expr 1-($sigmaAf/$sigmaMs)]
set Rm  0
set rBear [expr $Rm/$k1]
puts "beta=$beta"

#uniaxialMaterial SelfCentering $matTag $k1 $k2 $sigAct $beta <$epsSlip>
<$epsBear> <rBear>
uniaxialMaterial SelfCentering $SMA $k1 $k2 $sigAct $beta 0.0 $epsilonl
$rBear



uniaxialMaterial Steel01 1 240 2.059e5 0.01


#IPE 160
#section WFSection2d $secTag $matTag $d  $tw  $bf $tf $Nfw $Nff
section WFSection2d  1  3 145.2  5.0 82.0 7.4 5 5


#element nonlinearBeamColumn $eleTag $iNode $jNode $numIntgrPts $secTag
$transfTag

element nonlinearBeamColumn 1 1 2 7 1 1

# connectivity:
#element elasticBeamColumn 1 1 2 3600 3225 1080000 1; # element
elasticBeamColumn $eleTag $iNode $jNode $A $E $Iz $transfTag
```

```
# Define RECORDERS ----------------------------------------------------------
---
recorder Node -file Data/dis_sma.txt -node 2 -dof 2 disp;      #
displacements of free nodes
recorder Node -file Data/force_sma.txt -node 2 -dof 2 reaction;     # support
reaction
recorder Node -file Data/force_sma_base.txt -node 1 -dof 2 reaction;
#recorder Node -file Data/Disp2.txt -time -node 2 -dof 1 2 4 disp;
#recorder Node -file Data/Vel2.txt -time -node 2 -dof 1 2 4 vel;


recorder Element -file Data/SMA_stress_strain.txt -ele 1 section 1 fiber 1 1
stressStrain


# define GRAVITY -----------------------------------------------------------
-
# timeSeries Linear 1
# pattern Plain 1 1 {
 # load 2 0. -20. 0.;     # node#, FX FY MZ -- superstructure-weight
# }
 # constraints Plain;     # how it handles boundary conditions
 # numberer Plain;      # renumber dof's to minimize band-width
(optimization), if you want to
 # system BandGeneral;     # how to store and solve the system of equations
in the analysis
 # algorithm Linear;     # use Linear algorithm for linear analysis
 # integrator LoadControl 0.1;   # determine the next time step for an
analysis, # apply gravity in 10 steps
 # analysis Static;      # define type of analysis static or transient
 # analyze 10;       # perform gravity analysis
 # loadConst -time 0.0;    # hold gravity constant and restart time




# --------------------------cYCLIC aNALYSIS---------------
pattern Plain 3 Linear {
 load 2 0.0 0.1 0.0
 }

# pattern Plain $patternTag $tsTag <-fact $cFactor> {
# load...
    # load $nodeTag (ndf $LoadValues)
    # $nodeTag tag of node to which load is applied.
    # $loadvalues ndf reference load values.

# eleLoad...
# sp...
# ...
# }
```

```
# NOTES:

 # The command to generate a LoadPattern contains in { } the commands to
generate all the loads and single-point constraints..

# $patternTag unique tag among load patterns
# $tsTag the tag of the time series to be used in the load pattern
# $cFactor constant factor (optional, default=1.0)
# load... command to nodal load
# eleLoad ... command to generate elemental load
# sp ... command to generate single-point constraint


foreach Dincr {0 0.06375 -0.06375 0.07875 -0.07875 0.09375 -0.09375 0.1125 -
0.1125 0.13125 -0.13125 0.15 -0.15} {
 integrator DisplacementControl 2 2 $Dincr
 analysis Static
 analyze 1000
}



# integrator DisplacementControl $node $dof $incr <$numIter $?Umin $?Umax>
# $node  node whose response controls solution
# $dof degree of freedom at the node, valid options: 1 through ndf at node.
# $incr  first displacement increment ?Udof
# $numIter the number of iterations the user would like to occur in the
solution algorithm. Optional, default = 1.0.
# $?Umin the min stepsize the user will allow. optional, defualt = ?Umin =
?U0
# $?Umax the max stepsize the user will allow. optional, default = ?Umax =
?U0







# # pattern Plain $patternTag $tsTag <-fact $cFactor> {

# # load $nodeTag (ndf $LoadValues)
# # $nodeTag tag of node to which load is applied.
# # $loadvalues  ndf reference load values.


# # }
```

```
#pattern UniformExcitation 2 1 -accel 2;     # define where and how (pattern
tag, dof) acceleration is applied

# set damping based on first eigen mode
set freq [expr [eigen -fullGenLapack 1]**0.5]
set dampRatio 0.02
rayleigh 0. 0. 0. [expr 2*$dampRatio/$freq]


# display displacement shape of the column
recorder display "Displaced shape" 10 10 500 500 -wipe
prp 200. 50. 1;
vup 0 1 0;
vpn 0 0 1;
display 1 5 40

# create the analysis
wipeAnalysis;      # clear previously-define analysis parameters
# constraints Plain;      # how it handles boundary conditions
# numberer Plain;      # renumber dof's to minimize band-width
(optimization), if you want to
# system BandGeneral;      # how to store and solve the system of equations in
the analysis
# algorithm Linear      # use Linear algorithm for linear analysis
# integrator Newmark 0.5 0.25 ;  # determine the next time step for an
analysis
# analysis Transient;      # define type of analysis: time-dependent
# analyze 10000 0.02;      # apply 3995 0.01-sec time steps in analysis

# constraints Transformation
# numberer RCM
# system BandGeneral
# test EnergyIncr 1.0e-5 1000
# #test NormUnbalance 1.0e-5 1000

# #test NormDispIncr 1.0e-5 200
# algorithm ModifiedNewton -initial 0.001
# integrator Newmark 0.5 0.25
# analysis Transient
# #

# analyze 10012 0.01
#
puts "ok End"


puts "Done!"wipe
```

Appendix B MRF-based damper (1A)

```
wipe
puts "system"
model basic -ndm 3 -ndf 6
set OutputmaxwellMRF1 OutputmaxwellMRF1;
file mkdir $OutputmaxwellMRF1;


puts "node"
node 1 0 0 0
node 2 1 0 0
fix 1 1 1 1 1 1 1
fix 2 0 1 1 1 1 1

puts "element"
#uniaxialMaterial ViscousDamper $matTag $K $Cd $alpha <$LGap> < $NM $RelTol
$AbsTol $MaxHalf>
set Cof 1; # it is teh
set K [expr $Cof*1e3]
set Cd [expr $Cof*640*1e-3]
set alpha 0.1

#uniaxialMaterial Viscous 1 $Cd $alpha
uniaxialMaterial ViscousDamper 1 $K $Cd $alpha
element twoNodeLink 1 1 2 -mat 1 -dir 1

puts "recoeder"
recorder Node -file OutputmaxwellMRF1/node2k1e3_disp.txt -time -node 2 -dof 1
disp;
recorder Node -file OutputmaxwellMRF1/node2k1e3_vel.txt -time -node 2 -dof 1
vel;
recorder Element -file OutputmaxwellMRF1/ele1k1e3_f.txt -time -ele 1 -dof 1
force;

#pattern MultipleSupport $patternTag {
#groundMotion $gmTag Plain <-accel $tsTag> <-vel $tsTag> <-disp $tsTag> <-int
(IntegratorType intArgs)> <-fact $cFactor>
#imposedMotion $nodeTag $dirn $gMotionTag

# Displacement Loading Protocol ------------------------------------------
---------
set dt1 0.01;

# Displacement Loading Protocol
set fileName2 "ViscousD4.tcl";


set Scalefact [expr 1.00000];
# Set Displacement loading history
set DispSeries "Series -dt $dt1 -filePath $fileName2 -factor [expr
$Scalefact]"
```

```
# Set Applied Direction of loading history
set dir 1

# Set Dynamic Analysis Parameters # ----------------------------------------
-----------------
#
# Displacement Control
# Note: In order to calibrate the viscoelastic damper displacement control is
used
#  since the damper is time dependent and rate effects are needed to generate
force
# Steps:
#  1. A multisupport excitation is used in OpenSees with displacement history
input
#  2. The imposed displacement motion is applied to the free end of the
damper
#groundMotion $gmTag Plain <-accel $tsTag> <-vel $tsTag> <-disp $tsTag> <-int
(IntegratorType intArgs)> <-fact $cFactor>
#imposedMotion $nodeTag $dirn $gMotionTag


pattern MultipleSupport 5 {
groundMotion 2 Plain -vel $DispSeries
#   node  dir GMotion
imposedMotion 2 $dir   2
}
puts "analysis"
wipeAnalysis;
constraints Transformation
integrator Newmark 0.5 0.25 ;
numberer RCM
system UmfPack
test EnergyIncr 1.0e-8 100 2
algorithm Newton;
analysis Transient
analyze 20000 0.0
```

Appendix C Natural frequencies of a two-story frame with SMA-MRF bracing

```
################################################################################
########
#
# Modelling of two Story Shear Frame equipped with shape memory alloy(SMA)
#bars , magnetorheological fluid(MRF) damper , SMA-MRF damper
#
# Shahin Zareie, Ph.D.
# The University of British Columbia, British Columbia, Canada
#
#In order to develop this code: two references are used:
#              Source 1:
#http://opensees.berkeley.edu/wiki/index.php/Dynamic_Analyses_of_1-
#Story_Moment_Frame_with_Viscous_Dampers
#              Source 2:
#http://opensees.berkeley.edu/wiki/index.php/Dynamic_Analysis_of_2-
#Story_Moment_Frame
# Date: 23/11/2018
# Revised: -
#
#
################################################################################
########
# Define model
# All the units are in mm,KN,sec

wipe all;
       # clear memory of past model definitions
model BasicBuilder -ndm 2 -ndf 3; # Define the model builder, ndm =
#dimension, ndf = #dofs
set pi [expr acos(-1.0)]; # calcute the Pi number
set numModes 2



# create data directory
set Output Output;S
file mkdir $Output;
# define geometry


# Columns and Beam Properties
set Ac 40909.5;  # mm2 ---->63.41 in2 to 40909.5 mm2 benchmark in source 2
set Ic 133194056.32;# mm4 ---->320.0 in4 to mm4 benchmark in source 2
set E 206.84 ; # KN/mm2 --->30000 Ksi to 206.84 KN/mm2 benchmark in source 2
set Ib 41626e+12; # mm4 ---->rigid material
set Ab 40909.5; # mm2. ---->63.41 in2 to 40909.5 mm2 benchmark in source 2
```

```
set h 3657.6; #story heigth # mm
set L [expr 2*$h]; #bay width is eual to L=2*h




# nodal coordinates:
node 1 0. 0. ;
node 2 $L 0. ;
node 3 0. $h ;
node 4 $L $h ;
node 5 0. [expr 2*$h]; #bay width is eual to L=2*h
node 6 $L [expr 2*$h]; #bay width is eual to L=2*h



# Single point constraints -- Boundary Conditions
fix 1 1 1 1;
fix 2 1 1 1;


# MP constraints
equalDOF 3 4 2 3
equalDOF 5 6 2 3

# mass
set W 1000.; #KN
set g 9810.; #mm/sec2
set m [expr $W/$g];

# assign mass
mass 3 $m 0. 0. ;
mass 4 $m 0. 0. ;
mass 5 [expr $m/2.] 0. 0. ;
mass 6 [expr $m/2.] 0. 0. ;



# define geometric transformation:
set TransfTag 1;
geomTransf Linear $TransfTag ;

# define elements:
# columns
element elasticBeamColumn 1 1 3 $Ac $E [expr 2.*$Ic] $TransfTag;
element elasticBeamColumn 2 3 5 $Ac $E $Ic   $TransfTag;
element elasticBeamColumn 3 2 4 $Ac $E [expr 2.*$Ic] $TransfTag;
```

```
element elasticBeamColumn 4 4 6 $Ac $E $Ic   $TransfTag;
# beams
element elasticBeamColumn 5 3 4 $Ab $E $Ib   $TransfTag;
element elasticBeamColumn 6 5 6 $Ab $E $Ib   $TransfTag;




# record eigenvectors
#-----------------------
for { set k 1 } { $k <= $numModes } { incr k } {
 recorder Node -file [format "modes/mode%i.out" $k] -nodeRange 1 6 -dof 1 2 3
"eigen $k"
}

# perform eigen analysis
#-----------------------------
set lambda [eigen $numModes];

# calculate frequencies and periods of the structure
#---------------------------------------------------
set omega {}
set f {}
set T {}

foreach lam $lambda {
 lappend omega [expr sqrt($lam)]
 lappend f [expr sqrt($lam)/(2*$pi)]
 lappend T [expr (2*$pi)/sqrt($lam)]
}

puts "periods are $T"

# write the output file cosisting of periods
#-------------------------------------------
set period "modes/Periods.txt"
set Periods [open $period "w"]
foreach t $T {
 puts $Periods " $t"
}
close $Periods


# create display for mode shapes
#-------------------------------
#     $windowTitle $xLoc $yLoc $xPixels $yPixels
recorder display "Mode Shape 1" 10 10  500  500  -wipe
prp $h $h 1;           # projection reference point (prp); defines the center
of projection (viewer eye)
vup 0 1 0;           # view-up vector (vup)
vpn 0 0 1;           # view-plane normal (vpn)
viewWindow -2000 2000 -2000 2000;      # coordiantes of the window relative
to prp
```

```
display -1 5 20;          # the 1st arg. is the tag for display mode (ex. -1
is for the first mode shape)
              # the 2nd arg. is magnification factor for nodes, the 3rd arg.
is magnif. factor of deformed shape
recorder display "Mode Shape 2" 10 510 500 500 -wipe
prp $h $h 1;
vup 0 1 0;
vpn 0 0 1;
viewWindow -2000 2000 -2000 2000
display -2 5 20
 # Run a one step gravity load with no loading (to record eigenvectors)
#-------------------------------------------------------------------------
integrator LoadControl 0 1 0 0

# Convergence test
#      tolerance maxIter displayCode
test EnergyIncr  1.0e-10 100  0

# Solution algorithm
algorithm Newton

# DOF numberer
numberer RCM

# Constraint handler
constraints Transformation


# System of equations solver
system ProfileSPD

analysis Static
set res [analyze 1]
if {$res < 0} {
 puts "Modal analysis failed"
}
 # get values of eigenvectors for translational DOFs
#---------------------------------------------------
set f11 [nodeEigenvector 3 1 1]
set f21 [nodeEigenvector 5 1 1]
set f12 [nodeEigenvector 3 2 1]
set f22 [nodeEigenvector 5 2 1]
puts "eigenvector 1: [list [expr {$f11/$f21}] [expr {$f21/$f21}] ]"
puts "eigenvector 2: [list [expr {$f12/$f22}] [expr {$f22/$f22}] ]"



wipeAnalysis
```

Appendix D Time-history analysis a two-story frame with SMA-MRF bracing

```
#
##########################################################################
########
#
# Modelling of two Story Shear Frame equipped with shape memory alloy(SMA)
bars , magnetorheological fluid(MRF) damper , SMA-MRF damper
#
# Shahin Zareie, Ph.D.
# The University of British Columbia, British Columbia, Canada
#
#In order to develop this code: two refrences are used:
#              Source 1:
http://opensees.berkeley.edu/wiki/index.php/Dynamic_Analyses_of_1-
Story_Moment_Frame_with_Viscous_Dampers
#              Source 2:
http://opensees.berkeley.edu/wiki/index.php/Dynamic_Analysis_of_2-
Story_Moment_Frame
# Date: 23/11/2018
# Revised: -
#
#
##########################################################################
########
# Define model
# All the units are in mm,KN,sec

wipe all;
       # clear memory of past model definitions
model BasicBuilder -ndm 2 -ndf 3; # Define the model builder, ndm =
#dimension, ndf = #dofs
set pi [expr acos(-1.0)]; # calcute the Pi number
set Tn 0.7717; # sec (Natural Period)



# create data directory
set Output Output;
file mkdir $Output;
# define geometry


# Columns and Beam Properties
set Ac 40909.5;  # mm2 ---->63.41 in2 to 40909.5 mm2 benchmark in source 2
set Ic 133194056.32;# mm4 ---->320.0 in4 to mm4 benchmark in source 2
set E 206.84 ; # KN/mm2 --->30000 Ksi to 206.84 KN/mm2 benchmark in source 2
set Ib 41626e+12; # mm4 ---->rigid material
set Ab 40909.5; # mm2. ---->63.41 in2 to 40909.5 mm2 benchmark in source 2
```

```
set h 3657.6; #story heigth # mm
set L [expr 2*$h]; #bay width is eual to L=2*h



# nodal coordinates:
node 1 0. 0. ;
node 2 $L 0. ;
node 3 0. $h ;
node 4 $L $h ;
node 5 0. [expr 2*$h]; #bay width is eual to L=2*h
node 6 $L [expr 2*$h]; #bay width is eual to L=2*h


# # nodal coordinates:
# node 11 0. 0. ;
# node 22 $L 0. ;
# node 33 0. $h ;
# node 44 $L $h ;
# node 55 0. [expr 2*$h]; #bay width is eual to L=2*h
# node 66 $L [expr 2*$h]; #bay width is eual to L=2*h


# #equalDOF $rNodeTag $cNodeTag $dof1 $dof2
# equalDOF 1 11 1 2 3
# equalDOF 2 22 1 2 3
# equalDOF 3 33 1 2 3
# equalDOF 4 44 1 2 3
# equalDOF 5 66 1 2 3




# # middle nodal coordinates:
 set alpha 0.8; # define how much devison
 node 14 [expr $alpha*$L] [expr $alpha*$h] ;
 #node 23 [expr (1.0-$alpha)*$L] [expr $alpha*$h] ;
# node 36 [expr $alpha*$L] [expr ($alpha+1.0)*$h] ;
 node 45 [expr (1.0-$alpha)*$L] [expr ($alpha+1.0)*$h]

# Single point constraints -- Boundary Conditions
fix 1 1 1 1;
fix 2 1 1 1;


# MP constraints
```

```
equalDOF 3 4 2 3
equalDOF 5 6 2 3

# mass
set W 1000.; #KN
set g 9810.; #mm/sec2
set m [expr $W/$g];

# assign mass
mass 3 $m 0. 0. ;
mass 4 $m 0. 0. ;
mass 5 [expr $m/2.] 0. 0. ;
mass 6 [expr $m/2.] 0. 0. ;




# define geometric transformation:
set TransfTag 1;
geomTransf Linear $TransfTag ;

# define elements:
# columns
element elasticBeamColumn 1 1 3 $Ac $E [expr 2.*$Ic] $TransfTag;
element elasticBeamColumn 2 3 5 $Ac $E $Ic   $TransfTag;
element elasticBeamColumn 3 2 4 $Ac $E [expr 2.*$Ic] $TransfTag;
element elasticBeamColumn 4 4 6 $Ac $E $Ic   $TransfTag;
# beams
element elasticBeamColumn 5 3 4 $Ab $E $Ib   $TransfTag;
element elasticBeamColumn 6 5 6 $Ab $E $Ib   $TransfTag;







set TransfCorotationalTag 3;
geomTransf Corotational $TransfCorotationalTag; #brace
# SMA material
set SMA  3
set k1  28000
set k2  [expr 0.128*$k1]
set sigmaMs 375.0; # KN/mm2
set sigmaAf 160.0; # KN/mm2
set epsilonl 0.06

set sigAct $sigmaMs
set beta [expr 1-($sigmaAf/$sigmaMs)]
set Rm  0
set rBear [expr $Rm/$k1]
puts "beta=$beta"
```

```
set E_SMA [expr 40.0*1e3];; # KN/mm2

#uniaxialMaterial SelfCentering $matTag $k1 $k2 $sigAct $beta <$epsSlip>
<$epsBear> <rBear>
uniaxialMaterial SelfCentering $SMA $k1 $k2 $sigAct $beta 0.0 $epsilonl
$rBear



 # set Radious [expr (4*$Ic*$E/($pi*$sigmaMs))**0.25/10]; # Calculation of
Radiuos of SMA bars
 # set area  [expr $pi*$Radious**2];

 set MRF_force 75; # KN the maximum force of MRF damper
# # # set Radious [expr (4*$Ic*$E/($pi*$sigmaMs))**0.25]; # Calculation of
Radiuos of SMA bars
# # #set Radious [expr (4*$Ic*$E/($pi*$E_SMA))**0.25]; # Calculation of
Radiuos of SMA bars
 set Cof_r 1; # how to sclae the SMA's radious
 set Delta_L 21;
 # set area  [expr ($MRF_force*$Lenghth)/($E_SMA*$Delta_L)];
 set area  [expr ($MRF_force)/($sigmaMs)];
 set Radious [expr $Cof_r*($area/$pi)**0.5];
 set Im  [expr $Radious**4/$pi];

# #set Radious 0.50;

puts "-------------------------------------------------"
#puts "E_SMA=$E_SMA"
puts "Radious=$Radious"
#puts "E_SMA=$E_SMA"
puts "area=$area"
puts "Im=$Im"
puts "-------------------------------------------------"


set sma_sec 14

 section Fiber $sma_sec {
 #patch circ $matTag $numSubdivCirc $numSubdivRad $yCenter $zCenter $intRad
$extRad $startAng $endAng
 patch circ $SMA  16   4    0.0  0.0  0.0  $Radious 0.0  360
 }


 element elasticBeamColumn 9 1 14 $Ac $E $Ic   $TransfTag;
 element elasticBeamColumn 10 4 45 $Ac $E $Ic   $TransfTag;


 element forceBeamColumn 7 14 4 10 $sma_sec $TransfTag;
 element forceBeamColumn 8 45 5 10 $sma_sec $TransfTag;
#element elasticBeamColumn 7 1 4 $area $E [expr 2.*$Ic] $TransfTag;
```

```
# ------------------------------------------------------------------------
# ------------------------------ Damper  -------------------------
# ------------------------------------------------------------------------
# ------------------------------------------------------------------------
#Damper
#uniaxialMaterial ViscousDamper $matTag $K $Cd $alpha <$LGap> < $NM $RelTol
$AbsTol $MaxHalf>
set Cof 80.5; # it is teh
set K [expr $Cof*1e3];
set Cd [expr $Cof*680*1e-3];
set alpha 0.1;
set damper 5;
#uniaxialMaterial Viscous 1 $Cd $alpha
uniaxialMaterial ViscousDamper $damper $K $Cd $alpha

#element twoNodeLink $eleTag $iNode $jNode -mat $matTags -dir $dirs
element twoNodeLink 77 1 4 -mat $damper -dir 1
# element twoNodeLink 8 2 3 -mat $damper -dir 1
# element twoNodeLink 9 3 6 -mat $damper -dir 1
element twoNodeLink 1010 4 5 -mat $damper -dir 1
# ------------------------------------------------------------------------
# ------------------------------ Damper ----- -------------------------
# ------------------------------------------------------------------------
# ------------------------------------------------------------------------

# Record-----------------------------------------------------------------------

#timeSeries Path $tag -dt $dt -filePath $filePath <-factor $cFactor>
#timeSeries Path 1 -dt 0.01 -filePath TAKY.txt -factor [expr 0.5*$g]; #
define acceleration vector from file (dt=0.01 is associated with the input
file gm)
#timeSeries Path 1 -dt 0.005 -filePath Christchurch.txt -factor [expr
0.50*$g]; # define acceleration of Christchurch vector from file (dt=0.005 is
associated with the input file gm)
#timeSeries Path 1 -dt 0.005 -filePath Tarapaca.txt -factor [expr 0.50*$g]; #
define acceleration of Tarapaca vector from file (dt=0.005 is associated with
the input file gm)
# timeSeries Path 1 -dt 0.01 -filePath Tohoko.txt -factor [expr 0.50*$g]; #
define acceleration vector of Tohoko from file (dt=0.01 is associated with
the input file gm)


timeSeries Path 1 -dt 0.005 -filePath Parkfield.txt -factor [expr 0.50*$g]; #
define acceleration of Tarapaca vector from file (dt=0.005 is associated with
the input file gm)
#timeSeries Path 1 -dt 0.005 -filePath Darfield.txt -factor [expr 0.50*$g]; #
define acceleration of Tarapaca vector from file (dt=0.005 is associated with
the input file gm)
#timeSeries Path 1 -dt 0.005 -filePath Imperial_valley.txt -factor [expr
0.50*$g]; # define acceleration of Tarapaca vector from file (dt=0.005 is
associated with the input file gm)
#timeSeries Path 1 -dt 0.005 -filePath Christchurch.txt -factor [expr
0.50*$g]; # define acceleration of Tarapaca vector from file (dt=0.005 is
associated with the input file gm)
```

```
# set damping based on first eigen mode
set freq [expr [eigen 1]**0.5]
set period [expr 2*$pi/$freq]
puts $period
set damp 0.02;
rayleigh [expr 2*$damp*$freq] 0. 0. 0.

#pattern UniformExcitation $patternTag $dir -accel $tsTag <-vel0 $ver0>
pattern UniformExcitation 1 1 -accel 1;    # define where and how (pattern
tag, dof) acceleration is applied

# Define RECORDERS ----------------------------------------------------------
---
# Define RECORDERS ----------------------------------------------------------
---
recorder Node -file $Output/Disp6.txt -time -node 6 -dof 1 disp; # The Second
Floor
recorder Node -file $Output/Disp4.txt -time -node 4 -dof 1 disp; # The First
Floor
recorder Node -file $Output/Acc6.txt -timeSeries 1 -time -node 6 -dof 1
accel; # The Second Floor
recorder Node -file $Output/Acc4.txt -timeSeries 1 -time -node 4 -dof 1
accel; # The First Floor


# recorder Element -file $Output/SMA_disp.txt -time -ele 7 8 deformations ;
recorder Element -file $Output/SMA_stress_strain.txt -ele 7 8 section 1 fiber
1 1 stressStrain


recorder Element -file $Output/MRF_Force_loacl.txt -time -ele 77 1010 -dof 1
localForce;
recorder Element -file $Output/MRF_disp.txt -time -ele 77 1010 deformations ;




recorder Node -file $Output/Base.txt -time -node 1 2 -dof 1 reaction; #
support reaction

# drift recorder command: recorder Drift -file $filename -time -iNode
$NodeI_ID -jNode $NodeJ_ID -dof $dof -perpDirn
$Record.drift.perpendicular.to.this.direction
recorder Drift -file $Output/Drift-Story1.txt -time -iNode 1 -jNode 3 -dof 1
-perpDirn 2;
recorder Drift -file $Output/Drift-Story2.txt -time -iNode 3 -jNode 5 -dof 1
-perpDirn 2;


# display displacement shape of the column
```

```
recorder display "Displaced shape" 10 10 500 500 -wipe
prp 200. 50. 1;
vup 0 1 0;
vpn 0 0 1;
display 1 5 40

# create the analysis
wipeAnalysis;       # clear previously-define analysis parameters
wipeAnalysis;       # clear previously-define analysis parameters
constraints Transformation;    # how it handles boundary conditions
numberer RCM;       # renumber dof's to minimize band-width (optimization), if
you want to
system UmfPack;       # how to store and solve the system of equations in the
analysis (large model: try UmfPack)
test EnergyIncr 1.0e-8 100;    # test Eneregy incerment
algorithm KrylovNewton;     # use Kyrlow-Newton algorithm
integrator Newmark 0.5 0.25 ;  # determine the next time step for an analysis
analysis Transient;      # define type of analysis: time-dependent
analyze [expr 4*40096] 0.001;  # apply 10*4096 steps for 0.001-sec time steps
in analysis

puts "Done!"
wipe
```

Appendix E Matlab Code

```
clc
clear all;
close all;
P=acos(-1.0);% define Pi number

A=40909.5;  %mm2 ---->63.41 in2 to 40909.5 mm2 benchmark in source 2
I=133194056.32;% mm4 ---->320.0 in4 to mm4 benchmark in source 2
E=206.84 ; % KN/mm2 --->30000 Ksi to 206.84 KN/mm2 benchmark in source 2
h=3657.6; % %mm #story heigth # mm

W=1000.; % #KN
g=9810.; % #mm/sec2
m=W/g; % calculation of mass based on Source 2



f1=(3.464/(2*P))*sqrt(E*I/(m*h^3));
f2=(6.928/(2*P))*sqrt(E*I/(m*h^3));

T1=1/f1;
disp("the First natural period");
disp(T1);
T2=1/f2;
disp("the second natural period");
disp(T2);
```

Appendix F As-built drawing